

The role of guanine nucleotide exchange factors (GEFs) in EGF-receptor signalling

Screening for a small molecule inhibitor of the Rin1-mediated Rab5 activation

Dissertation

zur Erlangung des Doktorgrades (Dr. rer. nat.)
der Mathematisch-Naturwissenschaftlichen Fakultät
der Rheinischen Friedrich-Wilhelms-Universität Bonn

vorgelegt von

Maren Hamann

aus Hamburg

Bonn, 2017

Angefertigt mit Genehmigung der Mathematisch-Naturwissenschaftlichen Fakultät der
Rheinischen Friedrich-Wilhelms-Universität Bonn

1. Gutachter: PD Dr. med. Anton Schmitz
2. Gutachter: Prof. Dr. rer. nat. Günter Mayer
Tag der Promotion: 30.01.2018
Erscheinungsjahr: 2018

Contents

List of abbreviations	8
List of figures	12
List of tables	15
Zusammenfassung	16
Abstract	18
1 Introduction	19
1.1 Inter- and intracellular signalling: communication in living organisms	19
1.2 The role of small GTPases in cellular signalling	20
1.3 Activation of small GTPases	21
1.4 The Rab family of small GTPases	22
1.4.1 Rab GTPases as key regulators of vesicular transport	22
1.4.2 The role of Rab GTPases in endocytosis	23
1.5 Rab5 – regulator of the early steps in CME	25
1.5.1 Diversity in structure and function: Rab5 interaction partners	25
1.5.2 Rab5 GEFs contain a catalytic Vps9 domain	26
1.6 Rin1: multiple domains, multiple functions	27
1.6.1 The nucleotide exchange mechanism of Vps9 domain-containing GEFs	27
1.6.2 Rin1 enhances EGFR internalization, degradation and down-regulation	28
1.6.3 The role of Rin1 in ABL kinase signalling	28
1.6.4 Two sides of the coin – Rin1 in cancer	29
1.7 Small molecules as tools to modify single domains in multi-domain proteins	30
1.7.1 Ras superfamily GTPases as targets for small molecule inhibitors	30
1.7.2 GEFs as targets for small molecule inhibitors	31
1.7.3 Overview: Inhibitors of Ras superfamily small GTPases and their GEFs	31
1.7.3.1 Inhibitors of Ras GTPases	31
1.7.3.2 Inhibitors of GEF proteins	35
2 Aim of the Project	38
3 Results	39
3.1 Protein expression and purification	39
3.1.1 Rab5a	39
3.1.2 Rin1C	40
3.1.3 Rin1-TS	42
3.1.4 Rabex-5 _{GEF}	42
3.1.5 Rab1	43
3.1.6 DrrA	45
3.1.7 Rac2	45
3.1.8 Tiam1DHPH	46
3.1.9 Rac1	47
3.1.10 Vav1	48
3.1.11 NΔ17 Arf1, ARNO-Sec7 and IR-ICD	49
3.2 Nucleotide exchange activity of the recombinant proteins	50
3.3 Screening for small molecule inhibitors	52
3.3.1 Establishing the Bodipy-TR-GTP nucleotide exchange screening assay	52

3.3.2 Assay optimization for HTS	53
3.3.3 Calculation of the Z' factor	54
3.3.4 The compound library	55
3.3.5 High-throughput screening results	55
3.3.6 Identification of secondary hits	55
3.4 Characterization of secondary hit compounds	56
3.4.1 Compound activity profiles and structures	57
3.4.2 Specificity in other GEF/GTPase assays	60
3.4.2.1 ARNO-Sec7 and Arf1	60
3.4.2.2 Vav1 and Rac1	61
3.4.2.3 DrrA and Rab1	61
3.4.2.4 Tiam1 and Rac2	62
3.4.2.5 Rabex-5 _{GEF} and Rab5a	63
3.4.3 Aggregation properties of the secondary hit compounds	63
3.4.3.1 The centrifugation-based aggregation assay	63
3.4.3.2 The insulin receptor auto-phosphorylation assay	65
3.4.4 Purity of CG3 05 A02	65
3.4.5 Solubility of CG3 05 A02	66
3.4.6 Structure activity relationship of CG3 05 A02	67
3.4.7 Influence of CG3 05 A02 on the ABL1-mediated Rin1 phosphorylation	70
3.4.8 Influence of CG3 05 A02 on Bodipy-TR-GTP binding to Rab5a	71
3.4.9 CG3 05 A02 in the Rin1C/Rab5a Bodipy-FL-GTP nucleotide exchange assay	72
3.4.10 CG3 05 A02 in the Rin1C/Rab5a Bodipy-FL-GDP release assay	73
3.4.11 CG3 05 A02 in the [α - ³² P]-GTP nucleotide exchange assay	74
4 Discussion	76
4.1 Protein expression and purification	76
4.1.1 Rin1 constructs could only be retrieved from <i>Sf9</i> insect cells	76
4.2 All constructs were found to be active in nucleotide exchange assays	77
4.3 Screening for small molecule inhibitors	78
4.4 Concentration-dependent inhibition of the Rin1C/Rab5a Bodipy-TR-GTP nucleotide exchange assay	80
4.5 The majority of the secondary hits were either unspecific or aggregators	80
4.6 CG3 05 A02 specifically inhibited the Vps9 domain-containing Rab5a GEF constructs Rin1C and Rabex-5 _{GEF} without inducing aggregation	81
4.7 A methoxy group is important for CG3 05 A02 to exhibit its inhibitory effect	82
4.8 CG3 05 A02 inhibits the GEF function of Rin1 without affecting the interaction with ABL1	83
4.9 The inhibitory effect of CG3 05 A02 depends on the use of a labelled GTP analogue	84
5 Outlook	86
5.1 Perspectives for CG3 05 A02	86
5.2 Considerations for future screening approaches	86
5.2.1 Insights from the Rin1C/Rab5a Bodipy-TR-GTP nucleotide exchange assay	86

5.2.2 Successful HTS approaches crucially depend on library size and quality	86
6 Conclusions	88
7 Materials & Methods	90
7.1 Materials	90
7.1.1 Equipment	91
7.1.2 Chemicals	91
7.1.3 Consumables	92
7.1.4 Compounds	92
7.1.5 Nucleic acids	93
7.1.6 Enzymes & Proteins	93
7.1.7 Antibodies	94
7.1.8 Bacterial strains	94
7.1.9 Software	94
7.2 Methods	94
7.2.1 Miscellaneous Methods	94
7.2.1.1 SDS-PAGE	94
7.2.1.2 Coomassie staining of PAA-gels	95
7.2.1.3 Western blotting (Immunoblotting)	96
7.2.1.3.1 Semi-dry blotting	96
7.2.1.3.2 Wet blotting	96
7.2.2 Protein biosynthesis and purification	97
7.2.2.1 Transformation of BL21-CodonPlus [®] (DE3)-RIL competent cells	97
7.2.2.2 Protein expression in <i>E. coli</i>	97
7.2.2.2.1 Monitoring of protein expression in <i>E. coli</i> whole cell lysates	98
7.2.2.3 Protein expression in <i>Sf9</i> -cells	98
7.2.2.4 <i>E. coli</i> and <i>Sf9</i> -cell lysis	98
7.2.2.5 Affinity chromatography	100
7.2.2.5.1 Nickel-NTA affinity chromatography	100
7.2.2.5.2 Glutathione affinity chromatography	101
7.2.2.5.3 Strep-Tactin affinity chromatography	102
7.2.2.5.4 Streptavidin affinity chromatography	102
7.2.2.5.5 Reverse affinity chromatography after tag cleavage	103
7.2.2.6 Cleavage of purification tags	103
7.2.2.6.1 Cleavage by TEV digestion	103
7.2.2.6.2 Cleavage by Thrombin digestion	103
7.2.2.7 Size exclusion chromatography	104
7.2.2.8 Handling of purified proteins	104
7.2.2.8.1 Determination of protein concentration	104
7.2.2.8.1.1 Photometric determination of protein concentration	104
7.2.2.8.1.2 Determination of protein concentration via Bradford assay	105
7.2.2.8.2 Increasing the protein concentration and buffer exchange	105

7.2.3 Nucleotide exchange assays	105
7.2.3.1 Bodipy-TR and –FL-GTP exchange assay	106
7.2.3.1.1 Bodipy-TR-GTP high throughput screening (HTS) assay	106
7.2.3.2 Bodipy-FL-GDP release assay	107
7.2.3.3 [α - ³² P]-GTP exchange assay	107
7.2.4 Protein aggregation assay	107
7.2.5 The insulin receptor auto-phosphorylation assay	108
7.2.6 The ABL1-mediated Rin1 phosphorylation assay	108
7.2.7 Analysis of Bodipy-TR-GTP binding to Rab5a	109
7.2.8 Synthesis and characterization of compounds	109
7.2.8.1 Synthesis of Aniline Precursors	110
7.2.8.1.1 3-Methyl-4-Nitrobenzoic acid chloride (1)	110
7.2.8.1.2 <i>N</i> -(2-Hydroxy-6-methylphenyl)-3-methyl-4-nitrobenzamine (2a)	110
7.2.8.1.3 <i>N</i> -(2-Hydroxyphenyl)-3-methyl-4-nitrobenzamine (2b)	111
7.2.8.1.4 4-Methyl-2-(3-methyl-4-nitrophenyl benzoxazole (3a)	112
7.2.8.1.5 4-Methyl-2-(4-nitrophenyl benzoxazole (3b)	112
7.2.8.2 Synthesis of CG3 05 A02 Analogues	113
7.2.8.2.1 2-Methyl-4-(4-methylbenzoxazol-2-yl)benzamine (4a)	113
7.2.8.2.2 4-(Benzoxazol-2-yl)-2-methylaniline (4b)	114
7.2.8.2.3 4-(4-Methylbenzoxazol-2-yl)benzamine (4c)	114
7.2.8.2.4 4-(Benzoxazol-2-yl)benzamine (4d)	115
7.2.8.2.5 2-Methoxy- <i>N</i> -(2-methyl-4-(4-methylbenzol-2-yl)phenyl)benzamine (5a)	115
7.2.8.2.6 <i>N</i> -(2-Methyl-4-(4-methylbenzoxazol-2-yl)phenyl)benzamine (5b)	116
7.2.8.2.7 <i>N</i> -(4-(Benzoxazol-2-yl)-2-methylphenyl)-2-methoxybenzamine (5c)	116
7.2.8.2.8 <i>N</i> -(4-(Benzoxazol-2-yl)-2-methylphenyl)benzamine (5d)	117
7.2.8.2.9 2-Methoxy- <i>N</i> -(4-(4-methylbenzoxazol-2-yl)phenyl)benzamine (5e)	118
7.2.8.2.10 <i>N</i> -(4-(4-Methylbenzoxazol-2-yl)phenyl)benzamine (5f)	118
7.2.8.2.11 <i>N</i> -(4-(benzoxazol-2-yl)phenyl)-2-methoxybenzamine (5g)	119
7.2.8.2.12 <i>N</i> -(4-(Benzoxazol-2-yl)phenyl)benzamine (5h)	119
7.2.8.3 Synthesis of the Control Compounds	120
7.2.8.3.1 4-Methoxy- <i>N</i> -(2-methyl-4-(4-methylbenzol-2-yl)phenyl)benzamine (5i)	120
7.2.8.3.2 3-Methoxy- <i>N</i> -(2-methyl-4-(4-methylbenzol-2-yl)phenyl)benzamine (5j)	121
7.2.8.3.3 <i>N</i> -(2-Methyl-4-(4-methylbenzoxazol-2-yl)phenyl)acetamide (6)	122
7.2.8.3.4 2-Methoxy- <i>N</i> -methyl- <i>N</i> -(2-methyl-4-(4-methylbenzol-2-yl)phenyl)benzamine (7)	122
7.2.9 Handling of Compounds	123
7.2.9.1 HPLC-MS	123
7.2.9.2 Determination of solubility	123

8	Appendix	125
8.1	Sequences	125
8.1.1	Plasmid maps	125
8.1.2	Protein sequences	130
8.2	Original gels and blots	132
8.2.1	Protein expression and purification	132
8.2.2	Aggregation assay	141
8.2.3	The insulin receptor auto-phosphorylation assay	142
8.2.4	Influence of CG3 05 A02 on the ABL1-mediated Rin1 phosphorylation	143
8.3	Structures of the 26 secondary hits	145
8.4	Raw data of the IC ₅₀ measurements	147
8.4.1	Secondary hits	147
8.4.2	SAR compounds	148
8.4.2.1	Linear fits	148
8.4.2.2	IC ₅₀ calculations	150
8.4.3	CG3 05 A02 in the Rin1C/Rab5a Bodipy-FL-GTP nucleotide exchange assay	151
8.4.4	CG3 05 A02 in the Rin1C/Rab5a Bodipy-FL-GDP release assay	151
8.5	Solubility of the CG3 05 A02 derivatives	152
8.6	Bodipy-TR-GTP binding to Rab5a	152
8.7	IC ₅₀ of CG3 05 A02 in the Rabex-5 _{GEF} /Rab5a Bodipy-TR-GTP nucleotide exchange assay	153
8.8	MST binding studies	153
8.9	Expression, purification and nucleotide exchange activity of GAPVD1	155
	References	158
	Acknowledgements	184

List of abbreviations

ABL	Abelson tyrosine-protein kinase
AA12	Acrylamide 12
AEBSF	4-benzenesulfonyl fluoride hydrochloride
AGP	Andrographolide
Als2	Alsin2
Als2CL	Alsin2 C-terminal-like protein
Amp	Ampicillin
Ankrd27	Ankyrin repeat domain-containing protein 27
AP2	Adapter protein 2
API	Athmospheric pressure interface
APS	Ammonium persulfate
AREG	Amphiregulin
Arf	ADP ribolysation factor
ARNO	ADP ribosylation factor nucleotide bindingsite opener
ATP	Adenosine triphosphate
BCR	Breakpoint cluster region protein
BFA	Brefeldin A
Bodipy-FL	Bodipy-Fluorescein
Bodipy-TR	Bodipy-Texas Red
BSA	Bovine serum albumin
BTC	Betacellulin
Bub2	Mitotic check point protein Bub2
CCV	Clathrin-coated vesicle
Cdc	Cell division control protein
CME	Clathrin-mediated endocytosis
CML	Chronic myelogenous leukaemia
COS	CV-1 (simian) origin carrying SV40 gene
DbI	Diffuse B-cell lymphoma
DH	DbI homology
DIPEA	N, N-Diisopropylethylamine
DMSO	Dimethyl sulfoxide
Dock5	Dedicator of cyto genesis protein 5
DrrA	Daunorubicin/doxorubicin resistance ATP-binding protein
DTT	Dithiothreitol
E-64	Epoxide-64 protease inhibitor
EDTA	Ethylenediaminetetraacetic acid
EEA1	Early endosomal autoantigen 1
EGF	Epidermal growth factor
EGFR	Epidermal growth factor receptor
EI	Electron impact
Em.	Emission
EPGN	Epithelial mitogen (Epigen)
ER	Endoplasmic reticulum
EREG	Epiregulin
ESI	Electrospray ionization
Ex.	Excitation

FI	Fluorescence intensity
FP	Fluorescence polarization
FPLC	Fast protein liquid chromatography
GAP	GTPase activating protein
GAPex-5	GTPase activating protein and exchange factor 4
GAPVD1	GTPase-activating and VPS9 domain-containing protein 1
GDF	GDI displacement factor
GDI	GDP dissociation inhibitor
GDP	Guanosine diphosphate
GEF	Guanine nucleotide exchange factor
Gent	Gentamycin
GSH	Glutathione
GST	Glutathione S-transferase
GTP	Guanosine triphosphate
HBEGF	Heparin-binding EGF-like growth factor
HBS3	Hydrogen-bond surrogate 3
HEPES	2-[4-(2-hydroxyethyl)piperazin-1-yl]ethanesulfonic acid
HPLC	High-performance liquid chromatography
HPLC-MS	High-performance liquid chromatography-mass spectrometry
HRMS	High-resolution mass spectrometry
Hsc70	Heat shock 70 kDa protein
HTS	High-throughput screening
IC₅₀	Halfmaximal inhibitory concentration
ICD	Intracellular domain
IPTG	Isopropyl β -D-1-thiogalactopyranoside
IR	Insulin receptor
ITC	Isothermal titration calorimetry
JFC1	synaptotagmin-like protein 1
Kan	Kanamycin
LARG	Leukemia-associated Rho guanine nucleotide exchange factor
LB	Lysogeny broth
LCMS	Liquid chromatography-mass spectrometry
LED	Light-emitting diode
MBP	Maltose-binding protein
MCF-7	Michigan Cancer Foundation-7
MDCK	Multicystic dysplastic kidney - Wikipedia
MS	Mass spectrometry
MST	Microscale thermophoresis
MTS	Medium-throughput screening
MTX	Mitoxantrone
MWCO	Molecular weight cut off
NBS	Non-binding surface
Ni-NTA	Nickel- Nitrilotriacetic acid
NMR	Nuclear magnetic resonance
NSF	N-ethyl-maleimide-sensitive fusion protein
OCRL1	Inositol polyphosphate 5-phosphatase 1
OD	Optical density
OSCC	Oral squamous cell carcinoma

PAA	Polyacrylamide
PAGE	Polyacrylamide gelelectrophoresis
PH	Pleckstrin homology
P-loop	Phosphate-binding loop
PR	Proline-rich region
Pra1	Prenylated Rab acceptor protein 1
PRKD1	Serine/threonine-protein kinase D1
RA	Ras-association domain
Rab	Ras-related brain protein
Rabex-5	Rab5 GDP/GTP exchange factor
RabGEF1	Rab5 GDP/GTP exchange factor
Rac	Ras-related C3 botulinum toxin substrate
Raf	RAF proto-oncogene serine/threonine-protein kinase
Ral	Ras-related protein Ral
Ran	Ras-related nuclear protein
Rap	Ras-related protein
Ras	Rat sarcoma protein
Rho	Ras homology
Rin1-3	Ras-interaction/interference protein 1
RME-6	Receptor-mediated endocytosis protein 6
RNA	Ribonucleic acid
RNAi	RNA interference
RT	Room temperature
RTK	Receptor tyrosine kinase
SAR	Structure activity relationship
SDS	Sodium dodecyl sulfate
Sec7	Protein transport protein Sec7
SELEX	Systematic evolution of ligands by exponential enrichment
<i>Sf</i>	<i>Spodoptera frugiperda</i>
SH	Src homology
SNARE	soluble NSF attachment protein receptor
Sos	Son of sevenless
Src	Proto-oncogene tyrosine-protein kinase Src
STAM	signal-transducing adaptor molecule
SUMO	Small Ubiquitin-like Modifier
TBC	Tre2/Bub2/Cdc16
TBS-T	Tris-buffered saline with Tween20
TEMED	Tetramethylethylenediamine
TEV	Tobacco etch virus
TGFα	Transforming growth factor alpha
THF	Tetrahydrofuran
Tiam1	T-lymphoma invasion and metastasis-inducing protein 1
TLC	thin-layer chromatography
Tre2	Proto-oncogene Tre2
Trio	Triple functional domain protein
Tris	<i>Tris</i> (hydroxymethyl)-aminomethane
tRNA	transfer RNA

Varp	Ankyrin repeat domain-containing protein
Vav1	Proto-oncogene Vav 1
Vps9	Vacuolar sorting protein 9
Vps9p	Vps9p guanine nucleotide exchange factor
Wt	wild type

List of figures

Figure 1: Activation and inactivation of small GTPases	20
Figure 2: Overview over the 3D structure of H-Ras in complex with the non-cleavable GTP analogue GppNHp	21
Figure 3: Rab GTPases in the endocytic pathway	24
Figure 4: Domain structure of Rin1	27
Figure 5: Expression and purification of Rab5a	40
Figure 6: Purification of Rin1C	41
Figure 7: Purification of Rin1-TS	42
Figure 8: Expression and purification of Rabex-5 _{GEF}	43
Figure 9: Expression and purification of Rab1	44
Figure 10: Expression and purification of DrrA	45
Figure 11: Expression and purification of Rac2	46
Figure 12: Expression and purification of Tiam1DHPH	47
Figure 13: Expression and purification of Rac1	48
Figure 14: Expression and purification of Vav1	49
Figure 15: The structure of Bodipy-TR-GTP	50
Figure 16: GEF-concentration-dependent activation of GTPases	51
Figure 17: The Rin1C-mediated Bodipy-TR-GTP nucleotide exchange on Rab5a	52
Figure 18: Adjustment of the Bodipy-TR-GTP assay for a HTS approach	53
Figure 19: Determination of the Z' factor for the Bodipy-TR-GTP screening assay	55
Figure 20: Manual re-screening of the 239 primary hit compounds	56
Figure 21: Activity profiles of the secondary hits	58
Figure 22: Structures of the 10 secondary hits	59
Figure 23: Specificity of the 10 secondary hits in the ARNO-Sec7/Arf1 nucleotide exchange assay	60
Figure 24: CG3 05 A02, CG5 08 H06, CG6 24 G06 and CG6 25 G08 in the Vav1/Rac1 nucleotide exchange assay	61
Figure 25: CG3 05 A02 and CG6 25 G08 in the DrrA/Rab1 nucleotide exchange assay	62
Figure 26: CG3 05 A02 and CG6 25 G08 in the Tiam1/Rac2 nucleotide exchange assay	62
Figure 27: CG3 05 A02 and CG6 25 G08 in the Rabex-5 _{GEF} /Rab5a nucleotide exchange assay	63
Figure 28: Aggregation properties of the compounds CG3 05 A02, CG5 08 H06, CG6 24 G06 and CG6 25 G08	64
Figure 29: IR-ICD auto-phosphorylation assay in presence and absence of CG3 05 A02	65
Figure 30: HPLC-MS analysis of the compound CG3 05 A02	66
Figure 31: The ABL1-mediated Rin1 phosphorylation assay in presence and absence of CG3 05 A02	71
Figure 32: Influence of CG3 05 A02 on Bodipy-TR-GTP binding to Rab5a	72
Figure 33: CG3 05 A02 in the Rin1C/Rab5a Bodipy-FL-GTP nucleotide exchange assay	73
Figure 34: CG3 05 A02 in the Rin1C/Rab5a Bodipy-FL-GDP release assay	74
Figure 35: CG3 05 A02 in the [α - ³² P]-GTP exchange assay	75
Figure 36: Core structure of CG3 05 A02	82
Figure 37: Synthesis of Aniline Precursors	110
Figure 38: Synthesis of CG3 05 A02 Analogues	113
Figure 39: Synthesis of the control compounds	120
Supporting figure 1: Plasmid map of pDL2	125

Supporting figure 2: Plasmid map of pET19mod	125
Supporting figure 3: Plasmid map of pET15b	126
Supporting figure 4: Plasmid map of pET52b(+)	126
Supporting figure 5: Plasmid map of pET SUMO	127
Supporting figure 6: Plasmid map of pFBHT	127
Supporting figure 7: Plasmid map of pAB1	128
Supporting figure 8: Plasmid map of pGEX-2T	128
Supporting figure 9: Plasmid map of pIBA101HT	129
Supporting figure 10: Plasmid map of pMAL-C2	129
Supporting figure 11: Expression of Rab5a	132
Supporting figure 12: Purification of Rab5a	133
Supporting figure 13: Ni-NTA affinity chromatography of Rin1C	133
Supporting figure 14: First part of the Rin1C size exclusion chromatography	134
Supporting figure 15: Second part of the Rin1C size exclusion chromatography	134
Supporting figure 16: Purification of Rin1-TS	135
Supporting figure 17: Expression of Rabex-5 _{GEF} and Rab5c	135
Supporting figure 18: Purification of Rabex-5 _{GEF}	136
Supporting figure 19: Expression of Rab1, DrrA, Vav1 and Tiam1DHPH	136
Supporting figure 20: First part of the Rab1 purification	137
Supporting figure 21: Second part of the Rab1 purification	137
Supporting figure 22: Purification of DrrA	138
Supporting figure 23: Expression of Rac1 and Rac2	138
Supporting figure 24: Purification of Rac2	139
Supporting figure 25: Purification of Tiam1DHPH	139
Supporting Figure 26: Final sample of Tiam1DHPH	140
Supporting figure 27: Purification of Rac1	140
Supporting figure 28: Purification of Vav1	141
Supporting figure 29: Aggregation assay with the compounds CG3 05 A02 and CG6 25 G08	141
Supporting figure 30: Aggregation assay with the compounds CG55 08 H06, CG6 24 G06 and CG6 25 G08	142
Supporting figure 31: Coomassie gel of the insulin receptor auto-phosphorylation assay	142
Supporting figure 32: Western blot of the insulin receptor auto-phosphorylation assay	143
Supporting figure 33: Coomassie gel of the ABL1-mediated Rin1 phosphorylation assay	143
Supporting figure 34: Western blot of the ABL1-mediated Rin1 phosphorylation assay	144
Supporting figure 35: Structures of the 26 secondary hits	145
Supporting figure 36: Raw data of the IC ₅₀ measurements	147
Supporting figure 37: Raw data of the SAR studies	148
Supporting figure 38: IC ₅₀ calculations for the active SAR compounds	150
Supporting figure 39: Raw data of the IC ₅₀ measurement for CG3 05 A02 in the Bodipy-FL-GTP nucleotide exchange assay	151
Supporting figure 40: Raw data of the IC ₅₀ measurement for CG3 05 A02 in the Bodipy-FL-GDP release assay	151
Supporting figure 41: Raw data showing the loading of Rab5a with Bodipy-TR-GTP	152

Supporting figure 42: IC ₅₀ calculation of the compound CG3 05 A02 in the Rabex-5 _{GEF} /Rab5a Bodipy-TR-GTP nucleotide exchange assay	153
Supporting figure 43: MST binding studies for CG3 05 A02 on Rin1C and Rab5a	154
Supporting figure 44: MST binding studies for CG3 05 A02 on the complex between Rin1C and Rab5a	155
Supporting figure 45: Expression and purification of GAPDV1	156
Supporting figure 46: Activity testing of GAPVD1	157

List of tables

Table 1: Vps9 domain-containing Rab5 GEFs	26
Table 2: Inhibitors of Ras superfamily GTPases	33
Table 3: Inhibitors of GEF proteins	36
Table 4: Determination of the solubility of CG3 05 A02	67
Table 5: Structure activity relationship of the compound CG3 05 A02	67
Table 6: Equipment	90
Table 7: Chemicals	91
Table 8: Consumables	92
Table 9: Compounds	93
Table 10: Nucleic acids	93
Table 11: Enzymes & Proteins	93
Table 12: Antibodies	94
Table 13: Bacterial strains	94
Table 14: Software	94
Table 15: Composition of SDS-PAA-gels	95
Table 16: Lysis buffers	99
Table 17: Washing buffers for His-tagged proteins	100
Table 18: Elution buffers for His-tagged proteins	101
Table 19: Washing buffers for GSH-fusion proteins	101
Table 20: Elution buffers for GSH-fusion proteins	102
Table 21: Dialysis buffers for TEV digestions	103
Table 22: Dialysis buffers for Thrombin digestions	104
Table 23: Storage buffers for size exclusion chromatography	104
Table 24: GEF concentrations for Bodipy-GTP nucleotide exchange assay	106
Table 25: Determination of the solubility of 068A	152
Table 26: Determination of the solubility of 137B	152
Table 27: Buffers for Alexa-647 (NHS-ester) labelling	154

Zusammenfassung

Rab5 ist eine kleine GTPase, die maßgeblich an der Regulierung des Membrantransportes zu- und -an frühen Endosomen beteiligt ist. GTPasen sind molekulare Schalter, die durch Guaninnukleotid Austauschfaktoren (GEFs) aktiviert und durch die Hydrolyse von GTP mit Hilfe katalytischer GTPase aktivierender Proteinen (GAPs) inaktiviert werden. GEFs vermitteln den Austausch von GTPase-gebundenem GDP gegen freies GTP. Einer von mindestens neun bisher beschriebenen Rab5 GEFs ist Rin1. Die genauen Unterschiede in Funktion und Wirkungsweise der verschiedenen Rab5 GEFs sind derzeit noch nicht im Gesamten entschlüsselt. Rin1 ist ein Multidomänenprotein mit verschiedenen Funktionen in der intrazellulären Signaltransduktion. Neben der Aktivierung von Rab5 spielt Rin1 ebenfalls eine Rolle in ABL Kinasen Signalwegen. Hier verstärkt es die Aktivierung der ABL Kinasen.

Rab5 Überaktivierung wurde mit verschiedenen Krebsarten in Zusammenhang gebracht. In den meisten Fällen kann diese Überaktivierung auf Rin1 Überexpression zurückgeführt werden. Rin1 verfügt jedoch auch über eine krebsunterdrückende Funktion, die im Zusammenhang mit seiner Interaktion mit ABL Kinasen steht.

Diese Arbeit zielt auf die Identifikation eines niedermolekularen Inhibitors der Rin1-vermittelten Rab5 Aktivierung ab. Der Inhibitor könnte helfen, die komplexen Signalkaskaden, an denen Rab5 beteiligt ist, aufzuschlüsseln. Idealerweise wäre er spezifisch für Rin1 gegenüber anderen GEFs. Außerdem sollte er die Interaktion zwischen Rin1 und den ABL Kinasen nicht beeinflussen.

Hierfür wurde ein *in vitro* Hochdurchsatzscreening mit über 20 000 potentiellen niedermolekularen Inhibitoren durchgeführt. Das Screeningexperiment überwachte den Rin1-vermittelten Austausch von GDP gegen das Fluoreszenzmarkierte GTP Analogon Bodipy-TR-GTP an Rab5. So wurde unter Anderem der niedermolekulare Inhibitor CG3 05 A02 identifiziert. Während Spezifitäts- und Aggregationsstudien stellte sich dieser als der vielversprechendste Kandidat heraus.

Seine Charakterisierung ergab Spezifität für Rin1 und Rabex-5 an der GTPase Rab5a im Bodipy-TR-GTP Nukleotidaustauschexperiment. Verschiedene andere GEF/GTPase Paare wurden nicht beeinflusst, obwohl deren Austauschmechanismus dem von Rin1 und Rabex-5 an Rab5 ähnelt. Die IC_{50} Werte, die in den Austauschexperimenten mit Rin1 und Rabex-5 ermittelt wurden, liegen beide im niedrigen micromolaren Bereich. Beide GEFs verfügen über eine homologe katalytische Vps9 Domäne. Es kann derzeit nicht ausgeschlossen werden, dass CG3 05 A02 auch weitere Vps9 Domänen GEFs inhibiert. Der Inhibitor führte keine Aggregation von Rin1 oder Rab5 herbei und hatte auch keinen unspezifischen Effekt in einem unverwandten Insulinrezeptor Autophosphorylierungsexperiment. Außerdem beeinflusste er die Interaktion zwischen Rin1 und ABL1 nicht, was gegen eine intramolekulare, domänenunspezifische Inhibition sprach.

Bedauerlicherweise zeigte ein weiteres Kontrollexperiment keine Inhibition des Rin1-vermittelten Nukleotidaustausches, wenn radioaktiv markiertes GTP verwendet wurde. Dieses Ergebnis sprach für eine Bodipy-TR-GTP-Abhängigkeit der Inhibition. Diese stammt wahrscheinlich nicht von einer Interaktion zwischen dem Inhibitor und dem GTP Analog her, denn in diesem Fall wäre die Inhibition in allen Bodipy-TR-GTP Nukleotidaustauschexperimenten aufgetreten, auch wenn andere GEFs und GTPasen getestet wurden. Aufgrund dieser Markierungsabhängigkeit ist der Inhibitor für die zelluläre und die *in vivo* Anwendung ungeeignet.

An welches Protein CG3 05 A02 bindet konnte nicht final aufgeklärt werden. Das Beladen von Rab5a mit Bodipy-TR-GTP in Abwesenheit eines GEFs wurde von CG3 05 A02 nicht

beeinflusst, was gegen einen GTP-kompetitiven Mechanismus der Inhibition spricht. Der Inhibitor bindet entweder an die Vps9 Domänen von Rin1 und Rabex-5, in der Nähe von diesen, oder an den Komplex zwischen den GEFs und Rab5. Aufgrund der Datenlage wurde ein auf sterischer Hinderung basierender Inhibitionsmechanismus vermutet, bei dem der Bodipy-TR-Rest und der an den Proteinkomplex gebundene Inhibitor sich behindern, sodass das Nukleotid nicht in die Bindungstasche gelangen kann. Das deutlich kleinere, radioaktiv markierte GTP ist von dieser Hinderung nicht betroffen.

Kristallisation der Proteine im Komplex mit CG3 05 A02 könnte zur Identifizierung einer Bindestelle führen, die als Ausgangspunkt für zukünftige *in silico* Screenings dienen könnte. Aus einem derartigen Screening könnte dann eine zweite Generation von Inhibitoren der Rin1-vermittelten Rab5 Aktivierung hervorgehen.

Abstract

The small GTPase Rab5 is a key regulator of early endosomal trafficking. It functions as a molecular switch that can be activated by guanine nucleotide exchange factors (GEFs) and inactivated via hydrolysis of GTP with the help of catalytic GTPase activating proteins (GAPs). GEFs mediate the exchange of GTPase-bound GDP for GTP. One of at least nine Rab5 GEFs, that have been identified until today, is Rin1. However, the differences in the exact roles of these GEFs are not completely understood. Rin1 is a multi-domain protein that has multiple signalling functions alongside the Rab5 activation. It is for example also involved in ABL kinase signalling, where it increases ABL activation. Rab5 over-activation has been reported to be involved in the genesis and progression of many different types of cancer and it could often be traced back to Rin1 over-expression. On the other hand Rin1 has been found to have a tumour repressive effect, mediated by its ABL kinase signalling function.

This study aimed on the identification of a small molecule inhibitor of the Rin1-mediated Rab5 activation. Such a small molecule inhibitor could be used as a tool to unravel parts of the complex signalling networks around Rab5. Ideally the inhibitor should be specific for Rin1 over other GEFs and moreover not influence its ABL kinase signalling function.

A high-throughput *in vitro* screening of more than 20 000 small molecules has been performed. The screening assay monitored the Rin1-catalyzed nucleotide exchange on Rab5a by the use of the fluorescently labelled GTP analogue Bodipy-TR-GTP. Amongst other primary hits the compound CG3 05 A02 was identified. During specificity and aggregation studies it turned out to be the most promising candidate.

Characterization of CG3 05 A02 revealed that its inhibitory effect in the Bodipy-TR-GTP nucleotide exchange assay is specific for Rin1 and Rabex-5 on Rab5a over several other GEF/GTPase pairs. The IC_{50} values were in both cases found to be in the low micromolar range. Rin1 and Rabex-5 share the homologous catalytic Vps9 domain and the compound might also be able to inhibit other Vps9 domain-containing GEFs. The compound did not induce aggregation of Rin1 or Rab5a and had no unspecific off-target effects in an unrelated insulin receptor auto-phosphorylation assay. It moreover did not influence the interaction between Rin1 and ABL1, indicating no intramolecular domain-unspecific inhibition. Unfortunately a control experiment with radioactively labelled GTP showed no inhibitory effect of the compound. The inhibition therefore depends on the use of Bodipy-TR-GTP but unlikely originates from CG3 05 A02 binding to the GTP analogue. In this case it would have inhibited the Bodipy-TR-GTP nucleotide exchange assay when GEFs/GTPases other than Rin1/Rabex-5 and Rab5 were used. This label-dependence classifies the compound unsuitable for cellular or *in vivo* application.

The actual target of CG3 05 A02 could not be finally addressed but Bodipy-TR-GTP binding to Rab5a in absence of a GEF was not influenced by the compound. This argues against GTP-competitive binding as the mechanism of inhibition. The compound potentially targets either directly the Vps9 domains of Rin1 and Rabex-5, areas adjacent to these, or the complex between the GEFs and Rab5. A mechanism based on steric hindrance involving the compound and the Bodipy-TR moiety of the GTP analogue was proposed as the mode of action.

Identification of a binding site for CG3 05 A02 in ongoing crystallization approaches could provide a starting point for *in silico* screenings that can result in a second generation of inhibitors of the Rin1-mediated Rab5 activation.

1 Introduction

1.1 Inter- and intracellular signalling: communication in living organisms

All organisms on this planet are built from cells. There are unicellular organisms including archaea and most bacteria as well as multi-cellular organisms like plants, fungi and animals. Organisms are facing constant changes in their environmental conditions that they have to adapt to in order to survive. Survival depends on the ability to detect and react to changes in the extracellular space. Cells are separated from this extracellular environment by a plasma membrane that consists of a lipid bilayer¹. The plasma membrane is equipped with a multitude of different proteins that can act as receptors for stimuli like ligand binding, changes in temperature or osmolarity, mechanical forces and light²⁻⁵. Moreover there are proteins capable of performing transport of molecules over the membrane⁶. After detection of a stimulus, the cell transmits the signal in a series of molecular events leading to the coordination of a response. These signalling pathways or -cascades are tightly regulated as they are the basic mechanisms controlling cell proliferation, growth and metabolism. An imbalance in signalling, often caused by a mutation, can lead to pathological conditions including unregulated proliferation or cell growth like it is the case in cancer^{7,8}.

Eukaryotic cells are subdivided into different compartments executing special functions. They generate energy from nutrients, degrade substances, process genetic information and coordinate cargo transport. This cargo transport also takes place extensively between the compartments to secure provision with- and exchange of -molecules like proteins, ions, nutrients and nucleic acids. The cargo transport is mostly conducted in membrane enclosed particles called vesicles. Upon vesicle budding and fusion, the compartments also exchange parts of their membranes and the incorporated proteins⁹.

Membrane-bound receptors often get internalized in vesicles after activation. This internalization either terminates their signalling, transmits the signal to another cellular compartment or changes the signal quality^{10,11}. Signals can be amplified during the transduction process since the binding of one ligand molecule can generate a response involving multiple molecules.

Small GTPases are a protein family involved in modulation of signalling pathways and integration of signals. They are also known to regulate vesicle transport. GTPases usually get activated by interaction with guanine nucleotide exchange factors (GEFs) that exchange GTPase-bound guanosine diphosphate (GDP) for guanosine triphosphate (GTP). Inactivation occurs via GTP hydrolysis with the help of GTPase activating proteins (GAPs)¹². Defective regulation of small GTPases can lead to pathological conditions^{13,14}, therefore those proteins can be interesting targets for therapeutics¹⁵. Small molecule inhibitors and activators are widely used as therapeutics in general. Those modulators can often also be used as tools to study signalling pathways in greater detail. Some small molecule modulators of GTPases, GEFs and GAPs are already known. However, there are many interesting proteins that still remain to be targeted. This work aims at the identification of a small molecule inhibitor of the Ras interaction/interference protein 1 (Rin1) mediated Ras-related brain protein (Rab5) activation.

1.2 The role of small GTPases in cellular signalling

As previously mentioned in section 1.1 the activity of small GTPases depends on their nucleotide state¹⁶. In the inactive state GDP is bound. Upon activation a GEF exchanges GDP for GTP¹². The intrinsic GTPase activity of small GTPases is often low, therefore GAPs are recruited to trigger hydrolysis and transform the GTPase back to its inactive state¹⁷. For that activation mechanism small GTPases are often referred to as molecular switches¹⁸. Small GTPases in their active state can interact with multiple effector proteins to trigger cellular responses via various signalling cascades¹⁹ (figure 1).

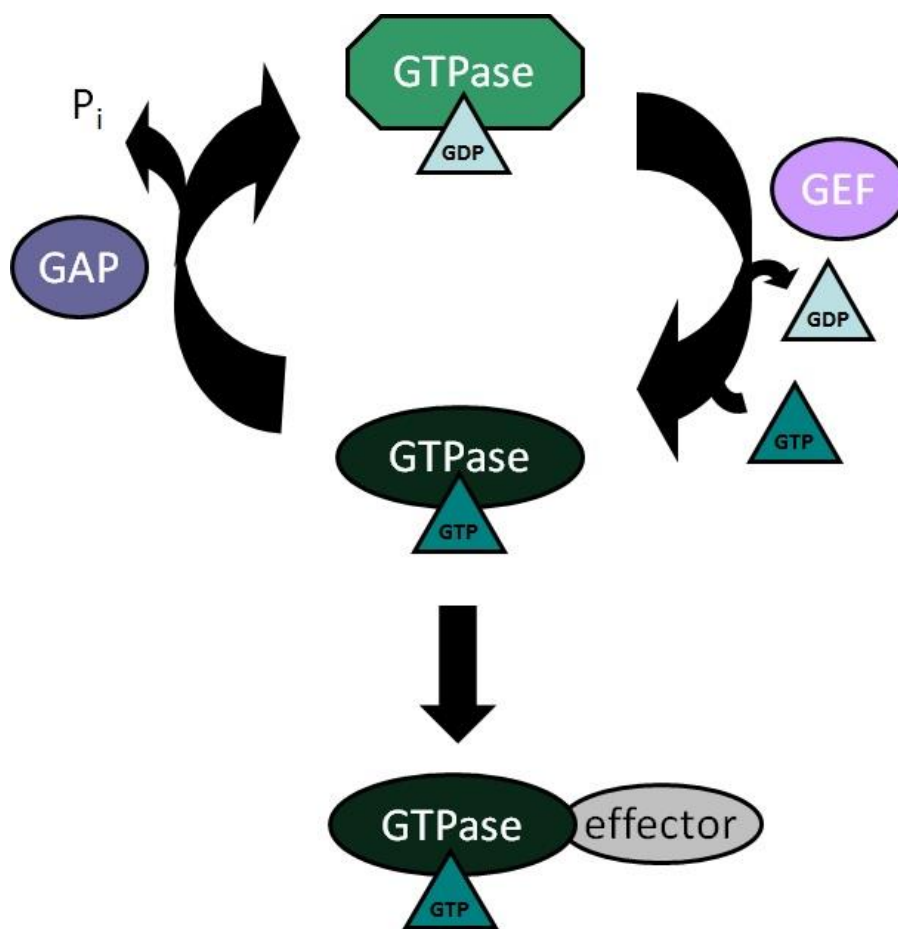


Figure 1: Activation and inactivation of small GTPases. The GTPase is inactive when GDP is bound and becomes activated upon GTP binding. The two nucleotide states are tightly regulated by GEFs and GAPs. GEFs exchange bound GDP for GTP while GAPs stimulate GTP hydrolysis. Active GTPases can bind multiple effector proteins to trigger cellular responses.

Rat sarcoma (Ras) was the first small GTPase to be discovered in 1979²⁰, giving its name to the Ras superfamily of small GTPases that by now covers over 150 members²¹. The superfamily is subdivided into five families: the Ras, ADP ribosylation factor (Arf), Ras homolog (Rho), Ras-related nuclear protein (Ran) and Rab family. Ras GTPases are engaged in cytoplasmic signalling cascades leading to changes in the expression of genes in relation with cell differentiation, proliferation and survival²². Arf and Rab GTPases are involved in

protein trafficking, vesicular transport and regulation of endocytosis^{23,24}. Modulation of the actin cytoskeleton and regulation of transcription factor activity is guided by Rho GTPases²⁵. The Ran family comprises only one member. Ran controls nuclear pore transport and organization of the mitotic spindle²⁶.

1.3 Activation of small GTPases

GTPases mostly become activated in close proximity to membranes²⁷⁻³⁰. A magnesium-ion is required as co-factor to stabilize nucleotide binding inside the binding pocket. GEFs destabilize magnesium and nucleotide binding. The exchange is therefore not directed towards GDP for GTP but the about ten times higher abundance of GTP in the cell favours GTP binding over GDP re-binding³¹. Figure 2 shows an overview of the three-dimensional structure of H-Ras in complex with the non-hydrolyzable GTP analogue GppNHp³². The structure of Ras superfamily GTPases is highly conserved. They all contain the switch regions I and II as well as a phosphate binding loop (P-loop) that are involved in magnesium-ion and nucleotide binding^{18,32}.

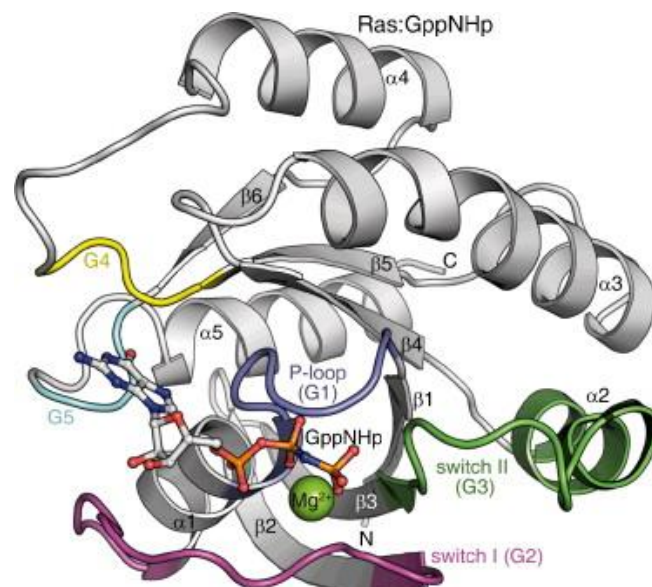


Figure 2: Overview over the 3D structure of H-Ras in complex with the non-cleavable GTP analogue GppNHp. Rab, Arf and Rho GTPases have the same basic secondary structure elements and G1-G5 regions. [...] Reprinted from Itzen and Goody, 2011³² with permission from Elsevier (4017670396307). The switch regions I (purple) and II (green) as well as the P-loop (blue) are involved in magnesium-ion (green ball) and nucleotide (ball and stick representation) binding.

The conformation of GTPases often differs depending on their nucleotide state (GDP-bound, GTP-bound or nucleotide free)^{33,34}. Effector proteins can bind to active GTPases leading to downstream signal transmission. The switch I, switch II and interswitch regions change most and often expose a hydrophobic patch upon GTP binding, accordingly many effectors are found to bind to those regions³². However, there are additional areas for effector binding in Rab GTPases. Some Rab effectors can recognize a combination of nucleotide-dependent and -independent areas^{35,36}. Since the different GTPases are highly similar, the complexity and versatility of GTPase-involving signalling pathways originates largely from the diversity of GTPase effectors and alterations in GTPase localization, making GTPases important modulators of many cellular processes.

1.4 The Rab family of small GTPases

The Rab family of small GTPases is the largest family within the Ras superfamily. It is encoded by more than 60 genes in the human genome^{34,35}. The family can be subdivided into several subfamilies: Rab1, Rab3, Rab4, Rab5, Rab6, Rab8, Rab11, Rab 14, Rab22, Rab27, Rab39 and Rab40. However, not all of the identified Rab proteins can be grouped into any of those subfamilies^{37,38}. The structure of Rab GTPases consists of a six-stranded β -sheet surrounded by five α -helices. This represents the common composition amongst GTPases of the Ras superfamily (cp. figure 2)³⁴. The C-terminus, involved in subcellular targeting, differs most between the Rab GTPases, whereas the nucleotide-binding switch regions I and II and the P-loop are highly conserved³⁹. Alternative splicing variants are also known⁴⁰. Some Rabs are expressed ubiquitously in human tissue but many are tissue specific. They are localized on the cytosolic face of cellular membranes. The distinct localization depends partly on post-translational modifications, mostly prenylations, on a cysteine motif in the C-terminus^{41,42}. Based on those prenylations Rab GTPases can cycle between membrane-bound and cytosolic states, depending on their activation state. GTPases can undergo several activation cycles before being released from the membrane³⁶. Rab membrane-binding is additionally regulated by interaction with GDP dissociation inhibitors (GDIs) and GDI displacement factors (GDFs). The GDIs prevent GTPases from interacting with the membrane by masking the prenyl modifications²². Rab GDIs stabilize the GDP-bound state and shuttle the GTPase back to its compartment of origin^{36,43}. A GDF for endosomal Rab GTPases (Rab5, Rab7 and Rab9) can release the GDI^{44,45}. However, the importance of GDIs and GDFs for the specific organelle-membrane localization has been challenged, suggesting GEFs and effector proteins to be crucially involved in this process instead^{46,47}. Possibly the specific localization is controlled by diverse mechanisms²⁸.

1.4.1 Rab GTPases as key regulators of vesicular transport

Rab GTPases control vesicular transport along cellular compartments including endosomes, lysosomes, endoplasmic reticulum (ER) and golgi apparatus⁴⁸. They regulate different stages of transport: vesicle formation, vesicle and organelle motility and vesicle docking⁴⁹.

The specific roles of Rab GTPases in vesicle formation are as yet emerging. Rabs seem to play a crucial role in endosomal cargo sorting mediated by retromer and sorting nexins⁵⁰⁻⁵². Also the cargo recruitment is mediated by direct or indirect interaction with Rab GTPases^{53,54}. It is speculated that Rab-mediated cargo selection and vesicle formation could involve specific lipids being recruited to the affected membrane areas⁵⁵.

Vesicle and organelle motility depends on microtubules. Rabs and their effector proteins regulate intracellular motility via recruitment of kinesin and dynein-dynactin motors to control cytoskeletal translocation⁵⁶⁻⁶². The endocytic compartments including endosomes, lysosomes and phagosomes can also move in an actin/myosin-dependent manner over shorter distances. Here Rab GTPases can recruit myosin to the organelle membranes to regulate motility^{63,64}.

Vesicle docking and fusion has to be highly specific in order to preserve organelle identity and to ensure the desired cargo distribution inside the cell²³. The regulatory mechanisms require Rabs to bind effector proteins that can then interact with proteins of the SNARE (soluble NSF attachment protein receptor, NSF stands for N-ethyl-maleimide-sensitive fusion protein) machinery. Cognate SNAREs interact with each other between two lipid bilayers and ensure precise tethering and membrane fusion^{65,66}. Certain SNAREs are enriched in the

different cellular compartments to limit unspecific fusion events. Parts of the membranes and the incorporated proteins, including SNAREs, inevitably spread through many organelles during vesicular trafficking. Therefore regulatory mechanisms, like those involving Rab effectors, are needed to allow fusion only at the appropriate time and place⁶⁵. Rab effectors are, unlike Rabs and SNAREs, not structurally conserved. The structural heterogeneity of Rab effectors implies that they are highly specialized for their functions. However, there are common motifs among Rab effectors like zinc-fingers and coiled-coil regions²³. Rab effectors can also be shared between different Rabs to functionally couple them in a signalling cascade^{24,67}.

1.4.2 The role of Rab GTPases in endocytosis

Lysosomes, phagosomes and endosomes are the cellular compartments of the endocytic pathway. Endosomes can be grouped into early endosomes, late endosomes and recycling endosomes⁶⁸. They are involved in the vesicular internalization of extracellular molecules and membrane-bound proteins. This process is called endocytosis and leads inevitably to changes in the plasma membrane composition. It controls signalling pathways via receptor up- or downregulation⁶⁸⁻⁷⁰. The internalized molecules can become degraded, shuttled to other compartments or recycled back to the plasma membrane⁷⁰. There are several types of endocytosis driven by different vesicle types and diverse mechanisms⁷¹. The best-described mechanism is clathrin-mediated endocytosis (CME), where Rab GTPases play a major role⁷²⁻⁷⁴. However, there are many other clathrin-independent mechanisms including the CLIC/GEEC endocytic pathway, flotillin-dependent endocytosis, arf6-dependent endocytosis, circular dorsal ruffles, phagocytosis, trans-endocytosis and macropinocytosis⁷¹. Many receptors and their ligands become, however, internalized via CME⁷⁵. Coupling proteins like the adaptor protein 2 (AP2) regulate cargo assembly and packing into clathrin-coated vesicles (CCVs)^{76,77}. Cargo and adaptor proteins are diverse, reflecting a complexity of the process that originates from adaptations to the various materials that are being packed. CCVs are budding from the plasma membrane as well as from various intracellular compartments⁷¹. In the beginning, clathrin nucleation is coordinated by adaptor and accessory proteins at the membrane sites that are destined to be internalized⁷⁷. This nucleation leads to clathrin polymerization into curved lattices⁷⁸. At this point membrane curvature occurs, affected by small GTPases of the Arf, Rab and Rho families⁷¹. The membrane scission protein dynamin then forms a helical polymer around the vesicles neck and detaches it from the membrane. Finally Auxilin and Hsc70 release the clathrin coat from the vesicle⁷⁹.

Rab GTPases can directly affect and recognize positive membrane curvature^{71,80}. The Rab GTPases are compartment-specific and enriched in rab microdomains⁸¹. They can therefore also be used as markers to identify the different organelles⁷¹. Other compartment-specific proteins are recruited by Rab GTPases that altogether define organelle identity^{67,81}. The compartment-specific Rab microdomains are visualized in figure 3. Rab GTPases all fulfil certain roles on their specific compartments, often additionally acting via effector proteins. Rab4 for example is essential for the recycling of receptors from the early endosome back to the plasma membrane⁴³. Rab GTPases regulate the endocytic pathway on various compartments by controlling vesicle formation as well as tethering and fusion (cp. section 1.4.1)

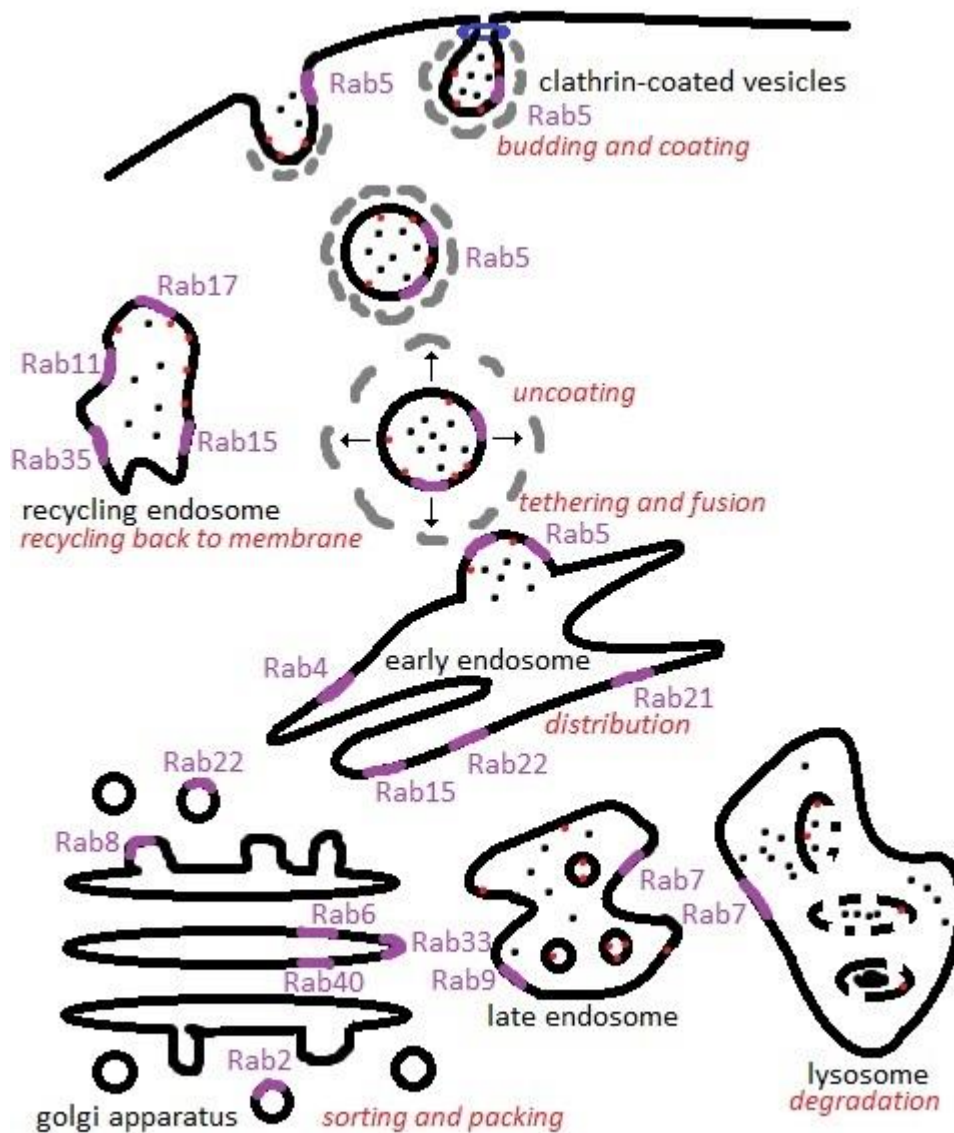


Figure 3: Rab GTPases in the endocytic pathway. Endocytosis describes the vesicular uptake of extracellular molecules and membrane-bound proteins. In clathrin-mediated endocytosis (CME), clathrin coated vesicles (CCVs, depicted with grey clathrin coat) are formed in membrane proximity. The vesicles get released from the membrane with help of the scission protein dynamin depicted in blue. Clathrin un-coating takes place in the cytoplasm followed by Rab- and SNARE-mediated tethering (as described in section 1.4.1) and fusion with early endosomes. From there, the cargo is transported to the late endosomes, the golgi apparatus for further sorting, packing and distribution, the lysosomes for degradation or recycled back to the plasma membrane via the recycling endosomes. Rab GTPases are depicted as purple microdomains on the compartment membranes. Rab5 is localized on the plasma membrane and on vesicles as well as on early endosomes, where also Rab4, Rab15, Rab22 and Rab21 microdomains can be found. Rab4 mediates recycling, Rab 22 controls transport from and to the golgi apparatus and Rab15 is involved in trafficking to the recycling endosomes. On the recycling endosomes Rab11 and Rab35 regulate the recycling. Rab2, Rab6, Rab8, Rab33 and Rab40 are localized on the golgi apparatus and contribute to cargo sorting, packing and further distribution. Rab7 and Rab9 can be found on the membranes of late endosomes where they control the transport to the lysosomes and the golgi, respectively.

The figure is partially adapted from Stenmark, 2009⁴³ and inspired by figure 3 from Wosnitza, 2013⁸².

1.5 Rab5 – regulator of the early steps in CME

Rab5 is localized on the plasma membrane, on vesicles and on the membrane of early endosomes. Rab5 controls the formation of CCVs by affecting membrane curvature and recruiting adaptor proteins. Tethering and fusion of vesicles on the early endosomes is also mediated by Rab5 and its effectors.

The Rab5 subfamily consists of seven members: Rab5a, Rab5b, Rab5c, Rab17, Rab21, Rab22a and Rab22b⁸³. The Rab5 isoforms a-c are highly conserved in terms of sequence, function and localization. However, there are certain functions described only for particular isoforms. Rab5a can, for example, enhance endocytosis of the epidermal growth factor receptor (EGFR)⁸⁴ and Rab5b is involved in neuroprotection against *N*-methyl-*D*-aspartate⁸⁵. Rab21 and Rab22 are, like Rab5, localized on early endosomes but also control trafficking at the golgi apparatus. Rab17 can be found on recycling endosomes and has recently been discovered to play a role in autophagy⁸⁶.

1.5.1 Diversity in structure and function: Rab5 interaction partners

The many different Rab5 interaction partners are functionally and structurally diverse. Their functions include adaptors, GDIs, GDFs, GAPs and GEFs but the specific signalling functions of many Rab interaction partners are still to be explored^{23,32}. Effectors are by definition proteins, that only interact with active, GTP-bound GTPases, so not all of the interacting proteins can be addressed as such³². The proteins mentioned in this section are a small selection to exemplify the different types of Rab5 interaction partners and there are many more proteins known for most of these types.

The early endosomal autoantigen 1 (EEA1) is an adaptor protein, acting as a Rab5 effector on early endosomes. It is essential for endosome fusion and can bind to the endosomes via a C-terminal interaction domain⁸⁷. EEA1 co-localizes with Rab5 on early endosomes due to direct interaction between the two proteins. An N-terminal zinc finger on EEA1 specifically recognizes the switch I, switch II and interswitch regions of active Rab5⁸⁸. The interaction epitope on Rab5 is similar to the epitopes observed in complexes between Rab5 and the effectors Rabaptin-5 and Rabenosyn-5^{89,90}. Rabaptin-5 can also interact with the Rab5-GEF Rabex-5, bringing GEF and GTPase in close proximity. This leads to locally increased Rab5 activation⁹¹. Adaptor proteins like these can mediate the formation of Rab microdomains on the organelles of the endocytic pathway⁶⁷.

As already mentioned in section 1.4, Rab GTPases cycle between a membrane-bound and a cytosolic state. In the cytosolic state they are bound to guanine nucleotide dissociation inhibitors (GDIs)⁸⁰. There are two isoforms known in humans: GDI α , which is predominantly expressed in brain tissue and GDI β , which is expressed ubiquitously⁹². GDIs can specifically target membranes of subcellular compartments and deliver GDI-bound Rab5^{29,30,93}.

Pra1 is one of only two GDI displacement factors (GDFs) that have been discovered. It can dissociate endosomal Rab5 from the GDIs to allow nucleotide exchange^{44,45}.

Adaptors, GDIs and GDFs contribute to the regulation of Rab5 localization on the specific membranes⁸⁰. They modulate the Rab5 distribution inside the cell. Besides, there are also proteins that modulate the activity of Rab5. GTPase activating proteins (GAPs) trigger the GTP hydrolysis activity of GTPases.

The intrinsic GTPase activity of Rab5 may be higher compared to, for example Arf1⁹⁴⁻⁹⁶, but is in general not sufficient to ensure coordinated switching off of the signal transmitted by the active GTPase^{32,96}. Rab5 GAPs stimulate the GTPase activity via a conserved

Tre2/Bub2/Cdc16 (TBC) domain containing a catalytic arginine residue^{96–98}. There are around 50 TBC domain-containing proteins in humans but most of them have not been characterized yet³⁵. A well-described one is TBC-2 that acts as a Rab5 GAP in *C. elegans*⁹⁹.

1.5.2 Rab5 GEFs contain a catalytic Vps9 domain

GEFs are Rab5 interaction partners that exchange Rab5-bound GDP for free GTP, leading to Rab5 activation. Rab5 activation is among other things required to complete vesicle targeting and fusion¹⁰⁰. Accordingly expression of a dominant-negative Rab5 mutant (S34N) inhibits endocytic fusion events and expression of a constitutively active mutant (Q79L) enhances them⁹⁵. The intrinsic nucleotide dissociation of GDP from Rab5 is very slow¹⁰¹, therefore little nucleotide exchange can take place, even when excess GTP is present. To switch between the inactive GDP-bound and the active GTP-bound state, GEFs are unconditionally required¹⁰⁰. There are at least nine GEFs described for Rab5, but their precise role in the regulation of the diverse Rab5 functions is yet not completely understood¹⁰⁰. All of them contain a homologous catalytic Vps9 domain^{102–112}. A list of the known Rab5 GEFs is provided in table 1. The Vps9 domain-containing GEFs are multi-domain proteins that additionally possess other signalling domains. They might serve to link Rab5 activation with different signal transduction cascades¹⁰⁰ and are involved in controlling Rab5 localization^{46,47}.

Table 1: Vps9 domain-containing Rab5 GEFs.

Name	Abbreviation	Alternative names	Rabs
Amyotrophic lateral sclerosis 2 protein	Als2	Alsin	Rab5
Als2 C-terminal-like protein	Als2CL		Rab5
Rab5 GDP/GTP exchange factor	Rabex-5	RabGEF1, Rap1	Rab5, Rab21, Rab22
Rab5-activating protein 6	Rap6	GAPVD1, RME-6, GAPex-5	Rab5
Ras and Rab interactor 1	Rin1	Ras interaction/interference protein 1	Rab5
Ras and Rab interactor 2	Rin2	Ras interaction/interference protein 2	Rab5
Ras and Rab interactor 3	Rin3	Ras interaction/interference protein 3	Rab5, Rab31
Ras and Rab interactor-like protein	Rin-like		Rab5, Rab22
Ankyrin repeat domain-containing protein 27	Ankrd27	Varp	Rab5, Rab21, Rab32, Rab38,
Vps9p guanine nucleotide exchange factor	Vps9p		Rab5, Vps21p

1.6 Rin1: multiple domains, multiple functions

The Ras and Rab interactor 1 (Rin1) is a soluble multi-domain protein localized at the plasma membrane and in the cytosol¹¹³. A schematic overview over the domain structure of Rin1 is provided in figure 4. The N-terminal Src homology 2 (SH2) domain can interact with receptor tyrosine kinases (RTKs) and increase their internalization and degradation^{114–116}. Rin1 moreover contains a proline-rich region (PR) that acts as Abelson tyrosine-protein kinase (ABL) interaction site. Upon interaction with ABL, Rin1 becomes phosphorylated at Tyr36^{113,117}. The central Vps9 domain catalyses the exchange of GDP for GTP on Rab5¹¹⁸. This activation enables Rab5 to interact with its effectors and mediate the effects described in section 1.5.1. The C-terminal Ras interaction site (RA) can directly bind to active Ras (Ras-GTP), competing with the RAF proto-oncogene serine/threonine-protein kinase 1 (Raf1). In this context Rin1 can inhibit cellular transformation induced by activated mutant Ras species. Many other Ras effectors have been described to enhance cellular transformation instead¹¹³. Rin1 contains several phosphorylation sites. Two of them, the best-described ones, are Tyr36 and Ser351, which get phosphorylated by ABL and the serine/threonine-protein kinase D1 (PRKD1), respectively^{113,119}. Phosphorylation of Ser351 enables Rin1 to interact with 14-3-3 proteins¹²⁰. This interaction controls the correct localization of Rin1 as well as its ability to compete with Raf1 and is controlled by PRKD1¹¹³. The diversity of Rin1 functions, caused by its multi-domain structure, results in complex signalling capabilities¹¹⁷. An imbalance in the regulation of Rin1 functions can lead to severe diseases like chronic myelogenous leukaemia (CML)^{121,122} and other types of cancer^{123–126}.

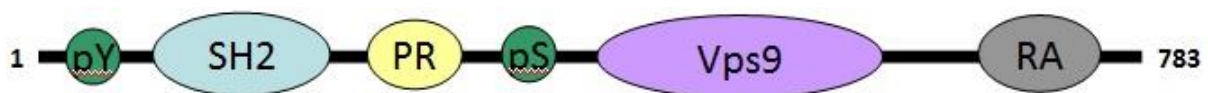


Figure 4: Domain structure of Rin1. Rin1 possesses an N-terminal Src homology 2 (SH2) domain that can bind receptor tyrosine kinases (RTKs) followed by a proline-rich region (PR) that represents the binding site for ABL. The central Vps9 domain catalyzes the nucleotide exchange on Rab5. Ras-interaction occurs via the C-terminus Ras association domain (RA). Rin1 contains several phosphorylation sites, the two labelled in this figure are the best-described ones: Tyr36 and Ser351, which get phosphorylated by ABL and the serine/threonine-protein kinase D1 (PRKD1), respectively. The phosphorylation of Ser351 induces interaction with 14-3-3 proteins.

1.6.1 The nucleotide exchange mechanism of Vps9 domain-containing GEFs

The Vps9 domain of Rin1 catalyzes the exchange of Rab5-bound GDP for free GTP. This exchange is not directed towards GTP, but the about ten times higher abundance of GTP inside the cell favours GTP binding instead of GDP re-binding^{31,127}. There is no structural data available for the Vps9 domain of Rin1 yet, but there is a crystal structure published for the homologous Rabex-5 Vps9 domain and helical bundle tandem in complex with nucleotide-free Rab21. The domain consists of six α -helices of which two form a hydrophobic groove that represents the binding site for Rab21¹²⁸. The P-loop, switch I, switch II and interswitch regions of Rab21 constitute the recognition site for the Vps9 domain^{32,128}. An aspartate residue from the hydrophobic groove of the Vps9 domain interacts with an invariant lysine in the P-loop of Rab21. This lysine originally contacts the β and γ phosphates of bound nucleotides and this contact gets disrupted by the interaction¹²⁸. Additionally, there is also

an aspartate in the interswitch region of Rab21 that directly interacts with the Mg^{2+} ion in absence of GEFs. Upon GEF binding, this aspartate loses contact with the ion and interacts with the conserved P-loop lysine instead, leading to further destabilization of the nucleotide binding³². The GEF/GTPase complex gets disrupted by allosteric competitive binding of excess GTP¹²⁹. This mechanism resembles the one described for Sec7 domain-containing GEFs on GTPases of the Arf family. The Sec7 domain contains a catalytic glutamate residue instead of the aspartate^{130,131}. It can be assumed, that the exchange mechanism of Rin1 on Rab5 is similar to the one described for Rabex-5 on Rab21, since both GEFs contain the homologous catalytic Vps9 domain.

1.6.2 Rin1 enhances EGFR internalization, degradation and down-regulation

The epidermal growth factor receptor (EGFR) is a receptor tyrosine kinase that can be found inside the plasma membrane and the membranes of endosomes, golgi apparatus, nucleus and endoplasmic reticulum (ER), anchored with a single transmembrane region^{114,132,133}. It consists of three major parts: an extracellular domain where ligand binding takes place, a transmembrane region and an intracellular kinase domain flanked by a juxtamembrane segment and a C-terminal tail^{134,135}. The intracellular domain contains several tyrosine residues that can become phosphorylated during receptor dimerization¹¹⁴. Upon ligand binding, the receptor usually dimerizes and one intracellular domain phosphorylates the other¹⁰². However, ligand-free dimers have also been described¹³⁶. Phosphotyrosines provide binding sites for adaptor proteins that can recruit Ras activators¹³⁷. There are at least seven EGFR ligands known: epidermal growth factor (EGF), transforming growth factor α (TGF α), heparin-binding EGF-like growth factor (HBEGF), betacellulin (BTC), amphiregulin (AREG), epiregulin (EREG) and epigen (EPGN). EGF, TGF α , HBEGF and BTC have a higher affinity to the EGFR than the other three ligands¹³⁸. Upon EGF binding the receptor becomes activated and gets internalized mainly via CME¹³⁹. As previously described in sections 1.4.2 and 1.5 active Rab5 is required for CME and Rin1 can activate Rab5 via its GEF function as explicated in section 1.6.1. Therefore, Rin1 can indirectly enhance EGFR internalization via Rab5 activation⁸⁴. Additionally Rin1 can directly interact with activated EGFR through its SH2 domain and with active H-Ras via its RA domain^{100,113-115,140,141}. Binding active H-Ras increases the GEF activity of Rin1¹⁰² and may also contribute to its membrane recruitment¹⁰⁰. Eventually, after endocytosis, the EGFR follows one of two possible paths: either it gets recycled back to the plasma membrane via the recycling endosomes¹⁴² or it is transported to the lysosomes for degradation¹⁴³. Rin1 has been found to interact with the signal-transducing adaptor molecule (STAM) leading to fortified RTK degradation¹¹⁶. EGFR down-regulation and degradation after EGF stimulation are promoted by the Rin1 mediated Rab5 activation¹¹⁴.

1.6.3 The role of Rin1 in ABL kinase signalling

Abelson tyrosine-protein kinases (ABL1 and ABL2) are non-receptor tyrosine kinases that regulate actin remodelling through direct binding to filamentous actin (F-actin) and phosphorylation of actin related proteins¹⁴⁴. The kinase activity of ABL is regulated on multiple levels. An N-terminal myristoylation supports an inactive kinase domain conformation¹⁴⁵. Additionally, the ABL SH2 and SH3 domains stabilize a low activity conformation of the kinase domain¹⁴⁶. Finally, there are tyrosine residues in the kinase domain that increase kinase activity upon (auto)phosphorylation^{147,148}. Rin1 can bind to the

ABL SH3 domain with its proline rich region (PR). This binding leads to phosphorylation of Rin1 at Tyr36, which thereby gets enabled to interact with the SH2 domain of ABL. The divalent interaction increases ABL kinase activation^{117,119} by releasing ABL SH2- and SH3-imposed auto-inhibition¹⁴⁹.

1.6.4 Two sides of the coin – Rin1 in cancer

On one hand, Rin1 up-regulation has been implicated in the development of different types of cancer including squamous cell carcinoma¹²³, colorectal cancer¹²⁴, melanoma¹⁵⁰ and non-small cell lung cancer¹²⁵. These studies suggest that Rin1 may play a role in enhancing cell proliferation. On the other hand a tumour suppressor function of Rin1 has been described in breast cancer, where it negatively regulates tumour invasive growth and inhibits the progression of tumourigenesis¹²⁶.

In oral squamous cell carcinoma (OSCC), an intra-chromosomal gene amplification of chromosome 11q13 encoding Rin1, amongst other proteins, has been found. This amplification may lead to a high Rin1 expression level¹²³.

52 of 101 colorectal cancer specimens have been found to over-express Rin1. Rin1 is, in those tumour cells, mainly bound to 14-3-3 proteins and localized in the cytoplasm. A lack of the ability to compete with Raf1 for binding of active Ras, due to a lack of plasma membrane localization, has been suggested. This may lead to enhanced Ras/Raf1 interaction compared to non-tumour cells, resulting in an increase of cell proliferation¹²⁴.

An over-expression of Rin1 could also be detected in melanoma samples and its accumulation could be associated with poor prognosis. Knock-down of Rin1 in A375 cells, a malignant melanoma cell line, suppresses cell proliferation and induces apoptosis¹⁵⁰.

Rin1 is expressed at high levels in many non-small cell lung adenocarcinoma cell lines including A549 cells. Depletion of Rin1 from A549 cells leads to a decrease in EGFR signalling and a correlating decrease in cell proliferation^{125,151}. This effect supposedly originates from the requirement of Rab5-GTP for effective EGFR signalling, which is provided by high levels of Rin1^{84,125}. As previously described in section 1.6.2, Rin1 can also directly interact with the EGFR through its SH2 domain and positively influence EGFR internalization¹¹⁵.

The RIN1-gene is silenced in several breast cancer cell lines, leading to reduced levels of Rin1 protein. Rin1 re-expression can inhibit the initiation and progression of tumourigenesis in a breast cancer mouse model. Moreover, tumour invasive growth has been shown to be negatively regulated by the ABL kinase signalling function of Rin1¹²⁶.

Rin1 also plays a role in chronic myelogenous leukaemia since it can activate the oncogenic BCR-ABL tyrosine kinase fusion protein. This activation strongly accelerates BCR-ABL induced leukaemia (CML) in mice^{121,122}. Alterations in the Rin1 expression level have not yet been reported in the context of CML.

Together these studies suggest that Rin1 can play controversial roles in cancer. At least in lung cancer, the oncogenic effects of Rin1 could be traced back to its Rab5-GEF function. The effects of Rin1 over-expression in OSCC and melanoma are not completely understood but may also arise from enhanced RTK signalling, promoted by an increase of Rab5 activation. The tumour suppressor function of Rin1 in breast cancer could be addressed to its ABL kinase signalling function. Conclusively Rin1 is a multi-domain protein with domain-specific effects in cancer development.

1.7 Small molecules as tools to modify single domains in multi-domain proteins

Since the discovery of penicillin by Alexander Fleming in 1929 at the latest, drug discovery became a huge field in pharmacology, medicine and chemistry¹⁵². Combinatory libraries of small molecules can be screened in high throughput approaches since the middle of the 20th century^{152,153}. Small molecules are not only suitable as therapeutics but also as tools to study signalling cascades by modification of the activity of one or more of the proteins involved¹⁵⁴. With small molecules it is moreover possible to target specific domains and thereby specific functions of multi-domain proteins without inevitably affecting their other functions or their expression level^{155,156}.

In contrast, knock-out or knock-down methods usually operate on the level of DNA or RNA instead and generally result in the loss of whole proteins and all their functions. Therefore the effects of small molecule inhibitors can, in some cases, be more accurate than methods like RNA interference (RNAi)¹⁵⁶. Knock-outs and knock-downs often have lethal effects on the organism, as described for a Rab5 knock-down in *C. elegans*¹⁵⁷, complicating *in vivo* research¹⁵⁴. Small molecules are normally easily synthesizable, relatively stable, often cell permeable and their effects are also reversible, since they usually can be metabolized^{154,156,158}. Multiple small molecules can be combined and applied in variable doses to allow a fine-tuning of the desired effects¹⁵⁸. Small molecule modifiers of specific protein functions are usually discovered in robot-assisted high throughput screening (HTS) approaches. For that, a suitable assay that meets certain criteria has to be developed. After identification of hit compounds in the HTS, the molecules can be characterized and optimized according to structure activity relationship studies. This often also helps to address the mechanism behind small molecule effects^{153,159}.

1.7.1 Ras superfamily GTPases as targets for small molecule inhibitors

Various members of the Ras superfamily of small GTPases have been reported to become over-activated during cancer development in many different types of cancer, as previously described for Rab5 in section 1.6.4. However, small GTPases are elusive drug targets due to their flat and flexible topology and their multiplicity of interaction partners^{21,160}. In principle, locking GTPases in any of the stages occurring during the canonical GTPase cycle (cp. figure 1) could lead to inhibition. This comprises anything from targeting the nucleotide binding pocket to stabilizing an inactive conformation (GDP-bound, GAP-bound or state I GTP-bound) and blocking GEF/effector binding sites either reversibly or covalently²¹. Finding a selective GDP- or GTP-competitive GTPase inhibitor is difficult. Due to the high affinity for GDP/GTP and conservation of the residues surrounding the nucleotide binding pocket, the risk of undesirable cross-inhibition throughout other GTPases is high. Such a nucleotide competitive pan-GTPase inhibitor has been described and appears to be long-term cytotoxic¹⁶¹.

The most effort has been directed towards inhibition of Ras, because mutant hyperactive Ras subfamily members are implicated in over 20 % of all cancers^{162–165}. The Rab subfamily is widely unexplored as target for small molecules with only a few novel binders discovered to date. To develop small molecules against other members of the Ras superfamily of GTPases, more data on structure and dynamics of Arf, Ran and Rho GTPases is required²¹.

Recent strides towards directly targeting Ras superfamily GTPases have refuted the 'undruggability' of these proteins and generated a strong interest in targeting them¹⁶⁵.

1.7.2 GEFs as targets for small molecule inhibitors

Hyper-activation of GTPases can not only be caused by mutations of the GTPases themselves, as it is the case for Ras in many tumours, but also by GTPase over-expression, loss of GAP-mediated inactivation and up-regulation of the corresponding GEFs¹⁶⁶. Therefore it is not surprising that over-expression of GEFs can be found in different cancers¹⁶⁷⁻¹⁷⁵, as already described also in section 1.6.4 for Rin1. One GTPase can be activated by a large variety of different GEFs¹⁰⁰. Therefore targeting a single GEF can more specifically influence a certain signalling cascade compared to targeting the GTPase itself. GEFs are not classically considered 'druggable' targets because they often lack grooves and pockets for small molecule interactions. They are covered with large contact surfaces for protein-protein interactions instead¹⁷⁶. Since GEFs are not as conserved in structure and catalytic domains as GTPases, the risk for off-target effects is lower and thus the chances to find a specific inhibitor are higher¹⁶⁶. GEF inhibition can be achieved by either targeting the catalytic GEF domain or by locking the GEF/GTPase complex in a way that prevents nucleotide exchange. As for Ras GTPases themselves, the strongest efforts have been directed towards finding inhibitors of Ras GEFs¹⁷⁷⁻¹⁸⁰. However, there are also several inhibitors described for GEFs activating other Ras superfamily GTPases¹⁸¹⁻¹⁸⁵.

Those examples illustrate that targeting GEFs, either directly at their catalytic domains or by targeting the GEF/GTPase complex, is possible and worth further trials in the future.

1.7.3 Overview: Inhibitors of Ras superfamily small GTPases and their GEFs

1.7.3.1 Inhibitors of Ras superfamily GTPases

Several inhibitors of small GTPases of the Ras superfamily have been described so far. Not all of them are small molecules, some peptide inhibitors have also been found. An overview over the inhibitors described below is given in table 2.

Inhibitors of Ras GTPases:

CID1067700 is a nucleotide-competitive pan-GTPase inhibitor discovered in a flow cytometry bead-based high-throughput screening (HTS). Inhibition could be shown for representative GTPases from the Ras, Rho and Rab subfamilies in biochemical, cellular protein-protein interaction and cellular functional assays¹⁶¹.

The small molecule Kobe0065 has been found in an *in silico* HTS approach and proved to prevent the interaction between H-Ras-GTP and c-Raf1 both, *in vitro* and *in vivo*¹⁸⁶.

SML-10-70-1 is a covalent GDP analogue created by rational design. It is selective for mutant K-Ras^{G12C} over wild-type (wt) Ras and it renders the protein in an inactive state. SML-10-70-1 is a 'caged' analogue of SML-8-73-1, which is thereby made cell permeable and showed anti-proliferative effects in A549, H23 and H358 cells¹⁸⁷.

An about 4-fold decrease in GTP affinity of K-Ras^{G12C} could be obtained with Acrylamide 12 (AA12) by allosteric binding. It abolishes activation of the mutant Ras by the GEF Son of sevenless (Sos) and promotes apoptosis of K-Ras^{G12C} expressing cell lines¹⁸⁸.

SCH-53239 targets GEF-Ras-GDP ternary complexes and could reduce cell growth. The definite mode of action remains elusive for this compound and its derivatives¹⁸⁹.

The hydrogen-bond surrogate 3 (HBS3) is a synthetic α -helix designed based on the wt Sos α H (929–944). It competes with Sos-binding. It could moreover reduce the Ras-GTP level and downstream Erk-activation in serum-starved, EGF stimulated HeLa cells¹⁹⁰.

Another synthetic α -helix designed based on the structure of Sos1 is SAH-SOS1, a stapled peptide inhibitor that interferes with wt Ras- and K-Ras-Sos1 interaction. It binds Ras-GDP and Ras-GTP with similar affinity and impairs viability of K-Ras dependent cell lines with an IC_{50} of 5 – 15 μ M¹⁹¹.

Andrographolide (AGP) is a natural product isolated from *Andrographis paniculata*. It was shown to interact with wt Ras and K-Ras and supposedly binds to a Ras-GEF interaction site. Intracellular levels of wt Ras-GTP as well as Erk-phosphorylation could be reduced by AGP in different cell lines with IC_{50} values between 4.5 and 9.7 μ M¹⁹².

The Sos-catalyzed nucleotide exchange and release on K-Ras could be impaired by DCAI *in vitro*. It binds to a hydrophobic pocket between switch I and II of K-Ras and inhibits the nucleotide exchange with an IC_{50} of 342 μ M and the nucleotide release with an IC_{50} of 155 μ M¹⁹³.

Zn²⁺- and Cu²⁺-cyclen stabilize H-Ras in state I GTP-bound conformation, which is a weak state for effector binding^{194,195}.

In a yeast two-hybrid screening approach the small molecule inhibitor MCP110 could be identified. It can disrupt the interaction between H-Ras and Raf1 *in vitro* and in cells and had an anti-proliferative effect in cells expressing constitutively active Ras¹⁹⁶.

BQU57 binds to RalB-GDP and supposedly locks this inactive state. It was identified in a structure-based virtual screening and binds adjacent to the switch II region of RalB. BQU57 can effectively reduce RalB-GTP in cells and inhibits colony formation in lung cancer cell lines¹⁹⁷.

Inhibitors of Rho GTPases:

Mitoxantrone (MTX) is a Rho-GTPase pan-inhibitor identified in an AlphaScreen® approach. It impairs GTP loading *in vitro* and has been shown to slow down cell migration in wound-healing assays¹⁹⁸.

The allosteric Cdc42 inhibitor CID29950007 locks the GTPase in an inactive conformation and induces nucleotide release. It can inhibit Cdc42-mediated cellular functions like filopodia formation¹⁹⁹.

EHT 1864 is an allosteric Rac1 inhibitor with an IC_{50} of 40 nM. It has been shown to reduce A β peptide levels in Alzheimers disease models²⁰⁰.

In a virtual screening approach the RhoA/RhoB/RhoC inhibitor Rhosin was identified. Rhosin blocks the interaction between Rho and its GEF LARG. Moreover it was shown that Rhosin can block Rho-specific downstream signalling and inhibits growth of MCF-7 cells in a dose-dependent manner²⁰¹.

The small molecule ZCL278 was found in an *in silico* HTS. It interferes with the interaction between Cdc42 and its GEF Intersectin and decreases the cellular level of Cdc42-GTP²⁰².

NSC23766 selectively inhibits the interaction of Rac1 with its GEFs Tiam1 and TrioN with an IC_{50} of about 50 μ M *in vitro*. An anti-proliferative and anti-invasive effect could be shown in prostate cancer cells²⁰³.

The small molecule EHop-016 has been designed based on the structure of NSC23766 and inhibits Rac activity with an IC_{50} of 1.1 μ M in cells. It significantly reduces tumour growth, metastasis and angiogenesis in breast cancer mouse models²⁰⁴.

1A-116 interferes with the interaction between Rac1 and its GEF P-Rex1 and could be shown to reduce the level of Rac1-GTP in breast cancer cells²⁰⁵.

Secramine A supposedly stabilizes the interaction between Cdc42 and RhoGDI, preventing membrane association and effector binding of Cdc42. It does not affect nucleotide binding and exchange²⁰⁶.

Inhibitors of Arf GTPases:

AMF-26 is a small molecule inhibitor that has been identified in an *in silico* approach based on the cellular effects of Brefeldin A (BFA). A logarithm has been used to compare the effects of BFA with those of 4000 compounds on a total of 39 cell lines. Reduction of ARF1 activation by AMF-26 could be shown in a pull down assay²⁰⁷.

Other inhibitors of proteins from the Arf subfamily of small GTPases are Brefeldin A and LM-11. These small molecules stabilize the complex between Arf1 and a GEF. They are listed in Section 1.7.3.2 (Inhibitors of GEF proteins).

Inhibitors of Rab GTPases:

The stapled peptide StRIP3 has been designed based on the structure of the Rab6-interacting protein 1 and locks Rab8a in its GDP-bound state. StRIP3 also interferes with the interaction of Rab8a and its effector OCRL1^{208,209}.

Nexinhib20 is a small molecule inhibitor that disrupts the interaction between Rab27a and its effector JFC1 that plays an important tethering role in neutrophil exocytosis²¹⁰.

Inhibitors of the Ran GTPase:

There is no inhibitor known for the small GTPase Ran to this day.

Table 2: Inhibitors of Ras superfamily GTPases.

Name	Type	Target	Mechanism	Screening	IC ₅₀	Ref.
CID1067700	Small molecule	pan-GTPases	Nucleotide competitive	Flow cytometry bead-based	Different for each GTPase	^{161,211}
Kobe0065	Small molecule	H-Ras-GTP	Inhibits effector interaction	<i>In silico</i> HTS	46 ± 13 μM	¹⁸⁶
SML-10-70-1	Small molecule	K-Ras ^{G12C}	Covalent, GDP analogue	Rational design	26.6 – 47.6 μM (in cells)	¹⁸⁷
AA12	Small molecule	K-Ras ^{G12C}	Allosteric, decreases affinity for GTP	Disulfide fragment-based tethering	0.32 μM (in cells)	¹⁸⁸
SCH53239	Small molecule	Ras-GDP	unknown	Rational design	0.5 μM	¹⁸⁹
HBS3	Synthetic α-helix	Nucleotide-free Ras	Sos competitive, inhibits interaction	Rational design	28 ± 4.8 μM	¹⁹⁰

SAH-SOS1	Stapled peptide	K-Ras and wt Ras	Sos-competitive	Rational design	60 – 140 nM	¹⁹¹
AGP	Small molecule	K-Ras and wt Ras	May inhibit K-Ras-GEF interaction	None (natural product)	4.5 – 9.7 μ M (in cells)	¹⁹²
DCAI	Small molecule	K-Ras	Inhibits Ras-Sos interaction	NMR-based fragment screen	342 μ M	¹⁹³
Cu ²⁺ /Zn ²⁺ -cyclen	Small molecule	H-Ras	Locks Ras-GTP in state I	NMR spectroscopy	Millimolar	^{194,195}
MCP110	Small molecule	H-Ras	Inhibits Ras-Raf interaction	Yeast two-hybrid screen	2 – 25 μ M	^{196,212}
BQU57	Small molecule	RalB-GDP	May lock GDP-bound state	<i>In silico</i> HTS	~ 2 μ M (in cells)	¹⁹⁷
CID29950007	Small molecule	Cdc42	Allosteric, locks inactive conformation and induces nucleotide release	<i>In vitro</i> GTP competitive HTS	2 – 3 μ M	¹⁹⁹
EHT1864	Small molecule	Rac1	Allosteric, induces nucleotide release	unknown	40 nM	^{200,213}
MTX	Small molecule	pan-Rho GTPases	Inhibits GTP loading	AlphaScreen®	Different for each GTPase	¹⁹⁸
Rhosin	Small molecule	RhoA, RhoB, RhoC	Inhibits Rho-LARG interaction	<i>In silico</i> HTS	Submicromolar	²⁰¹
ZCL278	Small molecule	Cdc42	Inhibits Cdc42-intersectin interaction	<i>In silico</i> HTS	Low micromolar	²⁰²
NSC23766	Small molecule	Rac1	Inhibits Rac1-Tiam1/TrioN interaction	<i>In silico</i> HTS	50 μ M	²⁰³
EHop-016	Small molecule	Rac1, Rac3	May inhibit Rac1-Vav2 interaction	Rational design	1.1 μ M (in cells)	²⁰⁴
1A-116	Small molecule	Rac1	Inhibits Rac1-P-Rex1 interaction	<i>In silico</i> HTS	4 μ M	²⁰⁵
Secramine A	Small molecule	Cdc42	May stabilize Cdc42-RhoGDI interaction	Phenotypic HTS	1 μ M (in cells)	²⁰⁶
AMF-26	Small molecule	Arf1	May inhibit Arf1-ArfGEF interaction	Drug sensitivity data base (<i>in silico</i>)	4.9 μ M (in cells)	²⁰⁷

StRIP3	Stapled peptide	Rab8a	Locks Rab8a-GDP, inhibits Rab8a-OCRL1 interaction	Rational design	22 μ M	165,208,209
Nexinhib20	Small molecule	Rab27a	Inhibits Rab27a-JFC1 interaction	<i>In vitro</i> FRET-based HTS	2.6 μ M	210

1.7.3.2 Inhibitors of GEF proteins

Some inhibitors of GEF proteins for GTPases of the Ras superfamily have been identified. There are small molecule inhibitors of GEF proteins, but also aptamers and stapled peptides have been found. Inhibitors that act by stabilization of GEF/GTPase complexes will be listed here, although they by definition also act on the GTPases. An overview over the inhibitors described below is given in table 3.

Inhibitors of Ras GEFs:

UC-773587 and UC-857993 are small molecule inhibitors of the Ras GEF Sos1. They have been identified in an *in silico* structural HTS approach followed by an *in vitro* HTS. The binding site could be mapped to the catalytic pocket of Sos1, preventing the interaction between Sos1 and Ras²¹⁴.

Another small molecule compound that interferes with the Sos1-Ras interaction is NSC-658497. It binds to the catalytic site of Sos1 and dose-dependently inhibits Sos1-mediated Ras activation *in vitro* as well as cell proliferation of prostate cancer cells²¹⁵.

Inhibitors of Rho GEFs:

The RNA aptamers K91 and K11 have been identified in a Systematic evolution of ligands by exponential enrichment (SELEX) approach. They inhibit the Tiam1-mediated activation of Rac1 and Rac2. The aptamer binding motif overlaps with the GTPase binding site of Tiam1 and involves the helix α 9²¹⁶.

Y16 is a small molecule inhibitor that dose-dependently blocks the activation of RhoA by its GEF LARG. It interacts with the DPH domain of LARG and could be shown to specifically inhibit RhoA activation in fibroblasts as well as growth, migration and invasion of breast cancer cells¹⁸².

Trip α is a peptide aptamer identified in a yeast-two-hybrid genetic screen that inhibits the C-terminal GEF domain of Trio (TrioC). Trio contains two different GEF domains: TrioC and TrioN that activate RhoA and RhoG/Rac1, respectively. Trip α could inhibit TrioC activity in COS cells^{183,217}.

TrioN can also be targeted by the small molecule NPPD that has been found in a medium-throughput screening (MTS) using a yeast exchange assay. It dose-dependently reduces the GEF activity of TrioN on RhoG *in vitro* but turned out to be cytotoxic in mammalian cells²¹⁸.

ITX3 was identified in the same yeast exchange assay screening as NPPD and could be shown to inhibit the TrioN-mediated nucleotide exchange on RhoG and Rac1. It could inhibit Rac1 activation in mammalian cells without showing cytotoxic effects¹⁸⁴.

In another yeast exchange assay setup C21 could be discovered. C21 is a small molecule inhibitor of the Rac1-GEF Dock5 that does not affect Rac1 activation by TrioN²¹⁹.

Inhibitors of Arf GEFs:

Brefeldin A (BFA) is the first GEF inhibitor that has ever been found, discovered in the 1950s. It is a natural product, isolated from the fungus *Eupenicillium brefeldianum*, which blocks the GEF activity of a subgroup of Sec7 domain-containing Arf1 nucleotide exchange factors as Gea1 in yeast or Big1 in higher eukaryotes. BFA acts by stabilizing the Arf1-GDP-Sec7 complex^{166,185}. This mode of action is known as ‘interfacial inhibition’ and suggests a promising strategy for targeting GEF/GTPase complexes²²⁰.

Another interfacial inhibitor called LM-11 stabilizes the complex between Arf1-GDP and the Sec7 domain of its GEF ARNO. LM-11 has been shown to block the ARNO-mediated migration of MDCK cells¹⁸⁵.

M69 is an RNA aptamer that binds to the catalytic Sec7 domain of Cytohesin1, ARNO (Cytohesin2) and Cytohesin3 and inhibits the nucleotide exchange on Arf1 and Arf6 with an IC₅₀ in the low micromolar range.

An aptamer displacement screen using the fluorescently-labelled M69 aptamer in a fluorescence polarization assay identified the small molecule SecinH3. It inhibits the Cytohesin-mediated nucleotide exchange on Arf1 and Arf6 in a concentration-dependent manner. Using SecinH3 it could be shown that cytohesins are involved in hepatic insulin signalling²²¹.

A virtual screening approach based on the structure of SecinH3 identified Secin16, that could inhibit the ARNO-mediated nucleotide exchange on Arf1 and reduce Cytohesin-dependent cell adhesion of human leukocytes²²².

Inhibitors of Rab GEFs:

The only inhibitor of a Rab GEF that has been discovered to this day is JH5. JH5 inhibits the Rabex-5-mediated nucleotide exchange on Rab5 *in vitro*, without affecting the Rin1-mediated nucleotide exchange. The small molecule contains a thiol group that has been shown to be important for the inhibitory effect, yet makes this compound sensitive to reducing conditions. A cellular effect of JH5 could not be shown⁸².

Inhibitors of Ran GEFs:

There is no inhibitor known for GEFs of the small GTPase Ran to this day.

Table 3: Inhibitors of GEF proteins.

Name	Type	Target	Mechanism	Screening	IC ₅₀	Ref.
UC-773587	Small molecule	Sos1	Inhibits Sos1-Ras interaction	<i>In silico</i> followed by <i>in vitro</i> HTS	< 50 μM	²¹⁴
UC-857993	Small molecule	Sos1	Inhibits Sos1-Ras interaction	<i>In silico</i> followed by <i>in vitro</i> HTS	< 50 μM	²¹⁴
NSC-658497	Small molecule	Sos1	Inhibits Sos1-Ras interaction	<i>In silico</i> followed by <i>in vitro</i> HTS	micromolar	²¹⁵
K91 & K11	RNA aptamers	Tiam1	Inhibit Tiam1-Rac1 – 2 interaction	SELEX	nanomolar	²¹⁶

Y16	Small molecule	LARG	Binds to catalytic DHPH domain	<i>In silico</i> HTS	Low micromolar	182
Tripα	Peptide aptamer	TrioC	May inhibit TrioC-RhoA interaction	Yeast-two-hybrid genetic screen	4 μM	183,217
NPPD	Small molecule	TrioN	May inhibit TrioN-RhoG/Rac1 interaction	Yeast exchange assay MTS	116 μM	218
ITX3	Small molecule	TrioN	May stabilize GTPase/TrioN complex	Yeast exchange assay MTS	76 μM	184
C21	Small molecule	Dock5	unknown	Yeast exchange assay MTS	Micromolar range	
BFA	Small molecule	Arf1-GDP-Gea1 Sec7 complex	Stabilizes Arf1-GDP-Gea1 Sec7 complex	None (natural product)	15 μM	166,185
LM-11	Small molecule	Arf1-GDP-ARNO-Sec7 complex	Stabilizes Arf1-GDP-ARNO-Sec7 complex	<i>In silico</i> HTS	150 – 200 μM	185
M69	RNA aptamer	Cytohesin 1-3	Binds to catalytic Sec7 domain	SELEX	Low micromolar range	223
SecinH3	Small molecule	Cytohesin 1-3	Binds to catalytic Sec7 domain	Aptamer displacement screen	2.4 – 5.6 μM	221
Secin16	Small molecule	Cytohesin 1-3	unknown	<i>In silico</i> HTS	3.1 μM	222
JH5	Small molecule	Rabex-5	May bind to catalytic Vps9 domain	<i>In vitro</i> HTS	0.3 μM	82

2 Aim of the Project

The small GTPase Rab5 is involved in early endosomal trafficking and vesicular transport. Its activity is regulated by various GEFs and, once activated, it can interact with a multitude of different effector proteins. Yet the specific contribution of single GEFs to the diverse Rab5 functions and interactions is far from being understood and also depends largely on Rab5 localization. Moreover an up-regulation of Rab5 or Rab5-GEFs can lead to pathological conditions like many different types of cancer.

GEFs are usually multi-domain proteins with specific functions besides GTPase activation. The Rab5-GEF Rin1 is of particular interest. It is on the one hand up-regulated in non-small cell lung adenocarcinoma and other cancer cell lines, contributing to their proliferative nature via excessive Rab5 activation, and on the other hand acts as a tumour suppressor in breast cancer cells via its ABL kinase signalling function.

Rin1 also increases EGFR internalization, degradation and down-regulation and can interact with active Ras to enhance Ras-dependent signalling. It has several phosphorylation sites and upon phosphorylation can interact with 14-3-3 proteins. The impact of Rin1 domain-specific functions on downstream signalling cascades can hardly be studied by knock-out or knock-down methods, because they usually affect rather the whole protein than certain subdomains. To dissect the complex network of protein-protein interactions involving Rin1 and Rab5, domain-specific small molecule inhibitors could be a useful tool. With such inhibitors it could be possible to investigate the influence of, for example, only the GEF function of Rin1 by selective inhibition of the Vps9 domain, without affecting its other domains. This approach would help elucidating the complex roles of Rin1 and subsequently Rab5 and might even contribute to a deeper understanding of other Rab5-GEFs and their ability to counteract Rin1 GEF-deficiency.

To this day there is no small molecule modulator of Rin1 or Rab5 available. The only small molecule modulator described for a Rab5-GEF is the Rabex-5_{GEF} inhibitor JH5. A cellular effect of JH5 could not be shown, possibly due to its sensitivity to reducing conditions.

The aim of this project is to identify a small molecule inhibitor of the Rin1-mediated Rab5 activation. Therefore it is necessary to establish and apply an *in vitro* nucleotide exchange assay suitable for high-throughput screening. This requires the purification of active recombinant Rin1- and Rab5 constructs first, followed by assay design and conversion to a robot-assisted format. After screening of a small molecule library with more than 20 000 compounds, the resulting hits should be evaluated and characterized *in vitro* in terms of their biochemical properties, structure-activity relationship and specificity over other GEF and GTPase pairs.

3 Results

3.1 Protein expression and purification

Several GTPases and GEFs have been expressed and purified during this project. First of all, active Rab5a and Rin1C had to be purified to establish the screening assay and perform the screening. To test for specificity of the hit compounds, other GEF/GTPase pairs have been purified: Rabex-5_{GEF}/ Rab5a, DrrA/Rab1, Tiam1DHPH/Rac2 and Vav1/Rac1. Strep-tagged full length Rin1 (Rin1-TS) has been purified to study the effects of the hit compound on the Rin1/ABL1 interaction.

3.1.1 Rab5a

Human Rab5a was expressed as an aa17-184 construct, lacking the hypervariable C-terminal region that contains the prenylation sites required for membrane anchorage and a short N-terminal part that is involved in endocytosis and fusion events^{36,39,224,225}. These parts are nonessential for nucleotide and GEF binding and a similar construct for Rab5c has been described to be active *in vitro*²²⁶. It was heterologously expressed in a pET15b vector with an N-terminal 10 x Histidine tag in *E. coli* BL21-CodonPlus®(DE3)-RIL cells. The protein expression before and after Isopropyl β-D-1-thiogalactopyranoside (IPTG) induction was monitored via SDS-PAGE as depicted in figure 5a. An increased abundance of a band at around 21 kDa was observed after induction, which correlates with the expected mass for the Rab5a construct, indicating successful protein expression. The analysis of the purification during every step is shown in figure 5b. The 21 kDa protein could be retrieved from the fractions 22 – 26 (figure 5b, lane 11) during a size exclusion chromatography. A yield of 83.6 mg Rab5a in a concentration of 198 μM could be obtained from 2 L of *E. coli* culture. The protein was mainly pure with only a few traces of impurities and could be largely enriched. During the Ni-NTA affinity chromatography some amount of the target protein could be found in the flow-through and the washing fraction. This might have been avoidable by using more of the Ni-NTA resin to avoid saturation.

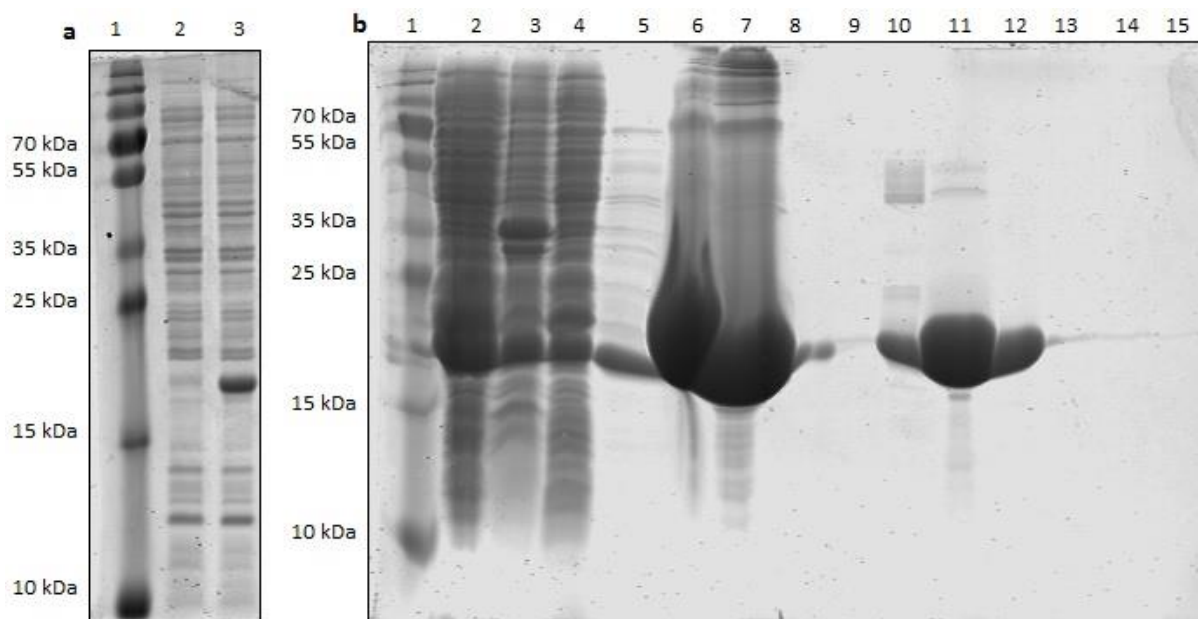


Figure 5: Expression and purification of Rab5a. 15 % SDS-PAGE gels stained with coomassie brilliant blue. A pre-stained molecular weight marker is loaded in lane 1 of each gel. **a:** Analysis of the protein expression before (lane 2) and after (lane 3) IPTG induction. **b:** Step-by-step analysis of the Rab5a purification. The *E. coli* lysate has been loaded in lane 1, followed by the insoluble cell debris in lane 2. Lane 3 shows the flow-through fraction after incubation with Ni-NTA beads. In lane 4 the wash fraction from the Ni-NTA chromatography has been loaded. The lanes 6 and 7 show the eluate fraction of the Ni-affinity chromatography before (6) and after (7) centrifugation to remove possible precipitate. In the lanes 8 – 14 the fractions (pooled by peaks) collected during size exclusion chromatography have been loaded. Lane 8: Fractions 1 + 2, lane 9: Fractions 5 – 7, lane 10: Fractions 18 – 20, lane 11: Fractions 22 – 26, lane 12: Fractions 27 – 29, lane 13: Fractions 33 – 35 and lane 14: Fractions 38 – 42. Lane 15 has been left empty.

3.1.2 Rin1C

Rin1C is an aa293 – 783 construct of human Rin1 that has been expressed in *Sf9* insect cells previously and was found to be active in *in vitro* assays after purification¹⁰². It lacks the N-terminal SH2 domain as well as the proline rich region required for ABL kinase interaction. It is built of the Vps9 domain that bares the Rab5-GEF activity as well as the C-terminal Ras interaction site and contains a 6 x histidine tag followed by a TEV cleavage site at the N-terminus. The Bac-to-Bac system has been used to generate the virus required for expression of the construct. The purification was analysed at every step on the SDS-PAGE gels that are depicted in figure 6. The 55 kDa protein could be collected from fractions 14 – 22 (figure 6b, lane 14 and c, lanes 2 – 9) during the size exclusion chromatography. A yield of 15.3 mg Rin1C in a concentration of 113 μ M could be obtained from 5 L of *Sf9* cell culture.

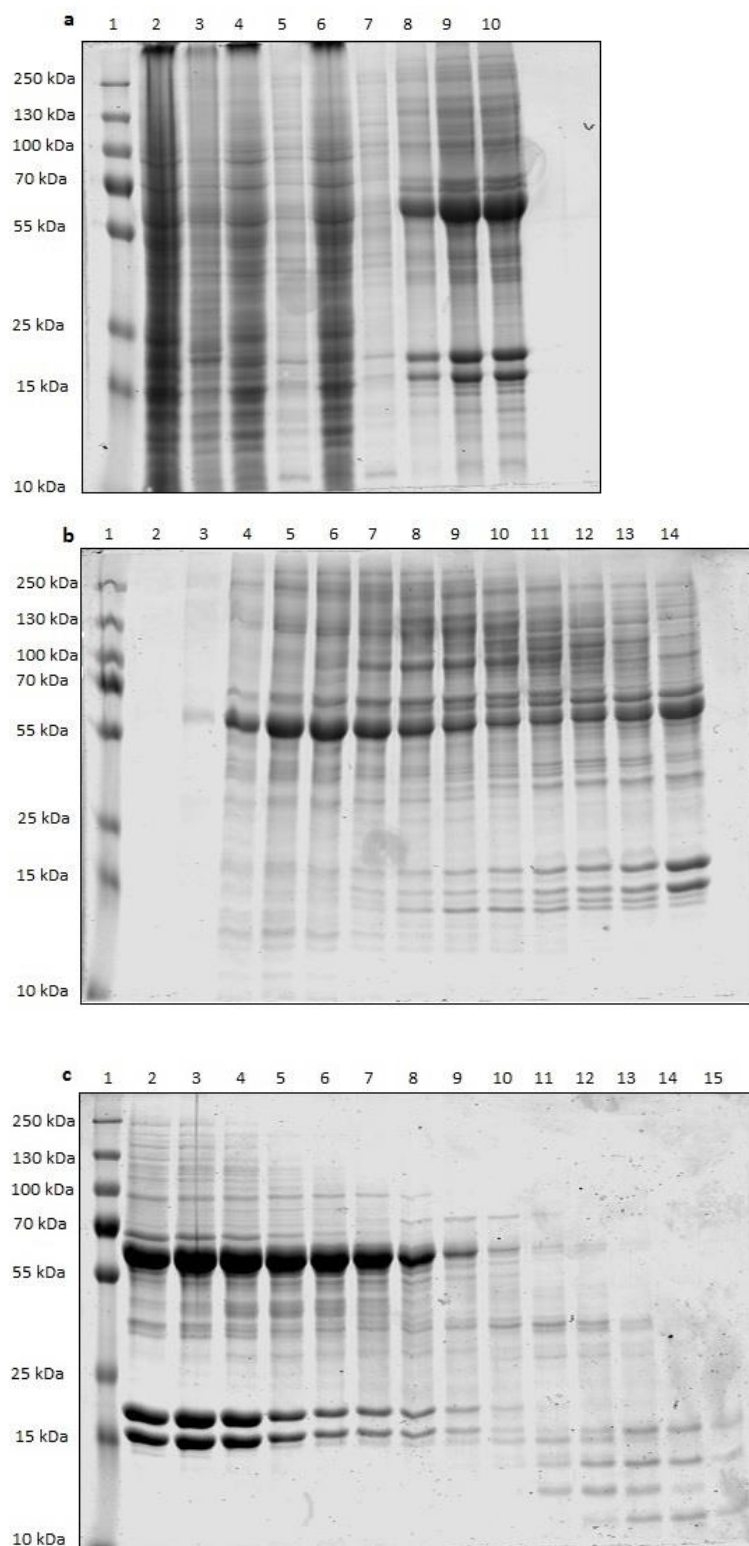


Figure 6: Purification of Rin1C. 10 % SDS-PAGE gels stained with coomassie brilliant blue. A pre-stained molecular weight marker is loaded in lane 1 of each gel. **a:** Analysis of the Ni-NTA affinity chromatography. The *Sf9* cell lysate is loaded in lane 2, followed by the insoluble cell debris in lane 3. The lysate was split into two tubes before incubation with the Ni-NTA beads (for volume reasons). Lanes 4 and 6 show the wash fractions of each split and lanes 5 and 7 the corresponding flow-through fractions. Lanes 8, 9 and 10 show the pooled eluate of the Ni-NTA beads: before concentration (8), after concentration (9) and after centrifugation to remove possible precipitate (10). **b:** Analysis of the size exclusion chromatography. Lane 2 – 14 are numbered after the fractions they contain (fractions 2 – 14). **c:** Continuation of the fractions from the size exclusion chromatography. Lanes 2 – 15 show the fractions 15 – 28, respectively.

3.1.3 Rin1-TS

Strep-tagged full length Rin1 has been expressed in *Sf9* insect cells. The construct comprises the aa 1-783 of human Rin1. It contains the N-terminal SH2 domain as well as the proline rich region required for ABL kinase interaction, the Vps9 domain that bares the GEF activity and the C-terminal Ras interaction site. A TEV protease cleavage site followed by a streptavidin-binding peptide²²⁷ have been attached at the C-terminus. The Bac-to-Bac system has been used to generate the virus required for expression of the construct. The purification via Streptavidin affinity chromatography followed by buffer exchange and sample concentration was analysed at every step on the SDS-PAGE gel depicted in figure 7. The protein of interest could be enriched (figure 7, lane 8). A yield of 24.1 µg Rin1-TS in a concentration of 2.7 µM could be obtained from 10 mL of *Sf9* cell culture.

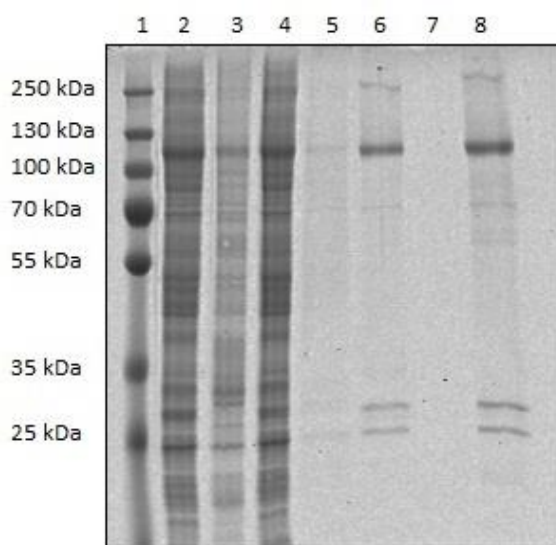


Figure 7: Purification of Rin1-TS. 10 % SDS-PAGE gel stained with coomassie brilliant blue. A pre-stained molecular weight marker has been loaded in lane 1. The gel shows the analysis of the Streptavidin affinity chromatography purification. The *Sf9* cell lysate is loaded in lane 2. Lane 3 shows the insoluble cell debris after clearance of the lysate. The flow-through, which contains unbound material after incubation with the Streptavidin beads, is depicted in lane 4, followed by the washing fraction in lane 5. The eluate has been loaded in lane 6. After buffer exchange and concentration, the flow-through from the spin concentrator and the final sample have been loaded in lanes 7 and 8, respectively.

3.1.4 Rabex-5_{GEF}

The construct Rabex-5_{GEF} contains only the Vps9 domain that holds the Rab5 GEF function as well as a helical bundle required for stabilization. This construct has been purified for *in vitro* assays before and was found to be highly active¹³¹. Furthermore it has been found that full-length Rabex-5 requires the effector Rabaptin-5 for full activity²²⁸. The construct comprises the aa132-391 of human Rabex-5. It has been expressed in *E. coli* BL21-CodonPlus®(DE3)-RIL cells with an N-terminal 6 x Histidine tag using a pDL2 vector as described by C. Wosnitza⁸² using a modified version of the protocol described by Delprato et al.¹³¹. The expression before and after IPTG induction was monitored on an SDS-PAGE gel prior to protein purification. This gel is depicted in figure 8a. An increase in band intensity for a band approx. at the expected mass of 31 kDa could be found, indicating inducible Rabex-5_{GEF} expression. The purification via Ni-NTA affinity chromatography and gel filtration has been analysed at

every step on the SDS-PAGE gel shown in figure 8b. During the size exclusion chromatography the target protein eluted in fractions 22 – 27 (figure 8b, lane 8). A yield of 27.1 mg Rabex-5_{GEF} in a concentration of 75 μ M could be obtained from 2 L of *E. coli* culture. The 31 kDa protein was found to be pure after gel filtration. Due to over-loading of the SDS-PAGE gel a statement about possible protein loss during the Ni-NTA chromatography could not be made.

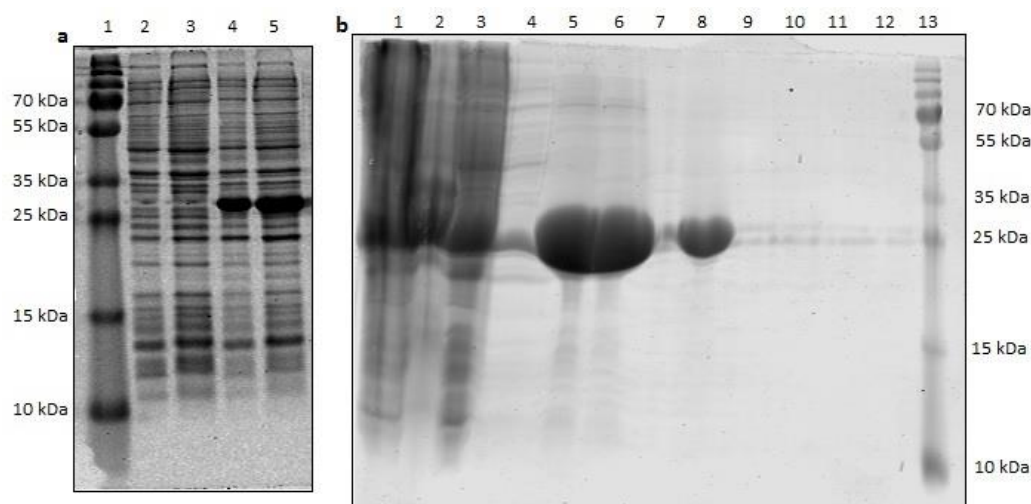


Figure 8: Expression and purification of Rabex-5_{GEF}. 15 % SDS-PAGE gels stained with coomassie brilliant blue. **a:** Analysis of the Rabex-5_{GEF} expression in *E. coli* lysates before (lanes 2 (3 μ L lysate) and 3 (7 μ L lysate)) and after (lanes 4 (3 μ L lysate) and 5 (7 μ L lysate)) IPTG induction. A pre-stained molecular weight marker has been loaded in lane 1. **b:** Step-by-step analysis of the purification of Rabex-5_{GEF} by Ni-NTA affinity chromatography and gel filtration. Lane 1 shows the *E. coli* lysate, followed by the insoluble cell debris in lane 2. In lane 3 the unbound material (flow-through) after Ni-NTA bead-binding has been loaded. The wash fraction is shown in lane 4. The lanes 5 and 6 contain the eluate from the Ni-NTA beads before (lane 5) and after (lane 6) centrifugation to remove possible precipitate. The lanes 7 – 12 show the different fractions from the size exclusion chromatography, pooled by peaks. Lane 7: Fractions 3 – 5, lane 8: Fractions 22 – 27, lane 9: Fractions 37 – 40, lane 10: Fractions 43 – 47, lane 11: Fractions 49 – 52 and lane 12: Fractions 61 – 62. In lane 13 a pre-stained molecular weight marker has been loaded.

3.1.5 Rab1

The GTPase Rab1 has been heterologously expressed in *E. coli* as an MBP fusion protein with an N-terminal 6 x Histidine tag using a pMAL vector. The tags could be cleaved by the TEV protease due to a cleavage site after the MBP sequence. The construct comprises the aa1 – 205 of human Rab1. An SDS-PAGE gel to analyse the protein expression before and after IPTG induction is depicted in figure 9a. After induction a strong band is visible at about 65 kDa, corresponding to the expected mass of the MBP-Rab1 fusion protein. This indicates that inducible expression occurred. MBP-Rab1 was then purified by Ni-NTA affinity chromatography followed by tag cleavage using the TEV protease. After the cleavage, the 6 x His tag remained on the N-terminus of MBP so it could be re-bound to Ni-NTA beads to separate it from Rab1. A step-by-step analysis of this affinity purification is depicted in figure 9b. The TEV cleavage could have been optimized by using a larger amount of TEV protease or a prolonged cleavage time. Due to incomplete cleavage a huge amount of un-cleaved protein was present in the sample applied to the reverse affinity chromatography. The incomplete separation during this second Ni-NTA binding step might have been avoidable by using a larger amount of resin to circumvent saturation. Finally, a gel filtration was

performed to increase the purity of Rab1 and an SDS-PAGE gel of the fractions is shown in figure 9c. The 22 kDa target protein eluted in the fractions 48 – 55 (figure 9c, lane 7) during the size exclusion chromatography. The protein of interest could be separated from the un-cleaved fusion protein. However, the final sample still contained traces of His₆-MBP. A yield of 4.5 mg Rab1 in a concentration of 51 μ M could be obtained from 2 L of *E. coli* culture. Since the Rab1 final protein sample turned out to be active (cp. section 3.2) the sample quality was sufficient to perform the desired nucleotide exchange assays.

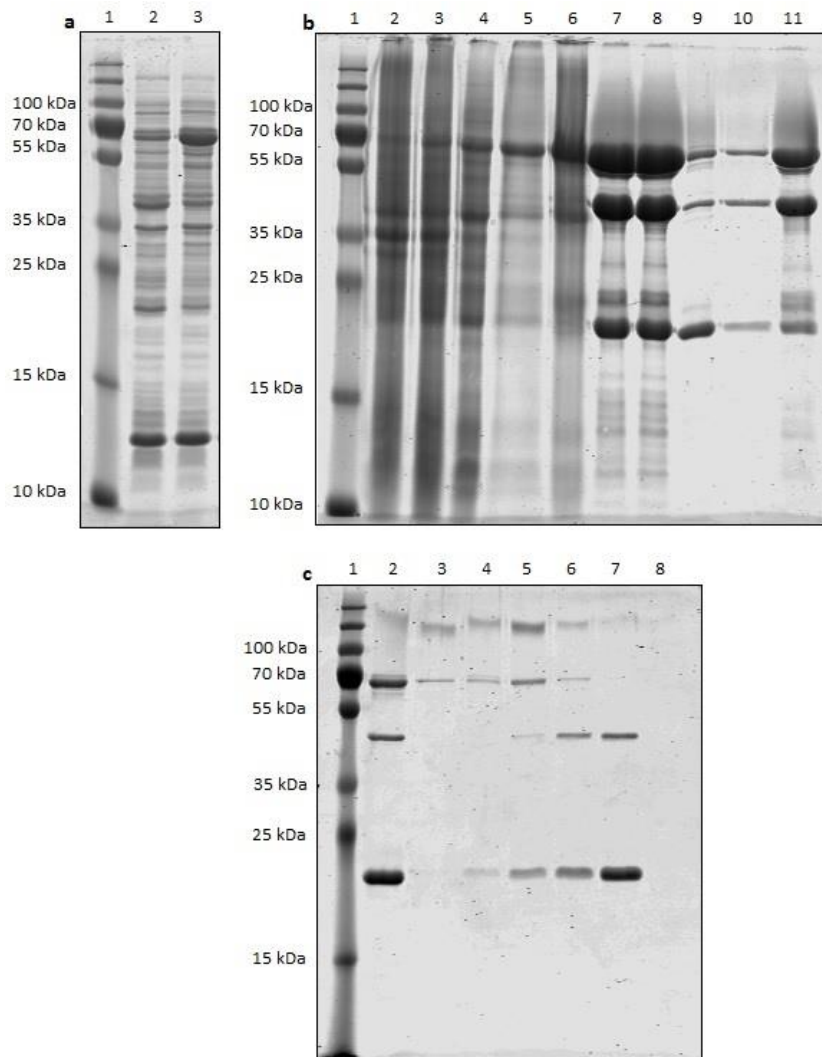


Figure 9: Expression and purification of Rab1. 12.5 % SDS-PAGE gels stained with coomassie brilliant blue. A pre-stained molecular weight marker has been loaded in lane 1 of each gel. **a:** Analysis of the MBP-Rab1 expression before (lane 2) and after (lane 3) IPTG induction. **b:** Step-by-step analysis of the Ni-NTA affinity chromatography, tag cleavage and reverse Ni-NTA affinity chromatography. Lane 2 shows the *E. coli* lysate followed by the insoluble cell debris in lane 3. In lane 4 the unbound cellular proteins (flow-through) were loaded. The washing fraction is shown in lane 5 and the eluate containing the MBP-Rab1 fusion protein is shown in lane 6. The sample after TEV cleavage has been loaded before (lane 7) and after (lane 8) centrifugation to remove possible precipitate. The flow-through fraction from the reverse affinity chromatography that contained the un-tagged Rab1 protein is loaded in lane 9, followed by the wash fraction in lane 10. The eluate retrieved during the reverse Ni-NTA binding is shown in lane 11. **c:** Size exclusion chromatography of the Rab1 sample. In lane 2 the starting material (flow-through from the reverse affinity chromatography) is shown. The fractions, pooled by peak, from the size exclusion chromatography have been loaded in the lanes 3 – 8. Lane 3: Fractions 4 – 9, lane 4: Fractions 32 – 36, lane 5: Fractions 37 – 43, lane 6: Fractions 44 – 47, lane 7: Fractions 48 – 55 and lane 8: Fractions 73 – 77.

3.1.6 DrrA

The Rab1-GEF DrrA has been expressed in *E. coli* using a modified pET19 vector. The construct contained a TEV-cleavable N-terminal 6 x Histidine tag and comprises the aa40 – 533 of human DrrA. The protein expression before and after IPTG induction was monitored on the SDS-PAGE gel shown in figure 10a. There was no definite increase in band intensity visible at the expected mass of approx. 24 kDa, but the basal expression level could have been high, so it was proceeded to purify the protein. First it was bound to Ni-NTA beads, followed by TEV cleavage of the Histidine tag and reverse Ni-affinity chromatography. The step-by-step analysis of this purification is depicted in figure 10b. The 24 kDa target protein could be retrieved from the flow-through fraction during reverse affinity chromatography (figure 10b, lane 9). A yield of 1.9 mg DrrA in a concentration of 44 μ M could be obtained from 2 L of *E. coli* culture.

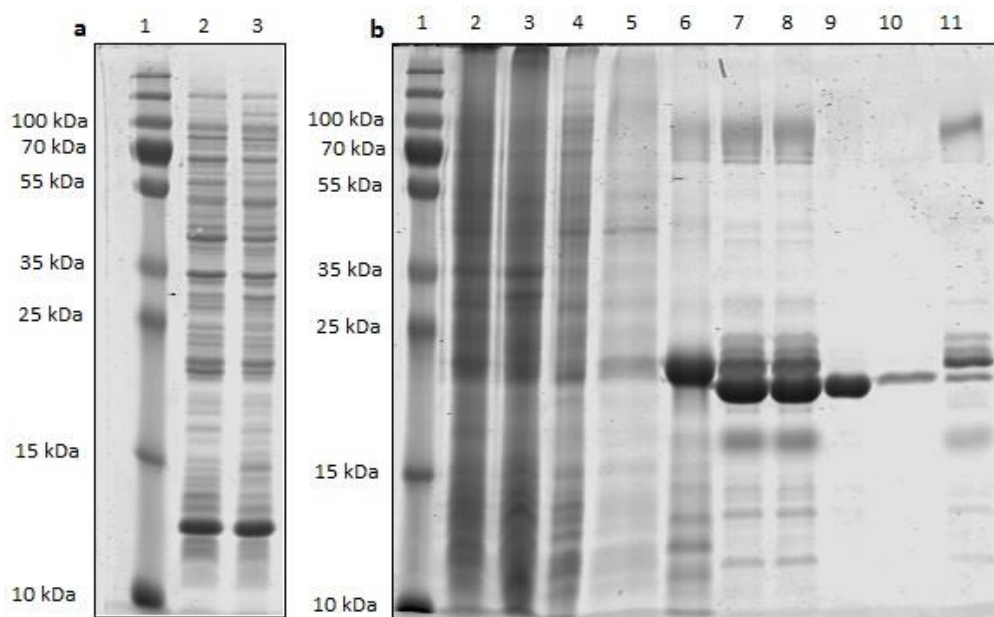


Figure 10: Expression and purification of DrrA. 12.5 % SDS-PAGE gels stained with coomassie brilliant blue. A pre-stained molecular weight marker has been loaded in lane 1 on both gels. **a:** Analysis of the DrrA expression before (lane 2) and after (lane 3) IPTG induction. **b:** Ni-NTA affinity chromatography, TEV cleavage and reverse Ni-NTA chromatography. In lane 2 the *E. coli* lysate has been loaded, followed by the insoluble cell debris in lane 3. Lane 4 contains the unbound protein mix after Ni-NTA affinity binding. The washing fraction is shown in lane 5. In lane 6 the eluate from the Ni-NTA beads is shown, containing HT-DrrA. The lanes 7 and 8 contain the cleaved sample before (lane 7) and after (lane 8) centrifugation to remove possible precipitate. The flow-through after reverse Ni-NTA chromatography is shown in lane 9 and contains the cut DrrA target protein. In lane 10 and 11 the washing fraction and the eluate from the reverse Ni-NTA chromatography have been loaded, respectively.

3.1.7 Rac2

The GTPase Rac2 has been expressed in *E. coli* using a pET SUMO vector. The construct comprises the aa1-192 of human Rac2 and contains N-terminal 6 x His- and SUMO tags. The IPTG inducible protein expression was monitored on the SDS-PAGE gel depicted in figure 11a. A strong band for a protein with a mass of approx. 35 kDa can be seen after induction. Rac2 was then purified via Ni-NTA affinity binding and size exclusion chromatography. The

purification has been analysed at every step on the SDS-PAGE gel shown in figure 11b. Large amounts of the protein of interest could be found in the cell debris fraction, indicating protein insolubility or incomplete cell lysis. Insoluble protein can result from folding problems during the expression and can sometimes be prevented by expression at lower temperatures over a longer period of time. Thereby the expression is slower and that results in some cases in larger amounts of soluble protein. Some amount of His₆-SUMO-Rac2 did not bind to the Ni-NTA resin during the affinity chromatography or got washed away in the following washing step. This might have been avoidable by using a larger amount of Ni-NTA resin to circumvent saturation. The 34.8 kDa protein Rac2 could be enriched and eluted in the fractions 23 – 29 (figure 11b, lane 11) during the gel filtration. A yield of 58 mg His₆-SUMO-Rac2 in a concentration of 119 μ M could be obtained from 2 L of *E. coli* culture. The final sample was mainly pure with only a few traces of impurities left. Aside from that the yield was utterly sufficient to perform the desired nucleotide exchange experiments.

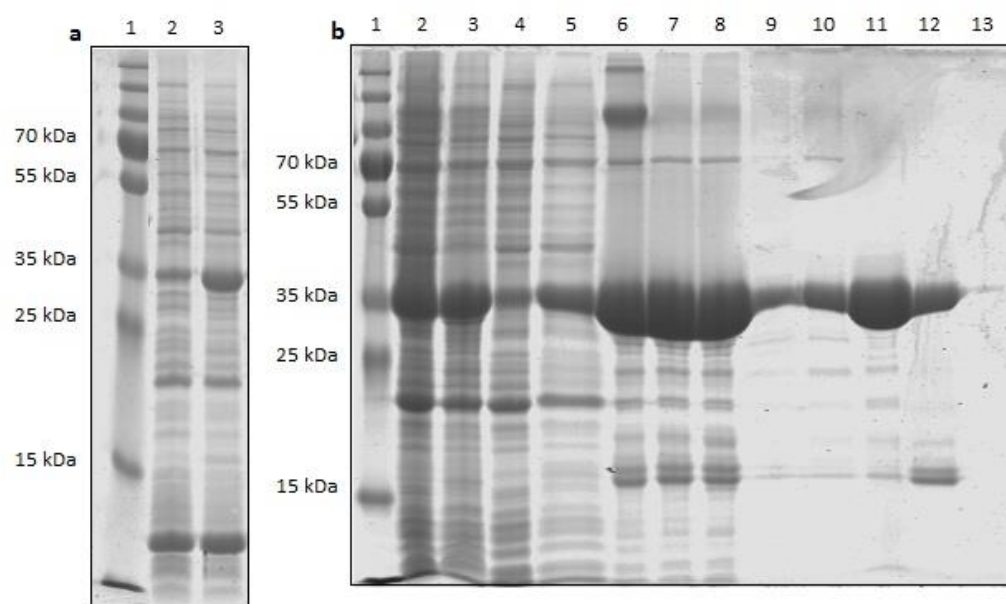


Figure 11: Expression and purification of Rac2. 12.5 % SDS-PAGE gels stained with coomassie brilliant blue. A pre-stained molecular weight marker has been loaded in lane 1 on both gels. **a:** Analysis of the Rac2 expression before (lane 2) and after (lane 3) IPTG induction. **b:** Purification of Rac2 by Ni-NTA affinity binding and size exclusion chromatography. The *E. coli* lysate has been loaded in lane 2 followed by the insoluble cell debris in lane 3. Lane 4 shows unbound material after the Ni-NTA affinity binding (flow-through) and lane 5 the wash fraction. The eluate is depicted in lanes 6 – 8: Lane 6: directly after elution, lane 7: after over-night storage at 4 °C and lane 8: after centrifugation to remove possible precipitate. The lanes 9 – 13 show the fractions collected during size exclusion chromatography, pooled by peak. Lane 9: Fractions 4 – 7, lane 10: Fractions 18 – 21, lane 11: Fractions 23 – 29, lane 12: Fractions 30 – 33 and lane 13: Fractions 59 – 63.

3.1.8 Tiam1DHPH

Murine Tiam1 has been expressed in *E. coli* with an N-terminal Strep-tag and a C-terminal, Thrombin-cleavable 6 x Histidine tag using a pET52b(+) vector. The aa1033 – 1406 construct comprises the Dbl homology (DH) domain and the pleckstrin homology (PH) domain of Tiam1. It has been shown that the DH domain carries the GEF activity but fails to activate Rac GTPases in absence of the PH domain²²⁹. Analysis of the protein expression was performed on the SDS-PAGE gel depicted in figure 12a. A strong increase in band intensity after IPTG induction was visible for a band of the expected mass (approx. 48 kDa), indicating

inducible protein expression. The purification was performed via Ni-NTA affinity binding followed by thrombin cleavage of the Histidine tag. The target protein was then collected by Strep-Tactin affinity chromatography. This purification was analysed step-by-step on the SDS-PAGE gel shown in figure 12b. A large amount of Strep-Tiam1DHPH was lost during Strep-Tactin affinity chromatography, likely due to incomplete elution. This might have been avoided by using a higher concentration of desthiobiotin in the elution buffer or a longer incubation of the Strep-Tactin resin with the elution buffer. Since the final sample as shown in figure 12b, lane 11 appeared blurry, it was concentrated and afterwards repeatedly analysed on an SDS-PAGE gel, which is shown in figure 12c. The target protein could be retrieved and used in further applications. A yield of 1.4 mg Tiam1DHPH in a concentration of 29 μ M could be obtained from 2 L of *E. coli* culture. The final sample showed four additional bands in the SDS-PAGE analysis, indicating traces of impurities but the main band corresponded to the 48 kDa protein of interest. The yield was sufficient to perform the desired nucleotide exchange experiments.

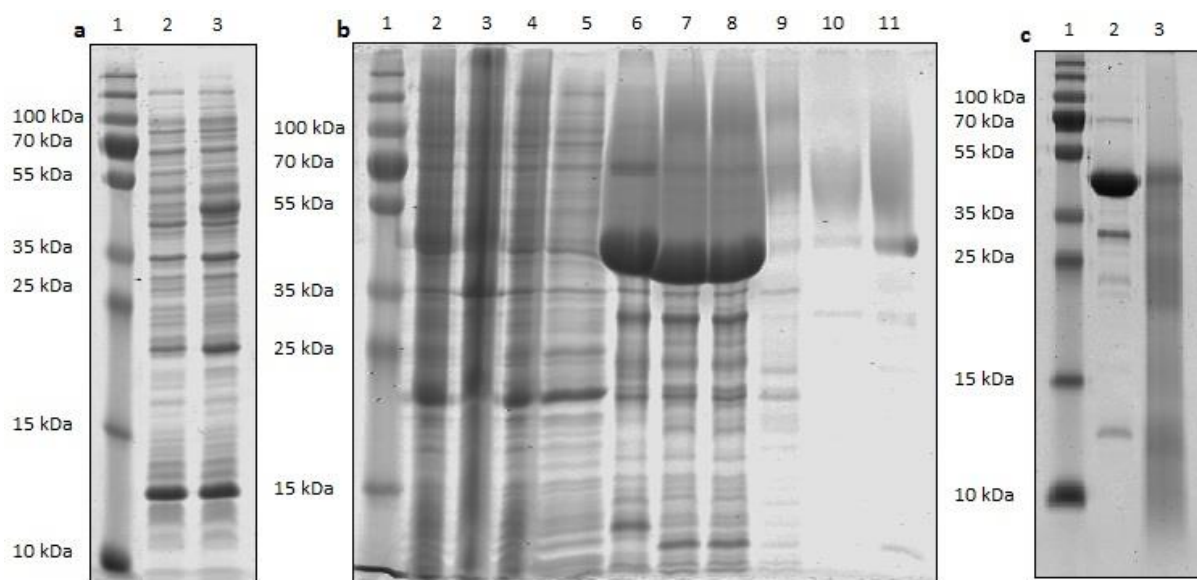


Figure 12: Expression and purification of Tiam1DHPH. A pre-stained molecular weight marker has been loaded in lane 1 on each gel. **a:** 12.5 % SDS-PAGE gel stained with coomassie brilliant blue. Analysis of the Tiam1DHPH expression before (lane 2) and after (lane 3) IPTG induction. **b:** 12.5 % SDS-PAGE gel stained with coomassie brilliant blue. Ni-NTA affinity chromatography followed by His-tag cleavage using thrombin and subsequent strep-Tactin affinity binding. The *E. coli* lysate has been loaded in lane 2, followed by the insoluble cell debris in lane 3. Unbound material after Ni-NTA affinity binding is shown in lane 4. Lane 5 shows the washing fraction from the Ni-NTA chromatography. The eluate is shown in lane 6 before over-night thrombin digestion and in lane 7 afterwards. Lane 8 shows the digested eluate after centrifugation to remove possible precipitate. The strep-Tactin affinity chromatography is shown in the lanes 9 – 11. Lane 9: Flow-through containing unbound material, lane 10: washing fraction and lane 11: eluate containing strep-Tiam1DHPH. **c:** 15% SDS-PAGE gel stained with coomassie brilliant blue. Comparison of the concentrated final sample (lane 2) and the sample collected during strep-Tactin affinity chromatography (lane 3).

3.1.9 Rac1

Human Rac1 (aa 1 – 184) has been expressed with a Thrombin-cleavable N-terminal GST tag. A pGEX2T vector was used for heterologous expression in *E. coli* BL21-CodonPlus®(DE3)-RIL cells. The protein expression before and after IPTG induction has been monitored on the SDS-PAGE gel shown in figure 13a. Inducible expression could be seen by an increase in band

intensity after induction for a band with the expected mass of approx. 48 kDa for GST-Rac1. GST-Rac1 was purified by Glutathione (GSH) affinity chromatography, Thrombin digestion and reverse GSH affinity chromatography. This purification was analysed at every step on the SDS-PAGE gel depicted in figure 13b. Un-tagged Rac1 (~ 22 kDa) could be retrieved from the flow-through during reverse affinity binding (figure 13b, lane 9). A yield of 3.7 mg Rac1 in a concentration of 34 μ M could be obtained from 2 L of *E. coli* culture. The sample was mainly pure with only one impurity band showing at the height of the 70 kDa marker band. The yield was also sufficient for the desired experiments.

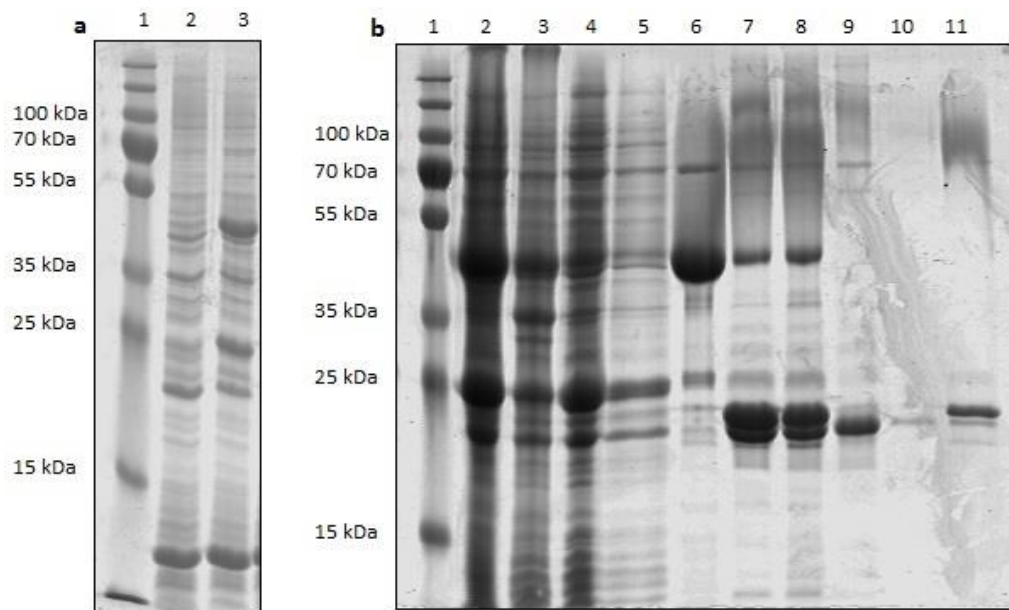


Figure 13: Expression and purification of Rac1. 12.5 % SDS-PAGE gels stained with coomassie brilliant blue. A pre-stained molecular weight marker has been loaded in lane 1 of each gel. **a:** Analysis of the GST-Rac1 expression before (lane 2) and after (lane 3) induction with IPTG. **b:** Analysis of the GSH affinity binding, Thrombin cleavage and reverse GSH affinity chromatography. The *E. coli* lysate has been loaded in lane 2, followed by the insoluble cell debris in lane 3. In lane 4 the unbound material (flow-through) after GSH affinity binding is shown. Lane 5 shows the washing fraction. The eluate containing GST-Rac1 is shown in lane 6. In lanes 7 and 8 the digested sample has been loaded before (lane 7) and after (lane 8) centrifugation to remove possible precipitate. The lower band of the duplet represents Rac1 while the upper one corresponds to GST. Lane 9 shows the flow-through of the reverse GSH affinity binding and contains the un-tagged Rac1. The lanes 10 and 11 show the washing fraction and the eluate from the reverse GSH chromatography, respectively.

3.1.10 Vav1

The aa189 – 575 construct of human Vav1 has been expressed in *E. coli* as a GST fusion protein with a TEV cleavage site to remove the GST tag. It contained the mutation M351T that has previously been described to increase the amount of soluble Vav1²³⁰. A pGEX2T vector has been used and the GST-Vav1 expression has been monitored on an SDS-PAGE gel before and after IPTG induction (figure 14a). A strong increase in band intensity for a band corresponding to a protein with a mass of about 72 kDa could be seen after induction. This indicated the inducible expression of GST-Vav1. The protein was then purified by GSH affinity chromatography, followed by TEV cleavage and reverse GSH affinity binding. Every step was analysed on the SDS-PAGE gel shown in figure 14b. During the *E. coli* cell lysis a large amount of GST-Vav1 could be found in the insoluble cell debris fraction (figure 14b, lane 3). This could either have been caused by folding problems during the protein

expression or by incomplete cell lysis (cp. section 3.1.7). There was no shift visible when comparing the undigested eluate (lane 6) with the digested sample (lane 7). Therefore the TEV protease-mediated tag cleavage appeared to be unsuccessful. Possible explanations could have been an inactive TEV protease sample or an inaccessible cleavage site caused by the folding properties of this fusion protein. Thus GST-Vav1 bound again to the GSH resin during the reverse affinity chromatography and was again found in the eluate (figure 14b, lane 11). Although the GST-tag could not be cleaved off, the fusion protein was active in the nucleotide exchange assay (cp. section 3.2) and it was used for the compound specificity testing experiments without further optimization of the purification protocol. A yield of 1 mg GST-Vav1 in a concentration of 29 μM could be obtained from 2 L of *E. coli* culture.

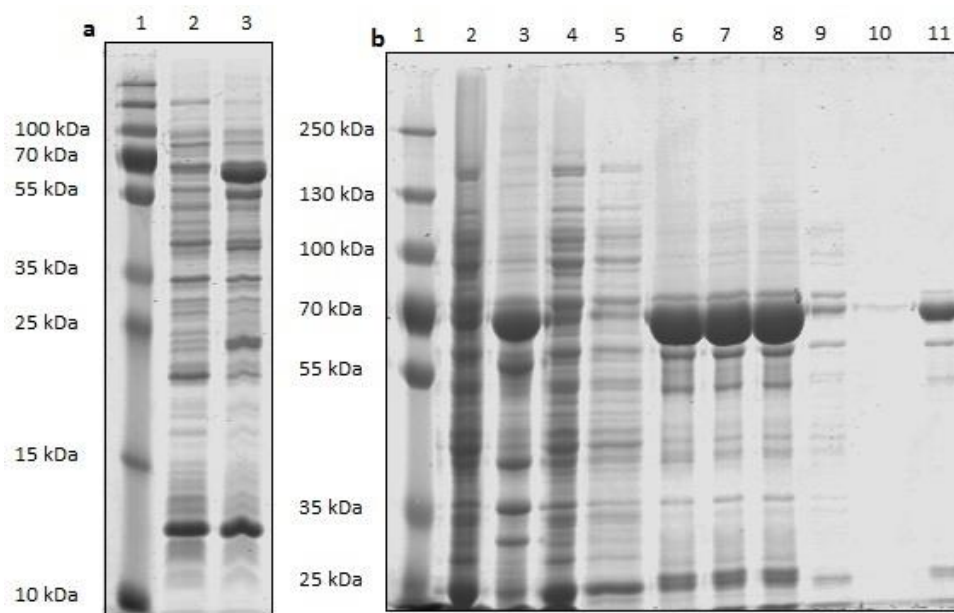


Figure 14: Expression and purification of Vav1. A pre-stained molecular weight marker has been loaded in lane 1 on both gels. **a:** 12.5 % SDS-PAGE gel stained with coomassie brilliant blue showing *E. coli* lysates before (lane 2) and after (lane 3) IPTG induction. **b:** 8 % SDS-PAGE gel stained with coomassie brilliant blue showing a step-by-step analysis of the purification by GSH affinity binding, GST-tag cleavage using the TEV protease and reverse GSH affinity chromatography. In lane 2 the *E. coli* lysate is shown, followed by the insoluble cell debris in lane 3. The unbound material after GSH affinity binding is depicted in lane 4. In lane 5 the washing fraction has been loaded. Lines 6, 7 and 8 contain the eluate, the eluate after over-night TEV digestion and the digested sample after centrifugation, respectively. In lane 9 the unbound material after reverse GSH affinity binding has been loaded, followed by the washing fraction in lane 10. Lane 11 shows the eluate from the reverse GSH affinity chromatography that contains undigested GST-Vav1.

3.1.11 N Δ 17 Arf1, ARNO-Sec7 and IR-ICD

The proteins N Δ 17 Arf1 and ARNO-Sec7 were kind gifts of Benjamin Weiche from the Famulok group. The insulin receptor intracellular domain (IR-ICD) was a kind gift of Christian Sieg, also from the Famulok group. Detailed information on the constructs can be found in section 7.1.5

3.2 Nucleotide exchange activity of the recombinant proteins

The fluorescently labelled GTP-analogue Bodipy-TR-GTP has been used to monitor the GEF-mediated nucleotide exchange on GTPases. The fluorescence intensity of Bodipy-TR-GTP was shown to increase upon binding to at least some GTP binding proteins²³¹. The fluorescence intensity was measured at 595 nm (excitation) and 620 nm (emission) and was expected to increase over time upon binding to the GTPase in presence of the corresponding GEF. Figure 15 shows the structure of Bodipy-TR-GTP. The fluorophore is attached to the ribose ring via an aminoethylcarbamoyl linker.

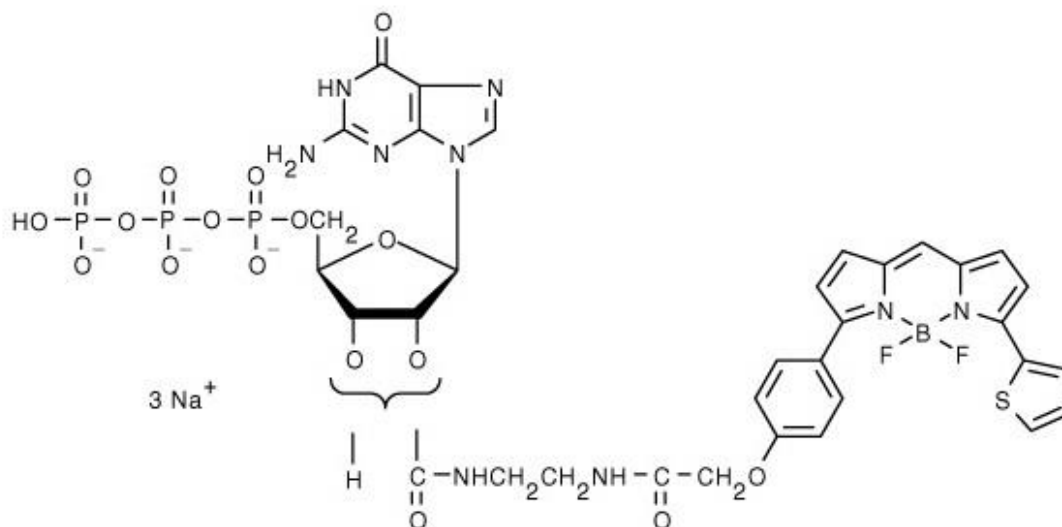


Figure 15: The structure of Bodipy-TR-GTP. In the mixed-isomer analogue the fluorophore is attached to the 2' or 3' position on the ribose ring via an aminoethylcarbamoyl linker.

The GEFs were expected to concentration-dependently catalyse the nucleotide exchange reaction on their corresponding GTPases^{33,131}. Different concentrations of the GEFs were assayed on a fixed GTPase concentration of 1 μ M with 2 μ M Bodipy-TR-GTP. The fluorescence intensity was plotted against the time and the resulting curves are shown in figure 16. All GEF constructs were capable to catalyse the nucleotide exchange on their corresponding GTPases. Rin1C, Rin1-TS and Rabex-5_{GEF} activated Rab5a with Rabex-5_{GEF} showing noticeably higher exchange activity than both Rin1-constructs (figure 16a – c). DrrA catalysed the nucleotide exchange on Rab1 (figure 16d). Both Rabs did not show a remarkable intrinsic nucleotide exchange activity as can be seen by essentially constant fluorescence intensity over time in the negative controls in absence of a GEF (black curves). Tiam1DHPH catalysed the nucleotide exchange on Rac2 only when used in considerably higher concentrations compared to all other GEFs (figure 16e). The intrinsic nucleotide exchange activity of Rac2 was high as reflected by a strong increase in fluorescence intensity over time in the negative control without Tiam1DHPH. Rac1 also showed a fairly strong intrinsic nucleotide exchange activity albeit not as strong as Rac2. Vav1 activated Rac1 even when used in concentrations below 25 nM (figure 16f). The ARNO-Sec7-mediated nucleotide exchange on Arf1 could be shown when ARNO-Sec7 was used in concentrations higher than 20 nM (figure 16f). The intrinsic nucleotide exchange activity was considerably high for Arf1. From those activity tests, the GEF concentrations that have later been used to assay compound specificity have been derived. The chosen concentrations can be found in section 7.2.3.1, table 24.

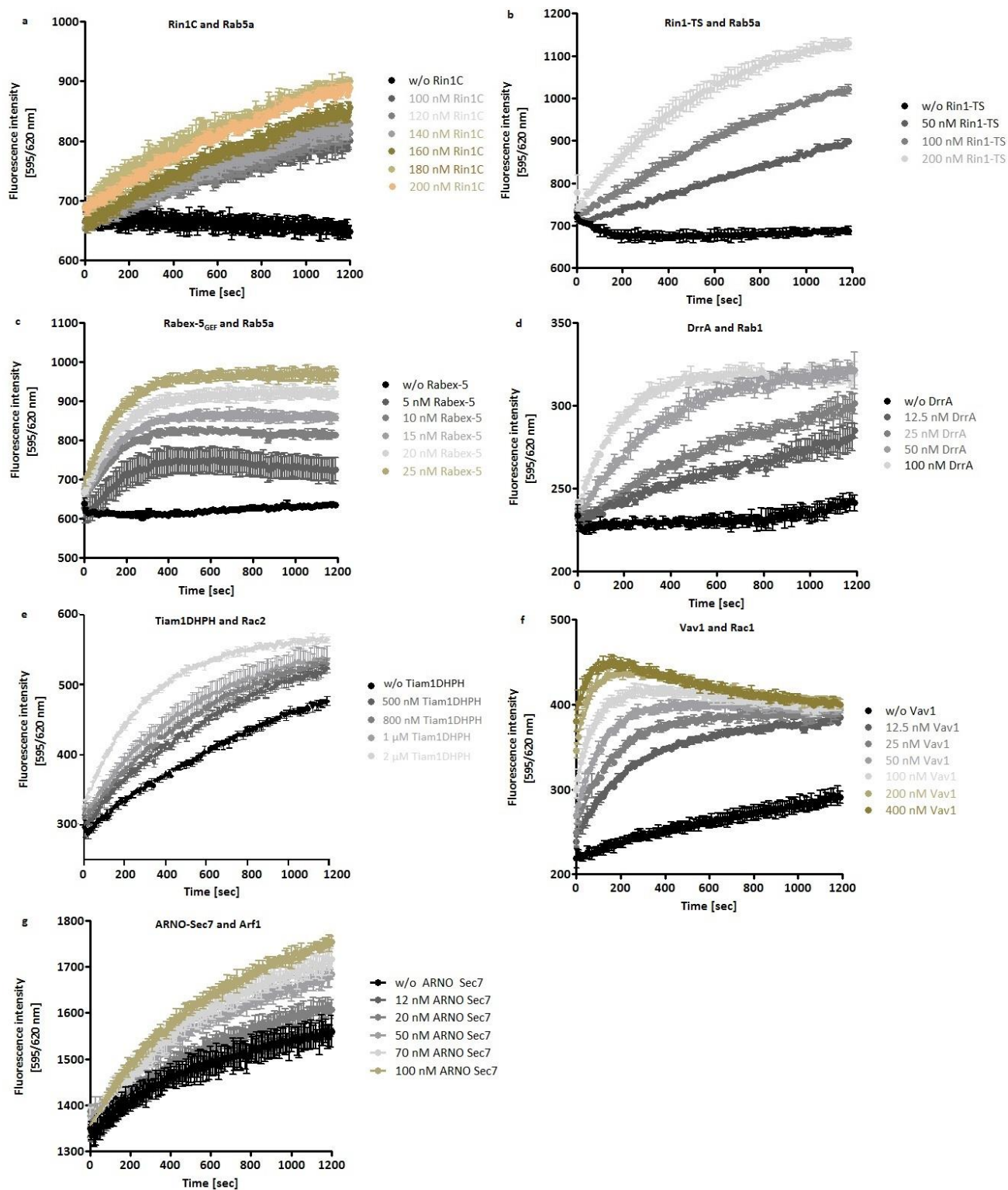


Figure 16: GEF-concentration-dependent activation of GTPases. The different GTPases were used at 1 μ M with 2 μ M of Bodipy-TR GTP. The GEFs were used at increasing concentrations to determine adequate conditions for the respective nucleotide exchange assays. **a:** Rin1C-mediated nucleotide exchange on Rab5a. **b:** Rin1-TS-mediated Rab5a activation. **c:** Rabex-5_{GEF}-mediated activation of Rab5a. **d:** Activation of Rab1 by DrrA. **e:** Tiam1DHPH dependent Rac2 activation. **f:** Vav1-mediated nucleotide exchange on Rac1. **g:** ARNO-Sec7-mediated Arf1 activation.

3.3 Screening for small molecule inhibitors

A functional nucleotide exchange assay was to be established with regard to screening for small molecule inhibitors of the Rin1-mediated Rab5 activation. The compounds were, as in most HTS approaches, only tested in single values. Therefore the assay had to be exact and sensitive in the identification of hits and also robust enough to avoid false positives²³². This required a wide span between the signals of the positive control (GEF-mediated nucleotide exchange) and the negative control (no GEF-mediated nucleotide exchange)²³³. The assay properties could be quantified by use of the Z' factor. It describes the assay quality and enables to judge, whether an assay is in general suitable for HTS approaches²³⁴.

3.3.1 Establishing the Bodipy-TR-GTP nucleotide exchange screening assay

The fluorescently labelled GTP analogue Bodipy-TR-GTP has previously been used in similar screening approaches and led to promising results^{214,235}. The Rin1C/Rab5a Bodipy-TR-GTP exchange assay was chosen to be optimized for HTS. Rin1C catalysed the nucleotide exchange on Rab5a in a concentration-dependent manner (cp. figure 16a), similar as previously described for Rabex-5¹³¹. First, different concentrations of Rin1C were tested again over a longer period to find conditions with a linear phase long enough to allow appropriate calculation of the slope. Figure 17 shows the Rin1C-mediated nucleotide exchange on Rab5a. As expected, higher concentrations of Rin1C again led to a faster nucleotide exchange. The reaction reached saturation at approx. 2100 fluorescence units. The use of 200 nM Rin1C resulted in a linear increase of the fluorescence intensity over the first 20 minutes and was therefore chosen as appropriate to be used during the screening.

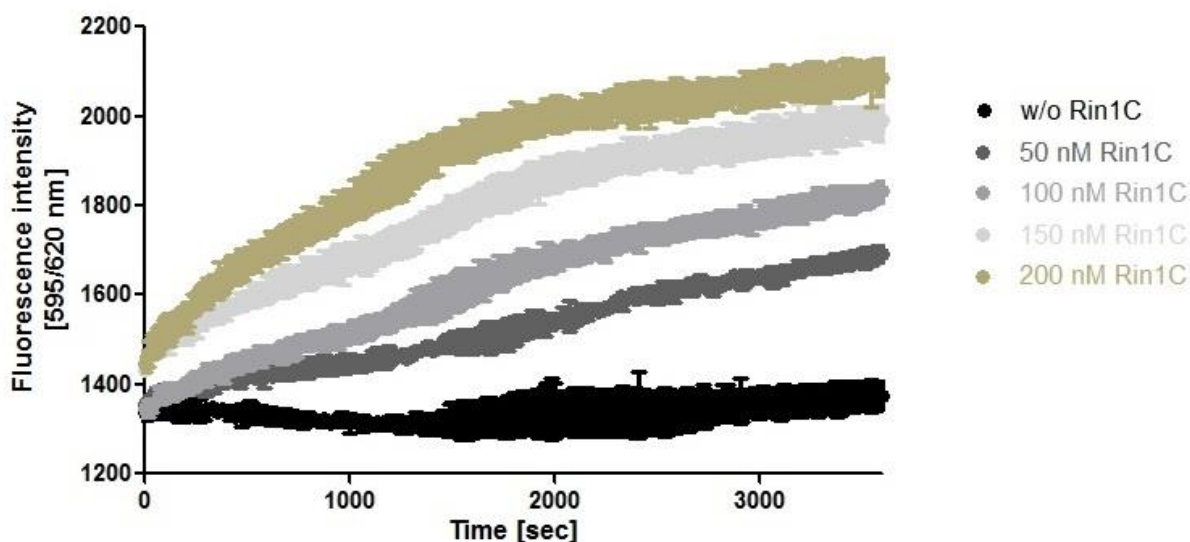


Figure 17: The Rin1C-mediated Bodipy-TR-GTP nucleotide exchange on Rab5a. Rin1C dose-dependently catalysed the nucleotide exchange on Rab5a. The nucleotide exchange was measured by monitoring the Bodipy-TR-GTP fluorescence at 595 / 620 nm (Ex. / Em.). Without Rin1C almost no nucleotide binding occurred (black curve). 1 μ M Rab5a and 2 μ M Bodipy-TR-GTP have been used. 200 nM Rin1C resulted in a linear increase of the fluorescence intensity over the first 1200 seconds.

3.3.2 Assay optimization for HTS

To increase the sample throughput, the assay had to be converted to an endpoint measurement instead of measuring the kinetics. This allowed the measurement of a whole 384 well plate at once in a time-delayed manner as described in section 7.2.3.1.1. The fluorescence intensity was measured once directly after Bodipy-TR-GTP addition ($t = 0$ min.) and then again after 20 minutes. From those values, the difference in fluorescence intensity (ΔFI) was calculated for each well. A small ΔFI could be measured for the negative control without Rin1C while the ΔFI in presence of 200 nM Rin1C was much higher. Figure 18a and b illustrate the conversion from the kinetic to the endpoint measurement. Since the library compounds were dissolved in dimethyl sulfoxide (DMSO), the DMSO tolerance had to be tested. The results are shown in Figure 18c. There was no significant difference between 0 – 6 % DMSO detectable. 4 % DMSO was necessary to use 40 μM as the final compound concentration and was found to be tolerated in the Bodipy-TR-GTP exchange assay.

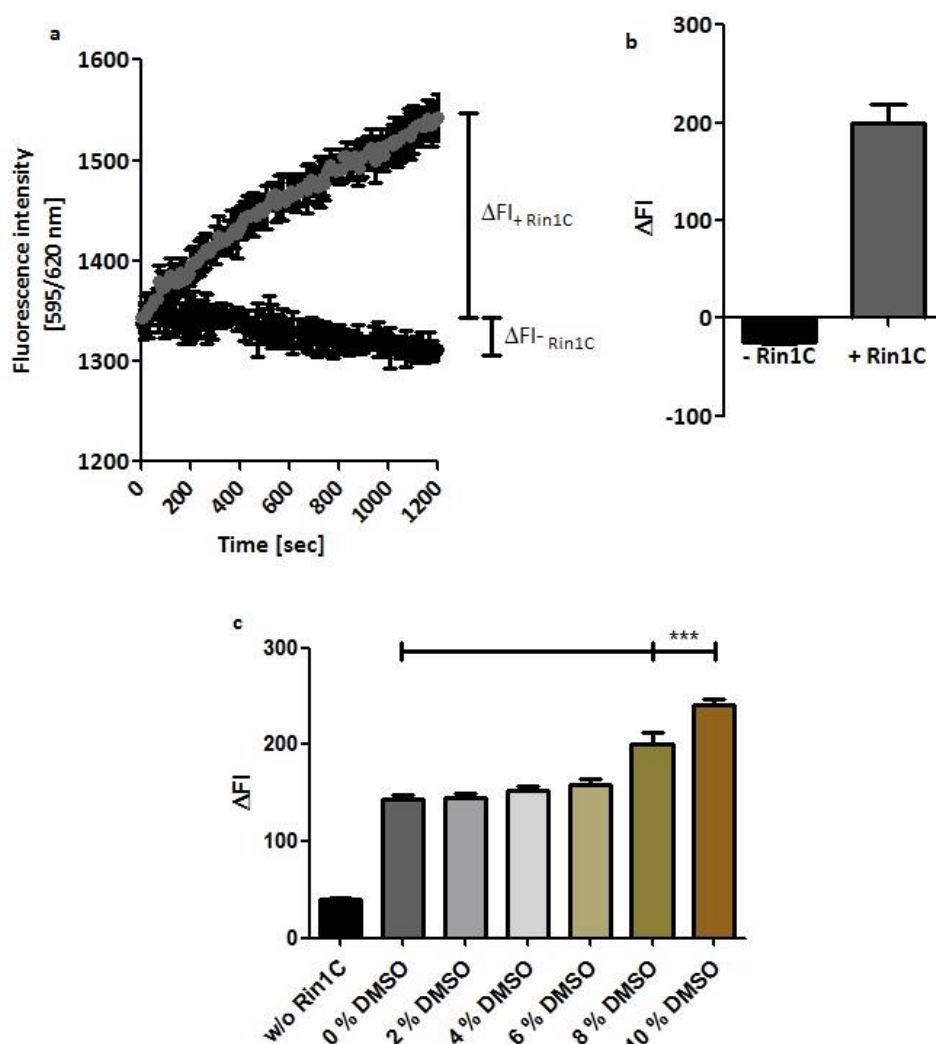


Figure 18: Adjustment of the Bodipy-TR-GTP assay for a HTS approach. a \rightarrow b: Conversion of the kinetic measurement to an endpoint measurement. ΔFI could be calculated from the fluorescence intensities at $t = 0$ min. and $t = 20$ min. **c:** DMSO tolerance of the Bodipy-TR-GTP exchange assay. There was no significant difference in the ΔFI between 0 – 6 % DMSO. The significance was calculated by one-way ANOVA, $p < 0.05$ using GraphPad Prism software.

With this conversion, the assay was expected to be suitable for HTS. During the screening the hits should exhibit lower ΔFI values compared to the DMSO controls (32 per plate). Other important considerations were the type of plate to be used, the buffer conditions and the order of sample preparation. Bodipy-TR-GTP turned out to be sticky on most plastic surfaces, therefore only plates with non-binding surface (NBS) yielded reasonable results. Moreover the use of detergents (tested: Tween-20, Triton X-100, Nonidet P-40, sodium cholate, CHAPS and IGEPAL CA-630, data not shown) dramatically increased the fluorescence signal of Bodipy-TR-GTP and simultaneously the error between replicates, leading to bad assay quality. In terms of assay preparation order, robot-assisted addition of compounds/DMSO into the plates followed by mixing Rab5a and Rin1C in exchange buffer and manual addition of the proteins gave the best results (lowest variance between replicates). Bodipy-TR-GTP was finally injected at the Tecan infinite M1000 pro plate reader directly before starting the time-delayed measurement.

3.3.3 Calculation of the Z' factor

To minimize the probability of false positives and false negatives during a HTS, the screening assay has to meet certain quality criteria. False positives would be time- and material consuming to be re-tested after the screening while false negatives would mean missing out on promising compounds. The Z' factor, a statistical parameter to judge assay quality, has been calculated as follows:

$$Z' factor = 1 - \frac{3(\sigma_p + \sigma_n)}{|\mu_p - \mu_n|}$$

It is defined in terms of the means (μ) and the standard deviations (σ) of the positive (p) and the negative (n) controls. The closer the Z' factor to its maximum 1, the higher the assay quality. A Z' factor between 0.5 and 1 defines an excellent assay that is suitable for HTS approaches²³⁴.

A 384 well plate with 192 positive controls and 192 negative controls (without Rin1C) has been measured in the time-delayed setup described in section 7.2.3.1.1. The corresponding results are shown in figure 19. The Z' factor was calculated to be 0.57 for the Bodipy-TR-GTP screening assay, indicating suitability for HTS.

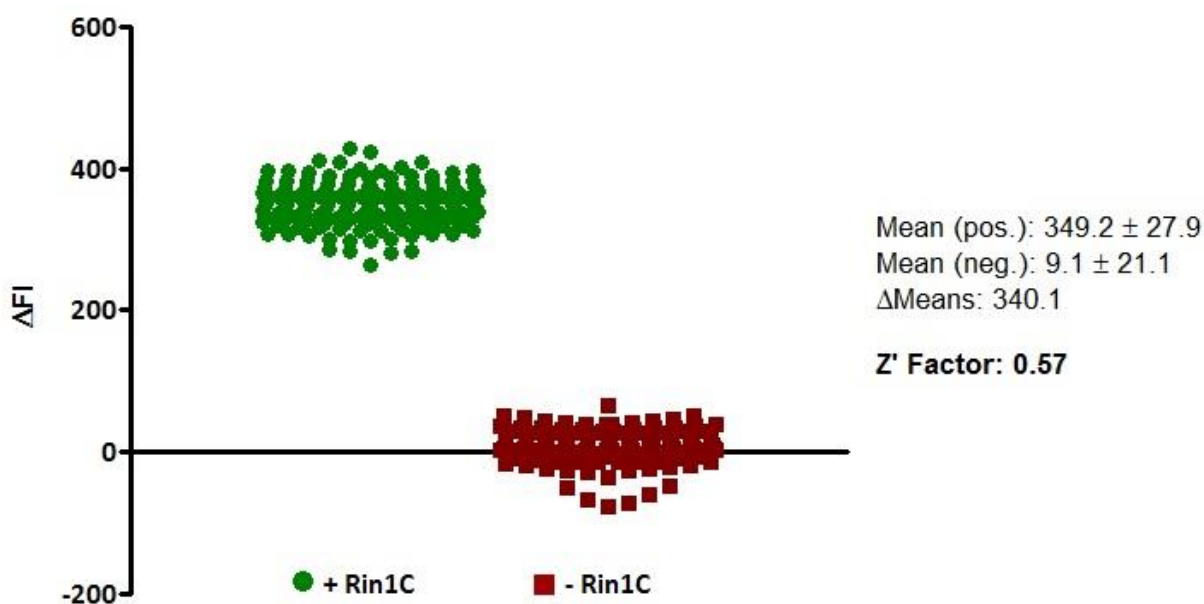


Figure 19: Determination of the Z' factor for the Bodipy-TR-GTP screening assay. 192 positive controls (green dots, 4% DMSO, 1 μ M Rab5a, 200 nM, Rin1C and 2 μ M Bodipy-TR-GTP) and 192 negative controls (red squares, without Rin1C) were measured in the time-delayed screening setup followed by calculation of the means \pm standard deviations. The Z' factor was calculated to be 0.57.

3.3.4 The compound library

An in-house compound library has been used for the screening. It contained 20 328 compounds in total of which the majority has been purchased at ComGenex. The library also contained many additional molecules that have been synthesized by members of the groups of Prof. Dr. M. Famulok, Prof. Dr. M. Gütschow and other groups from the University of Bonn.

3.3.5 High-throughput screening results

The screening of 20 328 compounds was performed under the conditions described in section 3.3.2 with 32 DMSO controls per plate (in columns 1 and 24). During the evaluation the Δ FI values for each compound sample and each control sample were calculated. Compounds that resulted in ≥ 80 % inhibition (equalling ≤ 20 % residual nucleotide exchange activity) compared to the DMSO controls from the same plate were defined as hits. This procedure identified 239 primary hits, which correlates to 1.2 % of the total compounds.

3.3.6 Identification of secondary hits

The primary hits were re-screened manually as duplicates in two different concentrations: 40 μ M and 10 μ M. By this, 26 secondary hits showing ≥ 50 % inhibition (at 40 μ M) could be identified. This equals 10.9 % of the primary hits. Correspondingly 213 (89.1 %) of the primary hits were found to be false positives of which some compounds had to be excluded due to strong quenching of the Bodipy-TR-GTP fluorescence signal. Quenchers usually interfere with the read-out rather than with the nucleotide exchange reaction. The results of the re-screen are depicted in figure 20. The 26 secondary hits were then tested from frozen 10 mM compound stock solutions to assure the inhibition does not result from degradation

products in the library plates. Degradation could have occurred during several thaw-freezing cycles in earlier screening approaches. Only 10 of the 26 secondary hits were found to inhibit the nucleotide exchange when the stock solution was tested. Due to insufficient information on possible degradation byproducts, the 16 compounds that did not show an inhibitory effect were omitted from further investigation. The 10 remaining compounds were chosen to be characterized. A complete list of the secondary hits is provided in the appendix (section 8.3).

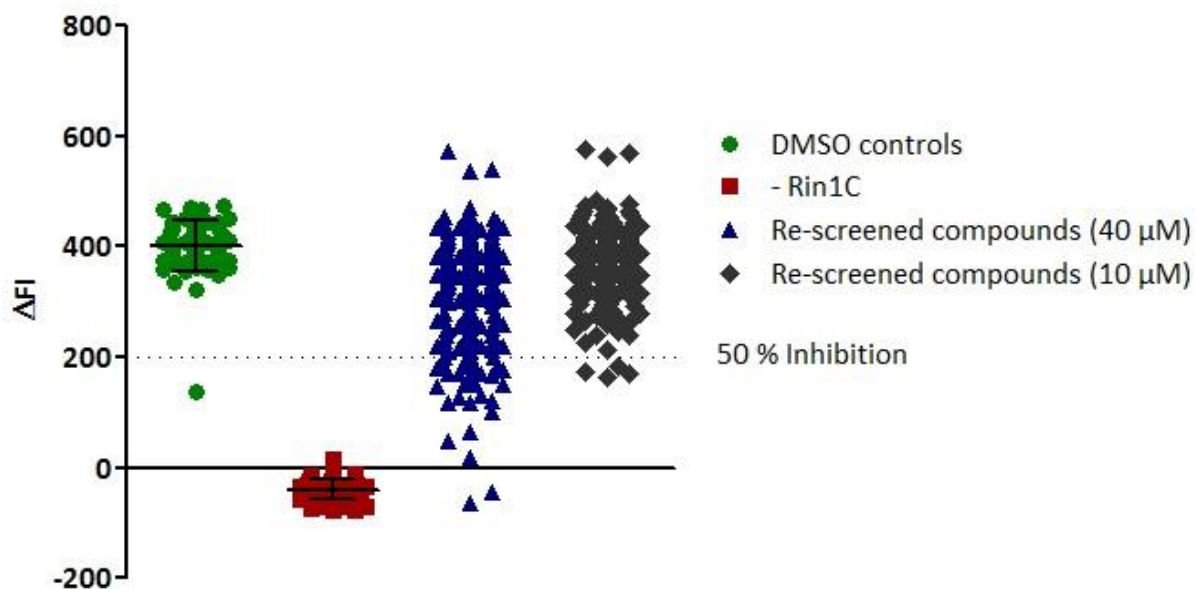


Figure 20: Manual re-screening of the 239 primary hit compounds. The positive controls (4 % DMSO, 1 μ M Rab5a200 nM, Rin1C and 2 μ M Bodipy-TR-GTP) are shown as green dots and the negative controls (without Rin1C) as red squares. The re-screened compounds (40 μ M, mean of duplicates) are depicted as blue triangles. Compounds that exhibited ≥ 50 % inhibition at 40 μ M were defined as secondary hits. Those are represented by the 26 blue triangles beneath the dotted line. The grey diamonds represent the compounds tested at a concentration of 10 μ M (mean of duplicates). Only four molecules showed ≥ 50 % inhibition at 10 μ M.

3.4 Characterization of secondary hit compounds

The 10 compounds chosen for characterization should be analysed in terms of their activity profile (IC_{50} and Hill coefficient), specificity for the Rin1C-mediated nucleotide exchange on Rab5a and their potential to induce protein aggregation. The IC_{50} and the Hill coefficient describe the potency and possible cooperative binding of small molecule inhibitors, respectively^{236,237}. Activity and specificity are crucial in the definition of a lead compound specified by J. G. Lombardino and J. A. Lowe as “a chemical structure or series of structures that show activity and selectivity in a pharmacological or biochemically relevant screen”²³⁸. Protein aggregation is a known source of promiscuous inhibition caused by small molecules. So-called aggregators are unlikely to act specifically and are prone to exhibit off-target effects²³⁹. By the characterization of these 10 compounds their suitability as lead structures should be surveyed.

3.4.1 Compound activity profiles and structures

The kinetic format of the Bodipy-TR-GTP exchange assay of the Rin1C-mediated Rab5a activation has been used to determine the IC_{50} values for the 10 secondary hits. They were tested as triplicates in concentrations between 0 and 50 μ M with a final DMSO concentration of 2 %. The structures were named after their position and well in the library e.g. CG1 05 F09. The activity profiles and the structures of those compounds are depicted in the figures 21 and 22, respectively. The IC_{50} and the Hill coefficient were determined using GraphPad Prism software by fitting the linear phases (the first 5 min.) of the kinetic reactions and calculation of the slopes. The slopes have then been plotted against the logarithmic compound concentrations and a sigmoidal fit (log(inhibitor) vs. response – variable slope) has been applied. The slopes of the negative and positive controls have been set as lower and upper limits for the fitting. The IC_{50} was given by the turning point of this curve while its slope at this point described the Hill coefficient. The Hill coefficient gives information on possible cooperative binding. A Hill coefficient of $|1|$ indicates non-cooperative/independent binding. Positively cooperative binding is assumed for a Hill coefficient $> |1|$, meaning once a ligand molecule is bound to a protein, its affinity for further ligand molecules increases. The other way around, a Hill coefficient between 0 and $|1|$ indicates negatively cooperative binding. In this case the binding of a ligand molecule decreases the proteins affinity for further ligand molecules²³⁷. The negative Hill coefficients found during the measurements result from the decreasing slopes with increasing compound concentration, leading to a decreasing sigmoidal curve. The raw data used for fitting can be found in section 8.4.1 in the appendix. The determined IC_{50} values all were in the low micromolar range qualifying the compounds as promising inhibitors at this point.

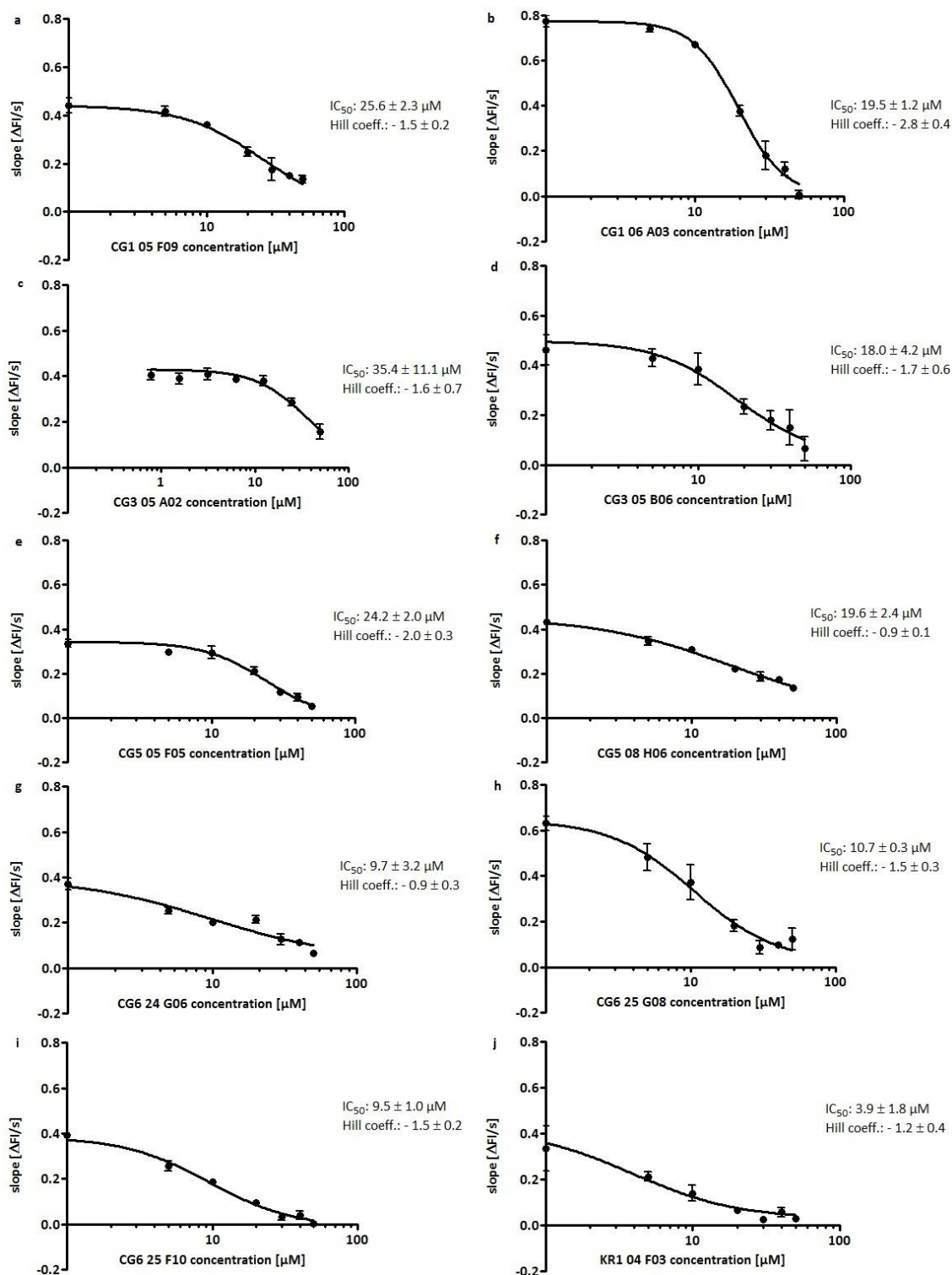


Figure 21: Activity profiles of the secondary hits. The compounds were tested as triplicates in concentrations between 1 and 50 μM in the kinetic Bodipy-TR-GTP nucleotide exchange assay. The Rin1C-mediated Rab5a activation was monitored as an increase in fluorescence intensity signal over time. 1 μM Rab5a, 150 nM Rin1C, 2 μM Bodipy-TR-GTP and a final DMSO concentration of 2 % have been used. A linear fit has been applied on the curves representing the nucleotide exchange over the first 5 minutes. The slopes of those curves have then been plotted against the logarithmic compound concentration and a sigmoidal fit has been applied, using the slopes of the positive control (1 μM Rab5a, 150 nM Rin1C, 2 μM Bodipy-TR-GTP and 2 % DMSO) and the negative control (without Rin1C) as boundaries. The IC_{50} values could be deduced from the turning points of these sigmoidal curves while their slopes represented the Hill coefficients. The values are given with the 95 % confidence intervals.

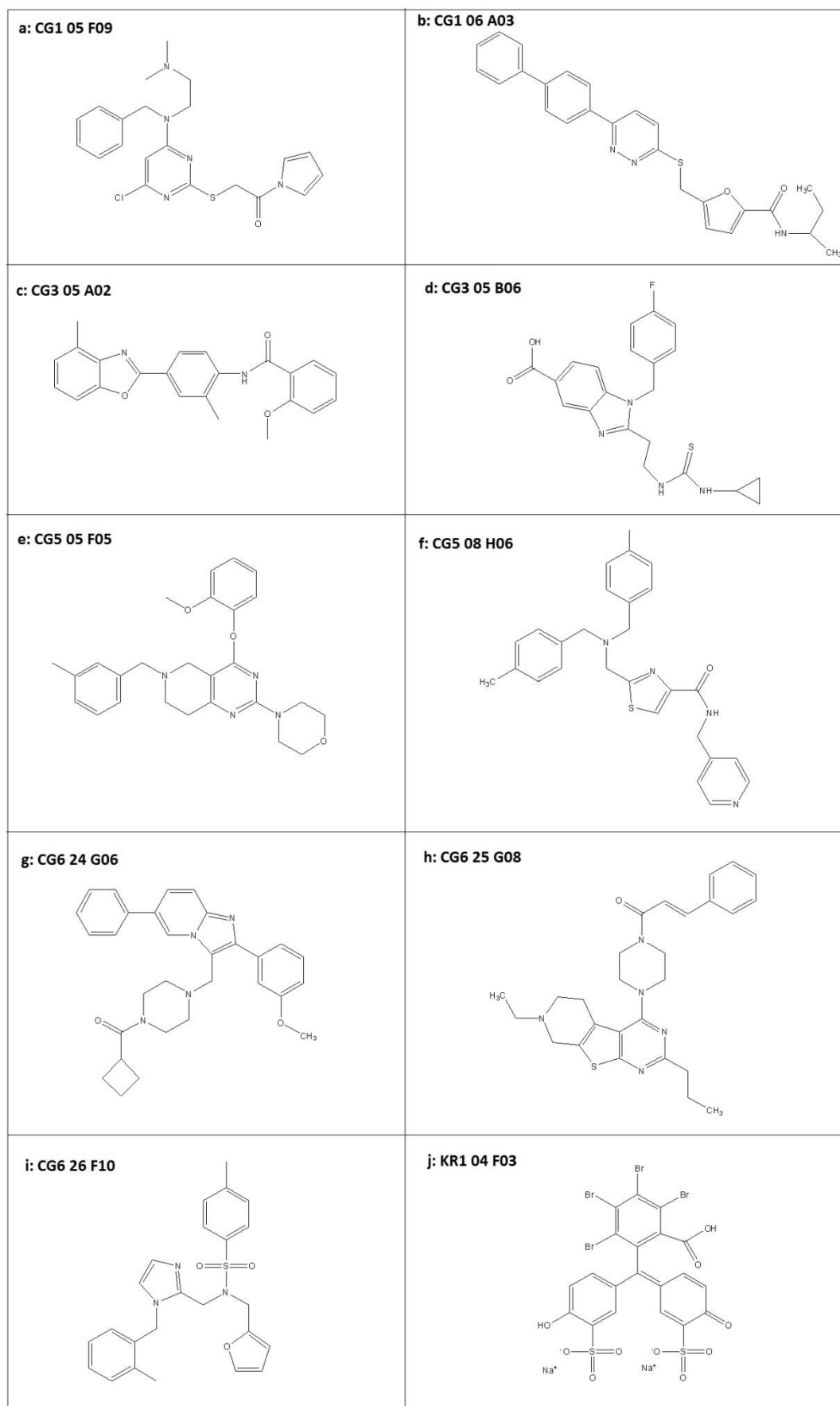


Figure 22: Structures of the 10 secondary hits. The 10 secondary hits that have been found to be active when the library stock solutions were tested are depicted here. There are no obvious structural similarities.

3.4.2 Specificity in other GEF/GTPase assays

Specificity has been tested by applying the compounds in nucleotide exchange assays using other GEF/GTPase pairs. The compounds were tested on the Sec7 domain-containing GEF ARNO and the GTPase Arf1, the Dbp homology domain-containing GEFs Vav1 and Tiam1 on the GTPases Rac1 and Rac2, and the *Legionella pneumophila* GEF DrrA and Rab1. Moreover the closely Rin1-related GEF Rabex-5 has been used to test the compounds for specificity. The GEFs ARNO and DrrA act through a mechanism similar to that of Rin1 but do not contain a catalytic Vps9 domain³². They are suitable controls to analyse specificity towards Vps9 domain-containing GEFs. Rabex-5 contains a Vps9 domain and, like Rin1, activates Rab5¹²⁸. A compound able to inhibit the Rin1-mediated Rab5 activation without interfering with the Rabex-5 GEF function would be considered highly specific. The GEFs Vav1 and Tiam1 are less related to Rin1 and built controls to analyse, whether a compound generally targets nucleotide exchange reactions on small GTPases^{216,240}. All nucleotide exchange assays were performed with Bodipy-TR-GTP in a similar way as the Rin1C/Rab5a nucleotide exchange assay. This additionally assured that compounds acting unspecific due to disturbance of the read out got sorted out during the characterization.

3.4.2.1 ARNO-Sec7 and Arf1

The 10 compounds have first been tested as triplicates at a concentration of 50 μ M with 2 % DMSO in the ARNO-Sec7-mediated nucleotide exchange assay on Arf1. The data points generated during the first 5 minutes of the kinetic measurements have been fitted linearly to calculate the slopes. These slopes have been compared to a positive control and a negative control (without ARNO-Sec7). The results are depicted in figure 23. The compounds CG1 05 F09, CG1 06 A03, CG3 05 B06, CG5 05 F05, CG6 26 F10 and KR1 04 F03 were found to inhibit the ARNO-Sec7-mediated nucleotide exchange on Arf1 and were therefore classified as unspecific. Little to no inhibitory effect could be seen for the compounds CG3 05 A02, CG5 08 H06, CG6 24 G06 and CG6 25 G08.

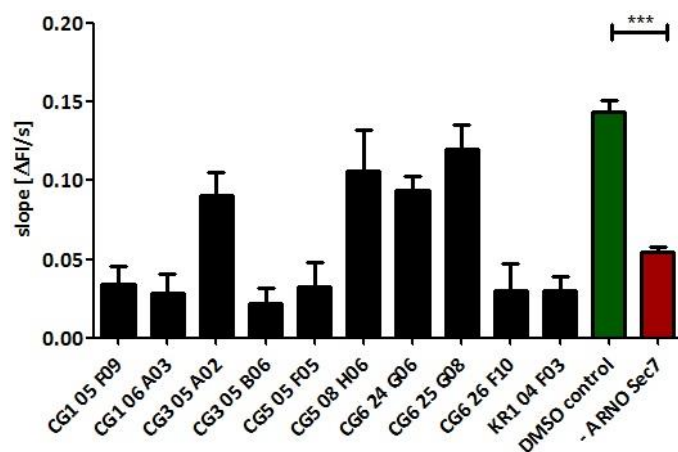


Figure 23: Specificity of the 10 secondary hits in the ARNO-Sec7/Arf1 nucleotide exchange assay. 50 μ M of each compound were tested on 100 nM ARNO-Sec7, 1 μ M Δ 17 Arf1 and 2 μ M Bodipy-TR-GTP with a final concentration of 2 % DMSO. CG1 05 F09, CG1 06 A03, CG3 05 B06, CG5 05 F05, CG6 26 F10 and KR1 04 F03 were found to inhibit the ARNO-Sec7-mediated nucleotide exchange on Arf1 while CG3 05 A02, CG5 08 H06, CG6 24 G06 and CG6 25 G08 showed little to no inhibitory effect. Pure DMSO was used in the positive control sample and the negative control lacked ARNO-Sec7. The significance was calculated by one-way ANOVA, $p < 0.05$ using GraphPad Prism software.

3.4.2.2 Vav1 and Rac1

The compound CG3 05 A02 was re-synthesized by Dr. Jeffrey Hannam from the Famulok group and CG6 25 G08 was commercially available (ChemDiv, V005-7464). The other two compounds, CG5 08 H06 and CG6 24 G06, that were found to be specific over ARNO-Sec7/Arf1, were used from the library stock solutions. The compounds were tested as triplicates at a concentration of 50 μ M with a final DMSO concentration of 2 % in the Vav1-mediated nucleotide exchange assay on Rac1. The Bodipy-TR-GTP fluorescence intensity was measured every 15 seconds and the data generated during the first 5 minutes was fitted linearly. From those fits the slopes were calculated and compared with a DMSO control and a negative control lacking Vav1. The results are depicted in figure 24. CG3 05 A02 did not inhibit the Vav1-mediated nucleotide exchange on Rac1. Slight inhibition could be found by the compounds CG6 24 G06 and CG6 25 G08. CH5 08 H06 led to a decrease in the nucleotide exchange of about 50 % and was classified as unspecific at this point.

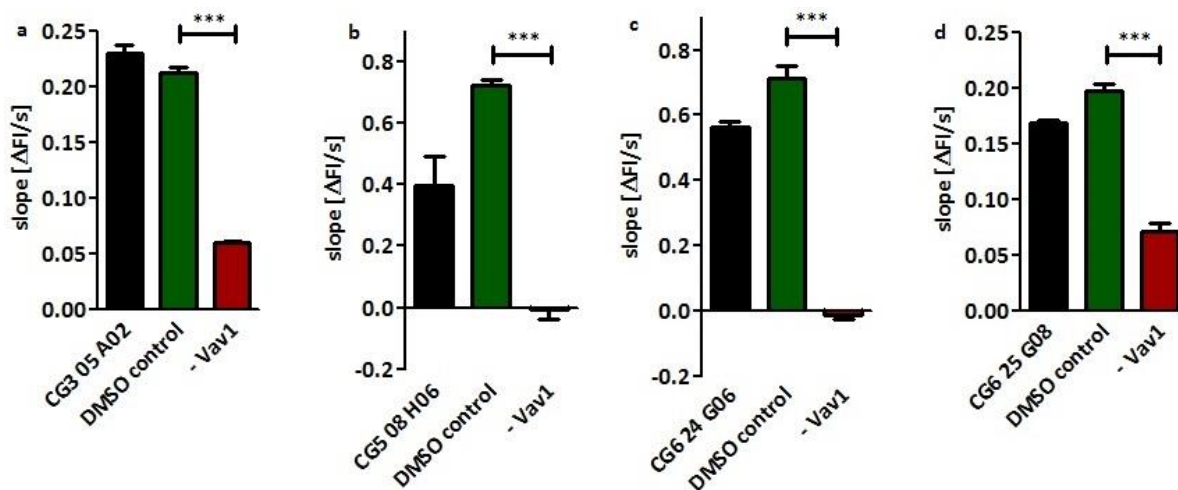


Figure 24: CG3 05 A02, CG5 08 H06, CG6 24 G06 and CG6 25 G08 in the Vav1/Rac1 nucleotide exchange assay. 50 μ M of each compound were tested on 25 nM Vav1, 1 μ M Rac1 and 2 μ M Bodipy-TR-GTP with a final concentration of 2 % DMSO. CG3 05 A02 did not show an inhibitory effect on the Vav1-mediated nucleotide exchange on Rac1. A slight inhibitory effect could be seen for the compounds CG6 24 G06 and CG6 25 G08. The compound CG5 08 H06 reduced the nucleotide exchange to about 50 % and was classified as unspecific at this point. DMSO was used in the positive control sample and the negative control lacked Vav1. The significance was calculated by one-way ANOVA, $p < 0.05$ using GraphPad Prism software.

3.4.2.3 DrrA and Rab1

Since CG5 08 H06 and CG6 24 G06 were only available in limited amounts from the library stocks, their aggregation properties were checked next as described in section 7.2.4. CG3 05 A02 and CG6 25 G08 were tested in further nucleotide exchange assays, starting with the DrrA-mediated nucleotide exchange on Rab1. 50 μ M of each compound were used as triplicates with a final assay DMSO concentration of 2 %. 25 nM DrrA and 1 μ M Rab1 have been used with 2 μ M of Bodipy-TR-GTP. The nucleotide exchange reaction was monitored by measuring the fluorescence of Bodipy-TR-GTP every 15 seconds. Data generated during the first 5 minutes was fitted linearly to calculate the slopes depicted in figure 25. No inhibitory effect on the DrrA-mediated nucleotide exchange on Rab1 could be detected for any of the compounds.

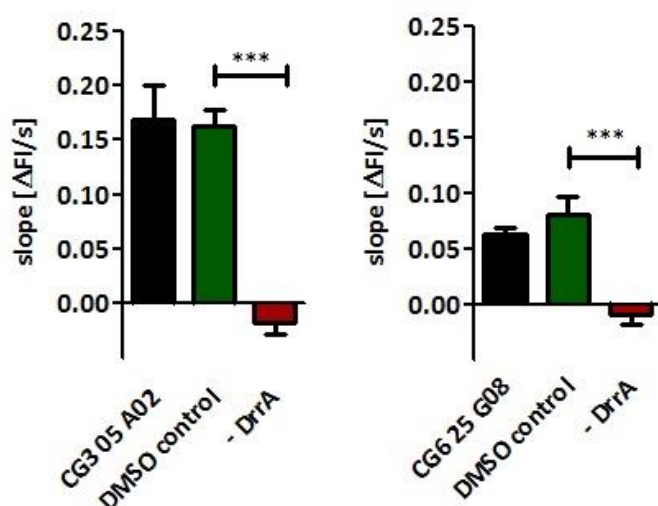


Figure 25: CG3 05 A02 and CG6 25 G08 in the DrrA/Rab1 nucleotide exchange assay. 50 μM of each compound were tested on 25 nM DrrA, 1 μM Rab1 and 2 μM Bodipy-TR-GTP with a final concentration of 2 % DMSO. No inhibitory effect could be observed for any of the compounds. DMSO was used as positive control and the negative control lacked DrrA. The significance was calculated by one-way ANOVA, $p < 0.05$ using GraphPad Prism software.

3.4.2.4 Tiam1 and Rac2

CG3 05 A02 and CG6 25 G08 were tested in the Tiam1-mediated nucleotide exchange on Rac2 next. 50 μM of each compound were used as triplicates with a final assay DMSO concentration of 2 %. 2 μM Tiam1 and 1 μM Rac1 have been used with 2 μM of Bodipy-TR-GTP. The fluorescence of Bodipy-TR-GTP was measured every 15 seconds and the data generated during the first 5 minutes was fitted linearly. The slopes of those linear fits are depicted in figure 26 and they were compared with those of a DMSO control and a negative control lacking Tiam1. No inhibition caused by any of the compounds could be observed.

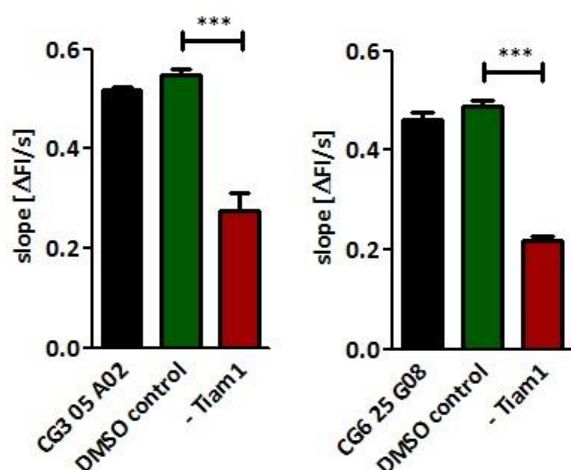


Figure 26: CG3 05 A02 and CG6 25 G08 in the Tiam1/Rac2 nucleotide exchange assay. 50 μM of each compound were tested on 2 μM Tiam1, 1 μM Rac2 and 2 μM Bodipy-TR-GTP with a final concentration of 2 % DMSO. No inhibitory effect could be seen for any of the compounds. DMSO was used as positive control and the negative control lacked Tiam1. The significance was calculated by one-way ANOVA, $p < 0.05$ using GraphPad Prism software.

3.4.2.5 Rabex-5_{GEF} and Rab5a

Lastly the compounds CG3 05 A02 and CG6 25 G08 were applied in the Rabex-5_{GEF}-mediated nucleotide exchange assay on Rab5a. 50 μ M of the compounds were tested as triplicates on 10 nM Rabex-5_{GEF} and 1 μ M Rab5a using 2 μ M Bodipy-TR-GTP and a final concentration of 2 % DMSO. DMSO has been used in the positive control sample and the negative control lacked Rabex-5_{GEF}. The Bodipy-TR-GTP fluorescence was measured every 15 seconds. The data generated during the first 5 minutes was fitted linearly to calculate the slopes depicted in figure 27. Both compounds significantly inhibited the nucleotide exchange.

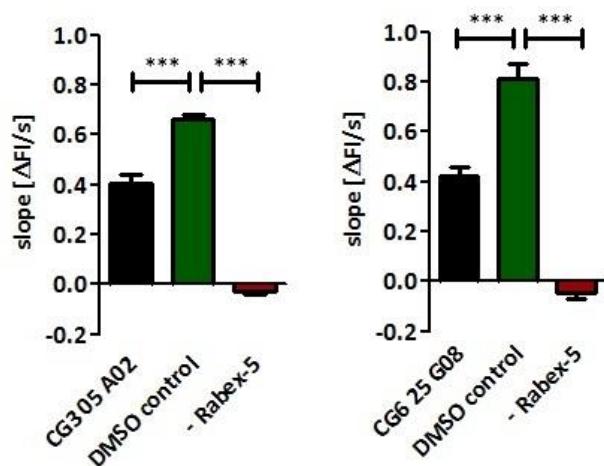


Figure 27: CG3 05 A02 and CG6 25 G08 in the Rabex-5_{GEF}/Rab5a nucleotide exchange assay. 50 μ M of each compound were tested on 10 nM Rabex-5_{GEF}, 1 μ M Rab5a and 2 μ M Bodipy-TR-GTP with a final concentration of 2 % DMSO. Both compounds significantly reduced the nucleotide exchange. DMSO was used in the positive control sample and the negative control lacked Rabex-5_{GEF}. The significance was calculated by one-way ANOVA, $p < 0.05$ using GraphPad Prism software.

3.4.3 Aggregation properties of the secondary hit compounds

Some small molecules are prone to form aggregates that may inhibit many proteins unspecifically. They form large aggregation colloids to which the proteins adsorb, making them unable to execute their functions²⁴¹. To test for aggregation, the compounds were incubated with Rin1C and Rab5a at room temperature for 20 minutes followed by centrifugation at maximum speed for 10 minutes. Afterwards the protein content of the supernatant was compared to a sample without compound addition (DMSO control). Another usual approach to test for aggregation is to apply compounds in a completely unrelated assay. In case of aggregation as the mechanism of inhibition, the compounds might also have an inhibitory effect in unrelated assays²⁴¹. Here the insulin receptor auto-phosphorylation assay has been performed to check for inhibition in an unrelated assay.

3.4.3.1 The centrifugation-based aggregation assay

In a simple centrifugation-based approach, Rin1C and Rab5a were mixed with 50 μ M of each compound and the amount of soluble protein was determined after 20 minutes of incubation. 2 % DMSO were used as a control. The compounds CG3 05 A02, CG5 08 H06, CG6 24 G06 and CG6 25 G08 were checked for their potential to aggregate with Rin1C and Rab5a and the results are depicted in the western blots shown in figure 28. An anti-His₅ primary

antibody has been used followed by incubation with a fluorescently labelled secondary antibody. The upper bands represent HT-Rin1C (~ 55 kDa) while the lower bands show HT-Rab5a (~ 21 kDa). The compound CG3 05 A02 was found not to induce aggregation of Rin1C or Rab5a (figure 28a, lane 3). About 50 % aggregation of Rin1C could be seen for CG5 08 H06 (figure 28b, lanes 3 and 4). The compounds CG6 24 G06 and CG6 25 G08 completely aggregated Rin1C (figure 28b, CG6 24 G06: lanes 5 and 7; CG6 25 G08: lanes 9 and 10). Since aggregation is likely to be unspecific and to cause promiscuous off-target inhibition, the compound CG3 05 A02 was considered the most promising candidate at this point.

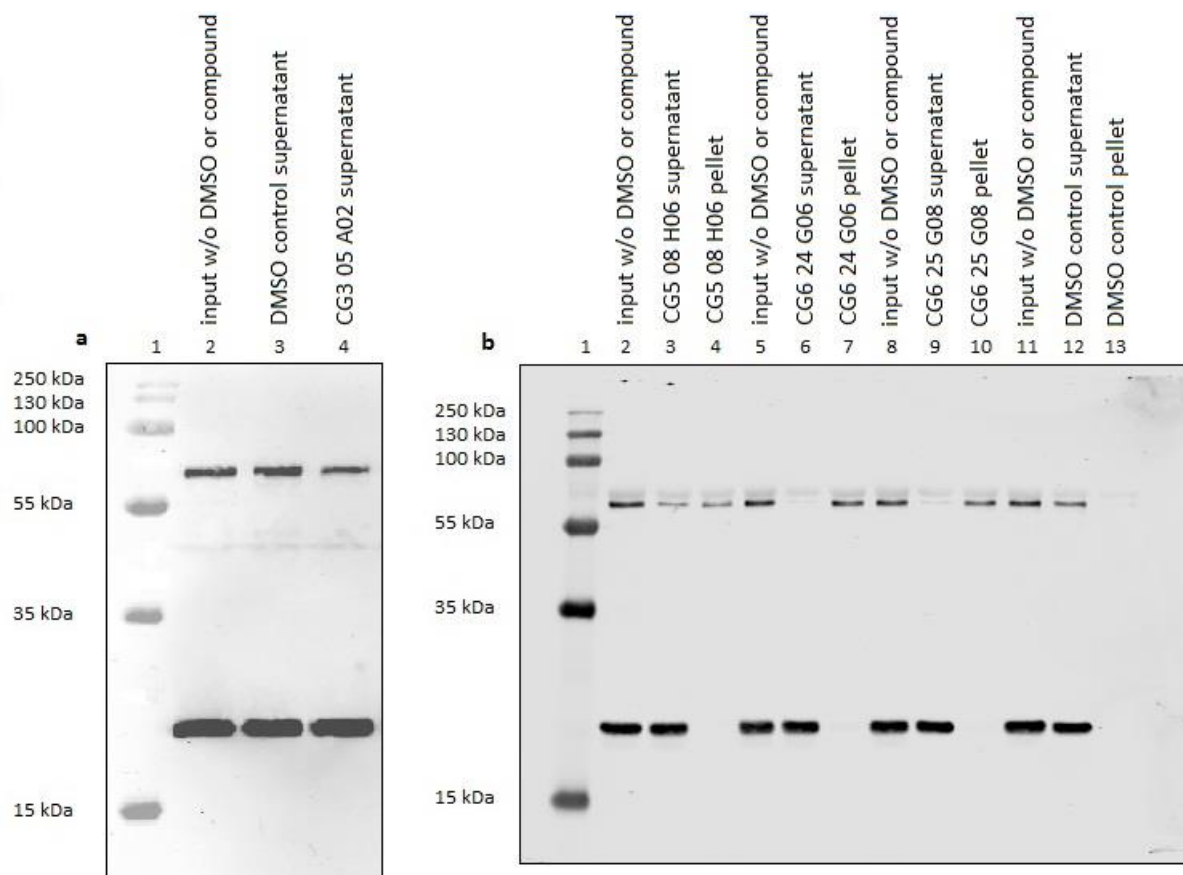


Figure 28: Aggregation properties of the compounds CG3 05 A02, CG5 08 H06, CG6 24 G06 and CG6 25 G08.

Western blots from 12.5 % SDS-PAGE gels. The proteins were histidine-tagged and visualized with an anti-His₅ primary antibody and a fluorescently labelled secondary antibody. A pre-stained molecular weight marker has been loaded in lane 1 on both blots. **a:** Aggregation assay with the compound CG3 05 A02. The initial sample before addition of compound/DMSO is shown in lane 2. Lane 3 shows the supernatant after 20 minutes of incubation with 2% DMSO and centrifugation. The sample in lane 4 represents the supernatant after 20 minutes of incubation with 50 μM CG3 05 A02 after centrifugation. Little to no difference in the amount of Rin1C (upper bands) and Rab5a (lower bands) could be seen when comparing the lanes 3 and 4. **b:** Aggregation assay with the compounds CG5 08 H06, CG6 24 G06 and CG6 25 G08. The initial samples before addition of compound/DMSO are shown in lanes 2, 5, 8 and 11. Lane 3 shows the supernatant after 20 minutes of incubation with 50 μM CG5 08 H06 and centrifugation. The corresponding pellet is shown in lane 4. About 50 % of the initial Rin1C (compare: lane 2 and lane 4) could be found in the pellet. Lane 6 shows the supernatant after 20 minutes of incubation with 50 μM CG6 24 G06 and centrifugation. The corresponding pellet is shown in lane 7. All of the initial Rin1C (compare: lane 5 and lane 7) could be found in the pellet. Lane 9 shows the supernatant after 20 minutes of incubation with 50 μM CG6 25 G08 and centrifugation. The corresponding pellet is shown in lane 10. Again all of the initial Rin1C (compare: lane 8 and lane 10) could be found in the pellet. The DMSO control is depicted in lane 12 (supernatant) and lane 13 (pellet). DMSO did not cause any aggregation as none of the proteins could be found in the pellet.

3.4.3.2 The insulin receptor auto-phosphorylation assay

The insulin receptor auto-phosphorylation assay has been used as an additional control to supposedly exclude aggregation as possible mechanism of inhibition. The ATP-dependent auto-phosphorylation of the insulin receptor intracellular domain (IR-ICD) has been monitored after 0, 20 and 60 seconds in presence and absence of 50 μ M of the compound CG3 05 A02. The phosphorylation has afterwards been visualized on a western blot using an anti-phospho-tyrosine antibody followed by a fluorescently labelled secondary antibody. Figure 29 shows the total amount of IR-ICD on a coomassie stained SDS-PAGE gel (a) and the degree of phosphorylation on a western blot (b) in samples without treatment, treated with DMSO and treated with CG3 05 A02. The compound had no effect on the IR-ICD auto-phosphorylation when compared to both controls. This argues against promiscuous unspecific aggregation around proteins as the mechanism of inhibition.

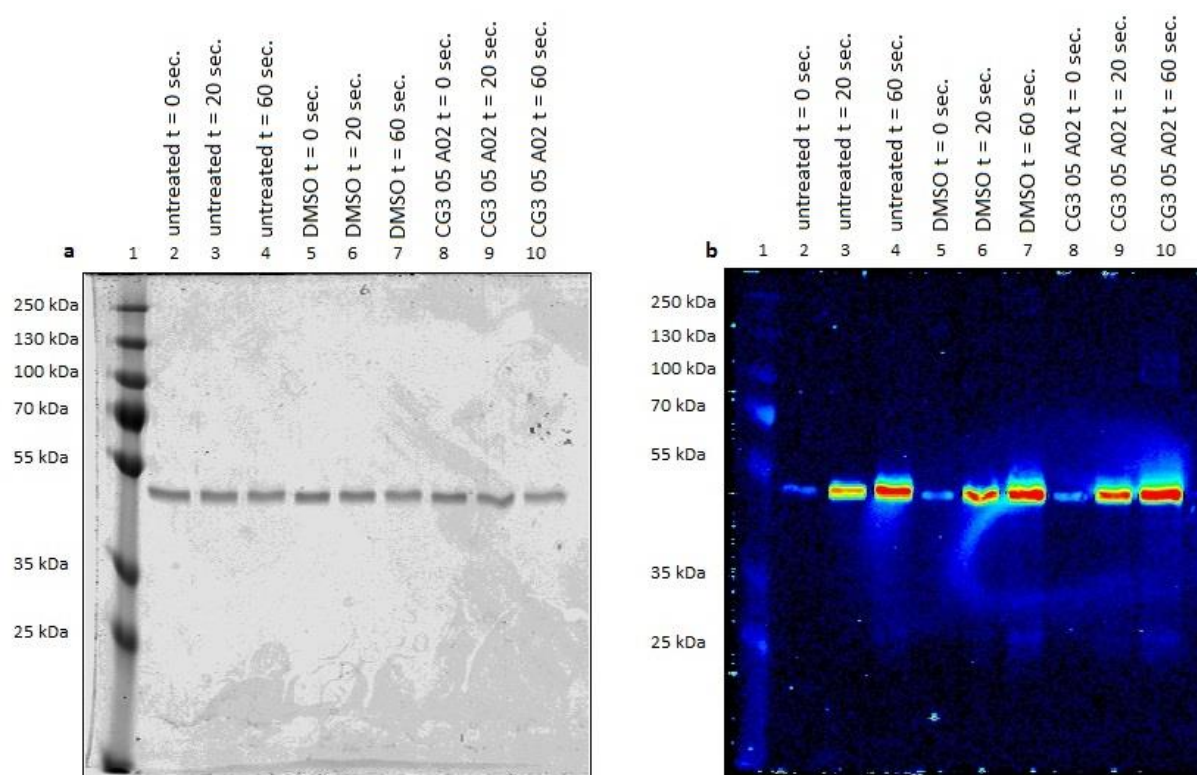


Figure 29: IR-ICD auto-phosphorylation assay in presence and absence of CG3 05 A02. **a:** 10 % SDS-PAGE gel stained with coomassie brilliant blue. A pre-stained molecular weight marker has been loaded in lane 1. The gel shows that equal amounts of IR-ICD (\sim 46 kDa) have been loaded (lanes 2 – 10). **b:** Western blot from a 10 % SDS-PAGE gel. An anti-phospho-tyrosine primary antibody has been used followed by incubation with a fluorescently labelled secondary antibody. A pre-stained molecular weight marker has been loaded in lane 1. The lanes 2, 3 and 4 show the auto-phosphorylation of untreated IR-ICD after 0, 20 and 60 seconds, respectively. In the lanes 5, 6 and 7 the auto-phosphorylation after 0, 20 and 60 seconds of the samples treated with DMSO is shown. The auto-phosphorylation after 0, 20 and 60 seconds of the samples treated with CG3 05 A02 is shown in lanes 8, 9 and 10. No difference in the degree of auto-phosphorylation could be seen for the samples treated with CG3 05 A02 in comparison to the controls.

3.4.4 Purity of CG3 05 A02

The purity of the CG3 05 A02 library stock was checked using HPLC-MS before re-synthesis to ensure the inhibitory effect stems from the compound expected to be present in the library.

0.1 mg/mL of the compound diluted in 10 % acetonitrile was subjected to a C18 reversed phase column and the eluate was analysed by MS (figure 30b). The library stock was found to be 81.4 % pure (peak 14, figure 30a) with a mass of 373.3 g/mol [CG3 05 A02 + H⁺]. The mass 431 g/mol could not be assigned to a structure and 767.5 g/mol most likely stemmed from [2 x CG3 05 A02 + Na⁺]. The theoretical mass of CG3 05 A02 was calculated to be 372.42 g/mol.

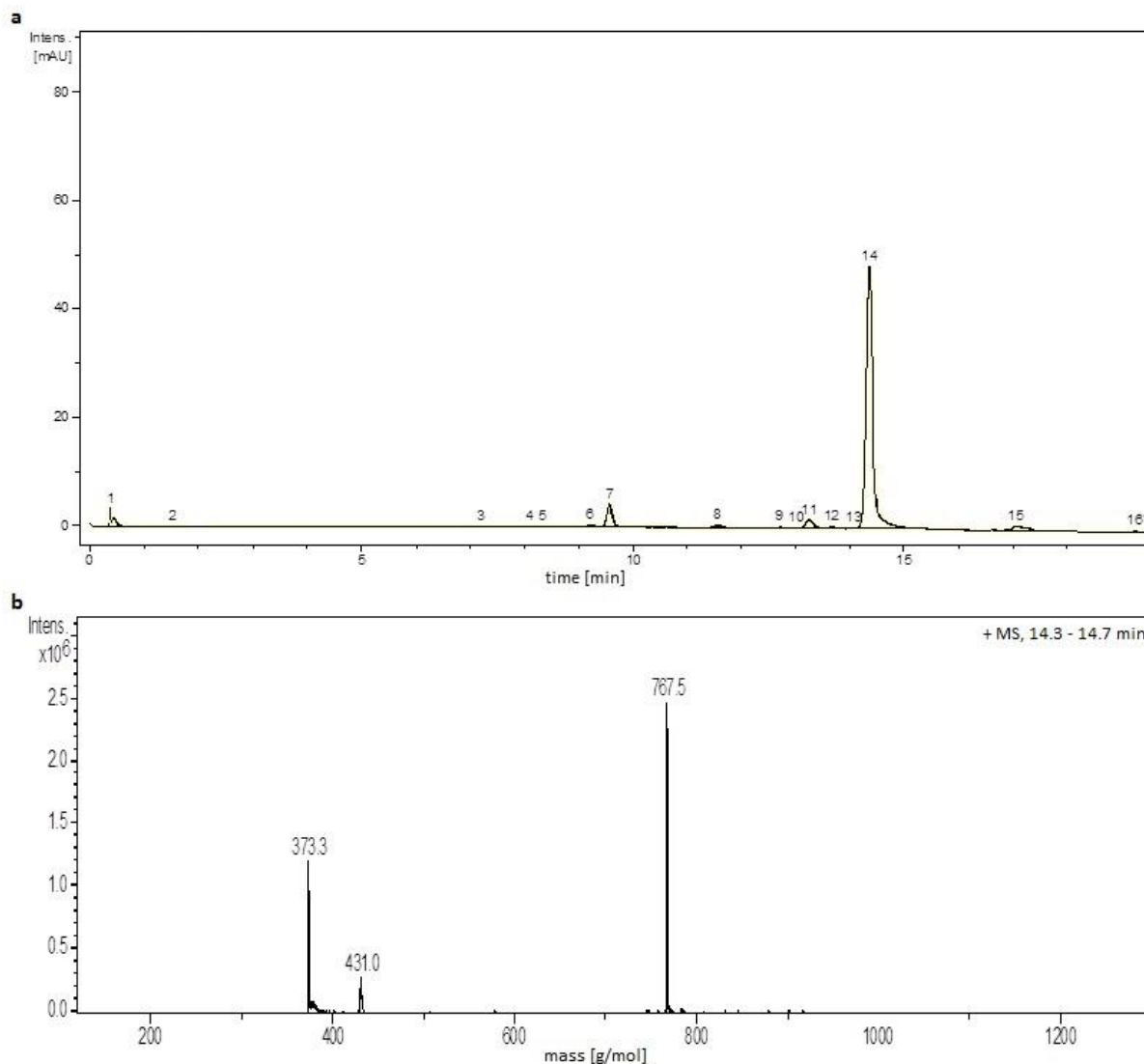


Figure 30: HPLC-MS analysis of the compound CG3 05 A02. **a:** HPLC chromatogram of the library stock. Several peaks could be found. The main peak (14) covers 81.4 % of the area under all peaks. **b:** MS analysis of peak 14. The chromatogram covers the masses found between 14.3 and 14.7 minutes during the HPLC run. Three masses could be found. 373.3 g/mol likely corresponded to the compound (theor. mass: 372.42 g/mol) [CG3 05 A02 + H⁺], 431 g/mol could not be assigned to a structure and 767.5 g/mol most likely stemmed from [2 x CG3 05 A02 + Na⁺].

3.4.5 Solubility of CG3 05 A02

Solubility of the compound was measured in a photometric approach on the NanoDrop 2000. The absorption maximum of CG3 05 A02 was determined in a spectral measurement using the compound at a concentration of 50 µM in buffer and was found to be at 350 nm. The compound was diluted in buffer in concentrations ranging from 1.6 – 200 µM with a

final DMSO concentration of 2 %. The absorption of the supernatant before and after centrifugation is shown in table 4. The compound was found to be insoluble at concentrations > 2.3 μM .

Table 4: Determination of the solubility of CG3 05 A02.

Concentration [μM]	A ₃₅₀ before centrifugation	A ₃₅₀ after centrifugation
200	0.148	0.001
150	0.156	0.001
100	0.135	0.000
75	0.118	0.002
50	0.070	0.003
37.5	0.074	0.002
25	0.056	0.000
18.75	0.044	- 0.001
12.5	0.030	0.001
9.4	0.026	0.003
6.25	0.020	0.003
4.7	0.017	0.001
3.13	0.013	0.002
2.3	0.010	0.008
1.6	0.008	0.005

3.4.6 Structure activity relationship of CG3 05 A02

Several derivatives of the compound CG3 05 A02 have been synthesized by Dr. J. Hannam from the Famulok group to examine the structure activity relationship. The analytical data for CG3 05 A02 and the derivatives can be found in section 7.2.8. Single functional groups have been removed, exchanged or repositioned and the inhibitory activity was checked in the kinetic Rin1C/Rab5a Bodipy-TR-GTP nucleotide exchange assay. The compounds were tested in different concentrations between 0.1 and 200 μM . If the derivatives had an inhibitory effect, the IC₅₀ was determined as described in section 3.4.1 and compared to that of the original structure. Table 5 summarizes the structures of the derivatives, the IC₅₀ values and the 95 % confidence intervals. The raw data used for linear fitting and the slopes plotted against the logarithmic compound concentrations can be found in section 8.4.2 in the appendix.

Table 5: Structure activity relationship of the compound CG3 05 A02.

Name	Structure	IC ₅₀ [μM]	95 % CI [μM]
CG3 05 A02		35.4	24.3 – 46.5
010A		n. i.	n. i.

066A		n. i.	n. i.
068A		28.9	21.7 – 38.5
071A		n. i.	n. i.
099A		n. i.	n. i.
103A		85.8	80.0 – 92.0
137B		21.3	17.3 – 26.2
146A		n. i.	n. i.

148A		n. i.	n. i.
160A		n. i.	n. i.
162A		63.5	56.0 – 72.0
163A		n. i.	n. i.
165A		38.8	32.1 – 46.9
166A		72.9	64.9 – 81.9
167A		138.8	127.6 – 151.1
170A		23.7	18.5 – 30.4
179A		n. i.	n. i.

The core structure of CG3 05 A02 that comprises four ring structures, a secondary amine and a ketone group has been conserved in all compounds. The compound was modified at the positions of the methyl- and methoxy groups attached to the heterocycle and the phenyl rings. Deletion of both methyl groups and the methoxy group as in compound 163A led to complete loss of the inhibitory effect. Deletion of either one of the methyl groups as in the compounds 165A and 170A did not affect the inhibition but deletion of both at the same time (compound 162A) led to an IC_{50} about two fold higher compared to the original structure. Removing the methoxy group in combination with either one of the methyl groups (compounds 166A and 167A) led to a 2 – 5-fold higher IC_{50} . A complete loss of inhibitory potential resulted from elimination of only the methoxy group as in compound 160A. The same was the case if the position of this group on the ring has been changed (compounds 179A and 010A). This led to the assumption, that the methoxy group might be needed to perform a ring closure with the secondary amine to unfold the full inhibitory effect. To test this hypothesis, compound 066A has been synthesized with a methyl group attached to the nitrogen originally employed in the secondary amine. This compound did not inhibit the Bodipy-TR-GTP nucleotide exchange. The collected results pointed towards a tolerance for changes at the position of the methyl group on the heterocycle. Two compounds with different groups at this position have been synthesized: 137B with a hydroxyl group and 068A with a methoxy group. Both groups did not influence the inhibition but they also did not improve the solubility (data in the appendix in section 8.5). This position has then been picked to try to attach a fluorescein label for binding studies via different linkers. First the compound has been modified with the linkers and tested for inhibition in the Bodipy-TR-GTP nucleotide exchange assay. Attachment of a *tert*-butyloxycarbonyl protecting group with a long linker led to loss of the inhibitory effect (compound 071A). The compound 103A with a shorter linker and a *tert*-butyloxycarbonyl protecting group had an IC_{50} about three times higher than CG3 05 A02. However, de-protection and fluorescein labelling resulted in the completely inactive compound 148A. The approach to use an ethanolamine group as linker to attach the fluorophore as in compound 146A also eliminated the inhibitory effect. In a final labelling approach the short linker with the *tert*-butyloxycarbonyl protecting group has been attached at the position of the methoxy group (compound 099A) but this structure also proved to be inactive.

3.4.7 Influence of CG3 05 A02 on the ABL1-mediated Rin1 phosphorylation

The screening was performed with Rin1C – a construct lacking the ABL kinase interaction site of Rin1. This made an influence of the compound CG3 05 A02 on the ABL1-mediated Rin1 phosphorylation unlikely. Nevertheless an ABL1/Rin1 phosphorylation assay has been performed to ensure the compound does not have a domain-unspecific effect on the ABL1-Rin1 interaction. Rin1-TS and ABL1-6 x His have been incubated with ATP and the compound at a concentration of 50 μ M. The phosphorylation state of both proteins has been analysed after 0, 1 and 15 minutes on a Western blot using an anti-phospho-tyrosine antibody followed by a fluorescently labelled secondary antibody. Figure 31 shows the total and equally loaded amounts of ABL1-6 x His (~ 125 kDa) and Rin1-TS (~ 89 kDa) on a coomassie stained SDS-PAGE gel (a) and the degree of phosphorylation on a western blot (b) in samples without treatment, treated with DMSO and treated with CG3 05 A02. Both proteins notably behaved untypically in the SDS-PAGE. They ran much higher than expected when compared to the molecular weight marker. This can be caused by certain hydrodynamic properties held by non-globular proteins. The compound had no effect on the phosphorylation of Rin1-TS.

This argues against a domain-unspecific inhibitory effect of the compound CG3 05 A02 on the proline rich region of Rin1. An increase in ABL1-6xHis auto-phosphorylation could not be detected during this assay.

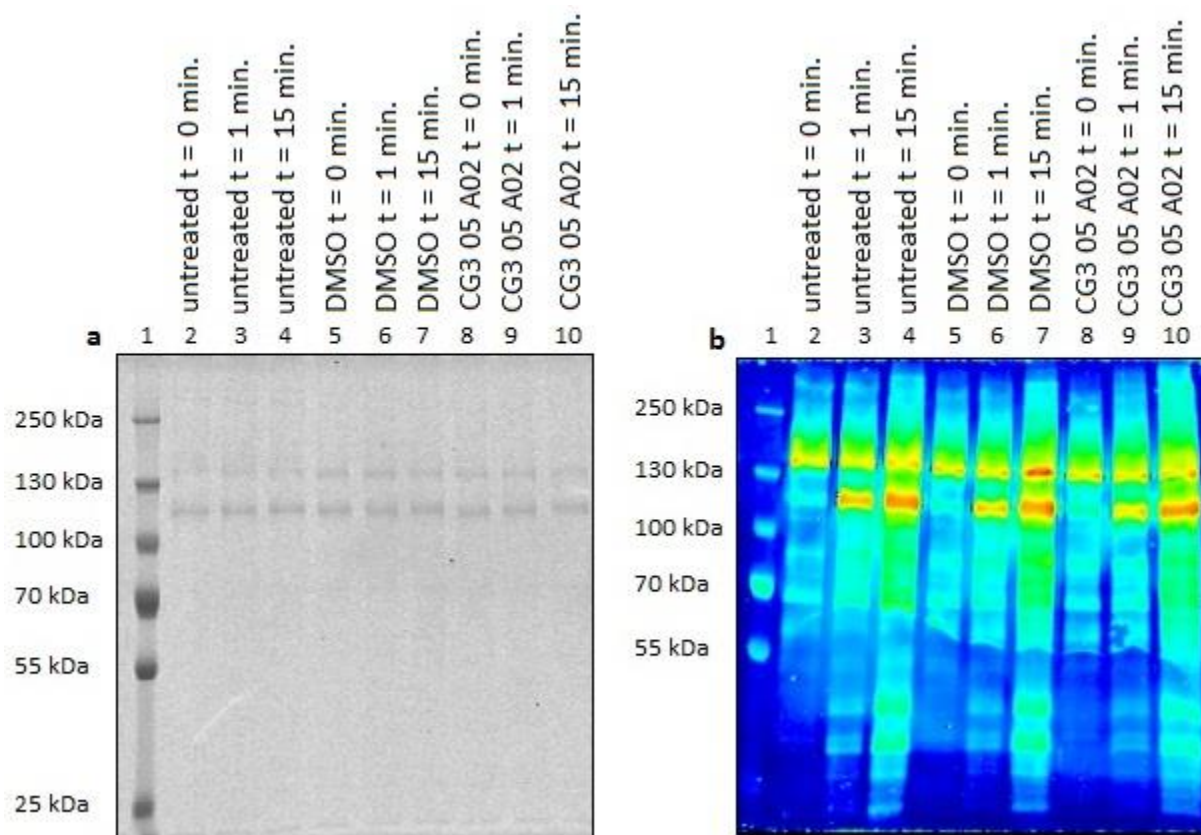


Figure 31: The ABL1-mediated Rin1 phosphorylation assay in presence and absence of CG3 05 A02. **a:** 8 % SDS-PAGE gel stained with coomassie brilliant blue. A pre-stained molecular weight marker has been loaded in lane 1. The gel shows that equal amounts of HT-ABL1 (~ 125 kDa) and Rin1-TS (~ 89 kDa) have been loaded (lanes 2 – 10). **b:** Western blot from an 8 % SDS-PAGE gel. An anti-phospho-tyrosine primary antibody has been used followed by incubation with a fluorescently labelled secondary antibody. A pre-stained molecular weight marker has been loaded in lane 1. The lanes 2, 3 and 4 show the phosphorylation of untreated HT-ABL1 and Rin1-TS after 0, 1 and 15 minutes, respectively. In the lanes 5, 6 and 7 the samples treated with DMSO for 0, 1 and 15 minutes are shown. The samples treated with CG3 05 A02 for 0, 1 and 15 minutes are shown in lanes 8, 9 and 10. No difference in the degree of Rin1-TS phosphorylation could be seen for the samples treated with CG3 05 A02 in comparison to the controls. HT-ABL1 auto-phosphorylation could not be seen in this assay.

3.4.8 Influence of CG3 05 A02 on Bodipy-TR-GTP binding to Rab5a

The influence of CG3 05 A02 on Bodipy-TR-GTP binding GEF-independently to Rab5a was analysed to gain insights on the mechanism of inhibition employed by the compound. Based on the setup of the screening assay it could not be estimated, whether it interacts with Rin1C and Rabex-5_{GEF}, with the complex between them and Rab5a or GTP-competitively with Rab5a alone. To investigate possible GTP-competitive binding, Rab5a was loaded with Bodipy-TR-GTP in the absence of a nucleotide exchange factor by treatment with EDTA as described in section 7.2.7 in presence of different concentrations of CG3 05 A02. During the 15 minutes of incubation the Bodipy-TR-GTP fluorescence was measured at 595 nm (excitation) and 620 nm (emission) and a linear fit was applied on the data generated in the first 100 seconds. The slopes were calculated and compared to that of a DMSO control. In

case of reduced Bodipy-TR-GTP binding, a decrease in steepness was to be expected. The results are depicted in figure 32. No concentration-dependent effect on the Bodipy-TR-GTP binding to Rab5a could be determined in presence of the compound. The raw data used for fitting, as well as an extended interpretation, can be found in the appendix in section 8.6.

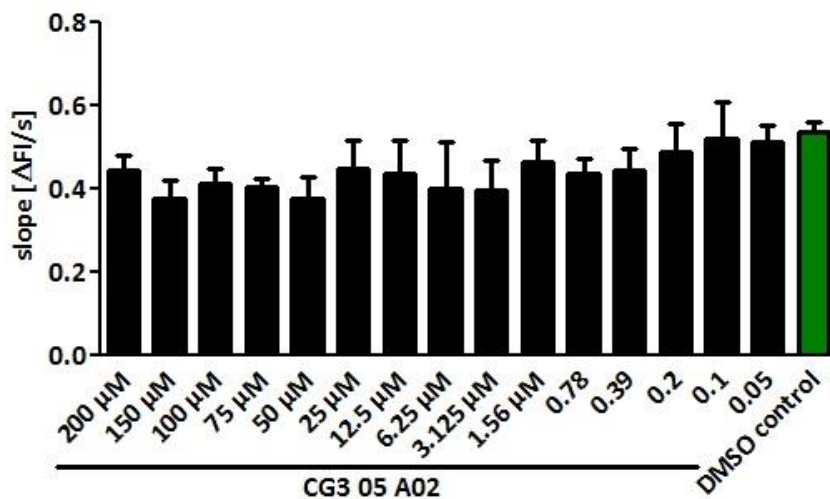


Figure 32: Influence of CG3 05 A02 on Bodipy-TR-GTP binding to Rab5a. Rab5a was loaded with Bodipy-TR-GTP in presence of CG3 05 A02 concentrations between 0.05 and 200 μ M. The Bodipy-TR-GTP fluorescence was measured over 15 minutes and a linear fit was applied to the data generated during the first 100 seconds. From those fits the depicted slopes were calculated and compared to that of a DMSO control. There was no significant difference between any of the samples in comparison to the control. The significance was calculated by one-way ANOVA, $p < 0.05$ using GraphPad Prism software.

3.4.9 CG3 05 A02 in the Rin1C/Rab5a Bodipy-FL-GTP nucleotide exchange assay

To exclude that the inhibitory effect of CG3 05 A02 in the Rin1C/Rab5a Bodipy-TR-GTP nucleotide exchange assay is artificially related to the use of Bodipy-TR-GTP, the GTP analogue Bodipy-FL-GTP has been used in another nucleotide exchange assay. Bodipy-FL is a smaller fluorophore attached via an aminoethylcarbamoyl linker to the 2' or 3' position of the GTP ribose ring. The fluorescence of Bodipy-FL-GTP may increase upon interaction with GTP-binding proteins and could be measured at 490 nm (excitation) and 520 nm (emission)²³¹. Bodipy-FL-GTP was used in a 1-fold excess over Rab5a. CG3 05 A02 was tested as triplicates in concentrations between 0.025 and 200 μ M. Figure 33 shows the structure of Bodipy-FL-GTP (a) as well as the concentration-dependent inhibition of the Bodipy-FL-GTP nucleotide exchange by CG3 05 A02 (b). The fluorescence intensity of Bodipy-FL-GTP has been measured every 15 seconds and the data generated during the first 5 minutes was fitted linearly to calculate the slopes depicted in figure 33b. The IC_{50} and the Hill coefficient were determined using GraphPad Prism software. The IC_{50} measured here was about seven times higher compared to that measured in the Bodipy-TR-GTP nucleotide exchange assay (cp. section 3.4.1). Thus, additional controls had to be performed to survey and ensure the inhibitory effect of the compound CG3 05 A02. The raw data used for linear fitting can be found in section 8.4.3 in the appendix.

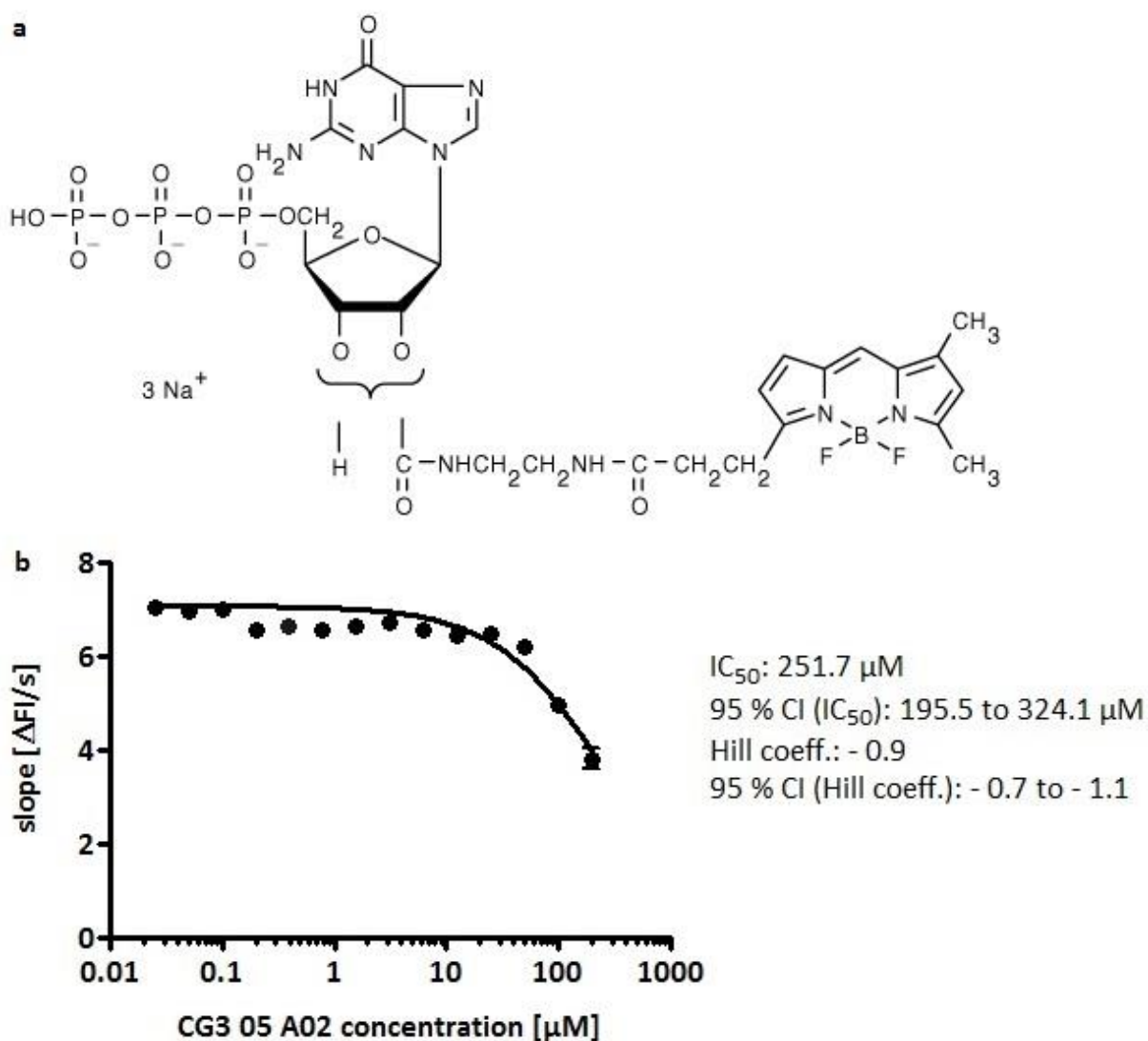


Figure 33: CG3 05 A02 in the Rin1C/Rab5a Bodipy-FL-GTP nucleotide exchange assay. **a:** Structure of Bodipy-FL-GTP. In the mixed-isomer analogue the fluorophore is attached to the 2' or 3' position on the ribose ring via an aminoethylcarbamoyl linker. **b:** Concentration-dependent inhibition of the Rin1C/Rab5a Bodipy-FL-GTP nucleotide exchange assay by the compound CG3 05 A02. The Rin1C-mediated nucleotide exchange on Rab5a was monitored as an increase in fluorescence intensity signal over time. A linear fit has been applied on the data collected during the first 5 minutes of the measurement to calculate the depicted slopes dep. The IC₅₀ and the Hill coefficient are given with the 95 % confidence intervals.

3.4.10 CG3 05 A02 in the Rin1C/Rab5a Bodipy-FL-GDP release assay

The Bodipy-FL-GDP release assay has been employed as an additional control to ensure the inhibitory effect of the compound CG3 05 A02 on the Rin1C-mediated nucleotide exchange on Rab5a. The compound was tested as triplicates in concentrations between 0.05 and 200 μM with a final DMSO concentration of 2 %. Rab5a has been pre-loaded with Bodipy-FL-GDP before addition of Rin1C and GTP. The Bodipy-FL-GDP release was measured every 15 seconds as a decrease in fluorescence intensity at 490 nm (excitation) and 520 nm (emission). Data generated during the first 5 minutes have been fitted linearly and the slope of each curve was calculated and plotted against the logarithmic compound concentration. The results are shown in figure 34. The IC₅₀ estimated here was about six times higher compared to that measured in the Bodipy-TR-GTP nucleotide exchange assay (cp. section

3.4.1). Since the use of two different fluorophores resulted in contradicting data, a fluorescence-independent assay had to be performed as a more native-like control to exclude artificial effects that could originate from the use of fluorophore labels. The raw data used for linear fitting can be found in section 8.4.4 in the appendix.

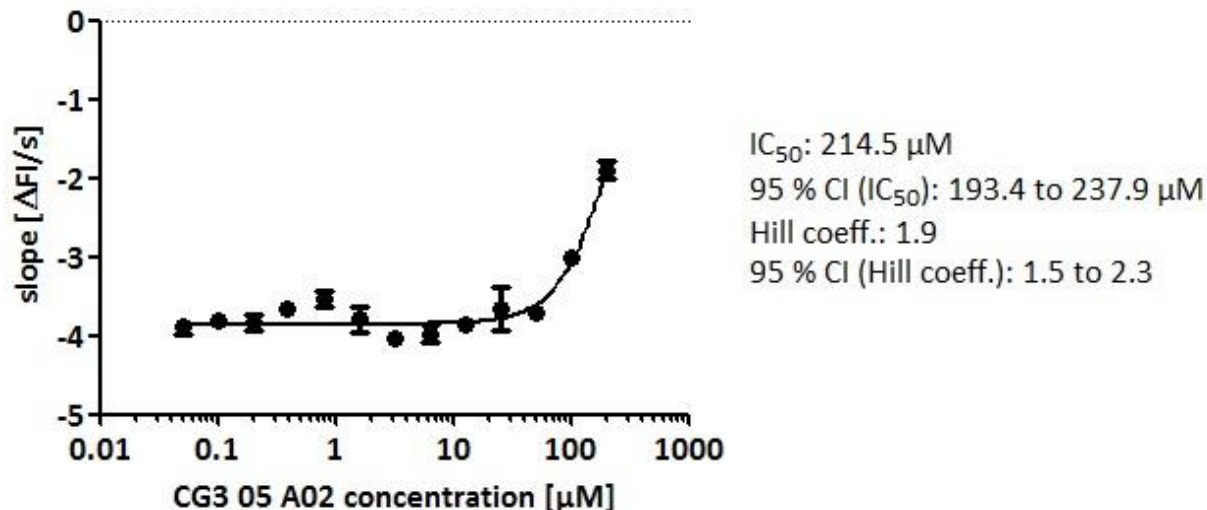


Figure 34: CG3 05 A02 in the Rin1C/Rab5a Bodipy-FL-GDP release assay. Concentration-dependent inhibition of the Rin1C/Rab5a Bodipy-FL-GDP release assay by the compound CG3 05 A02. Rab5a has been pre-loaded with Bodipy-FL-GDP prior to the addition of Rin1C and excess GTP. The Rin1C-mediated nucleotide exchange on Rab5a was monitored as a decrease in fluorescence intensity signal over time when Rab5a-bound Bodipy-FL-GDP got released. A linear fit has been applied on the data collected during the first 5 minutes of the measurement to calculate the depicted slopes. The IC_{50} and the Hill coefficient are given with the 95 % confidence intervals and could merely be estimated, since the concentration range of the IC_{50} was not covered during the measurement..

3.4.11 CG3 05 A02 in the [α - ^{32}P]-GTP nucleotide exchange assay

GTP labelled with radioactive ^{32}P in the α -position has been used in a Rin1C/Rab5a nucleotide exchange assay to perform a more native-like control. The results using two different fluorescence-labelled GTP analogues have been contradictory (cp. sections 3.4.1 and 3.4.9), suggesting one data set to be erroneous. Therefore a fluorescence-independent approach has been necessary to survey the inhibitory effect of the compound CG3 05 A02. The compound has been tested as triplicates in concentrations between 1.56 and 100 μM . The amount of Rab5a-bound [α - ^{32}P]-GTP was analysed by filter binding and scintillation counting after 20 minutes of incubation with Rin1C. The results were compared to a DMSO control and a negative control lacking Rin1C as depicted in figure 35. No concentration-dependent inhibition of the nucleotide exchange by CG3 05 A02 could be seen.

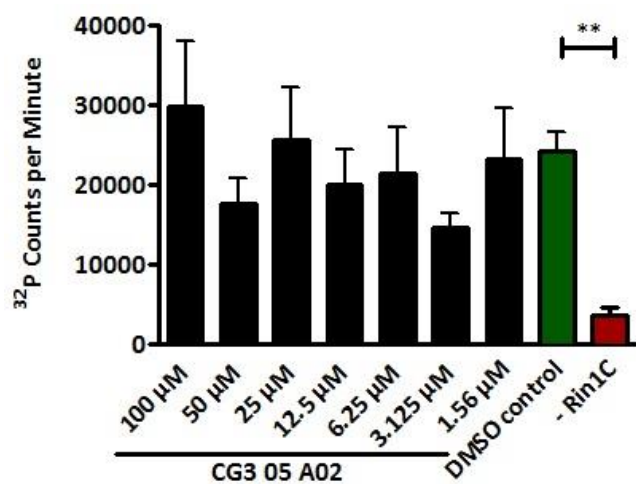


Figure 35: CG3 05 A02 in the $[\alpha\text{-}^{32}\text{P}]\text{-GTP}$ exchange assay. The compound was used in concentrations between 1.56 and 100 μM on Rin1C and Rab5a in presence of excess nucleotide. After 20 minutes the amount of protein-bound $[\alpha\text{-}^{32}\text{P}]\text{-GTP}$ was measured by filter binding and scintillation counting. 2 % DMSO have been used in the positive control sample and the negative control lacked Rin1C. No concentration-dependent inhibition by the compound CG3 05 A02 could be seen. The significance was calculated by one-way ANOVA, $p < 0.05$ using GraphPad Prism software.

4 Discussion

Small molecule modulators have proven to be powerful tools to study the functions and interactions of proteins *in vitro* and *in vivo*. This project aimed on the identification of a small molecule inhibitor of the Rin1-mediated Rab5 activation. Ten secondary hits were found in an *in vitro* HTS approach using a fluorescently labelled GTP analogue. During the characterization of those molecules the compound CG3 05 A02 turned out to be the most specific and aggregation seemed unlikely to be the cause of inhibition. Further controls revealed that the compound was only active under certain conditions.

4.1 Protein expression and purification

Several proteins had to be expressed and purified to perform the experiments performed during this project. In the beginning active Rab5a and Rin1C needed to be purified to establish the screening assay and perform the high throughput screening (HTS). To test for specificity of the resulting hit compounds, other GTPases and GEFs have been purified: Rab5a/Rabex-5_{GEF}, Rab1/DrrA, Rac2/Tiam1DHPH and Rac1/Vav1. Strep-tagged full length Rin1 (Rin1-TS) was purified to study the effects of the hit compound on the Rin1/ABL1 interaction. All constructs could successfully be purified and were found to be active in the desired assays. However, there were several issues with the expression and purification of Rin1 constructs.

4.1.1 Rin1 constructs could only be retrieved from *Sf9* insect cells

After failing to purify a Rin1 construct similar to Rabex-5_{GEF} in *E. coli* and *Sf9* insect cells, His-tagged Rin1C was purified from *Sf9* insect cells as described in Tall, 2001¹⁰², followed by an additional gel filtration step to increase the purity. Yin Dongsheng from the Famulok group simultaneously tried to express and purify several different shorter Rin1 constructs in *E. coli* as well as in *Sf9* cells over the last years but all his efforts to retrieve a shorter construct failed. Aim of his approach was to generate a construct covering only the minimal motif necessary for Rin1-GEF activity. By now Rin1C is still the shortest GEF-active construct. Rin1C could be enriched in the Ni-NTA affinity chromatography and eluted in fractions 14-22 during the gel filtration. The sample contained several impurities that could not be separated from the target protein during the purification process. Especially two strong bands could be found that corresponded to proteins with molecular weights between 15 and 25 kDa. Those two bands were detected in every HT-Rin1C purification attempt and they most likely contained degradation products of the target protein itself. HT-Rin1C has a molecular weight of approx. 55 kDa. However, it notably behaved untypically during SDS-PAGE, running considerably above the 55 kDa marker band. This behaviour can be caused by posttranslational modifications or the proteins folding and the resulting hydrodynamic properties. Since the impurities could not be further separated and HT-Rin1C was found to be active after the purification (cp. section 3.2), the quality was decided to be sufficient to perform the screening.

Moreover a small amount of full-length Rin1-TS has been purified, again from baculovirus-infected *Sf9* insect cells. 24.1 µg were yielded from a 10 mL culture. The 89.4 kDa protein of interest was mainly pure, containing only a few traces of impurities. Noticeably similar low molecular weight impurities as during the purification of Rin1C could be found. This further

supported the hypothesis that they might originate from Rin1 itself. A small amount of Rin1-TS appeared to be insoluble as it could be found in the cell debris fraction after clearance of the lysate. Moreover some amount was lost during the Streptavidin affinity binding. There, unbound Rin1-TS could be found in the flow-through fraction. This might have been avoidable by using a larger amount of Streptavidin resin to circumvent saturation. Nevertheless the yield was high enough to perform the ABL1-mediated Rin1-phosphorylation assay.

4.2 All constructs were found to be active in nucleotide exchange assays

The activity of the purified proteins was subsequently determined. Therefore the nucleotide exchange activity of the GEFs was assayed in different GEF concentrations on the corresponding GTPases. It was aimed to find conditions that allow testing of the hit compounds after the screening. A critical point here was the intrinsic nucleotide exchange activity of the GTPases. Strong intrinsic nucleotide exchange activity can lead to a small measurement window between the samples with and without GEF, making it hard to observe a potential concentration-dependent inhibition.

The intrinsic nucleotide exchange activity of Rab5a was reported to be relatively low. Tall et al. observed about 20 % nucleotide exchange in 30 minutes in absence of a GEF¹⁰². Using Bodipy-TR-GTP and Rab5a no nucleotide exchange could be detected in absence of Rin1C or Rabex-5_{GEF}. This might have been caused by a lower affinity of Rab5a for Bodipy-TR-GTP compared to GTP.

For Rab1 only about 5 – 10 % Bodipy-TR-GTP association within 20 minutes could be seen in absence of DrrA.

The strongest intrinsic Bodipy-TR-GTP binding capacity was seen for Rac2. Even in absence of Tiam1DHPH about 55 % of Bodipy-TR-GTP bound to Rac2 within 20 minutes. Similar results have already been obtained for GTP by B. Niebel from the Famulok group during an earlier project²⁴².

Approximately 45 % of intrinsic Bodipy-TR-GTP binding within 20 minutes could be seen for Rac1. This was contradictory to the < 10 % intrinsic GTP binding observed by B. Niebel²⁴².

Likewise results were found for Arf1. The approximately 50 % of intrinsic nucleotide exchange activity within 20 minutes observed when Bodipy-TR-GTP was used dissented from data observed by B. Weiche from the Famulok group, who only found about 20 % of intrinsic nucleotide exchange when using GTP²⁴³. A phenomenon like this has been discussed extensively in Goody, 2014²⁴⁴. Here the author elaborates how fluorescently labelled GTP analogues can bind to GTPases in absence of a GEF, even when they have a lower affinity compared to GDP and GTP. By simple considerations of equilibria it becomes clear why the analogues can bind to GTPases, depending of course on the concentrations of GTPase, GDP and GTP-analogue used in an experiment. From this it also becomes apparent that intrinsic nucleotide exchange does not only depend on the GTPases affinity for the GTP analogue but also on the GDP dissociation rate. The faster GDP can dissociate from a GTPase, the more GTP (or analogue) can bind. However, the intrinsic GDP dissociation rate should not be influenced by the use of GTP analogues instead of GTP, presupposed they have a similar affinity towards the GTPase. Therefore this does not explain the differences in the results obtained with Bodipy-TR-GTP compared to those obtained with GTP. These results suggest that Rac1 and Arf1 possess a stronger affinity for Bodipy-TR-GTP than they do for GTP (and GDP, therefore the faster dissociation).

When looking at the GEF-mediated nucleotide exchange, Rin1C, Rin1-TS and Rabex-5_{GEF} concentration-dependently catalysed the Bodipy-TR-GTP association on Rab5a. When Rabex-5_{GEF} was used at 25 nM the Bodipy-TR-GTP association reached saturation after around 400 seconds. With 200 nM of Rin1C saturation was not reached within the measurement time of 20 minutes. 200 nM of Rin1-TS led to saturation after 20 minutes. Resultant the catalytic effect was much stronger for Rabex-5_{GEF} than for the two Rin1-constructs as was to be expected and conclusive with data found in the literature^{82,102,131}.

DrrA catalysed the Bodipy-TR-GTP association on Rab1 concentration-dependently and with 100 nM of DrrA saturation was reached after about 400 seconds.

Tiam1DHPH had to be used in much higher concentrations compared to all the other GEFs in order to efficiently catalyse the nucleotide exchange. With 2 μ M of Tiam1DHPH the nucleotide exchange reaction on Rac2 reached saturation after approximately 900 seconds. Using 800 nM of Tiam1DHPH the reaction did not reach saturation within the 20 minutes measurement time. Consistently B. Niebel observed saturation only after 8000 seconds with 770 nM Tiam1DHPH using GTP²⁴².

Vav1 strongly catalysed the Bodipy-TR-GTP association on Rac1. With the highest concentration (400 nM) tested the reaction was saturated within the first 100 seconds. Using this concentration the linear phase of the reaction was way too short to appropriately calculate a slope. 25 nM Vav1 yielded saturation after around 400 seconds. This concentration was eventually chosen to be used during compound specificity measurements.

ARNO-Sec7 was capable to concentration-dependently catalyse the Bodipy-TR-GTP association on Arf1. The highest concentration (100 nM) tested did not lead to saturation of the reaction within the 20 minutes measured.

In both cases (GEF-mediated catalysis of the nucleotide exchange and intrinsic GTPase nucleotide binding capacity) the literature comparisons can only serve as reference points, as Bodipy-TR-GTP has been used in all nucleotide exchange assays performed during this study while the literature describes the activities when using GTP. It is well possible that the affinity of the proteins for Bodipy-TR-GTP differs from that observed with GTP.

The GEF concentrations listed in section 7.2.3.1, table 24 were chosen for specificity testing of the hit compounds because a linear increase in fluorescence intensity could be observed during at least the first five minutes.

4.3 Screening for small molecule inhibitors

Establishing a suitable screening assay to target a certain protein or a single domain within a multi-domain protein can be challenging. The screenings described throughout the history of drug discovery differ e.g. in format, library design and read-out. Screening approaches monitoring protein activity are often advantageous over those assaying the compounds ability to bind the target protein since here the read-out gives direct information on whether inhibition occurs. Binding does not necessarily equal inhibition, therefore several inactive compounds have been found in screenings monitoring target binding^{193,242,245}. Based on this knowledge a functional assay using Rin1C, Rab5a and a fluorescently labelled GTP analogue was to be designed. A drawback of this assay might be that inhibition could arise from targeting either of the two proteins or the complex between them. For example the screening could yield a GTP-competitive Rab5a-binder. Since there is no inhibitor known for Rin1 as well as Rab5, both proteins were attractive targets and the actual target should later be determined during characterization of the hit compounds.

Another disadvantage could be the use of a fluorophore label (Bodipy-TR) on the nucleotide. This always bears the risk of changing the interaction properties between the nucleotide and the nucleotide-binding protein. Using nucleotide-dependent changes in the intrinsic tryptophan fluorescence of Rab5a as read-out could have helped to overcome this problem. However, during an earlier screening approach with the same small molecule library, many compounds were found to be highly auto-fluorescent at the wavelengths required to monitor tryptophan fluorescence⁸². It has been previously reported that the UV range generally is the characteristic absorbance range for many different small molecules²⁴⁶. Thus, not only autofluorescence of the compounds but also quenching of the tryptophane signal by the compounds limits the usability of the tryptophane fluorescence assay for screening.

Another common approach would be the use of a radioactively labelled GTP analogue and a filter retention read-out. The major drawback of this kind of assays is that they are very time-consuming and usually not suitable for a high sample throughput. Such a radioactive assay should later be used to verify the inhibitory effect of promising compounds in a fluorescence-independent setup.

During an earlier screening approach, a reduction-sensitive lead compound has been identified by a member of the Famulok group⁸². Compounds that are inactive under reducing conditions are unlikely to exhibit an effect in an intracellular environment⁴⁸. To prevent the finding of a reduction-sensitive small molecule during the present screening, the screening buffer has been equipped with 1 mM DTT to apply reducing conditions.

To use the 1 mM library compounds in a final concentration of 40 μ M the assay had to tolerate 4 % DMSO. DMSO concentrations between 0 and 10 % have been tested in the nucleotide exchange assay. The Δ FI was not significantly influenced by DMSO concentrations between 2 and 6 % when compared to the 0 % DMSO sample. 8 and 10 % DMSO led to significantly higher Δ FI values compared to the control. This effect might have either been caused by an influence of DMSO on the fluorescence properties of Bodipy-TR-GTP, by DMSO increasing the general solubility of the assay components or by an increase in the GEF-independent nucleotide exchange.

With those adjustments a Z' factor of 0.57 could be calculated for the Rin1C/Rab5a Bodipy-TR-GTP nucleotide exchange assay. The assay was therefore suitable for HTS²³⁴ and the screening was subsequently performed with a library of 20 328 small molecule compounds. Compounds that reduced the Δ FI by ≥ 80 % (equalling ≤ 20 % residual nucleotide exchange activity) compared to the DMSO controls on the same plate were defined as primary hits. The screening identified 239 primary hits, representing 1.2 % of the total compounds that have been tested. Primary hit rates between 0.6 and 1.6 % are commonly found in HTS approaches²⁴⁷⁻²⁴⁹. Notably the in-house compound library used during this screening was considerably small compared to those used in other recent screening approaches²⁵⁰⁻²⁵³.

The primary hits were then tested as duplicates in two different concentrations in a manual re-screening. Here 213 of the primary hits were found to be false positives. It is common that many of the primary hits found during HTS approaches are false positives that can not be confirmed in a re-screening²⁵⁴. The false positives here were mainly caused by compounds either quenching the fluorescence signal of Bodipy-TR-GTP or being auto-fluorescent at 595/620 nm. This could not be deduced from the Δ FI values calculated during the HTS but was easily detectable as an up- or downshift of the FI value measured at $t = 0$ min when compared to that of the DMSO control. Another reason for false positive results could have been air bubbles in the wells that occurred during injection of Bodipy-TR-GTP at the plate reader. 26 compounds inhibited the nucleotide exchange by ≥ 50 % at a concentration of 40 μ M and were defined as secondary hits.

The compound library plates have been stored at -20 °C for some time and have been exposed to several thaw/freezing cycles during earlier screening approaches. Those conditions can lead to degradation and insolubility of instable compounds as explained in greater detail in section 5.2.2. It had to be assured that the inhibitory effect originates from the compounds expected at the corresponding library positions and not from degradation products of those. Subsequently the secondary hits were re-tested from frozen library stock solutions. Those solutions have been stored at -80 °C without recurring thaw/freezing cycles. Only 10 of the 26 secondary hits were found to inhibit the nucleotide exchange when the stock solutions were tested. For the other 16 compounds the inhibitory effect likely stemmed from degradation products that accumulated in the compound library plates. They were excluded from further analysis due to lack of structural knowledge of the inhibitory molecules.

4.4 Concentration-dependent inhibition of the Rin1C/Rab5a Bodipy-TR-GTP nucleotide exchange assay

The 10 secondary hits all inhibited the Rin1C-mediated Bodipy-TR-GTP nucleotide exchange on Rab5a in a concentration-dependent manner. The IC_{50} and the Hill coefficient describe the potency and possible cooperative binding of small molecule inhibitors, respectively^{236,237}. Activity and specificity are crucial in the concept of a lead compound as defined by J. G. Lombardino and J. A. Lowe as “a chemical structure or series of structures that show activity and selectivity in a pharmacological or biochemically relevant screen”²³⁸.

The IC_{50} values of the 10 secondary hits all were in the low micromolar range, characterizing them as potential inhibitors.

Their Hill coefficients were between -0.9 and -2.8 so some compounds were likely to bind independently while others seemed to bind positively cooperative. Independent binding was assumed for the compounds CG3 05 B06, CG5 08 H06, CG6 24 G06 and KR1 04 F03. The compounds CG1 05 F09, CG1 06 A03, CG5 05 F05, CG6 25 G08 and CG6 25 F10 showed Hill coefficients that indicated positive cooperative binding. The compounds CG3 05 A02 and CG3 05 B06 exhibited Hill coefficients of -1.6 ± 0.7 and -0.7 ± 0.6 , respectively. Because of the large standard deviations no conclusions could be drawn whether independent or positively cooperative binding might take place in those cases.

The 10 secondary hit compounds were moreover not noticeable structurally related.

4.5 The majority of the secondary hits were either unspecific or aggregators

During specificity testing using other GEF/GTPase pairs, most of the 10 secondary hits exhibited unspecific off-target effects on one or more of the selected protein pairs. The compounds CG1 05 F09, CG1 06 A03, CG3 05 B06, CG5 05 F05, CG6 26 F10 and KR1 04 F03 were found to also inhibit the ARNO-Sec7/Arf1 nucleotide exchange assay. They were therefore classified as unspecific and unsuitable as lead compounds. CH5 08 H06 caused approximately 50 % inhibition in the nucleotide exchange assay using Vav1 and Rac1 and was therefore also categorized as unspecific.

Many small molecule compounds are known to form colloidal aggregates around and with proteins, leading to promiscuous artificial inhibition^{239,241,255}. A compound can for example bridge protein monomers, leading to inappropriate polymerization, disordered protein domains and aggregation²⁵⁶. The compounds were therefore tested in a simple

centrifugation-based aggregation assay. During this analysis the compound CG5 08 H06 was found to take about 50 % of Rin1C out of solution. The compounds CG6 24 G06 and CG6 25 G08 completely aggregated Rin1C. Surprisingly none of the compounds aggregated with Rab5a. Supposing that bridging of monomers would be the mechanism behind the Rin1C aggregation, an explanation could be a lack of the cavities required for bridging in Rab5a. Moreover there are a few examples of specific aggregator described in the literature^{255,256}. Since aggregators usually are prone to exhibit off-target effects²³⁹, these compounds were excluded from further investigations.

4.6 CG3 05 A02 specifically inhibited the Vps9 domain-containing Rab5a-GEF constructs Rin1C and Rabex-5_{GEF} without inducing aggregation

The compound CG3 05 A02 inhibited the Rin1C- and Rabex-5_{GEF}-mediated Bodipy-TR-GTP nucleotide exchange on Rab5a with IC₅₀ values of 35.4 ± 11.1 µM and 40.7 ± 4.1 µM (data in the appendix, section 8.7), respectively. Since Rabex-5 and Rin1 share the homologous catalytic Vps9 domain it was not unexpected that a compound might be able to inhibit both GEFs. Another possibility would be that CG3 05 A02 interacts with Rab5a instead as this would also lead to inhibition in both setups.

Binding studies using microscale thermophoresis (MST, data in the appendix, section 8.8) unfortunately did not deliver reasonable results indicating binding to either of the two proteins or both proteins combined. The latter was done to analyse possible binding to the complex between Rin1C and Rab5a.

Other methods to generate binding data also failed for different reasons. Isothermal titration calorimetry (ITC) would have required higher solubility of the compound in buffer, ideally in a range at least 10-fold higher than the IC₅₀.

The solubility of CG3 05 A02 was found to be poor. An explanation for the measured IC₅₀ values in a range far above the determined solubility could be that the compound gets solubilized upon binding to proteins. During the exchange assays the compound was at no time exposed to buffer without the presence of the two proteins. The compounds synthesized for structure activity relationship (SAR) studies that had an inhibitory effect comparable to that of CG3 05 A02 did not show improved solubility in buffer (data in the appendix in section 8.5).

For fluorescence polarization (FP) experiments the compound needed to be labelled with a fluorophore. During the SAR studies several linkers at different positions have been tested and even a fluorescein-labelled compound was synthesized. All modifications led to a partial or complete loss of the inhibitory effect.

To assess the possibility that CG3 05 A02 might interact GTP-competitively with Rab5a, Rab5a was loaded GEF-independently with Bodipy-TR-GTP in presence of different concentrations of the compound. No concentration-dependent effect on the GTP-binding could be found, therefore it seemed unlikely that GTP-competitive binding is the mechanism of inhibition employed by the compound CG3 05 A02. It could not be determined at this point whether CG3 05 A02 interacts with Rin1C and Rabex-5_{GEF} or with the GEF/GTPase complex.

CG3 05 A02 did not inhibit any of the other GEF/GTPase pairs although the exchange mechanisms of some of the GEF domains are similar³². DrrA and ARNO-Sec7 built quite rigorous controls due to similarity in the catalytic nucleotide exchange mechanism. To further analyse the inhibition on another Vps9 domain-containing GEF, GAPVD1 has been tried to be purified. Unfortunately the resulting protein turned out to be inactive after each

purification attempt (data in the appendix, section 8.9). At this point it could be concluded that CG3 05 A02 specifically inhibits the nucleotide exchange of at least two Vps9 domain-containing Rab5 GEFs. It remains to be tested whether this is the case for other Vps9 domain-containing Rab5 GEFs as well.

Little to no aggregation of Rin1C and Rab5a could be seen in the centrifugation-based aggregation assay when CG3 05 A02 has been tested. To investigate possible off-target effects that could arise from unspecific protein aggregation, the compound was tested in the GEF/GTPase unrelated insulin receptor (IR) auto-phosphorylation assay. CG3 05 A02 exhibited no effect on the IR auto-phosphorylation, rating IR aggregation unlikely. To further exclude off-target effects, whether they are aggregation-based or not, compound-centric proteomics²⁵⁷ could have been performed. However, this would have required labelling the compound with a structure that allows immobilization. Since modification of CG3 05 A02 with different linkers led to partial or complete loss of inhibition this approach has been omitted.

4.7 A methoxy group is important for CG3 05 A02 to exhibit its inhibitory effect

During SAR studies on the compound CG3 05 A02 several functional groups have been removed, exchanged or repositioned. Some derivatives have been synthesized to modify the compound with a label or to improve the solubility in buffer as already shortly discussed in section 4.6. Others were generated to gain insights on the substituents required for inhibition. The core structure of CG3 05 A02 is depicted in figure 36. This structure was modified at the positions R1, R2 and R3 as well as on the secondary amine during the SAR studies.

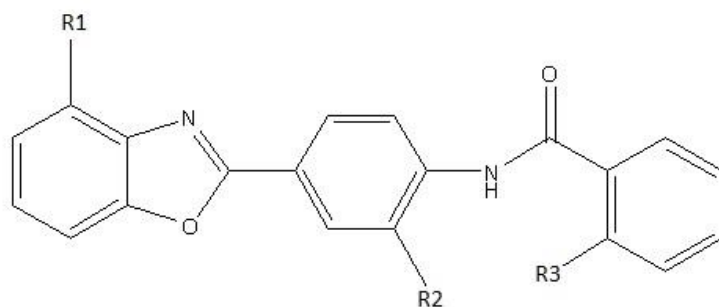


Figure 36: Core structure of CG3 05 A02. It comprises four ring structures, a secondary amine and a ketone group that have been conserved in all derivatives. The molecule was modified at the positions R1, R2 and R3 as well as on the position of the amine during the SAR studies.

A methoxy group is attached at position R3 in CG3 05 A02. This group turned out to be crucial for the compound to exhibit its full inhibitory effect. Removing or repositioning of this group to meta- or para position led to a loss of activity. These observations suggested that a covalent ring closure might take place between the methoxy group and the secondary amine, attended by the release of H₂. To further investigate this possibility the compound 066A has been synthesized. A methyl group has been attached, generating a tertiary amine and preventing the formation of a covalent bond. This compound was completely inactive. It was therefore possible that the inhibitory structure is actually the closed form.

Removing the methyl group at position R1 had no effect on the inhibition, neither had replacing it with a methoxy or a hydroxyl group. This certain tolerance for changes at the R1 position led to the attempt to label the compound at this position. However, attachment of different linkers and a fluorophore led to partial or complete loss of the inhibitory potential. This could possibly arise from the sheer increase in molecule size, hindering it from interaction with the target or from intramolecular interactions between the linker and a substituent required for inhibition.

Attachment of the linker at position R3 also extinguished the inhibition. This could result from preventing the ring closure mentioned above, in case this is the actual inhibitory form of the compound.

No effect on the inhibitory potential was observed when the methyl group at position R2 was removed. This indicated a certain tolerance towards changes at this position as well. However, the R2 position is more in the centre of the molecule, therefore it was assumed that modifications there could more likely cause intramolecular reactions than modifications at the R1 position.

When both methyl groups at the R1 and R2 positions were removed, the IC_{50} approximately doubled. This indicated that their presence is not completely irrelevant. They might somehow stabilize the correct orientation of the compound within a potential binding site.

The compound 166A is the only derivative that delivered results that were inconclusive with the remaining SAR data. This compound had an inhibitory effect, although the methoxy group at position R3 is lacking. The IC_{50} was about two times as high compared to CG3 05 A02. To gain further insights on the SAR and this specific matter some more derivatives should be synthesized. For example molecules with various substituents at the position R3, differing for example in size and reactivity.

Nevertheless the methoxy group at position R3 seems to be important for the compound CG3 05 A02 to exhibit its full inhibitory potential. Without this group the potency either decreased drastically or completely vanished. Unfortunately no gain of potency or solubility could be obtained with any of the molecules synthesized for the SAR studies.

4.8 CG3 05 A02 inhibits the GEF function of Rin1 without affecting the interaction with ABL1

In a Rin1-phosphorylation assay using full-length Rin1-TS and ABL1 the effect of CG3 05 A02 on the interaction between Rin1 and ABL1 has been investigated. It was analysed whether inhibition of the GEF domain influences the function of a neighbouring domain, the proline-rich region. This region interacts with ABL kinases, leading to Rin1-phosphorylation at Tyr36^{113,258}. By binding to a certain domain on a multi-domain protein, a compound could affect neighbouring domains for example by inducing conformational changes, by blocking them with overhanging substituents or by sheer bulkiness. The phosphorylation of Rin1-TS was not altered by CG3 05 A02. Hence, the compound either interacts specifically with the Vps9 domain without influencing the proline-rich region required for interaction with ABL1 or does not interact with Rin1 at all. Additionally, this result once again argues against the compound acting as a general protein aggregator. As already previously discussed in section 4.6 CG3 05 A02 possibly interacts with the complex between the GEF domains of Rin1/Rabex-5 and Rab5a. To further analyse this matter the Rin1-TS-phosphorylation in presence of Rab5a should be contemplated. In a cellular environment a Vps9 domain-specific small molecule inhibitor could be used to smother tumorigenic effects resulting from

Rin1-mediated Rab5 over-activation without influencing the tumour suppressive ABL1 signalling functions of Rin1^{123–126,150}.

4.9 The inhibitory effect of CG3 05 A02 depends on the use of a labelled GTP analogue

During the course of this study additional control experiments were performed that aimed on showing the inhibitory effect of CG3 05 A02 is not related to the use of Bodipy-TR-GTP. The use of Bodipy-TR-GTP in the specificity studies with other GEF/GTPase pairs already excluded that the effect simply stemmed from interaction of the compound with Bodipy-TR-GTP. If that was the case, the compound should have had an effect in every one of the consulted assays. It therefore seemed unlikely that the inhibition was linked to the use of Bodipy-TR-GTP at this point. Since there are differences in the affinities and binding properties of GTPases reported for GTP analogues compared to GTP²⁴⁴ the controls have been performed nevertheless. However, their priority was set low in comparison to the characterization experiments performed beforehand.

First, another GTP analogue has been used: Bodipy-FL-GTP. Surprisingly the IC₅₀ for CG3 05 A02 was estimated to be about 7-fold higher with Bodipy-FL-GTP compared to the experiments performed with Bodipy-TR-GTP. The IC₅₀ could merely be estimated here due to the compound concentration range used (0.025 – 200 µM) for solubility reasons. At this point it could not be concluded which one of those results is erroneous. Actually, the biochemically most relevant situation is that where GTP is used instead of a labelled analogue. To overcome this issue and get a more native-like glimpse on the situation, an experiment using radioactively labelled GTP has been performed. Unfortunately, no concentration-dependent inhibition of the Rin1C-mediated nucleotide exchange on Rab5a could be found.

As already mentioned above, the inhibition seen in the Bodipy-TR-GTP nucleotide exchange assay is unlikely to originate from the compound directly interacting with Bodipy-TR-GTP. Moreover the GEF-independent loading of Rab5a with Bodipy-TR-GTP in presence of CG3 05 A02 showed no effect of the compound on nucleotide binding. GTP-competitive binding to Rab5a is therefore also unlikely. This means in turn that, if there is an effect of CG3 05 A02 that does not descend from assay artefacts, the compound likely interacts with either Rin1C/Rabex-5_{GEF} or the complex of those with Rab5a. Supposing that CG3 05 A02 interacts specifically with or adjacent to the Vps9 domain of the GEFs in complex with Rab5a, or close to the GTP binding site with the complex itself, it could prevent Bodipy-TR-GTP from entering the binding site due to steric hindrance, caused by the Bodipy-TR moiety. The complex would normally get disrupted by high concentrations of GTP in the cell¹²⁹. The much smaller GTP without a fluorescent label is still able to bind to Rab5a in presence of CG3 05 A02, as seen in the radioactive approach. The Bodipy-FL label is smaller than the Bodipy-TR label (cp. structures from figures 15 and 33). Bodipy-FL-GTP can accordingly, to some extent, still bind to Rab5a even in presence of high concentrations of the compound. However, the binding of the “bulkier” Bodipy-TR-GTP is inhibited by CG3 05 A02 with an IC₅₀ of 35.4 µM. This also can explain the lack of inhibition in the Bodipy-FL-GDP release assay. Here Rab5a got pre-loaded with Bodipy-FL-GDP in absence of CG3 05 A02 and then mixed with Rin1C and the compound. Upon interaction with Rin1C, Bodipy-FL-GDP gets released as expected, independent of the presence of the compound. GTP binding should afterwards not be influenced by the compound binding to Rin1C or the Rin1C/Rab5a complex. To further investigate this hypothesis other fluorescently labelled GTP analogues could be tested. The

fluorophores should differ in size but they should all be attached to the ribose ring as it was the case for the Bodipy labels used in this study.

These findings unfortunately classify the compound unsuitable for cellular application because no inhibitory effect is to be expected, since the nucleotide exchange for GTP is not influenced by CG3 05 A02 *in vitro*.

5 Outlook

5.1 Perspectives for CG3 05 A02

Although CG3 05 A02 seems to be highly specific for at least two Vps9 domain-containing Rab5 GEFs, Rin1 and Rabex-5, its dependence on the use of a fluorescently labelled GTP analogue prevents its use as a tool to study these GEFs *in vivo*. It can be used to modify *in vitro* kinetic experiments and may help to gain insights on the differences between Rin1- and Rabex-5-mediated Rab5 activation in the presence of Bodipy-TR-GTP.

Clarifying the inhibitory mechanism of this compound could be interesting to obtain a deeper understanding of the effects the addition of a label can have on GTP binding to GTPases. Therefore it would be helpful to generate structural data of CG3 05 A02 in complex with Rin1, Rabex-5 or the complex between those and Rab5. X-ray crystallization efforts have already been initiated by D. Yin from the Famulok group. This could also answer the question, whether the compound really interacts with the complex between the Rab5 GEFs and Rab5 as assumed based on the data generated during this study.

Identification of the binding site of CG3 05 A02 could help to model potential inhibitory molecules into this protein cavity. Finding suitable cavities on GEFs and GTPases can often be challenging due to their globular surface lacking obvious grooves and pockets¹⁷⁶. This could be a good starting point for *in silico* screenings that have yielded promising results in other screening approaches for GTPase and GEF inhibitors^{182,185,186,197,201,222}. By this a second generation of Rin1 inhibitors might be identified that may also be able to inhibit the nucleotide exchange in presence of unlabelled GTP.

5.2 Considerations for future screening approaches

5.2.1 Insights from the Rin1C/Rab5a Bodipy-TR-GTP nucleotide exchange assay

Scientists planning on performing a HTS can certainly benefit from this study.

First of all it has to be kept in mind that the use of fluorophore labels influences the assay conditions in one way or the other. Therefore a fluorescence-independent control should be performed at an early stage after the screening, when a fluorescence-based method has been employed. By this, artefacts resulting from the use of fluorescently labelled material can be sorted out at an early time.

Next the use of a detergent in the screening buffer might have prevented hitting compounds that later turned out to be aggregators. This is, of course, only possible when the detergent does not interfere with the assay read-out, as it was seen in this study.

Lastly it has to be noted that in retrospect an assay monitoring the release of fluorescently labelled GDP (rather than the association of fluorescently labelled GTP) would have been preferable as in this setting CG3 05 A02 had no inhibitory effect.

5.2.2 Successful HTS approaches crucially depend on library size and quality

Many recent HTS approaches have been performed with libraries containing a way larger number of small molecules than the library used during this study^{250–253}. Certainly a larger number of compounds raises the probability to find a suitable inhibitor.

Moreover the appropriate storage of compound libraries was described to be as important as the HTS itself²⁵⁹. Reoccurring freeze-thaw cycles have been reported to induce compound precipitation and therefore change the compound concentration in the long term²⁶⁰. A mixture of water, DMSO and glycerol (10:45:45) was described to prevent compound precipitation and could be contemplable as a solvent for long-term storage²⁶¹.

Compounds were also described to decay over longer storage periods, leading to the accumulation of impurities in the library²⁶². Impurities can falsify screening results as they either might show effects in the screening assay, leading to false positive hits, or are inactive in contrast to the compound they originate from. The latter would result in false negative data, meaning missing out on a potentially promising compound.

Automated compound quality control should be undertaken at frequent intervals to assure the actual compound concentrations correspond to the theoretically desired library concentrations²⁶³. Solubility and purity should also be checked during quality controls.

Library composition, age and storage conditions influence the outcome of HTS approaches and should always be considered during the planning of such.

6 Conclusions

GTPases are molecular switches that are extensively involved in the regulation of gene expression, membrane trafficking and endocytosis¹⁸. They become activated by GEFs and inactivated via the hydrolysis of GTP with the help of catalytic GAPs¹². Often a variety of different GEFs can activate the same GTPase and their distinct functions in the affected signalling cascades are not completely understood. The GTPase Rab5 can get activated by several GEFs, amongst them Rin1 and Rabex-5. Rab5 GEFs contain a catalytic Vps9 domain that mediates the nucleotide exchange¹⁰⁰.

Small molecule inhibitors have proven to be valuable tools in the investigation of protein-protein interactions¹⁵⁴. GTPases and GEFs are interesting and yet challenging targets due to their smooth surface that lacks obvious grooves and pockets suitable for small molecule interactions^{21,160,176}. The homologous Vps9 domain shared by Rab5 GEFs makes it moreover difficult to target them specifically¹⁰⁰. Small molecule inhibitors of Rab5 GEFs would help to shine light on the complex signalling networks around Rab5.

This study aimed on the identification of an inhibitor of the Rin1-mediated Rab5 activation in an *in vitro* high-throughput screening (HTS) approach. The screening yielded the small molecule CG3 05 A02 that specifically inhibited the Rin1C and Rabex-5_{GEF}-mediated Bodipy-TR-GTP nucleotide exchange on Rab5a without aggregating the proteins involved. The IC₅₀ values of CG3 05 A02 in both cases were in the low micromolar range. The compound did not inhibit the Bodipy-TR-GTP nucleotide exchange between several other GEF/GTPase pairs, although the exchange mechanisms were described to be similar. However, it might still be able to inhibit other Vps9 domain containing Rab5 GEFs, as by now only Rin1C and Rabex-5_{GEF} have been tested. No unspecific inhibition could be seen in an unrelated insulin receptor auto-phosphorylation assay and the compound did moreover not influence the interaction between Rin1 and ABL1. This interaction is mediated by the proline-rich region of Rin1 that is located adjacent to the Vps9 domain. Accordingly CG3 05 A02 did not show a domain-unspecific intramolecular effect on the proline-rich region of Rin1. A compound like this could, theoretically, be used to oppress tumorigenic effects mediated by Rab5 over-activation without influencing the tumour suppressive ABL1 signalling functions of Rin1^{123-126,150}.

During several control experiments it became, however, apparent that CG3 05 A02 does not inhibit the Rin1C and Rab3x-5_{GEF}-mediated nucleotide exchange when radioactively labelled GTP is being used. This unfortunately characterizes the compound as unsuitable for cellular or *in vivo* applications.

Structure-activity relationship analyses revealed the importance of a methoxy group that might perform a ring closure reaction with a neighbouring secondary amine. This group seems to be crucial for the compound to exhibit its inhibitory effect.

Binding studies failed to unravel whether Rin1C/Rabex-5_{GEF}, Rab5a or the complex between those proteins is the actual target of CG3 05 A02. However, loading of Rab5a with Bodipy-TR-GTP was not influenced by CG3 05 A02 and therefore GTP-competitive binding to Rab5a is unlikely. The compound could hypothetically bind close to the GTP binding site on the complex between Rin1C/Rabex-5_{GEF} and Rab5a and prevent Bodipy-TR-GTP binding due to steric hindrance. The Bodipy-TR moiety could prevent the nucleotide from entering the binding site when CG3 05 A02 is attached to the complex. This mode of action could also apply when the compound binds Rin1C and Rabex-5_{GEF} at or adjacent to the Vps9 domain and this protein-compound complex stays intact upon interaction with Rab5a. The much smaller GTP can, however, still enter the binding pocket, even when CG3 05 A02 is bound.

To avoid investing in label-dependent compounds that might be found in future screenings a fluorescence-independent control should be performed promptly after the HTS. The right choice of the compound library to be screened is also an important issue that has to be thoroughly considered when a HTS should be performed²⁵⁹.

Identification of a possible binding site of CG3 05 A02 on Rin1C/Rabex-5_{GEF} or the complex of those with Rab5a in crystallization studies might pinpoint a protein cavity that could potentially be used for *in silico* HTS approaches. By this a second generation of inhibitors of the Rin1-mediated Rab5 activation could be identified. These second generation compounds could help to create a greater understanding of the signalling cascades involving Rab5 activation.

7 Materials & Methods

7.1 Materials

7.1.1 Equipment

Table 6: Equipment.

Equipment	Manufacturer
Agilent 1100 HPLC	BRUKER
ÄKTA FPLC	GE Healthcare
Analytical balance CPA 324S	sartorius AG
Balance BL 1500S	sartorius AG
Blotting chamber (semi dry)	PHASE HL
Blotting chamber (wet) Criterion	BioRad
Centrifuge 5427 R	Eppendorf
Centrifuge 5804 R	Eppendorf
Centrifuge Avanti J-26S XP	Beckman Coulter
Electrophoresis power supply E802	CONSORT
Esquire HCT (ESI MS & ion trap)	BRUKER
French Press cell disrupter	Thermo Scientific
Gelfiltration column Superdex 200 HiLoad 16/600 pg	GE Healthcare
HPLC column MultoHigh Bio 200-5 C18	CS-Chromatography
Incubator (bacteria) Multitron pro	INFORS-HT
Incubator (bacteria) HERatherm	Thermo Scientific
Incubator (<i>Sf9</i> cells) innova 42	Eppendorf
Liquid Scintillation Counter 1409	Wallac
Magnetic stirrer IKAMAG RCT	IKA Works
Magnetic rack	Promega
Microscope Eclipse TS 100	Nikon
MST Monolith NT.115	NanoTemper
Multipette Advanced	Eppendorf
NanoDrop 2000	Thermo Scientific
Odyssey gel documentation system 9260	LI-COR
Over head tumbler PTR-30	Grant-bio
Peristaltic pump 2115 Multiperpex	LKB Bromma
pH-meter FiveEasy	Mettler Toledo
Pipettes research plus	Eppendorf
Plate Reader infinite M1000 pro & injector	TECAN
Screening Robot Freedom Evo	TECAN
SDS-Page electrophoresis apparatus	BioRad
Sonifier Sonics Vibra Cell	Heinemann
Spectrophotometer BioSpectrometer basic	Eppendorf
Thermomixer comfort	Eppendorf
Vortexer MS2 Minishaker	IKA Works
Water bath 1008	GFL
Water purification system MicroPure UV	Thermo Scientific

7.1.2 Chemicals

Table 7: Chemicals.

Reagent	Manufacturer
[α - ³² P] GTP	PerkinElmer
β -mercaptoethanol	Roth
Acetic acid	Roth
Acetonitrile, LC-MS grade	Merck
Agar agar	Fluka Chemica
Alexa Fluor 647 NHS-ester	invitrogen
Ammonium persulfate	Roth
Ampicillin	Roth
ATP	AppliChem
Bac-to-Bac system	Thermo Scientific
Bodipy-TR GTP	life technologies
Bodipy-FL GTP	life technologies
Bodipy-FL GDP	life technologies
Bromophenol blue	Merck
Chloramphenicol	Sigma Aldrich
ComGenex compound library	ComGenex
Coomassie brilliant blue G-250	Serva
DMSO (anhydrous)	Sigma Aldrich
Dithiothreitol	Roth
EDTA	AppliChem
Ethanol	Roth
GDP	Sigma
Gentamycin	AppliChem
Glutathione	AppliChem
Glutathione Sepharose 4B	GE Healthcare
Glycerol	Roth
Glycine	Roth
GppNHp	JenaBioscience
GTP	Sigma
Hydrochloric acid	VWR Chemicals
Imidazole	Roth
IPTG	AppliChem
Isopropanol	Roth
Kanamycin	Roth
LB Medium	Roth
Methanol	Roth
MgCl ₂	Fluka Chemica
NaCl	Roth
NaOH	Roth
NHS-Fluorescein	Thermo Scientific
Ni-NTA Agarose Beads	Macherey-Nagel
100 x Protease Inhibitor Mix: 1 mM AEBSF	Components by Serva In-house preparation of stock

5 μ M E-64	
5 μ M Bestatin	
5 μ M Phosphoramidon	
Protein Assay Dye Reagent Concentrate	BioRad
Protein Ladder PageRuler Plus Prestained	Thermo Scientific
SDS	AppliChem
Strep-Tactin Superflow	Iba
Streptavidin Superflow	Iba
TEMED	Roth
Tween20	AppliChem
Rotiphorese Gel 30	Roth
Ultima Gold LSC Cocktail	Perkin Elmer

7.1.3 Consumables

Table 8: Consumables.

Product	Manufacturer
384 well plates, NBS, black, flat bottom	Corning
96 well plates, half area, MB, black, flat bottom	Greiner Bio One
96 well plates, transparent, round bottom	Greiner Bio One
Blotting paper	Macherey-Nagel
Capillaries, standard treated	NanoTemper
Centrifugation tubes (15 mL / 50 mL)	Sarstedt
Dialysis tubing SpectraPor PC 10 K MWCO	SpectrumLabs
Disposable columns	BioRad
Disposable cuvettes	Roth
Multipette combitips advanced	Eppendorf
NAP-5 columns	GE Healthcare
Needles	Henke Sass Wolf
Nitrocellulose membrane	GE Healthcare
Petridishes	Sarstedt
Pipette tips	Sarstedt
Protein LoBind reaction tubes (1.5 mL)	Eppendorf
Reaction tubes (1.5 mL / 2 mL)	Sarstedt
Reaction tubes (0.2 mL)	Sarstedt
Sterile filters	GE Healthcare
Super Polyethylene LSC Vials	Perkin Elmer
Syringes	BD Discardit
VivaSpin turbo 15 centrifugal filters	sartorius AG

7.1.4 Compounds

Table 9: Compounds.

Name	Manufacturer	Corresponding library No.
V005-7464	ChemDiv, Inc.	CG6 25 G08
Sulfobromophthalein	Sigma Aldrich	KR1 04 F03

7.1.5 Nucleic acids

Table 10: Nucleic acids.

Plasmid	Cloning sites	Resistance	Purification Tag	Cleavage site	Insert
pAB1	NcoI NotI	Gent	Strep	TEV	Rin1-TS (human, aa 1-783)
pDL2	BamHI Sall	Amp	6 x His	none	Rabex-5 _{GEF} (human, aa 132-391)
pET19mod	NdeI XhoI	Amp	6 x His	TEV	DrrA (human, aa 40-533)
pET15	NcoI EcoRV	Amp	6 x His	Thrombin	NΔ17 Arf1 (aa 1-164)
pET15b	NdeI BamHI	Amp	10 x His	none	Rab5a (human, aa 17-184)
pET52b(+)	XmaI Sall	Amp	6 x His / Strep	Thrombin	Tiam1DHPH (mouse, aa 1033-1406)
pET SUMO	TA cloning	Kan	6 x His / SUMO	none	Rac2 (human, aa 1-192)
pFBHT	EcoRI XhoI	Gent	6 x His	TEV	Rin1C (human, aa 293-783)
pFBHT	EheI Sall	Amp	6 x His	TEV	IR-ICD (human, aa 953-1355)
pGEX2T	BamHI EcoRI	Amp	GST	TEV	Vav1 (human, aa 189-575, M351T)
pGEX2T	BamHI EcoRI	Amp	GST	Thrombin	Rac1 (human, aa 1-184)
pIBA101HT	BsmBI HindIII	Amp	6 x His	TEV	ARNO-Sec7 (human, aa 61-246)
pMAL	NdeI XhoI	Amp	6 x His / MBP	TEV	Rab1 (human, aa 1-205)
pMAL-C2	SacI BamHI	Amp	7 x His / MBP	TEV	TEV Protease (tev, aa 1-304, S219V)

7.1.6 Enzymes & Proteins

Table 11: Enzymes & Proteins.

Protein	Manufacturer
ABL1 (His ₆ -tagged)	ThermoFisher
ARNO-Sec7	In-house production, Benjamin Weiche
BSA	PAN Biotech
EGF	PeptoTech Inc.
Insulin receptor (intracellular domain)	In-house production, Christian Sieg
Lysozyme	Thermo Scientific
NΔ17 Arf1	In-house production, Benjamin Weiche
TEV Protease	In-house production, Volkmar Fieberg
Thrombin, bovine	Calbiochem

7.1.7 Antibodies

Table 12: Antibodies.

Target	Species	Dilution	Manufacturer, No.
5 x His	mouse	1:1000	Qiagen, 34660
Phospho-Tyrosine	mouse	1:500	Santa Cruz, sc-7020
Rab5	mouse	1:1000	Santa Cruz, sc-46692 (D11)
Rab5a	rabbit	1:500	Santa Cruz, sc-309 (S-19)
EGFR-CT	rabbit	1:1000	Santa Cruz, sc-03
Mouse IgG IRDye [®] 800CW	goat	1:20000	LI-COR
Rabbit IgG IRDye [®] 800CW	goat	1:20000	LI-COR

7.1.8 Bacterial strains

Table 13: Bacterial strains.

Strain	Genotype	Manufacturer
BL21-CodonPlus [®] (DE3)-RIL	<i>E. coli</i> B F ⁻ ompT hsdS(r _B ⁻ m _B ⁻) dcm ⁺ Tet ^r gal λ(DE3) endA Hte [argU ileY leuW Cam ^r]	Agilent Technologies

7.1.9 Software

Table 14: Software.

Software	Manufacturer
ChemDraw Prime 15.1	PerkinElmer
GraphPad Prism [®]	GraphPad Software Inc.
Image Studio Lite	LI-COR
Office 2003	Microsoft

7.2 Methods

7.2.1 Miscellaneous Methods

7.2.1.1 SDS-PAGE

SDS-PAGE was used to separate proteins according to their mass as described by Laemmli^{264,265}. The anionic detergent sodium dodecyl sulfate (SDS) was used to denature the proteins and charge them negatively. The longer the peptide chain, the stronger the negative charge. This allowed a separation by protein size in an electric field using a polyacrylamide (PAA) gel. The gel consisted of a 4 % acrylamide stacking gel on top of an 8 – 15 % acrylamide separating gel. The percentage of the separating gel depended on the size range of the proteins desired to separate. Low percentages were advantageous to resolute big proteins whilst high percentages have been used for small ones. The gels have been prepared according to table 15. Polymerisation was initiated by addition of ammonium persulfate (APS) and the catalyst N,N,N',N'-tetramethylethylenediamine (TEMED). The gel was prepared between two glass plates held apart by spacers with a thickness of 1 mm. A comb was inserted into the stacking gel prior to polymerisation to create pockets for sample loading. The gel was placed inside a running chamber filled with 1 x running buffer. Protein samples were mixed with loading buffer in a final concentration of 1 x and boiled at 95 °C for

5 minutes before loading them to the gel pockets. 3 μL of a pre-stained protein marker were loaded as a size reference. The gel was run at 200 V for approx. 1 h and afterwards either stained with coomassie brilliant blue or used for western blotting as described in section 7.2.1.3.

4 x stacking gel buffer:

0.5 M Tris, pH 6.8
14 mM SDS

4 x separating gel buffer:

1.5 M Tris pH 8.8
14 mM SDS

5 x running buffer:

125 mM Tris
960 mM Glycine
17 mM SDS

6 x loading buffer

1 M Tris pH 6.8
30 % Glycerol
15 % w/v SDS
600 mM DTT
Small amount of bromophenol blue

Table 15: Composition of SDS-PAA-gels.

Amounts for 1 gel	Separating gel				Stacking gel
	8 %	10 %	12.5 %	15 %	4 %
Acrylamide [μL]	1333	1667	2083	2500	213
Water [μL]	2379	2045	1629	1212	975
Separating gel buffer [μL]	1250				-
Stacking gel buffer [μL]	-				400
TEMED	8				2
APS	30				10.4

7.2.1.2 Coomassie staining of PAA-gels

The coomassie blue staining method was adapted from the protocol described by Sasse²⁶⁶. The gel was incubated in coomassie staining solution for 30 minutes at room temperature on an orbital shaker. Afterwards the gel was rinsed with water and destained in destaining solution until the background staining faded away. The destaining solution was exchanged every 15 minutes. Finally the gel was documented in the Odyssey scanner system using the 700 nm channel. Protein bands could be quantified using the Image Studio Lite software.

Coomassie staining solution:

30 % v/v Methanol
10 % v/v Acetic acid
0.82 mM Coomassie brilliant blue G-250

Destaining solution:

10 % v/v Acetic acid

7.2.1.3 Western blotting (Immunoblotting)

Immunoblots were performed to detect, analyze and quantify proteins. The protein samples were run on PAA-gels as described in section 7.2.1.1 and then transferred to a nitrocellulose membrane by either semi dry or wet blotting. The membrane was then blocked with 5 % w/v BSA in TBST for 1 h at room temperature. Afterwards it was incubated with the desired primary antibody in the corresponding dilution (see section 7.1.7) in TBST + 5 % w/v BSA either 1 h at room temperature or over night at 4 °C on an orbital shaker. The membrane was washed three times for 5 minutes at room temperature under agitation before the fluorescently labelled secondary antibody was added. The secondary antibody was diluted in TBST with 5 % w/v BSA and 0.02 % w/v thimerosal as described in section 7.1.7. After another 1 h incubation at room temperature under light protection and agitation the blot was washed with TBST as before. Finally the proteins of desire were visualized using the 800 nm channel in the odyssey scanner to detect the secondary antibodies. Protein bands could be quantified using the Image Studio Lite software.

TBST:

20 mM Tris, pH 7.6

136 mM NaCl

0.1 % v/v Tween 20

7.2.1.3.1 Semi-dry blotting

Semi dry blotting was performed as described by Kyhse-Andersen²⁶⁷ in 1984 with slight buffer modifications. The gel and membrane were stacked between pieces of blotting paper equilibrated in different buffers (cathode, three pieces of paper equilibrated with cathode buffer, gel equilibrated with cathode buffer, membrane equilibrated with anode buffer II, two pieces of paper equilibrated with anode buffer II, one piece of paper equilibrated with anode buffer I, anode). The proteins were transferred by applying a current of 2 mA/cm² gel (108 mA for a 6 x 9 cm gel) for 50 minutes in a PHASE HL blot chamber.

Cathode buffer:

25 mM Tris, pH 9.4

40 mM Glycine

Anode buffer I:

300 mM Tris, pH 10.4

Anode buffer II:

25 mM Tris, pH 10.4

7.2.1.3.2 Wet blotting

Wet blotting was performed similar to the protocol described by Towbin²⁶⁸ in 1979 but in a methanol-free buffer. Gel, membrane, two sponges (parts of the Criterion wet blot chamber) and two pieces of blotting paper were equilibrated with cold wet blot buffer. The blot was assembled in a blot holder (starting from the black cathode side of the holder: one sponge, one piece of paper, gel, membrane, the second piece of paper, the second sponge, the red anode side of the blot holder). The blot holder, a – 20 °C cold thermal pack and a magnetic

stir bar were placed inside the Criterion wet blot chamber filled with wet blot buffer. The proteins were transferred by applying a total current of 2000 mA for 50 minutes.

Wet blot buffer:

25 mM Tris

192 mM Glycine

7.2.2 Protein biosynthesis and purification

7.2.2.1 Transformation of BL21-CodonPlus[®](DE3)-RIL competent cells

The *E. coli* strain BL21-CodonPlus[®](DE3)-RIL was used for protein expression. This strain supplies additional copies of tRNAs genes that are naturally rare in *E. coli* (arginine, leucine and isoleucine), thereby the protein expression level can be enhanced. 1×10^7 cells were thawed on ice, mixed with 100 ng plasmid DNA and incubated on ice for 10 minutes. A heat shock was performed for 1 minute at 42 °C in a thermomixer under agitation. Afterwards the cells were incubated for another 5 minutes on ice before 900 µL of LB medium were added followed by 1 h incubation in the thermomixer at 37 °C and 750 rpm. Finally the cells were plated onto a LB-agar-plate containing the appropriate antibiotic for selection of cells carrying the desired resistance encoded in the plasmid (see section 7.1.5). For the BL21-CodonPlus[®](DE3)-RIL strain chloramphenicol was always added to the plate to maintain the plasmid encoding the additional tRNAs. The plate was incubated upside down at 37 °C over night.

LB medium:

20 g/L LB broth in water

LB-agar-plates:

15 g/L agar agar in LB medium

Antibiotic concentrations:

Ampicillin: 100 µg/mL

Chloramphenicol: 50 µg/mL

Kanamycin: 50 µg/mL

Gentamycin: 7 µg/mL

7.2.2.2 Protein expression in *E. coli*

To express the protein of interest, a single clone from the plate generated during the transformation (see section 7.2.2.1) was picked to inoculate 100 mL LB medium supplemented with the appropriate antibiotic (see section 7.1.5) and chloramphenicol. Alternatively a glycerol cryoculture prepared during an earlier expression of the same protein could be used to inoculate the pre-culture. To conserve a certain clone after transformation, 500 µL of a 100 mL pre-culture were mixed with 500 µL glycerol and stored at – 80 °C. The pre-culture was incubated at 37 °C and 120 rpm in a Multitron pro incubator overnight. For large scale protein expression 2 L of LB medium supplemented with the appropriate antibiotics were inoculated with the 100 mL pre-culture. This main culture was grown at 37 °C until the OD₆₀₀ reached 0.4 – 0.5. The OD could be measured repeatedly using a spectrophotometer and disposable cuvettes. Gene expression of the desired protein was induced by addition of 0.1 mM IPTG. IPTG releases the lac repressor from the lac operon so genes encoded under its promoter can be expressed. The cells were then grown at 21 °C

and 120 rpm overnight. The final OD₆₀₀ was measured before the cells were harvested by centrifugation at 8000 x g and 4 °C for 30 minutes. Cell pellets could be stored at – 80 °C until further use. All proteins except for Rin1C, which was expressed in *Sf9*-cells, were expressed in *E. coli*.

7.2.2.2.1 Monitoring of protein expression in *E. coli* whole cell lysates

To verify that the protein of interest has been expressed, a whole cell lysate of *E. coli* cells before and after induction of the expression was prepared and run on a PAA-gel. 1 mL samples of the main culture before and after induction were harvested at 1000 x g and 4 °C for 5 minutes, respectively. The supernatant was discarded and the pellets were re-suspended in an appropriate amount of quicklysis buffer (amount [μL] = OD₆₀₀ · 100 μL). After 30 minutes of incubation at room temperature, loading buffer has been added to a final concentration of 1 x (for buffer formulation see section 7.2.1.1). The samples were sonicated with 5 pulses (1 second on / 1 second off, 40 % Amplitude) to shear genomic DNA, boiled at 95 °C for 5 minutes and finally loaded on a PAA-gel. SDS-PAGE was performed as described in section 7.2.1.1 followed by coomassie blue staining (see section 7.2.1.2).

Quicklysis buffer:

50 mM Tris, pH 7.8

50 mM NaCl

0.1 % v/v β-Mercaptoethanol

1 x Protease inhibitor mix (from 100 x)

Small amount of lysozyme

7.2.2.3 Protein expression in *Sf9*-cells

The proteins Rin1C and Rin1-TS were expressed in baculovirus-infected *Sf9* (*Spodoptera frugiperda*)-cells by Yvonne Aschenbach-Paul from the Famulok group. The pFBHT-Rin1C and pFB-Rin1-TS constructs were designed by Dr. Anton Schmitz. The virus was used for infection in a ratio of 1:1000 and the protein was expressed for three days at 27 °C. *Sf9*-cells were harvested by centrifugation at 500 x g and 4 °C for 20 minutes.

7.2.2.4 *E. coli* and *Sf9*-cell lysis

Prior to protein purification the cells were lysed using the French Press. The frozen cell pellet from the main culture was re-suspended in 10 mL of cold lysis buffer, sucked up into the pre-chilled French Press chamber and released under a pressure of approx. 18000 psi through a small hole. This process of sucking up and releasing was repeated a total of five times for *E. coli* cells and three times for *Sf9* cells until the cells were completely disrupted. Finally the lysate was cleared by centrifugation at 48 000 x g and 4 °C for 40 minutes.

Table 16: Lysis buffers.

Buffer	Composition
Lysis Buffer DrrA	50 mM Tris, pH 8 300 mM NaCl 20 mM Imidazole 0.1 % v/v β -Mercaptoethanol 1 x Protease inhibitor mix (from 100 x)
Lysis Buffer Rab1	50 mM Tris, pH 8 300 mM NaCl 20 mM Imidazole 0.1 % v/v β -Mercaptoethanol 1 x Protease inhibitor mix (from 100 x)
Lysis Buffer Rab5a	50 mM Tris, pH 7.8 50 mM NaCl 0.1 % v/v β -Mercaptoethanol 1 x Protease inhibitor mix (from 100 x)
Lysis Buffer Rabex-5 _{GEF}	50 mM Tris, pH 7.8 50 mM NaCl 0.1 % v/v β -Mercaptoethanol 1 x Protease inhibitor mix (from 100 x)
Lysis Buffer Rac1	50 mM Tris, pH 7.8 300 mM NaCl 0.1 % v/v β -Mercaptoethanol 1 x Protease inhibitor mix (from 100 x)
Lysis Buffer Rac2	50 mM Tris, pH 7.8 300 mM NaCl 20 mM Imidazole 0.1 % v/v β -Mercaptoethanol 1 x Protease inhibitor mix (from 100 x)
Lysis Buffer Rin1C	50 mM Tris, pH 8 300 mM NaCl 20 mM Imidazole 0.1 % v/v β -Mercaptoethanol 1 x Protease inhibitor mix (from 100 x)
Lysis Buffer Rin1-TS	20 mM MES, pH 6 300 mM NaCl 1 x Protease inhibitor mix (from 100 x)
Lysis Buffer Tiam1DHPH	50 mM Tris, pH 8 300 mM NaCl 20 mM Imidazole 0.1 % v/v β -Mercaptoethanol 1 x Protease inhibitor mix (from 100 x)
Lysis Buffer Vav1	50 mM Tris, pH 7.8 300 mM NaCl 0.1 % v/v β -Mercaptoethanol 1 x Protease inhibitor mix (from 100 x)

7.2.2.5 Affinity chromatography

Affinity chromatography was used to separate the expressed protein carrying an affinity tag from other proteins in a cell lysate. The proteins either carried a Histidine tag that can bind to a Ni-NTA resin by complexing nickel ions immobilized on agarose beads²⁶⁹ or were expressed as Glutathione S-transferase (GST)-fusion proteins²⁷⁰. GST is a short protein that binds glutathione. Glutathione can be immobilized on sepharose beads. After binding the protein of interest can be eluted using a competitor: imidazole for His-tagged proteins and glutathione for GST-fusion proteins, respectively.

7.2.2.5.1 Nickel-NTA affinity chromatography

Approx. 10 mL of the cleared cell lysate from a 2 L culture were incubated with 5 mL of the Ni-NTA resin (50 % slurry, equilibrated with cold lysis buffer) for 1 h at 4 °C in an overhead tumbler. The mixture was transferred to a 10 mL disposable column and the flow through was collected. 50 mL cold washing buffer were added step by step and the wash fraction was collected. Afterwards the protein of interest was eluted by adding five times 1 mL cold elution buffer to the beads. The elution fractions were collected and pooled on ice. The insoluble pellet from the cleared lysate was re-suspended in 10 mL lysis buffer. A 30 µL aliquot for SDS-PAGE analysis was taken at each step: lysate (soluble), lysate (pellet), flow through, wash and elution. The lysate samples and the flow through were diluted 1:2 with lysis buffer before addition of loading buffer in a final concentration of 1 x, the other samples were not pre-diluted. SDS-PAGE was performed as described in section 7.2.1.1 followed by coomassie blue staining (see section 7.2.1.2).

Table 17: Washing buffers for His-tagged proteins.

Buffer	Composition
Washing Buffer DrrA	50 mM Tris, pH 8 300 mM NaCl 20 mM Imidazole
Washing Buffer Rab1	50 mM Tris, pH 8 300 mM NaCl 20 mM Imidazole
Washing Buffer Rab5a	50 mM Tris, pH 7.8 50 mM NaCl
Washing Buffer Rabex-5 _{GEF}	50 mM Tris, pH 7.8 50 mM NaCl
Washing Buffer Rac2	50 mM Tris, pH 7.8 300 mM NaCl 20 mM Imidazole
Washing Buffer Rin1C	50 mM Tris, pH 8 300 mM NaCl 20 mM Imidazole
Washing Buffer Tiam1DHPH	50 mM Tris, pH 8 300 mM NaCl 20 mM Imidazole

Table 18: Elution buffers for His-tagged proteins.

Buffer	Composition
Elution Buffer DrrA	50 mM Tris, pH 8 300 mM NaCl 300 mM Imidazole
Elution Buffer Rab1	50 mM Tris, pH 8 300 mM NaCl 300 mM Imidazole
Elution Buffer Rab5a	50 mM Tris, pH 7.8 50 mM NaCl 300 mM Imidazole
Elution Buffer Rabex-5 _{GEF}	50 mM Tris, pH 7.8 50 mM NaCl 300 mM Imidazole
Elution Buffer Rac2	50 mM Tris, pH 7.8 300 mM NaCl 300 mM Imidazole
Elution Buffer Rin1C	50 mM Tris, pH 8 300 mM NaCl 300 mM Imidazole
Elution Buffer Tiam1DHPH	50 mM Tris, pH 8 300 mM NaCl 300 mM Imidazole

7.2.2.5.2 Glutathione affinity chromatography

3 mL of Glutathione Sepharose resin (75 % slurry) were equilibrated with cold lysis buffer and then incubated with approx. 10 mL cleared cell lysate from a 2 L culture for 1 h at 4 °C in an overhead tumbler. The mixture was transferred to a 10 mL disposable column and the flow-through was collected. 50 mL cold washing buffer were added step by step and the wash fraction was collected. Afterwards the protein of interest was eluted by adding five times 1 mL cold elution buffer to the beads. The elution fractions were collected and pooled on ice. The insoluble pellet from the cleared lysate was re-suspended in 10 mL lysis buffer. A 30 µL aliquot for SDS-PAGE analysis was taken at each step: lysate (soluble), lysate (pellet), flow through, wash and elution. The lysate samples and the flow through were diluted 1:2 with lysis buffer before addition of loading buffer in a final concentration of 1 x, the other samples were not pre-diluted. SDS-PAGE was performed as described in section 7.2.1.1 followed by coomassie blue staining (see section 7.2.1.2).

Table 19: Washing buffers for GSH-fusion proteins.

Buffer	Composition
Washing Buffer Rac1	50 mM Tris, pH 7.8 300 mM NaCl
Washing Buffer Vav1	50 mM Tris, pH 7.8 300 mM NaCl

Table 20: Elution buffers for GSH-fusion proteins.

Buffer	Composition
Elution Buffer Rac1	50 mM Tris, pH 7.8 300 mM NaCl 10 mM Glutathione
Elution Buffer Vav1	50 mM Tris, pH 7.8 300 mM NaCl 10 mM Glutathione

7.2.2.5.3 Strep-Tactin affinity chromatography

10 mL of Strep-Tactin resin (50 % slurry) were transferred to a 15 mL tube and equilibrated with dialysis buffer for Tiam1DHPH (cp. section 7.2.2.6.2) and then incubated with the sample containing the target protein for 1 h at 4 °C in an over-head tumbler. The mixture was transferred to a 10 mL disposable column and the flow-through was collected. After washing the beads with 50 mL dialysis buffer and collection of the washing fraction the target protein was eluted by addition of five times 1 mL elution buffer. The eluate was collected on ice. 30 µL aliquots for SDS-PAGE analysis were taken from the flow-through, the washing fraction and the eluate. SDS-PAGE was performed as described in section 7.2.1.1 followed by coomassie blue staining (see section 7.2.1.2).

Elution buffer Strep-tagged Tiam1DHPH:

50 mM Tris, pH 7.8
150 mM NaCl
2.5 mM Desthiobiotin

7.2.2.5.4 Streptavidin affinity chromatography

1 mL (per 10 mL of expression culture volume) of Streptavidin resin (50 % slurry) was transferred to a 15 mL tube and equilibrated with lysis buffer for Rin1-TS (cp. section 7.2.2.4) and then incubated with the sample containing the target protein for 1 h at 4 °C in an over-head tumbler. The mixture was transferred to a 10 mL disposable column and the flow-through was collected. After washing the beads with 50 mL washing buffer and collection of the washing fraction the target protein was eluted by addition of five times 1 mL elution buffer. The eluate was collected on ice. 30 µL aliquots for SDS-PAGE analysis were taken from the flow-through, the washing fraction and the eluate. SDS-PAGE was performed as described in section 7.2.1.1 followed by coomassie blue staining (see section 7.2.1.2).

Washing buffer Strep-tagged Tiam1DHPH:

20 mM MES, pH 6
300 mM NaCl

Elution buffer Strep-tagged Rin1:

20 mM MES, pH 6
300 mM NaCl
5 mM Desthiobiotin

7.2.2.5.5 Reverse affinity chromatography after tag cleavage

After tag cleavage as described in section 7.2.2.6 the cleaved protein could be separated from the former tag and the protease using reverse affinity chromatography. For that the dialyzed 5 mL sample was re-used for affinity binding as described in section 7.2.2.5. Since the protein of interest no longer contained a purification tag, it did not bind to the resin but appeared in the flow-through fraction while the tag and the protease bound and could and be eluted later on. Reverse affinity chromatography was applied during the purification of DrrA, Rab1, Rac1, Tiam1 and Vav1.

7.2.2.6 Cleavage of purification tags

The presence of a purification tag can sometimes influence the activity and stability of the protein of interest^{271–273}. To avoid this, the tags were cleaved using protease digestion when an appropriate cleavage site was present (see section 7.1.5).

7.2.2.6.1 Cleavage by TEV digestion

The TEV protease is a cysteine protease that originates from the tobacco etch virus. It was expressed and purified as a maltose binding protein (MBP)-fusion protein with the mutation S219V by Volkmar Fieberg from the Famulok group. The protein contained a TEV cleavage site so it could be separated from MBP after self-cleavage. TEV protease was added to the protein of interest in a molar ratio of 1:50 (TEV protease:protein of interest) and the mixture was transferred to a dialysis tubing with a molecular weight cut off of 10 kDa. The tubing was incubated in 2 L dialysis buffer at 4 °C on a magnetic stirrer over night. During dialysis, imidazole/glutathione was removed from the buffer containing the protein of interest via dilution. TEV digestion was used during the purification of DrrA, Rab1 and Vav1 followed by reverse affinity chromatography (see section 7.2.2.5.5).

Table 21: Dialysis buffers for TEV digestions.

Buffer	Composition
Dialysis Buffer DrrA1	50 mM Tris, pH 8 300 mM NaCl 20 mM Imidazole
Dialysis Buffer Rab1	50 mM Tris, pH 8 300 mM NaCl 20 mM Imidazole
Dialysis Buffer Vav1	50 mM Tris, pH 7.8 150 mM NaCl

7.2.2.6.2 Cleavage by Thrombin digestion

Thrombin is a serine protease that is commercially available and was bought at Calbiochem. 100 units of Thrombin were used for the purification yield from a 2 L culture and the mixture was transferred to a dialysis tubing with a molecular weight cut off of 10 kDa. Dialysis was performed as described in section 7.2.2.6.1. Thrombin digestion was used during the purification of Rac1 and Tiam1 followed by reverse affinity chromatography (see section 7.2.2.5.5).

Table 22: Dialysis buffers for Thrombin digestions.

Buffer	Composition
Dialysis Buffer Rac1	50 mM Tris, pH 7.8 300 mM NaCl
Dialysis Buffer Tiam1DHPH	50 mM Tris, pH 7.8 150 mM NaCl

7.2.2.7 Size exclusion chromatography

Size exclusion chromatography was used to increase the purity of proteins after affinity chromatography. Proteins were separated according to their size since the porous column material allows small substances to enter its holes while large ones flow through faster without entering. A Superdex 200 HiLoad 16/600 µg column was attached to the Äkta FPLC system and equilibrated with two column volumes of filtered and degassed storage buffer using a flow rate of 1 mL/min. The 5 mL elution fraction from an affinity chromatography was loaded onto the column and the run was performed at 1 mL/min flow rate. The peaks visible in the UV monitoring at 280 nm were collected in 2 mL fractions. Aliquots of 30 µL were taken from each peak, loading buffer was added in a final concentration of 1 x and SDS-PAGE analysis was performed as described in section 7.2.1.1. Size exclusion chromatography was used during the purification of Rab1, Rab5a, Rabex-5_{GEF}, Rac2 and Rin1C.

Table 23: Storage buffers for size exclusion chromatography.

Buffer	Composition
Storage Buffer Rab5a	50 mM Tris, pH 7.8 100 mM NaCl 2 mM MgCl ₂
Storage Buffer Rabex-5 _{GEF}	50 mM Tris, pH 7.8 50 mM NaCl
Storage Buffer Rac2	50 mM Tris, pH 7.8 300 mM NaCl 2 mM MgCl ₂
Storage Buffer Rin1C	50 mM Tris, pH 7.8 300 mM NaCl

7.2.2.8 Handling of purified proteins

After purification the proteins had to be prepared for the experiments to follow. The protein concentration had to be determined and in most cases increased before proceeding.

7.2.2.8.1 Determination of protein concentration

The protein concentration could be determined either by a photometric approach or by using the Bradford Assay that provides a colorimetric readout.

7.2.2.8.1.1 Photometric determination of protein concentration

The protein concentration can be calculated from the absorbance at 280 nm based on Tryptophan, Tyrosine, Histidine, Cysteine and Phenylalanine residues inside the peptide

chain. Every protein has a certain molar absorption coefficient (ϵ) that can be calculated as described by Pace et al. in 1995²⁷⁴. The protein concentration could then be calculated via the law of Lambert-Beer:

$$A_{280} = \epsilon \cdot l \cdot c$$

A_{280} : Absorption at 280 nm, ϵ : molar absorption coefficient ($M^{-1} \text{ cm}^{-1}$), l : length of cuvette (cm) and c : protein concentration (M)

The absorption has been measured using a spectrophotometer or a NanoDrop 2000. The buffer in which the protein of interest was dissolved was used as blank sample.

7.2.2.8.1.2 Determination of protein concentration via Bradford assay

The Bradford Assay is based on the absorption of Coomassie brilliant blue G-250 that binds to basic and aromatic amino acid residues²⁷⁵. The absorption of protein-bound dye could be measured at 595 nm. From that, the protein concentration could be estimated by comparing the measured absorption with that of a bovine serum albumin (BSA) standard of known concentrations (167 $\mu\text{g/mL}$ – 3 mg/mL). The Protein Assay Dye Reagent Concentrate was diluted 1:5 with ddH₂O and 150 μL of that were mixed with 2 μL of the protein sample or lysate that was to be quantified. Lysates were diluted 1:10 before the concentration was measured. The mixture was transferred to a transparent 96 well plate and the absorbance was measured using the infinite M1000 pro plate reader.

7.2.2.8.2 Increasing the protein concentration and buffer exchange

After purification the protein concentration often had to be increased in order to use the protein in different assays later on. VivaSpin Turbo ultrafiltration spin columns were used for that. The molecular weight cut off (MWCO) of the column was chosen to be at least 50 % smaller than the molecular weight of the protein of interest. The concentrator was filled up with the protein sample and centrifuged at 3000 x g and 4 °C until the desired protein concentration was reached. For buffer exchange or desalting, the protein sample was concentrated until the desired concentration, then the column was filled up with the final buffer and the sample was concentrated again. After three such cycles about 99 % of the initial salt content was removed.

7.2.3 Nucleotide exchange assays

Nucleotide exchange assays were performed to monitor GEF activity. GEF and GTPase were united followed by nucleotide addition. The nucleotide exchange was then monitored using a fluorescently labelled nucleotide analogue. Many fluorophores show altered fluorescence intensity when free in solution compared to when they are in close proximity to e.g. a protein¹³. This effect could be used to detect binding of the fluorescently labelled nucleotides to GTPases. A fluorescence-independent method has also been used. Here radioactively labelled GTP was bound to a GTPase in presence of the corresponding GEF. The amount of GTPase-bound [α -³²P]-GTP was then determined in a filter retention approach.

7.2.3.1 Bodipy-TR and –FL-GTP exchange assay

The fluorophores Bodipy-FL and Bodipy-TR are strongly quenched in solution. They are attached to the 2' or 3' position of the ribose ring of GTP via an aminoethylcarbamoyl linker. Upon GTP binding to a GTPase, the fluorescence signal increases. Generally 1 μM of the GTPases has been used with GEF concentrations between 10 nM – 2 μM , depending on the GEF activity (see table 24). 2 μM (final concentration) of Bodipy-GTP were added via injection prior to repeated fluorescence measurements every 10 – 15 seconds over 30 – 60 minutes. The fluorescence could be measured in black 384-well plates with non-binding surface at 490/520 nm (FL) and 595/620 nm (TR) using the infinite M1000 pro plate reader. Compounds were usually tested as triplicates ranging from 0 to 200 μM with a final assay concentration of 2 % DMSO. The linear range of the resulting curves was used to calculate the slope. To analyze potential concentration-dependent inhibitory effects, the slope was plotted against the logarithmic compound concentration.

Table 24: GEF concentrations for Bodipy-GTP nucleotide exchange assay.

GEF	Concentration
ARNO-Sec7	100 nM
DrrA	25 nM
Rabex-5 _{GEF}	20 nM
Rin1C	100 – 200 nM (batch to batch variations)
Tiam1DHPH	2 μM
Vav1	25 nM

Nucleotide exchange buffer:

20 mM MES, pH 6

100 mM NaCl

2 mM MgCl₂

1 mM DTT

7.2.3.1.1 Bodipy-TR-GTP high throughput screening (HTS) assay

The Bodipy-TR GTP exchange assay described in section 7.2.3.1 has been modified in order to generate an assay potentially suitable for HTS. 40 μM (final concentration) of each library compound were tested only once using 1 μM Rab5a and 200 nM Rin1C. The final DMSO concentration in the screening assay was again 2 %. The compounds were added to 384-well plates using a screening robot followed by manual addition of the proteins diluted in nucleotide exchange buffer. The plate was subdivided into eight parts comprising three columns each Rab5a and Rin1C were incubated with the compounds for eight minutes at room temperature during manual protein addition before injection of Bodipy-TR-GTP to the columns 1 – 3 of the 384-well plate. After the injection the fluorescence at 595/620 nm has been measured once ($t = 0$ minutes) and then again after 20 minutes ($t = 20$ minutes). In between injection into the columns 4 – 5 followed exactly one minute after the injection into the first three columns, followed by fluorescence measurement. This time-delayed pattern was continued until the last three columns were injected and measured twice. From those values the difference in fluorescence intensity (ΔFI) could be calculated. Compounds reducing the ΔFI to ≤ 20 % (compared to mean ΔFI of DMSO controls) were defined as hits. The nucleotide exchange buffer described in section 7.2.3.1 has been supplemented with 1

μM BSA during the screening to reduce protein and Bodipy-TR-GTP adsorption to plastic surfaces.

7.2.3.2 Bodipy-FL-GDP release assay

The Bodipy-FL GDP release assay is another method to analyze GEF activity. In contrast to the previously described nucleotide exchange assays, where the association of GTP is monitored, this assay focuses on the release of GTPase-bound GDP. To pre-load the GTPase with the Bodipy-labelled nucleotide, it was incubated in nucleotide exchange buffer without MgCl_2 but with 1 mM EDTA in presence of 2 μM Bodipy-FL-GDP at 37 °C for 15 minutes. 2 mM MgCl_2 were added to stabilize nucleotide binding followed by another 5 minutes incubation at 37 °C. The pre-loaded GTPase was used in a final concentration of 1 μM with GEF concentrations as described above (section 7.2.3.1). 100 μM GTP were added to start the nucleotide exchange. The fluorescence at 490/520 nm was measured every 10 – 15 seconds for 30 – 60 minutes. Compounds were usually tested as triplicates ranging from 0 to 200 μM with a final assay concentration of 2 % DMSO. Upon exchange of Bodipy-FL GDP for GTP a decrease in fluorescence intensity was to be expected. The linear range of the resulting curves was used to calculate the slope. To analyze potential concentration-dependent inhibitory effects, the slope was plotted against the logarithmic compound concentration.

7.2.3.3 [α - ^{32}P]-GTP exchange assay

The [α - ^{32}P]-GTP exchange assay provides a fluorescence-independent approach to monitor GEF activity *in vitro*. 1 μM of the GTPase was mixed with the correspondent GEF in the concentration described in table 24, section 7.2.3.1 in nucleotide exchange buffer. A mixture of GTP and [α - ^{32}P]-GTP was added: 0.4 $\mu\text{Ci}/\mu\text{L}$ [α - ^{32}P]-GTP, adjusted to 100 μM total GTP with GTP. Compounds were usually tested as triplicates ranging from 0 to 100 μM with a final assay concentration of 2 % DMSO. The amount of protein-bound [α - ^{32}P]-GTP was analyzed after 20 minutes by filter binding followed by scintillation counting. 10 μL of the samples were added as triplicates to approx. 1 x 1 cm sheets of nitrocellulose membrane. The proteins were allowed to bind for 5 minutes at room temperature before the sheets were washed three times for 5 minutes with nucleotide exchange buffer (see section 7.2.3.1) under agitation. The sheets were transferred to scintillation vials and the counts per minute (CpM) were measured in each vial. The assay was either performed kinetically with time points from 2 – 120 minutes or as an endpoint measurement after 20 minutes.

7.2.4 Protein aggregation assay

Compounds inducing protein aggregation are well known to have unspecific side effects on a wide variety of different proteins^{239,276}. To test, whether hit compounds found during the HTS are aggregators, a simple centrifugation assay was performed. 1 μM HT-Rab5a and 300 nM HT-Rin1C were mixed with 2 μM GTP in nucleotide exchange buffer (see section 7.2.3.1). A 30 μL sample of that was taken and SDS-PAGE loading buffer (see section 7.2.1.1) was added to a final concentration of 1 x. Then 50 μM of the compounds were added in a final DMSO concentration of 2 %. DMSO was also used as a positive control. The samples were incubated at room temperature for 20 minutes followed by centrifugation at 20 000 x g at room temperature for 10 minutes. A 30 μL sample was taken from each supernatant and

loading buffer was added to a final concentration of 1 x. The remaining supernatant was removed carefully and the pellet was resuspended in an equal amount of buffer. A 30 μ L aliquot was taken from each pellet sample and loading buffer was added to a final concentration of 1 x. All samples were boiled for 5 minutes at 95 °C and then subjected to SDS-PAGE and semi-dry western blotting as described in sections 7.2.1.1, 7.2.1.3 and 7.2.1.3.1. Anti-His₅ antibody was added over night at 4 °C under agitation followed by 1 h incubation with the secondary fluorescently labelled goat-anti-mouse antibody at room temperature under light protection (for antibody dilutions and specifications see section 7.1.7). The amount of soluble HT-Rin1C and HT-Rab5a in the supernatants and pellets was compared to the amount in the DMSO control as well as in the input sample.

7.2.5 The insulin receptor auto-phosphorylation assay

Compounds are often tested in an unrelated assay to check for promiscuous inhibition by aggregation²⁴¹. The insulin receptor auto-phosphorylation assay has been performed to check for unspecific inhibition. 250 nM of the insulin receptor intracellular domain (IR-ICD) were mixed in IR-ICD Phosphorylation Buffer with 50 μ M of the compound to be tested in a final assay concentration of 2 % DMSO. Two controls were performed: one with 2 % DMSO and one without compound or DMSO. A 30 μ L aliquot was taken and SDS-PAGE loading buffer (see section 7.2.1.1) was added to a final concentration of 1 x (t = 0 sec.). The sample was boiled for 5 min. at 95 °C and then stored at room temperature until SDS-PAGE analysis was performed. ATP was added to the remaining sample in a final concentration of 1 mM. Further 30 μ L aliquots were taken after 20 sec. and 60 sec. and treated as the one before. All samples were subjected to SDS-PAGE, coomassie staining and semi-dry western blotting as described in sections 7.2.1.1, 7.2.1.2, 7.2.1.3 and 7.2.1.3.1. Anti-phospho-tyrosine antibody has been added diluted 1:500 in TBST with 5 % BSA. The blot was incubated with the antibody overnight at 4 °C under agitation and washed three times for five minutes with TBST before incubation with the secondary goat-anti-mouse antibody as described in section 7.2.1.3 (for antibody dilution and specifications see section 7.1.7). The intensities of the bands corresponding to phosphorylated IR-ICD were compared between the samples with and without compound.

IR-ICD phosphorylation buffer:

20 mM HEPES, pH 7.2

100 mM NaCl

30 mM MgCl₂

7.2.6 The ABL1-mediated Rin1 phosphorylation assay

To exclude a domain-unspecific effect on the Rin1/ABL interaction by the hit compound an ABL1-mediated Rin1 phosphorylation assay has been performed. 500 nM Rin1-TS and 50 nM HT-ABL1 were mixed in Rin1 Phosphorylation Buffer before 50 μ M of the compound to be tested were added in a final assay concentration of 2 % DMSO. Two controls were performed: one with 2 % DMSO and one without compound or DMSO. A 30 μ L aliquot was taken and SDS-PAGE loading buffer (see section 7.2.1.1) was added to a final concentration of 1 x (t = 0 sec.). The sample was boiled for 5 min. at 95 °C and then stored at room temperature until SDS-PAGE analysis was performed. ATP was added to the remaining sample in a final concentration of 1 mM. Further 30 μ L aliquots were taken after 1 minute

and 15 minutes and treated as the one before. All samples were subjected to SDS-PAGE, coomassie staining and semi-dry western blotting as described in sections 7.2.1.1, 7.2.1.2, 7.2.1.3 and 7.2.1.3.1. Anti-phospho-tyrosine antibody has been added diluted 1:500 in TBST with 5 % BSA. The blot was incubated with the antibody overnight at 4 °C under agitation and washed three times for five minutes with TBST before incubation with the secondary goat-anti-mouse antibody as described in section 7.2.1.3 (for antibody dilution and specifications see section 7.1.7). The intensities of the bands corresponding to phosphorylated Rin1-TS and HT-ABL1 were compared between the samples with and without compound.

Rin1 phosphorylation buffer:

50 mM Tris, pH 7.2

100 mM NaCl

2 mM MgCl₂

7.2.7 Analysis of Bodipy-TR-GTP binding to Rab5a

To analyse the influence of the hit compound on GTP-binding to Rab5a, Rab5a was loaded with Bodipy-TR-GTP in presence of the compound in different concentrations between 0.05 and 200 μM. 1 μM of Rab5a was incubated with 1 mM EDTA in presence of 2 μM Bodipy-TR-GTP at 37 °C for 15 minutes. The fluorescence of Bodipy-TR-GTP was measured every 20 seconds at 595 nm (excitation) and 620 nm (emission). A linear fit was applied on the data generated in the first 100 seconds. The slopes were calculated and compared to that of a DMSO control.

7.2.8 Synthesis and characterization of compounds

All compounds listed below were kindly synthesized by Dr. Jeffrey Hannam from the Famulok Group. He also delivered the synthesis protocols in this section. Chemicals were bought from Acros, Sigma Aldrich, Fluorochem, Alfa Aesar, Iris Biotech or Fisher Scientific. Diisopropylethylamine (DIPEA) was distilled over CaH₂ under argon and stored over potassium hydroxide pellets.

NMR spectra (¹H NMR and ¹³C NMR) were recorded in deuterated dimethyl sulfoxide (*d*₆-DMSO) or deuterated chloroform (CDCl₃) on DPX 400, DRX 300, DMX 500 MHz or DPX 600 MHz Spectrometers from BRUKER, Karlsruhe. The chemical shifts were plotted as δ-values in ppm (multiplicity, coupling constant *J* in Hz, number of protons) for ¹H NMR spectra and chemical shift δ in ppm for ¹³C NMR spectra. Multiplicities are abbreviated as follows: s = singlet, d = doublet, t = triplet, q = quartet, m = multiplet, or combinations thereof. Residual solvent peaks of DMSO (δ_H = 2.50 ppm, δ_C = 39.5 ppm) were used as an internal reference. NMR spectra were assigned using information ascertained from COSY and DEPT135.

ESI-Mass spectra were measured on a MAT-95XL from Finnigan, Bremen. ESI-Mass spectra were measured with a microTOF-Q flight time spectrometer from Bruker, Daltonik. Samples were analysed by HPLC MS on an Agilent 1100 HPLC system with an Agilent Zorbax RP SB-C18 (2.1 x 50 mm, 5 μm) coupled to a Bruker HTC Esquire mass spectrometer. LCMS analyses were performed using an acetonitrile and water (formic acid 0.1 % v/v) based gradient from 5 – 100 % acetonitrile over 15 minutes with a flow rate of 0.5 mL/min.

Reactions were monitored by thin-layer chromatography (TLC) with aluminium sheets coated with silica gel 60 F254 (Merck) and visualized by exposure to ultraviolet light (λ = 254

nm and $\lambda = 365$ nm). Flash column chromatography was performed using silica gel (60 Å, 40-63 μ m, Merck) and a forced flow of eluent. All yields are isolated, unless otherwise specified.

7.2.8.1 Synthesis of Aniline Precursors

Aniline precursors were synthesized as described in figure 37.

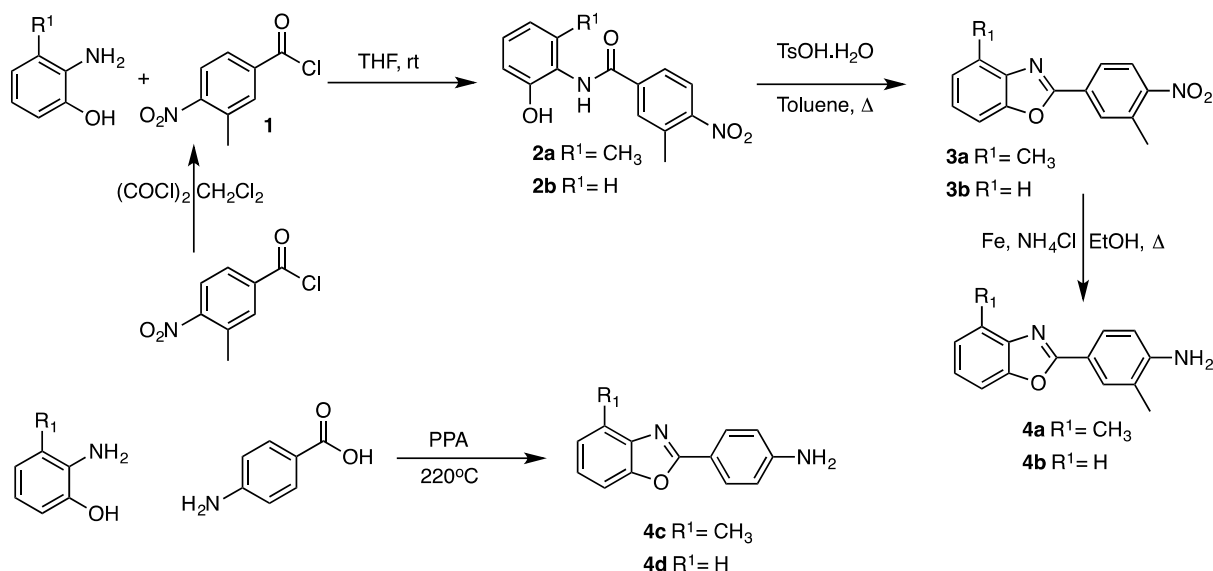
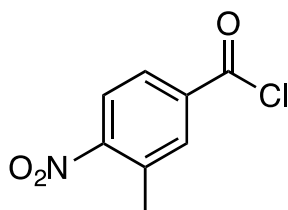


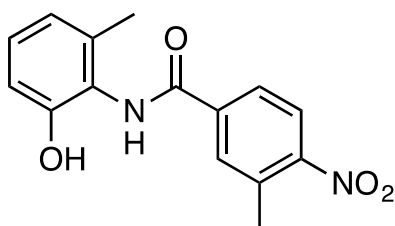
Figure 37: Synthesis of Aniline Precursors.

7.2.8.1.1 3-Methyl-4-Nitrobenzoic acid chloride (1)



Oxalyl Chloride (22.6 mL of a 1 M solution in CH_2Cl_2) was added dropwise to a stirred solution of 3-methyl-4-nitrobenzoic acid (10.0 g, 55.2 mmol) in THF (330 mL) at RT. The reaction mixture was stirred at RT for 2 h. The reaction mixture was concentrated under reduced pressure. The resulting residue was distilled under high vacuum to give **1** as a yellow solid, which was used without further analysis. Yield 10.0 g, 91 %.

7.2.8.1.2 *N*-(2-Hydroxy-6-methylphenyl)-3-methyl-4-nitrobenzamine (2a)



2-Hydroxy-6-methyl aniline ($R^1 = \text{CH}_3$) (8.64 g in 50 mL THF, 23.7 mmol) was added dropwise to a stirred solution of **1** (7.0 g, 10.8 mmol) in THF (250 mL) at RT over 10 min. The reaction mixture was stirred overnight for 18 h and afterwards concentrated under reduced pressure. The remaining residue was dissolved in ethyl acetate (250 mL) and was washed with 1 N aq. HCl (3 x 75 mL), sat. aq. NaHCO_3 (3 x 75 mL), sat. aq. NaCl (1 x 50 mL), dried (MgSO_4) and concentrated under reduced pressure to give **2a** as a red solid.

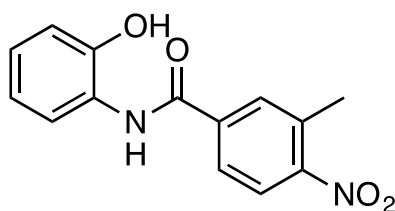
Yield: 9.51 g, 95 %

^1H NMR (300 MHz, d_6 -DMSO, 298 K) δ 9.74 (s, 1H), 9.70 (s, 1H), 8.09 (d, $J = 8.4, 2.0$ Hz, 1H), 8.07 (d, $J = 2.0$ Hz, 1H), 7.98 (dd, $J = 8.4, 2.0$ Hz, 1H), 7.63 (dd, $J = 8.1, 1.5$ Hz, 1H), 7.09-7.05 (m, 1H), 6.94 (dd, $J = 8.1, 1.5$ Hz, 1H), 6.84 (td, $J = 7.6, 1.4$ Hz), 2.58 (s, 3H).

^{13}C NMR (75 MHz, d_6 -DMSO, 298 K) δ 163.7 (s), 153.3 (s), 150.4 (s), 138.4 (s), 136.8 (s), 132.7 (s), 132.0 (d), 127.4 (d), 126.5 (d), 124.4 (d), 123.4 (s), 120.4 (d), 113.6 (d), 19.4 (q), 17.9 (q).

HRMS (ESI+): Calcd for $\text{C}_{15}\text{H}_{14}\text{N}_2\text{O}_2\text{Na}$: 309.0846 $[\text{M} + \text{Na}]^+$ Found 309.0839.

7.2.8.1.3 *N*-(2-Hydroxyphenyl)-3-methyl-4-nitrobenzamine (**2b**)



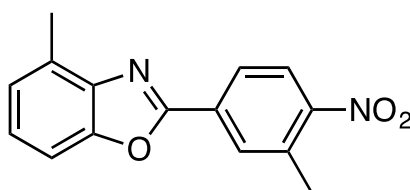
2-Aminophenol ($R^1 = \text{H}$) (0.995 g in 5 mL THF, 23.7 mmol) was added dropwise to a stirred solution of **1** (2.0 g, 10.8 mmol) in THF (25 mL) at RT over 10 min. The reaction mixture was stirred overnight for 18 h. The reaction mixture was concentrated under reduced pressure and the remaining residue was dissolved in ethyl acetate (250 mL) and was washed with 1N aq. HCl (3 x 75 mL), sat. aq. NaHCO_3 (3 x 75 mL), sat. aq. NaCl (1 x 50 mL), dried (MgSO_4) and reduced under reduced pressure to give **2b** as a red solid.

Yield: 2.65 g, 90 %

^1H NMR (600 MHz, d_6 -DMSO, 298 K) δ 9.74 (s, 1H), 9.70 (s, 1H), 8.09 (d, $J = 8.4$ Hz, 1H), 8.07 (d, $J = 2.0$ Hz, 1H), 7.98 (dd, $J = 8.3, 2.0$ Hz, 1H), 7.63 (dd, $J = 8.0, 1.6$ Hz, 1H), 7.09-7.05 (m, 1H), 6.94 (dd, $J = 8.0, 1.4$ Hz, 1H), 6.84 (td, $J = 7.6, 1.4$ Hz, 1H), 2.58 (s, 3H).

^{13}C NMR (200 MHz, d_6 -DMSO, 298 K) δ 163.7 (s), 150.5 (s), 149.9 (s), 138.4 (s), 132.7 (s), 131.9 (d), 126.4 (d), 126.2 (d), 125.2 (s), 124.9 (d), 124.4 (d), 118.9 (d), 116.0 (d), 19.3 (q).

7.2.8.1.4 4-Methyl-2-(3-methyl-4-nitrophenyl benzoxazole (3a)



p-toluenesulfonic acid monohydrate (12.4 g, 65.3 mmol) was added in one portion to a stirred suspension of **2a** (8.5 g, 29.7 mmol) in toluene (300 mL) at RT. The reaction mixture was heated at 110 °C for 3 h. The reaction mixture was cooled and washed with sat. aq. NaHCO₃ (3 x 50 mL), water (1 x 50 mL), sat. aq. NaCl (1 x 50 mL), dried (MgSO₄) and concentrated under reduced pressure to give **3a** as a red solid.

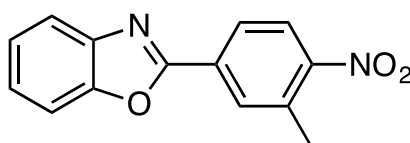
Yield: 7.85 g, 99 %

¹H NMR (300 MHz, CDCl₃, 298 K) δ 8.29 (d, *J* = 1.9 Hz 1H), 8.23 (dd, *J* = 8.5 Hz, 1.9 Hz, 1H), 8.12 (d, *J* = 8.5 Hz 1H), 7.44 (d, *J* = 8.5 Hz 1H), 7.31 (t, *J* = 7.8 Hz, 1H), 7.20 (dt, *J* = 7.4 Hz, 1H), 2.73 (s, 3H), 2.70 (s, 3H).

¹³C NMR (75 MHz, CDCl₃, 298 K) δ 159.9 (s), 150.7 (s), 150.3 (s), 141.2 (s), 134.3 (s), 131.6 (d), 131.3 (s), 131.2 (s), 125.8 (d) 125.7 (d), 125.5 (d), 125.3 (d), 108.0 (s), 20.4 (q), 16.5 (q).

HRMS (ESI+): Calcd for C₁₅H₁₄N₂O₂Na: 309.0846 [M+ Na]⁺ Found 309.0839.

7.2.8.1.5 4-Methyl-2-(4-nitrophenyl)benzoxazole (3b)



p-toluenesulfonic acid monohydrate (6.92 g, 36.4 mmol) was added in one portion to a stirred suspension of **2b** (4.5 g, 16.5 mmol) in toluene (200 mL) at RT. The reaction mixture was heated at 110°C for 3 h. The reaction mixture was cooled and washed with sat. aq. NaHCO₃ (3 x 50 mL), water (1 x 50 mL), sat. aq. NaCl (1 x 50 mL), dried (MgSO₄) and concentrated under reduced pressure to give **3b** as a red solid.

Yield: 3.92 g, 93 %

¹H NMR (300 MHz, CDCl₃, 298 K) δ 8.28-8.26 (m, 1H), 8.21 (dd, *J* = 8.4 Hz, 2.1, 1H), 8.11 (d, *J* = 8.4 Hz, 1H), 7.85-7.78 (m, 1H), 7.66-7.60 (m, 1H), 7.47-7.40 (m, 2H), 2.71 (s, 3H).

¹³C NMR (75 MHz, CDCl₃, 298 K) δ 160.7 (s), 150.9 (s), 150.6 (s), 141.7 (s), 134.4 (s), 131.7 (d), 131.0 (s), 126.2 (d), 125.8 (d) 125.4 (d), 125.1 (d), 120.5 (d), 110.9 (d), 20.4 (q).

HRMS (ESI+): Calcd for C₁₃H₁₁N₂O₃: 255.0764 [M+ H]⁺ Found 255.0753.

7.2.8.2 Synthesis of CG3 05 A02 Analogues

The CG3 05 A02 Analogues were synthesized as described in figure 38.

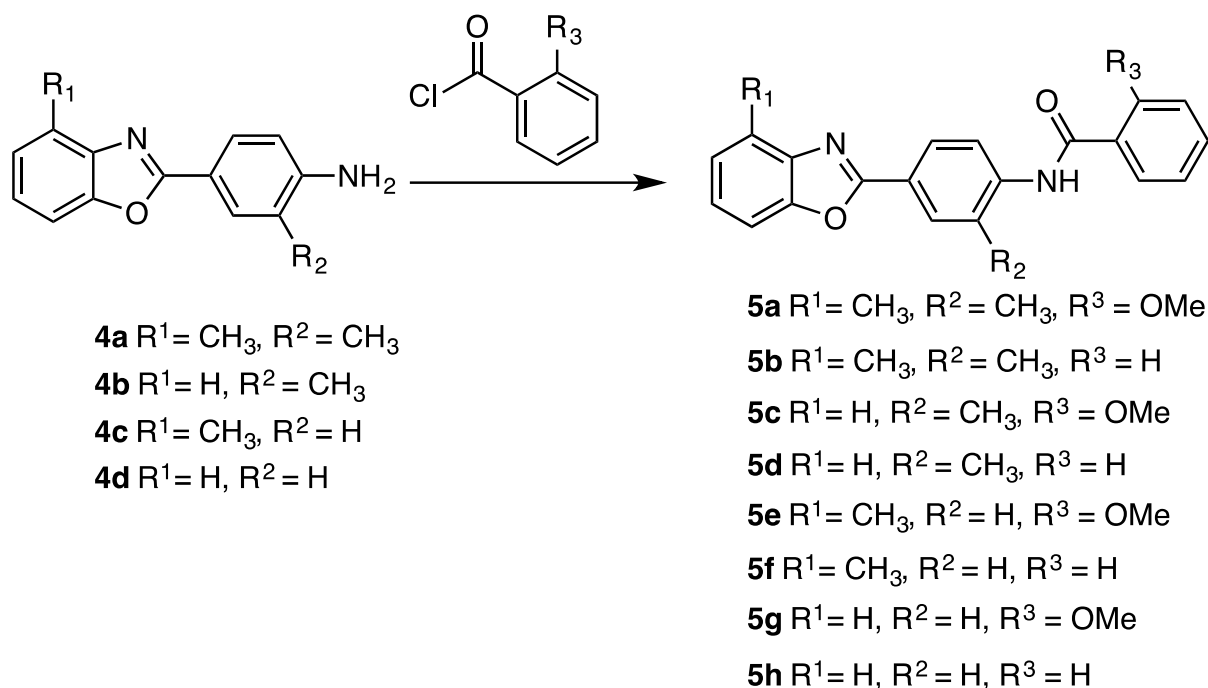
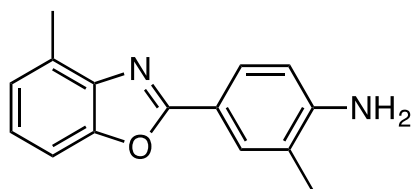


Figure 38: Synthesis of CG3 05 A02 Analogues.

7.2.8.2.1 2-Methyl-4-(4-methylbenzoxazol-2-yl)benzamine (4a)



3a (6.05 g, 22.5 mmol) was suspended in ethanol (300 mL) and water (50 mL). Ammonium chloride (6.03 g, 113 mmol), followed by iron powder (6.30 g, 113 mmol) were added both on one portion at RT. The reaction mixture was heated to 80 °C for 2 h. The reaction mixture was cooled to RT and concentrated under reduced pressure. The remaining residue was dissolved in ethyl acetate (500 mL) and washed with sat. aq. NaHCO₃ (2 x 50 mL), sat. aq. NaCl (1 x 50 mL), dried (MgSO₄) and again concentrated under reduced pressure. The residue was dry loaded onto silica gel and purified using column chromatography (SiO₂) using a gradient elution 10% EtOAc in Cyclohexane → 50 % EtOAc to give **4a** as a beige solid.

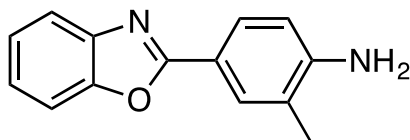
Yield: 4.84 g, 90 %

¹H NMR (300 MHz, *d*₆-DMSO, 298 K) δ 7.79 (dd, *J* = 2.0 Hz 0.9 Hz, 1H), 7.76 (dd, *J* = 8.3 Hz, 2.1, 1H), 7.51-7.42 (m, 1H), 7.18 (t, *J* = 7.7 Hz 1H), 7.12 (dt, *J* = 2.0 Hz 0.9 Hz, 1H), 6.74 (d, *J* = 8.3 Hz, 1H), 5.70 (s, 2H), 2.54 (s, 3H), 2.16 (s, 3H).

^{13}C NMR (75 MHz, d_6 -DMSO, 298 K) δ 162.9 (s), 150.5 (s), 149.5 (s), 141.2 (s), 129.3 (d), 128.6 (d), 126.5 (s), 124.7 (s), 123.6 (d), 120.9 (d), 113.5 (d), 113.2 (s), 107.5 (s), 17.3 (q), 16.3 (q).

HRMS (ESI⁺): Calcd for $\text{C}_{15}\text{H}_{14}\text{N}_2\text{ONa}$: 261.0998 $[\text{M} + \text{Na}]^+$ Found 261.0999.

7.2.8.2.2 4-(Benzoxazol-2-yl)-2-methylaniline (4b)



3b (3.42 g, 13.5 mmol) was suspended in ethanol (150 mL) and ammonium chloride (3.60 g, 67.3 mmol), followed by iron powder (3.76 g, 67.3 mmol) were added both on one portion at RT. The reaction mixture was heated to 80 °C for 2 h. The reaction mixture was cooled to RT and concentrated under reduced pressure. The remaining residue was dissolved in ethyl acetate (200 mL) and washed with sat. aq. NaHCO_3 (2 x 20 mL), sat. aq. NaCl (1 x 20 mL), dried (MgSO_4) and concentrated under reduced pressure. The residue was dry loaded onto silica gel and purified using column chromatography (SiO_2) using a gradient elution 10 % EtOAc in Cyclohexane \rightarrow 50 % EtOAc to give **4b** as a colorless solid.

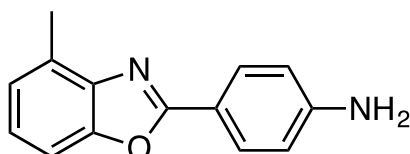
Yield: 2.38 g, 79 %

^1H NMR (600 MHz, d_6 -DMSO, 298 K) δ 7.80 (dd, $J = 2.1, 0.9$ Hz, 1H), 7.76 (dd, $J = 8.3, 2.1$ Hz, 1H), 7.68-7.63 (m, 2H), 7.33-7.27 (m, 2H), 6.75 (d, $J = 8.3$ Hz, 1H), 5.72 (s, 2H), 2.16 (s, 3H).

^{13}C NMR (200 MHz, d_6 -DMSO, 298 K) δ 163.6 (s), 150.6 (s), 149.9 (s), 142.1 (s), 129.3 (d), 126.6 (d), 124.2 (d), 123.9 (d), 120.9 (s), 118.6 (d), 113.5 (d), 113.0 (s), 110.2 (d), 17.3 (q).

HRMS (ESI⁺): Calcd for $\text{C}_{14}\text{H}_{13}\text{N}_2\text{O}$: 225.1022 $[\text{M} + \text{H}]^+$ Found 225.1023.

7.2.8.2.3 4-(4-Methylbenzoxazol-2-yl)benzamine (4c)



Polyphosphoric Acid (50 mL) was added to a round-bottomed flask and heated to 120 °C. 2-hydroxy-6-methylaniline (5.02 g, 40.8 mmol) was added, followed by 4-Aminobenzoic acid (5.59 g, 40.8 mmol) with mechanical stirring. After dissolution of the solids, the reaction mixture was heated to 220 °C for 4 h. The reaction mixture was cooled and neutralized carefully with cooled sodium hydroxide (2 M) and the resulting precipitate was filtered and dried overnight under high vacuum (P_2O_5). The residue was dry loaded onto silica gel and purified using column chromatography (SiO_2) using a gradient elution 10 % EtOAc in Cyclohexane \rightarrow 50 % EtOAc to give **4c** as a colorless solid.

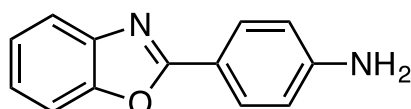
Yield: 5.48 g, 60 %

¹H NMR (600 MHz, *d*₆-DMSO, 298 K) δ 7.89-7.85 (m, 2H), 7.45 (dt, *J* = 8.0 0.9 Hz, 1H), 7.18 (t, *J* = 7.7 Hz 1H), 7.12 (dt, *J* = 7.4, 0.9 Hz, 1H), 6.72-6.69 (m, 2H), 5.94 (s, 2H), 2.53 (s, 3H).

¹³C NMR (200 MHz, *d*₆-DMSO, 298 K) δ 162.8 (s), 152.3 (s), 149.5 (s), 142.2 (s), 128.8 (d), 128.6 (s), 124.7 (d) 123.6 (d), 113.5 (d), 113.0 (s), 107.5 (d), 16.2 (q).

HRMS (ESI+): Calcd for C₁₄H₁₃N₂O: 225.1022 [M+ H]⁺ Found 225.1027.

7.2.8.2.4 4-(Benzoxazol-2-yl)benzamine (4d)



Polyphosphoric Acid (160 mL) was added to a round-bottomed flask and heated to 140°C. Aminophenol (11.55 g, 106 mmol) was added, followed by 4-Aminobenzoic acid (14.52 g, 106 mmol) with mechanical stirring. After dissolution of the solids, the reaction mixture was heated to 220°C for 4 hours. The reaction mixture was cooled and neutralized carefully with cooled sodium hydroxide (2M) and the resulting precipitate was filtered and dried overnight under high vacuum (P₂O₅). The residue was dry loaded onto silica gel and purified using column chromatography (SiO₂) using a gradient elution 10% EtOAc in Cyclohexane → 50% EtOAc to give **4d** as a colorless solid.

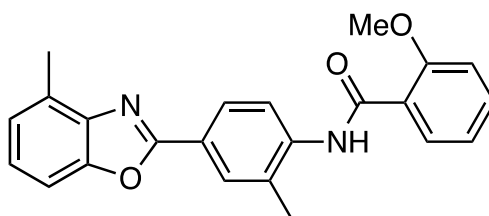
Yield: 11.8 g, 53 %

¹H NMR (300 MHz, *d*₆-DMSO, 298 K) δ 7.90-7.85 (m, 2H), 7.66-7.64 (m, 2H), 7.34-7.27 (m, 2H), 6.74-6.68 (m, 2H), 5.98 (s, 2H).

¹³C NMR (75 MHz, *d*₆-DMSO, 298 K) δ 163.6 (s), 152.5 (s), 149.8 (s), 142.1 (s), 128.9 (d), 124.3 (d) 124.0 (d), 118.7 (d), 113.5 (d), 112.7 (s), 110.2 (d).

HRMS (ESI+): Calcd for C₁₃H₁₁N₂O: 211.0866 [M+ H]⁺ Found 211.0883.

7.2.8.2.5 2-Methoxy-*N*-(2-methyl-4-(4-methylbenzol-2-yl)phenyl)benzamine (5a)



4a (0.50 g, 2.10 mmol) was dissolved in acetonitrile (25 mL), DIPEA (914 μL, 5.13 mmol) was added in one portion and then 2-methoxybenzoyl chloride (423 μL in 5 mL acetonitrile, 3.15 mmol) was added dropwise over 10 min with stirring at 0 °C. The reaction mixture was stirred 1 h and the resulting precipitate was filtered and washed with cold acetonitrile to give **5a** as a colorless solid.

Yield: 0.578 g, 74 %

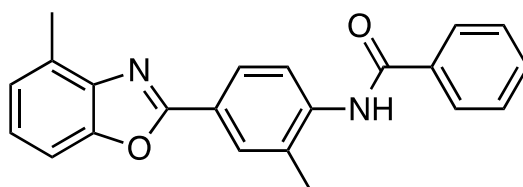
¹H NMR (300 MHz, *d*₆-DMSO, 298 K) δ 10.12 (s, 1H), 8.40 (d, *J* = 8.5 Hz, 1H), 8.12 (d, *J* = 2.0 Hz, 1H), 8.06 (dd, *J* = 8.5, 2.0 Hz, 1H), 8.00 (d, *J* = 7.8, 1.8 Hz, 1H), 7.63-7.53 (m, 2H), 7.33-7.25 (m, 2H), 4.05 (s, 3H), 2.59 (s, 3H), 2.47 (s, 3H).

¹³C NMR (75 MHz, *d*₆-DMSO, 298 K) δ 163.1 (s), 161.5 (s), 157.0 (s), 149.8 (s), 140.8 (s), 140.0 (s), 133.4 (d), 131.1 (d), 129.6 (s), 129.1 (d), 128.9 (s), 125.7 (d), 125.1 (d), 124.9 (d), 121.9 (s), 121.7 (d), 121.0 (d), 112.4 (d), 108.0 (d), 56.4 (q), 17.6 (q), 16.3 (q).

LCMS (ESI) 373.34 [M+H]⁺ R_t = 15.6 mins (99 %)

HRMS (ESI⁺): Calcd for C₂₃H₂₀N₂O₃Na: 395.1366 [M+ Na]⁺. Found 395.1366.

7.2.8.2.6 *N*-(2-Methyl-4-(4-methylbenzoxazol-2-yl)phenyl)benzamide (5b)



4b (0.688 g, 2.50 mmol) was dissolved in acetonitrile (50 mL), DIPEA (1.39 mL, 5.13 mmol) was added in one portion and then 2-methoxybenzoyl chloride (423 μL in 5 mL acetonitrile, 3.15 mmol) was added dropwise over 10 min with stirring at 0 °C. The reaction mixture was stirred 1 h and the resulting precipitate was filtered and washed with cold acetonitrile to give **5b** as a colorless solid.

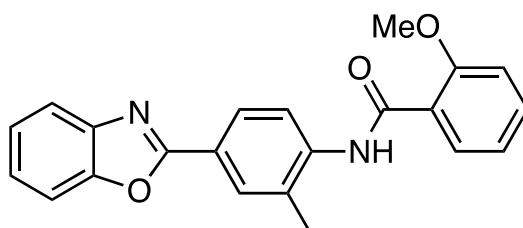
Yield: 0.736 g, 86 %

¹H NMR (300 MHz, *d*₆-DMSO, 298 K) δ 10.02 (s, 1H), 8.23-8.16 (m, 2H), 8.10-8.04 (m, 2H), 8.02-7.96 (m, 2H), 7.80-7.73 (m, 2H), 7.65-7.52 (m, 3H), 7.43-7.36 (m, 2H).

¹³C NMR (75 MHz, *d*₆-DMSO, 298 K) δ 165.4 (s), 161.4 (s), 149.9 (s), 140.8 (s), 139.8 (s), 134.3 (s), 133.8 (s), 131.7 (d), 129.7 (s), 129.1 (d), 128.4 (d), 127.7 (d), 126.4 (d), 125.13 (d), 125.09 (d), 125.0 (d), 123.5 (s), 108.1 (d), 17.9 (q), 16.2 (q).

HRMS (ESI⁺): Calcd for C₂₂H₁₉N₂O₂: 343.1441 [M+H]⁺. Found 343.1438.

7.2.8.2.7 *N*-(4-(Benzoxazol-2-yl)-2-methylphenyl)-2-methoxybenzamide (5c)



4b (0.688 g, 2.50 mmol) was dissolved in acetonitrile (20 mL), DIPEA (676 μ L, 5.13 mmol) was added in one portion and then 2-methoxybenzoyl chloride (313 μ L in 5 mL acetonitrile, 3.15 mmol) was added dropwise over 10 min with stirring at 0 °C. The reaction mixture was stirred 1 h and the resulting precipitate was filtered and washed with cold acetonitrile to give **5b** as a colorless solid.

Yield: 0.510 g, 92 %

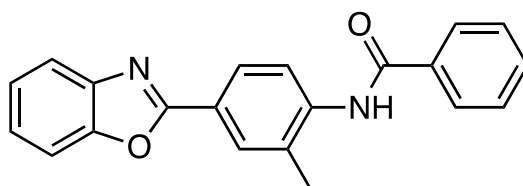
^1H NMR (600 MHz, d_6 -DMSO, 298 K) δ 10.12 (s, 1H), 8.40 (d, J = 8.5 Hz, 1H), 8.12 (dd, J = 2.0, 0.9 Hz, 1H), 8.07 (dd, J = 8.5, 2.0 Hz, 1H), 8.01 (dd, J = 7.5, 2.0 Hz, 1H), 7.80-7.74 (m, 2H), 7.59 (ddd, J = 8.5, 7.5, 2.0 Hz, 1H), 7.44-7.37 (m, 2H), 7.28 (d, J = 8.5 Hz, 1H), 7.15 (td, J = 7.5 Hz, 1H), 4.05 (s, 3H), 2.47 (s, 3H).

^{13}C NMR (200 MHz, d_6 -DMSO, 298 K) δ 163.1 (s), 162.2 (s), 157.0 (s), 150.1 (s), 141.6 (s), 140.1 (s), 133.4 (d), 131.0 (d), 129.1 (d), 128.9 (s), 125.7 (d), 125.1 (d), 124.7 (d), 121.9 (s), 121.7 (d), 121.5 (s), 121.0 (d), 119.5 (d), 112.4 (d), 110.7 (d), 56.4 (q), 17.5 (q).

LCMS (ESI) 359.2 [M+H]⁺ R_t = 14.4 min

HRMS (ESI+): Calcd for C₂₃H₁₉N₂O: 359.1390 [M+H]⁺. Found 359.1394.

7.2.8.2.8 *N*-(4-(Benzoxazol-2-yl)-2-methylphenyl)benzamide (**5d**)



4b (0.50 g, 2.50 mmol) was dissolved in acetonitrile (25 mL), DIPEA (388 μ L, 5.13 mmol) was added in one portion and then benzoyl chloride (423 μ L in 5 mL acetonitrile, 3.15 mmol) was added dropwise over 10 min with stirring at 0 °C. The reaction mixture was stirred 1 h and the resulting precipitate was filtered and washed with cold acetonitrile to give **5b** as a colorless solid.

Yield: 0.636 g, 87 %

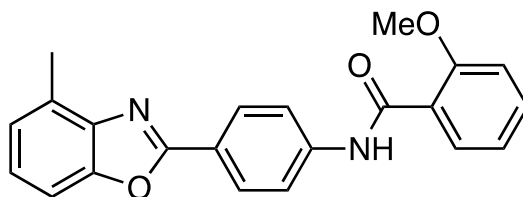
^1H NMR (500 MHz, d_6 -DMSO, 298 K) δ 10.03 (s, 1H), 8.15-8.13 (m, 1H), 8.07 (dd, J = 8.3, 2.1 Hz, 1H), 8.03-8.00 (m, 2H), 7.82-7.77 (m, 2H), 7.72 (d, J = 8.3 Hz, 1H), 7.64-7.60 (m, 1H), 7.56 (dd, J = 8.3, 6.7 Hz, 2H), 7.45-7.39 (m, 2H), 2.40 (s, 3H).

^{13}C NMR (125 MHz, d_6 -DMSO, 298 K) δ 165.4 (s), 162.1 (s), 150.2 (s), 141.6 (s), 140.0 (s), 134.3 (s), 133.9 (s), 131.8 (d), 129.2 (d), 128.4 (d), 127.7 (d), 126.4 (d), 125.3 (d), 125.2 (d), 124.8 (d), 123.4 (s), 119.7 (d), 110.8 (d), 17.9 (q).

LCMS (ESI) 329.23 [M+H]⁺ R_t = 13.5 mins (90 %)

HRMS (ESI+): Calcd for C₂₁H₁₆N₂O₂Na: 351.1104 [M+ Na]⁺. Found 351.1115.

7.2.8.2.9 2-Methoxy-*N*-(4-(4-methylbenzoxazol-2-yl)phenyl)benzamide (5e)



4b (0.5 g, 2.50 mmol) was dissolved in acetonitrile (25 mL), DIPEA (964 μ L, 5.13 mmol) was added in one portion and then 2-methoxybenzoyl chloride (450 μ L in 5 mL acetonitrile, 3.15 mmol) was added dropwise over 10 min with stirring at 0 °C. The reaction mixture was stirred 1 h and the resulting precipitate was filtered and washed with cold acetonitrile to give **5b** as a colorless solid.

Yield: 0.631 g, 79 %

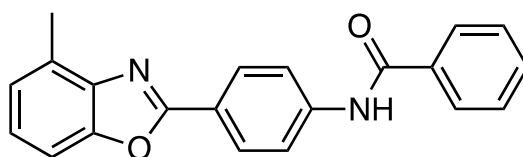
^1H NMR (600 MHz, d_6 -DMSO, 298 K) δ 10.45 (s, 1H), 8.18 (d, J = 8.6 Hz, 2H), 7.99 (d, J = 8.6 Hz, 2H), 7.64 (dd, J = 7.5, 1.8 Hz, 1H), 7.58-7.55 (m, 1H), 7.53 (ddd, J = 8.6, 7.4, 1.8 Hz 1H), 7.30 (t, J = 7.4 Hz 1H), 7.22-7.19 (m, 2H), 7.09 (td, J = 7.4, 0.9 Hz, 1H), 3.91 (s, 3H), 2.59 (s, 3H).

^{13}C NMR (200 MHz, d_6 -DMSO, 298 K) δ 165.0 (s), 161.5 (s), 156.5 (s), 149.8 (s), 142.1 (s), 140.8 (s), 132.2 (d), 129.6 (d), 128.0 (d), 125.1 (d), 124.84 (d), 124.80 (s), 121.2 (s), 120.5 (d), 119.7 (d), 112.0 (d), 55.9 (q), 16.2 (q).

LCMS (ESI) 359.18 [M+H]⁺ R_t = 14.7 min

HRMS (ESI+): Calcd for C₂₂H₁₉N₂O₂: 359.1390 [M+ H]⁺. Found 359.1383.

7.2.8.2.10 *N*-(4-(4-Methylbenzoxazol-2-yl)phenyl)benzamide (5f)



4b (0.5 g, 2.50 mmol) was dissolved in acetonitrile (25 mL), DIPEA (964 μ L, 5.13 mmol) was added in one portion and then 2-methoxybenzoyl chloride (388 μ L in 5 mL acetonitrile, 3.15 mmol) was added dropwise over 10 min with stirring at 0 °C. The reaction mixture was stirred 1 h and the resulting precipitate was filtered and washed with cold acetonitrile to give **5b** as a colorless solid.

Yield: 0.658g, 90 %

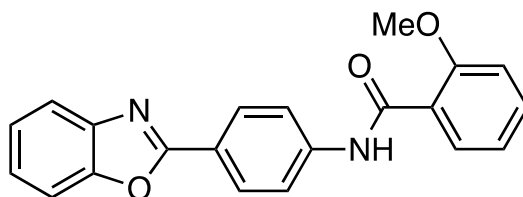
^1H NMR (500 MHz, d_6 -DMSO, 298 K) δ 10.58 (s, 1H), 8.19 (d, J = 8.4 Hz, 2H), 8.06 (d, J = 8.4 Hz, 2H), 8.02-7.96 (m, 2H), 7.65-7.59 (m, 1H), 7.58-7.53 (m, 3H), 7.28 (t, J = 7.8 Hz 1H), 7.19 (d, J = 7.4 Hz, 1H), 2.58 (s, 3H).

^{13}C NMR (125 MHz, d_6 -DMSO, 298 K) δ 165.9 (s), 161.5 (s), 149.8 (s), 142.4 (s), 140.8 (s), 134.6 (s), 131.8 (d), 129.6 (s), 128.4 (d), 127.9 (d), 127.8 (d), 125.1 (d), 124.8 (d), 121.4 (s), 120.3 (d), 108.0 (d), 16.2 (q).

LCMS (ESI) 329.18 $[\text{M}+\text{H}]^+$ $R_t = 13.7$ min (99 %)

HRMS (ESI+): Calcd for $\text{C}_{21}\text{H}_{16}\text{N}_2\text{O}_2\text{Na}$: 351.1104 $[\text{M}+\text{Na}]^+$. Found 351.1105.

7.2.8.2.11 *N*-(4-(benzoxazol-2-yl)phenyl)-2-methoxybenzamide (5g)



4b (0.65 g, 2.50 mmol) was dissolved in acetonitrile (25 mL), DIPEA (1.34 mL, 5.13 mmol) was added in one portion and then 2-methoxybenzoyl chloride (623 μL in 5 mL acetonitrile, 3.15 mmol) was added dropwise over 10 min with stirring at 0 °C. The reaction mixture was stirred 90 min and the resulting precipitate was filtered and washed with cold acetonitrile to give **5b** as a colorless solid.

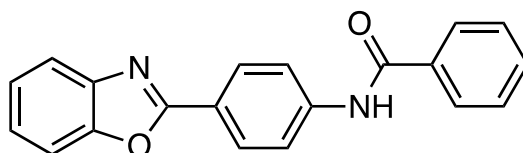
Yield: 0.883 g, 83 %

^1H NMR (300 MHz, d_6 -DMSO, 298 K) δ 10.48 (s, 1H), 8.19 (d, $J = 8.8$ Hz, 2H), 7.99 (d, $J = 8.8$ Hz, 2H), 7.81-7.73 (m, 2H), 7.65 (dd, $J = 7.6, 1.8$ Hz, 1H), 7.53 (ddd, $J = 9.0, 7.4, 1.8$ Hz, 1H), 7.43-7.37 (m, 2H), 7.20 (d, $J = 8.4$ Hz, 1H), 7.09 (td, $J = 7.4, 1.0$ Hz, 1H), 3.91 (s, 3H).

^{13}C NMR (75 MHz, d_6 -DMSO, 298 K) δ 165.0 (s), 162.2 (s), 156.5 (s), 150.1 (s), 142.3 (s), 141.6 (s), 132.2 (d), 129.6 (d), 128.2 (d), 125.2 (d), 124.8 (d), 124.7 (d), 121.1 (s), 120.5 (d), 119.7 (d), 119.5 (d), 112.0 (d), 110.7 (d), 55.9 (q).

HRMS (ESI+): Calcd for $\text{C}_{21}\text{H}_{16}\text{N}_2\text{O}_3\text{Na}$: 367.1053 $[\text{M}+\text{Na}]^+$. Found 367.1057.

7.2.8.2.12 *N*-(4-(Benzoxazol-2-yl)phenyl)benzamide (5h)



4b (0.7 g, 2.50 mmol) was dissolved in acetonitrile (25 mL), DIPEA (1.45 mL, 5.13 mmol) was added in one portion and then benzoyl chloride (580 μL in 5 mL acetonitrile, 3.15 mmol) was added dropwise over 10 min with stirring at 0 °C. The reaction mixture was stirred 1 h and the resulting precipitate was filtered and washed with cold acetonitrile to give **5b** as a colorless solid.

Yield: 0.836 g, 80 %

¹H NMR (300 MHz, *d*₆-DMSO, 298 K) δ 10.59 (s, 1H), 8.23-8.16 (m, 2H), 8.10-8.04 (m, 2H), 8.02-7.96 (m, 2H), 7.80-7.73 (m, 2H), 7.65-7.52 (m, 3H), 7.43-7.36 (m, 2H).

¹³C NMR (75 MHz, *d*₆-DMSO, 298 K) δ 165.9 (s), 162.2 (s), 150.1 (s), 142.5 (s), 141.6 (s), 134.6 (s), 131.8 (d), 128.4 (d), 128.0 (d), 127.8 (d), 125.1 (d), 124.7 (d), 121.2 (s), 120.3 (d), 119.5 (d), 110.7 (d).

LCMS (ESI) 315.10 [M+H]⁺ R_t = 13.6 min (99 %).

HRMS (ESI⁺): Calcd for C₂₀H₁₄N₂O₂Na: 337.0947 [M+ Na]⁺. Found 337.0959

7.2.8.3 Synthesis of the Control Compounds

The control compounds were synthesized as described in figure 39.

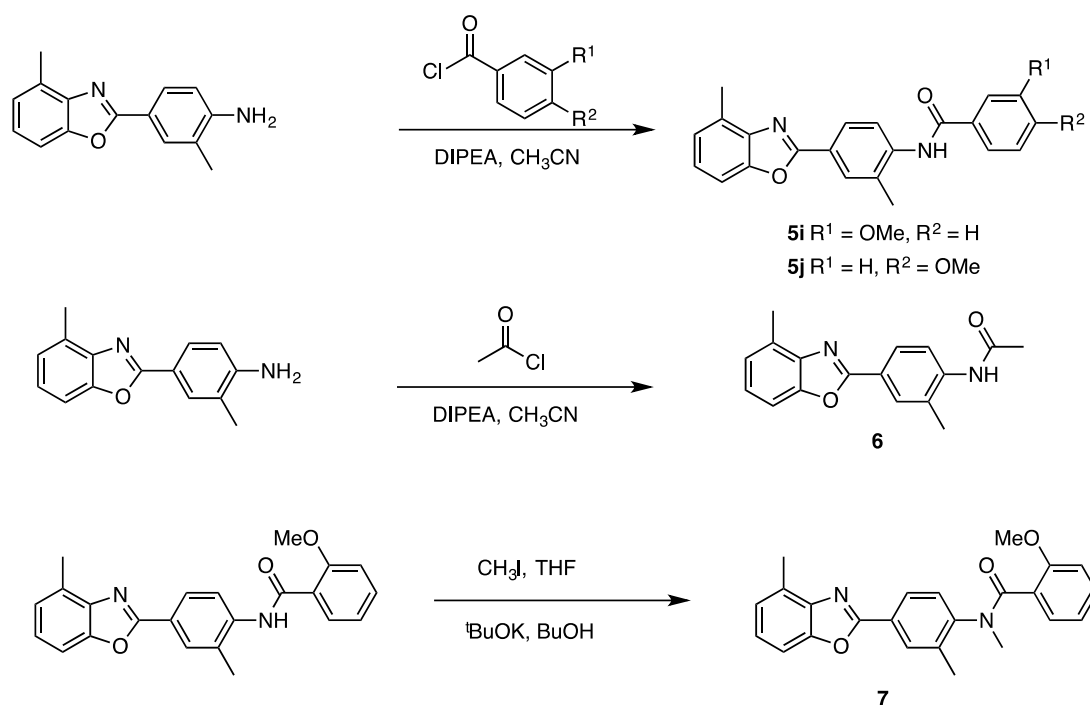
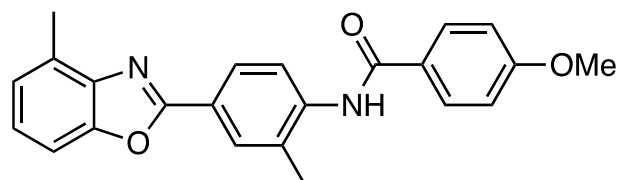


Figure 39: Synthesis of the control compounds.

7.2.8.3.1 4-Methoxy-*N*-(2-methyl-4-(4-methylbenzol-2-yl)phenyl)benzamine (5i)



4b (0.50 g, 2.50 mmol) was dissolved in acetonitrile (25 mL), DIPEA (914 μ L, 5.13 mmol) was added in one portion and then 2-methoxybenzoyl chloride (423 μ L in 5 mL acetonitrile, 3.15 mmol) was added dropwise over 10 min with stirring at 0 °C. The reaction mixture was stirred 1 h and the resulting precipitate was filtered and washed with cold acetonitrile to give **5b** as a colorless solid.

Yield: 0.620 g, 79 %

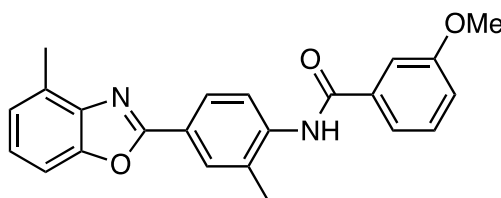
¹H NMR (600 MHz, *d*₆-DMSO, 298 K) δ 9.84 (s, 1H), 8.11 (dd, *J* = 2.1, 0.9 Hz, 1H), 8.05 (dd, *J* = 8.3, 2.1 Hz, 1H), 8.00 (d, *J* = 8.8 Hz, 2H), 7.70 (m, *J* = 8.3 Hz, 1H), 7.58-7.56 (m, 1H), 7.30 (t, *J* = 7.8 Hz, 1H), 7.22-7.20 (m, 1H), 7.08 (d, *J* = 8.8 Hz, 2H), 3.85 (s, 3H), 2.60 (s, 3H), 2.39 (s, 3H).

¹³C NMR (200 MHz, *d*₆-DMSO, 298 K) δ 164.8 (s), 162.0 (s), 161.4 (s), 149.9 (s), 140.8 (s), 140.0 (s), 133.7 (s), 129.68 (s), 129.64 (d), 129.1 (d), 126.35 (s), 126.30 (d), 125.11 (d), 125.04 (d), 124.96 (d), 123.3 (s), 113.6 (d), 108.0 (d), 55.4 (q), 17.9 (q), 16.2 (q).

LCMS (ESI) 373.22 [M+H]⁺ R_t = 13.8 min (98 %)

HRMS (ESI+): Calcd for C₂₃H₂₁N₂O₃: 373.1547 [M+H]⁺. Found 373.1545.

7.2.8.3.2 3-Methoxy-*N*-(2-methyl-4-(4-methylbenzol-2-yl)phenyl)benzamide (5j)



4b (0.688 g, 2.50 mmol) was dissolved in acetonitrile (25 mL), DIPEA (914 μL, 5.13 mmol) was added in one portion and then 2-methoxybenzoyl chloride (423 μL in 5 mL acetonitrile, 3.15 mmol) was added dropwise over 10 min with stirring at 0 °C. The reaction mixture was stirred 1 h and the resulting precipitate was filtered and washed with cold acetonitrile to give **5b** as a colorless solid.

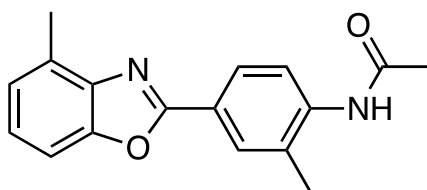
Yield: 0.566 g, 72 %

¹H NMR (600 MHz, *d*₆-DMSO, 298 K) δ 9.98 (s, 1H), 8.12 (d, *J* = 2.0 Hz, 1H), 8.05 (dd, *J* = 8.3, 2.0 Hz, 1H), 7.68 (d, *J* = 8.3 Hz, 1H), 7.59 (dt, *J* = 7.8, 1.0 Hz, 1H), 7.56 (d, *J* = 8.3 Hz, 1H), 7.55-7.53 (m, 1H), 7.46 (t, *J* = 7.8 Hz, 1H), 7.29 (t, *J* = 7.8 Hz, 1H), 7.22-7.19 (m, 1H), 7.18 (ddd, *J* = 8.3, 2.7, 1.0 Hz, 1H), 3.84 (s, 3H), 2.59 (s, 3H), 2.39 (s, 3H).

¹³C NMR (200 MHz, *d*₆-DMSO, 298 K) δ 165.1 (s), 161.4 (s), 159.2 (s), 149.9 (s), 140.8 (s), 139.7 (s), 135.7 (s), 134.0 (s), 129.7 (s), 129.7 (d), 129.6 (d), 129.1 (d), 126.5 (d), 125.12 (d), 125.07 (d), 124.99 (d), 123.6 (s), 119.9 (d), 117.5 (d), 112.9 (d), 108.0 (d), 55.3 (q), 17.9 (q), 16.2 (q).

LCMS (ESI) 373.22 [M+H]⁺ R_t = 13.9 min (95 %)

HRMS (ESI+): Calcd for C₂₃H₂₁N₂O₃: 373.1547 [M+H]⁺. Found 373.1551.

7.2.8.3.3 *N*-(2-Methyl-4-(4-methylbenzoxazol-2-yl)phenyl)acetamide (**6**)

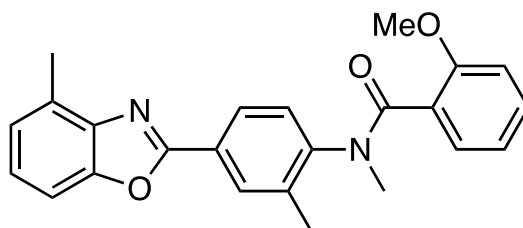
4b (0.25 g, 2.50 mmol) was dissolved in acetonitrile (15 mL), DIPEA (817 μ L, 5.13 mmol) was added in one portion and then acetyl chloride (224 μ L, 3.15 mmol) was added dropwise over 10 min with stirring at 0 °C. The reaction mixture was stirred 3 h and reaction mixture. The residue purified using column chromatography (SiO₂) using a gradient elution 10 % EtOAc in Cyclohexane \rightarrow 75 % EtOAc to give **6** as a colorless solid.

Yield: 83 mg, 31 %

¹H NMR (400 MHz, *d*₆-DMSO, 298 K) δ 9.41 (s, 1H), 8.03 (d, *J* = 2.1 Hz 1H), 7.98 (dd, *J* = 8.5, 2.1 Hz, 1H), 7.83 (d, *J* = 8.5 Hz, 1H), 7.54 (d, *J* = 8.1 Hz, 1H), 7.28 (t, *J* = 7.8 Hz, 1H), 7.19 (dt, *J* = 7.5, 1.0 Hz, 1H), 2.57 (s, 3H), 2.35 (s, 3H), 2.13 (s, 3H).

¹³C NMR (100 MHz, *d*₆-DMSO, 298 K) δ 166.6 (s), 161.4 (s), 149.8 (s), 140.8 (s), 139.9 (s), 130.9 (s), 129.6 (s), 129.1 (d), 125.09 (d), 125.08 (d), 124.9 (d), 124.1 (d), 108.0 (d), 23.6 (q), 17.8 (q), 16.2 (q).

HRMS (ESI⁺): Calcd for C₁₇H₁₆N₂O₂Na: 303.1104 [M+ Na]⁺. Found 303.1106.

7.2.8.3.4 2-Methoxy-*N*-methyl-*N*-(2-methyl-4-(4-methylbenzoxazol-2-yl)phenyl)benzamine (**7**)

5a (0.438 mg, 0.934 mmol) was dissolved in dry THF (15 mL) under argon at room temperature. Subsequently, the reaction mixture was cooled to 0 °C and potassium *t*-butoxide (934 μ L of a 1M solution in ^tBuOH, 0.934 mmol) was added dropwise over 10 min. The reaction mixture was maintained at 0 °C for further 30 min, after which time methyl iodide (64 μ L, 1.03 mmol) was added in one portion. The reaction mixture was allowed to warm to RT and stirred overnight for 16 h. The reaction mixture was quenched with water and concentrated under reduced pressure. The resulting residue was dissolved in ethyl acetate (100 mL) and washed with water (2 x 20 mL) and sat. aq. NaCl (1 x 10 mL), dried (MgSO₄) and concentrated under reduced pressure. The residue was purified using column chromatography (SiO₂) using a gradient elution 20 % EtOAc in cyclohexane \rightarrow 50 % EtOAc to give **7** as a colorless solid.

Yield: 280 mg, 78 %

¹H NMR (2.5:1 rotamer ratio, asterisks denote minor rotamer peaks, **600 MHz, d₆-DMSO, 298 K**) δ 8.17* (d, *J* = 2.1 Hz, 1H), 8.11* (d, *J* = 8.1, 2.1 Hz, 1H), 7.95 (d, *J* = 2.1 Hz, 1H), 7.78 (d, *J* = 8.1 Hz, 1H), 7.60-7.57* (m, 1H), 7.51 (dt, *J* = 8.1, 0.9 Hz, 2 x 1H), 7.47* (ddd, *J* = 8.3, 7.4, 1.7 Hz, 1H), 7.37* (d, *J* = 7.3 Hz, 1H), 7.32* (t, *J* = 7.8 Hz, 1H), 7.30-7.26 (m, 2 x 1H), 7.28 (t, *J* = 7.8 Hz, 2 x 1H), 7.24-7.21 (m, 1H), 7.19 (dt, *J* = 7.5, 1.0 Hz, 1H), 7.17-7.15* (m, 1H), 7.15* (dd, *J* = 1.7, 0.9 Hz, 1H), 7.14* (d, *J* = 1.7 Hz, 1H), 7.08* (td, *J* = 7.4, 0.9 Hz, 1H), 6.80 (td, *J* = 7.4, 0.9 Hz, 1H), 6.78-6.75 (m, 1H), 3.91* (s, 3H), 3.64 (s, 3H), 3.27 (s, 3H), 3.06* (s, 3H), 2.60* (s, 3H), 2.54 (s, 3H), 2.39* (s, 3H), 2.35 (s, 3H).

¹³C NMR (asterisks denote minor rotamer peaks, **200 MHz, d₆-DMSO, 298 K**) δ 167.7 (s), 161.1* (s), 160.8 (s), 155.0 (s), 154.6* (s), 150.0* (s), 149.9 (s), 145.2* (s), 144.9 (s), 140.7* (s), 140.6 (s), 136.8* (s), 136.3 (s), 130.7* (d), 130.3 (d), 129.9* (s), 129.8 (s), 129.5 (d), 129.4* (d), 129.2 (d), 128.4 (d), 125.4 (s), 125.3 (s), 125.21 (d), 125.19 (d), 125.16 (d), 124.7 (d), 120.8* (d), 119.7 (d), 111.5* (d), 110.8 (d), 108.1* (d), 108.0 (d), 55.7* (q), 54.9 (q), 38.4* (q), 35.6 (q), 17.3 (q), 17.2* (q), 16.2 (q), 16.1* (q).

LCMS (ESI) 387.27 [M+H]⁺ R_t = 13.7 min (99 %)

7.2.9 Handling of compounds

The small molecules used during the screening as well as the re-synthesized hits and derivatives were dissolved in anhydrous DMSO. The ComGenex library compounds were stored as 10 mM stock solutions as well as ready-to-use 2 mM solutions in 96-well plates at – 20 °C. Solid compound stock powders of in-house synthesized compounds were stored at 4 °C in the dark. 10 mM stock solutions of the in-house synthesized compounds were stored at room temperature in the dark. The compounds were synthesized by Dr. Jeffrey Hannam from the Famulok lab.

7.2.9.1 HPLC-MS

Compounds were analyzed with HPLC-MS to check their mass and purity. The samples were diluted in 20 % acetonitrile (LCMS grade) to a concentration of 0.1 mg/mL. The samples were analyzed using an Agilent Zorbax SB-C18 (2.1 x 5 mm) column followed by a Bruker Esquire HTC mass spectrometer with atmospheric pressure interface-electrospray ionisation (API-ESI). Compounds and impurities were detected by absorption measurement at 254 nm. A gradient of 20 – 100 % acetonitrile was run over 20 minutes with a flow rate of 0.4 mL/minute.

Eluent A:

0.1 % formic acid in water (LCMS grade)

Eluent B:

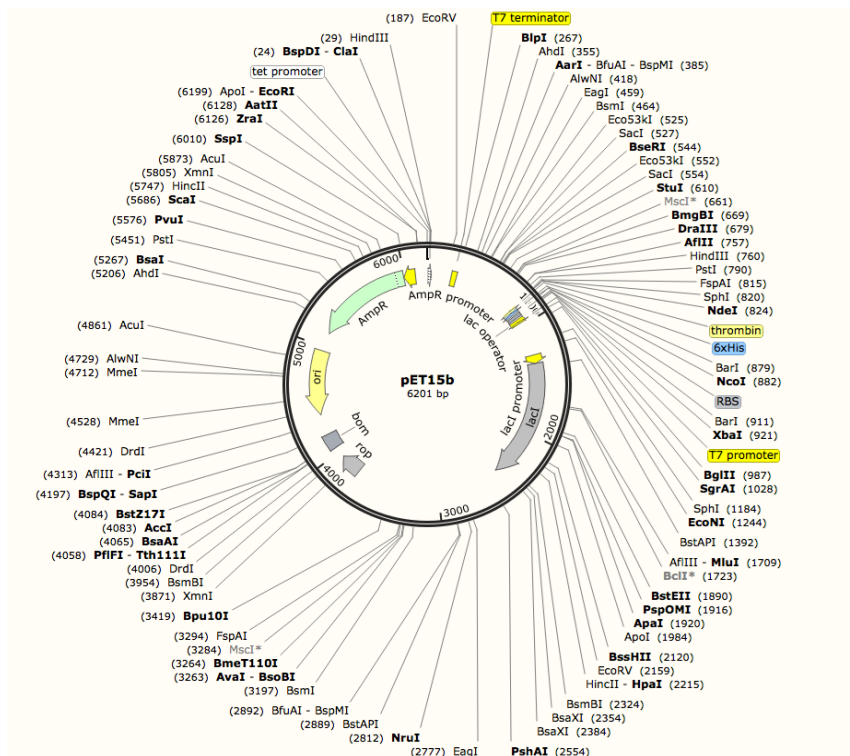
Acetonitrile (LCMS grade)

7.2.9.2 Determination of solubility

The solubility of the compounds in buffer was determined by absorption measurements²⁷⁷. The wavelength of maximal absorption for the specific compounds was identified in an

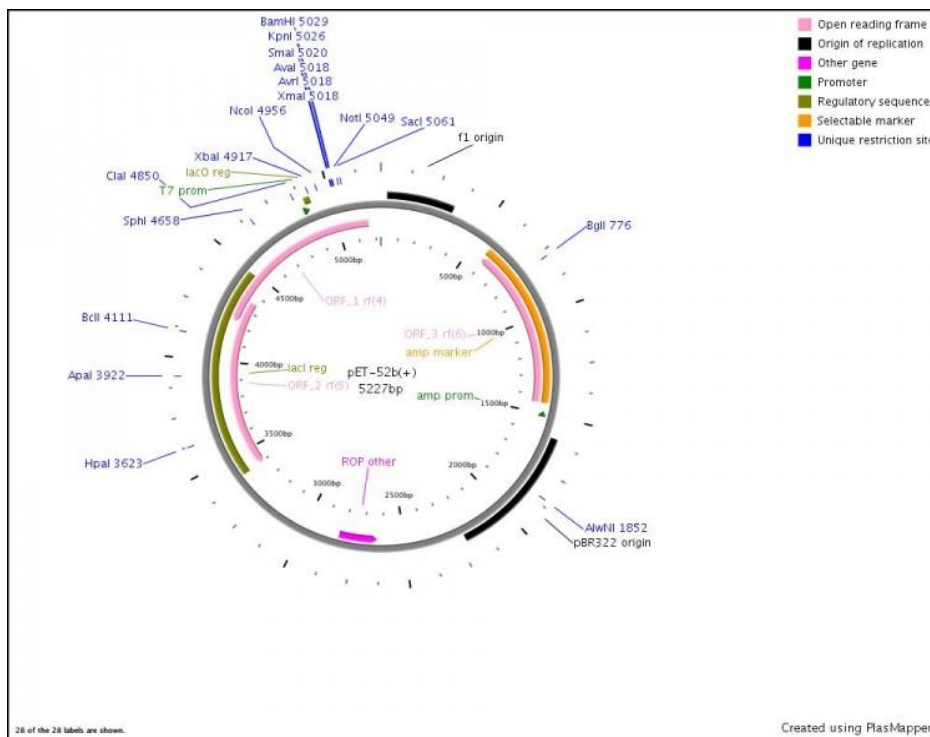
absorption scan using the NanoDrop 2000 and 50 μM of the compound in buffer with 2 % final DMSO concentration. A serial dilution of the compound ranging from 200 μM to 0.1 μM was prepared in the buffer of interest with 2 % DMSO. The absorption of the individual samples was measured at the previously determined wavelength. The samples were then incubated at room temperature for 20 minutes followed by centrifugation at 20 000 x g for 10 minutes. Finally the absorption of the supernatants was measured at the same wavelength as before. A decrease in the absorption signal compared to before centrifugation indicated that precipitation or aggregation of the compound had occurred.

pET15b



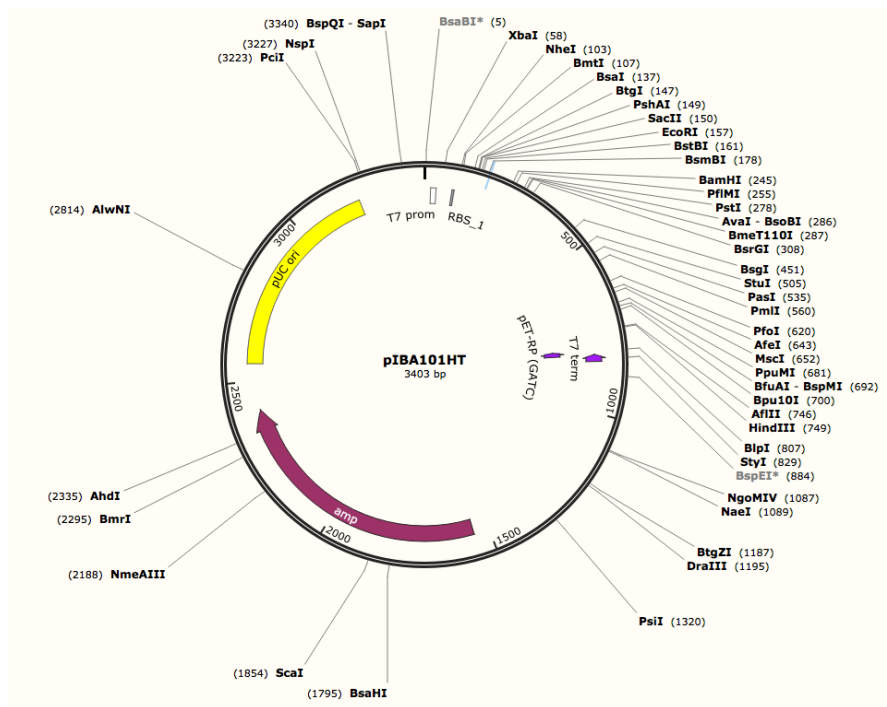
Supporting figure 3: Plasmid map of pET15b.

pET52b(+)



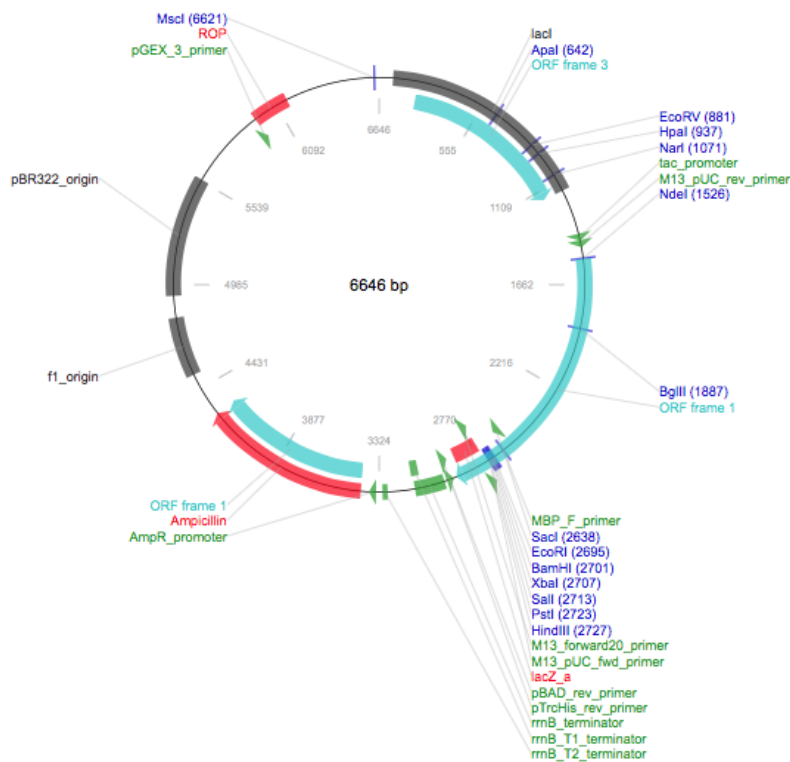
Supporting figure 4: Plasmid map of pET52b(+).

pIBA101HT



Supporting figure 9: Plasmid map of pIBA101HT.

pMAL-C2



Supporting figure 10: Plasmid map of pMAL-C2.

8.1.2 Protein sequences

ARNO-Sec7

MASRGSHHHH HHGAGDRGPE FENLYFQSET RNRKMAMGRK KFNMDPKKGI QFLVENELLQ
 NTPPEIARFL YKGEGLNKTA IGDYLGEEER LNLAVLHAFV DLHEFTDLNL VQALRQFLWS
 FRLPGEAQKI DRMMEAFQQR YCLCNPGVFQ STDTCYVLSF AVIMLNTSLH NPNVRDKPGL
 ERFVAMNRGI NEGGDLPEEL LRNLVDSIRN EPFKIP

DrrA

MVTRIEENLEN AKKLWDNANS MLEKGNISGY LKAANELHKF MKEKNLKEDD LRPELSDKTI
 SPKGYAILQS LWGAASDYSR AAATLTESTV EPGLVSAVVK MSAFFMDCKL SPNERATPDP
 DFKVGVSKIL VGIMQFIKDV ADPTSKIWMH NTKALMNHKI AAIQKLEERSN NVNDETLESV
 LSSKGENLSE YLSYK

IR-ICD

MSHHHHHHEN LYFQGARKRQ PDGPLGPLYA SSNPEYLSAS DVFPCSVYVP DEWEVSREKI
 TLLRELQGS FGMVYEGNAR DIIKGEAETR VAVKTVNESA SLRERIEFLN EASVMKGFTC
 HHVVRLGTV SKGQPTLVVM ELMAGDLKS YLRSLRPEAE NNPGRPPPTL QEMIQMAAEI
 ADGMAYLNAK KFHVRDLAAR NCMVAHDFTV KIGDFGMTRD IYETDYRKG GKGLLPVRWM
 APESLKDGVF TTSSDMWSFG VVLWEITSLA EQPYQGLSNE QVLKFVMDGG YLDQPDNCPE
 RVTDLRMCW QFNPKMRPTF LEIVNLLKDD LHPSFPEVSF FHSEENKAPE SEELEMEFED
 MENVPLDRSS HCQREEAGGR DGGSSLGFKR SYEEHIPYTH MNGGKKNRI LTLPRSNPS

NΔ17 Arf1

MGSSHHHHHH SSGLVPRGSH MCMRILMVGL DAAGKTTILY KLKLGIVTT IPTIGFNVET
 VEYKNISFTV WDVGGQDKIR PLWRHYFQNT QGLIFVVDNS DRERVNEARE ELMRMLAEDE
 LRDAVLLVFA NKQDLPNAMN AAEITDKLGL HSLRHRNWI QATCATSGDG LYEGLDWLSN
 QLRNQK

Rab1

MNPEYDYLK LLLIGDSGVG KSCLLLRFD DTYTESYIST IGVDKIRTI ELDGKTIKLO
 IWDTAGQERF RTITSSYYRG AHGIIVVYDV TDQESYANVK QWLQEIADRYA SENVNKLLVG
 NKSDLTTKKV VDNTTAKEFA DSLGIPFLET SAKNATNVEQ AFMTMAAEIK KRMGPGAASG
 GERPNLKIDS TPVKPAGGGC C

Rab5a

MGSSHHHHHH SSGLVPRGSH MKICQFKLV LGSASVSKSS LVLRFVKGQF HEFQESTIGA
 AFLTQTVCLD DTTVKFEIWD TAGQERYHSL APMYYRGAQA AIVVYDITNE ESFARAKNVV
 KELQRQASPN IVIALSGNKA DLANKRAVDF QEAQSYADDN SLLFMETSAK TSMNVNEIFM
 AIAKKLPKN

Rabex-5_{GEF}

MGHHHHHHGS IETDRVSKEF IEFLKTFHKT GQEIYKQTKL FLEGMHYKRD LSIEEQSECA
 QDFYHNVAER MQTRGKVPPE RVEKIMDQIE KYIMTRLYKY VFCPETDDE KKDIAIQKRI
 RALRWVTPQM LCVPVNEDIP EVSDMVVKAI TDIIEMDSKR VPRDKLACIT KCSKHIFNAI
 KITKNEPASA DDFLPTLIYI VLKGNPPRLQ SNIQYITRFC NPSRLMTGED GYYFTNLCCA
 VAFIEKLDQA SLNLSQEDFD RYMSGQTSP

Rac1

MSPILGYWKI KGLVQPTLL LEYLEEKYEE HLYERDEGDK WRNKKFELGL EFPNLPYYID
 GDVKLTQ SMA IIRYIADKHN MLGGCPKERA EISMLEGAVL DIRYGVSRIA YSKDFETLKV
 DFLSKLP EML KMFEDRLCHK TYLNGDHVTH PDFMLYDALD VVLYMDPMCL DAFPKLVCFK
 KRIEAIPQID KYLKSSKYIA WPLQGWQATF GGGDHPPKSD LVPRGSMQAI KCVVVG DGAV
 GKTCLLISYT TNAFPGEYIP TVFDNYSANV MVDGKPVNLG LWDTAGQEDY DRLRPLSY PQ
 TDVFLICFSL VSPASFENVR AKWYPEVRHH CPNTPIILVG TKLDRDDKD TIEKLKEKKL
 TPITYPQGLA MAKEIGAVKY LECSALTQRG LKT V FDEAIR AVLCPPPVKK RKRKCLLL

Rac2

MGSSHHHHH GSGLVPRGSA SMSDSEVNQE AKPEVKPEVK PETHINLKVS DGSSEIFFKI
 KKTTPLRRLM EFAFAKRGKE MDSLRFLYDG IRIQADQTE DLDMEDNDII EAHREQIGGM
 QAIKCVVVG D GAVGKTCLLI SYTTNAFPGE YIPTVFDNYS ANVMVDSKPV NLGLWDTAGQ
 EDYDRLRPLS YPQTDVFLIC FSLVSPASYE NVRAKWFPEV RHHCPSTPII LVGTKLDRD
 DKDTIEKLKE KKLAPITYPQ GLALAKEIDS VKYLECSALT QRGLKTVFDE AIRAVLCPQP
 TRQQKRACSL L

Rin1C

MSHHHHHHEN LYFQGAMEFV GYRVPAGSGP SLPPMPSLQE VDCGSPSSSE EEGVPGSRGS
 PATSPHLGRR RPLLRMSAA FCSSLAPERQ VGRAAAALMQ DRHTAAGQLV QDLLTQVRAG
 PEPQELQ GIR QALSRRAML SAELGPEKLL SPKRLEHVLE KSLHCSVLKP LRPILAARLR
 RRLAADGSLG RLAEGLRLAR AQGPGAFGSH LSLPSPVELE QVRQKLLQLL RTYSPSAQVK
 RLLQACKLLY MALRTQEGEG AGADEFLPLL SLVLAHCDLP ELLLEAEYMS ELLEPSLLTG
 EGGYYLTSLS ASLALLSGLG QAHTLPLSPV QELRRSLSLW EQRRLPATHC FQHLLRVAYQ
 DPSSGCTSKT LAVPPEASIA TLNQLCATKF RVTQPNTFGL FLYKEQGYHR LPPGALAHRL
 PTTGYLVYRR AEWPETQGAV TEEEGSGQSE ARSRGEEQGC QGDGDAGVKA SPRDIREQSE
 TTAEGGQQA QEGPAQPGE EAEGRAAEE

Rin1-TS

MESPGESGAG SPGAPSPSSF TTGHLAREKP AQDPLYDVPN ASGGQAGGPQ RPRGVVSLRE
 RLLLTRPVWL QLQANAAAAL HMLRTEPPGT FLVRKSNTRQ CQALCMRLPE ASGPSFVSSH
 YILESPGGVS LEGSELMFPD LVQLICAYCH TRDILLPLQ LPRAIHHAAT HKELEAISHL
 GIEFWSSSLN IKAQRGPAGG PVL PQLKARS PQELDQGTGA ALCFFNPLFP GDLGPTKREK
 FKRSFKVRVS TETSSPLSPP AVPPPPVPVL PGAVPSQTER LPPCQLLRRE SSVGYRVPAG
 SGPSLPPMPS LQEVDCGSPS SSEE EGVPGS RGSPATSPHL GRRRPLLRSM SAAFCSL LAP
 ERQVGRAAAA LMQDRHTAAG QLVQDLLTQV RAGPEPQELQ GIRQALSRRAR AMLS AELGPE
 KLLSPKRLEH VLEKSLHCSV LKPLRPILAA RLRRRLAADG SLGR LAEGLR LARAQGPAGF
 GSHLSLSPV ELEQVRQKLL QLLRTYSPSA QVKRLLQACK LLYMALRTQE GEGAGADEFL
 PLLSLVLAHC DLPELLLEAE YMSELLEPSL LTGEGGYLT SLSASLALLS GLGQAHTLPL
 SPVQELRRSL SLWEQRR LPA THCFQHLLRV AYQDPSSGCT SKTLAVPPEA SIATLNQLCA
 TKFRVTQNT FGLFLYKEQG YHRLPPGALA HRLPTTGYLV YRRAEWPETQ GAVTEEEGSG
 QSEARSRGEE QGCQGDGDAG VKASPRDIRE QSETTAEGGQ GQAQEGPAQP GEPEAEGRSRA
 AEEENLYFQG MDEKTTGWRG GHVVEGLAGE LEQLRARLEH HPQGQREPSG

TEV Protease

MKIEEGK LVI WINGDKGYNG LAEVGKKFEK DTGIKVTVEH PDKLEEKFPQ VAATGDGPD I
 IFWAHDRFGG YAQSGLLAEI TPKAFQDKL YPFTWDAVRY NGKLIAYPIA VEALS LIYNK
 DLLPNPKTW EEIPALDKEL KAKGKSALMF NLQEPYFTWP LIAADGGYAF KYENK YDIK
 DVGVDNAGAK AGLTFLVDLI KNKHMNADTD YSIAEAAFNK GETAMTINGP WAWSNIDTSK
 VNYGVTVLPT FKGQPSKPFV GVLSAGINAA SPNKE LAKEF LENYLLTDEG LEAVNKDKPL
 GAVALKSYEE ELAKDPRIAA TMENAQKGEI MPNIPQMSAF WYAVRTAVIN AASGRQTVDE
 ALKDAQTNSS SNNNNNNNN NLGIEGRGEN LYFQGHHHH HHGESL FKG P RDYNPISSTI

```

CHLTNESDGH TTSLYGIGFG PFIITNKHLF RRRNGTLLVQ SLHGVFKVKN TTTLQQHLID
GRDMIIIRMP KDFPPFPQKL KFREPQREER ICLVTTNFQT KSMSSMVSDT SCTFPSSDGI
FWKHWIQTKD GQCGSPLVST RDGFIVGIHS ASNFTNTNNY FTSVPKNFME LLTNQEAQQW
VSGWRLNADS VLWGGHKVFM VKPEEPFQPV KEATQLMNR RRR

```

Tiam1DHPH

```

MASWSHPQFE KGALEVLVQFQ PGRQLSDADK LRKVICELLE TERTYVKDLN CLMERYLKPL
QKETFLTQDE LDVLFGNLTE MVEFQVEFLK TLEDGVRLVP DLEKLEKVDQ FKKVLFSLGG
SFLYYADRFK LYSAFCASHT KVPKVLVKAK TDATFKAFLD AQNPRQQHSS TLESYLIKPI
QRVLKYPLLL RELFALDAAE SEEHYHLDVA IKTMNKVASH INEMQKIHEE FGAVFDQLIA
EQTGEKKEVA DLSMGDLLLH TSVIWLNPPA SLGKWKKEPE LAAFVFKTAV VLVYKDGSKQ
KKKLVGSHRL SIYEEWDPFR FRHMIPTAL QVRALPSADA EANAVCEIVH VKSESEGRPE
RVFHLCCSSP ESRKDFLKS SVHSILRDKHRR QLLKTEVDAA AELALVPRGS SAHHHHHHHHH
HH

```

Vav1

```

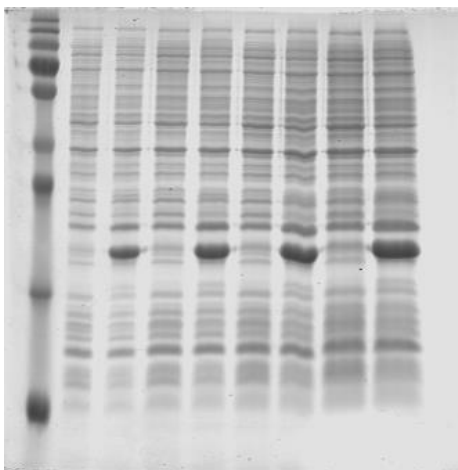
MSPILGYWKI KGLVQPTLL LEYLEEKYEE HLYERDEGDK WRNKKFELGL EFPNLPYYID
GDVKLTQ SMA IIRYIADKHN MLGGCPKERA EISMLEGAVL DIRYGVSR IA YSKDFETLKV
DFLSKLP EML KMFEDRLCHK TYLNGDHVTH PDFMLYDALD VVLYMDPMCL DAFPQQYIA
WPLQGWQATF GGGDHPPKSD LVPRGSDYDI PTTENLYFQG AHMGGSMTEY DKRCCCLREI
QQTEEKYTD T LGSIQQHFLK PLQRFLKPQD IEIIFINIED LLRVHTHFLK EMKEALGTPG
AANLYQVFIK YKERFLVYGR YCSQVESASK HLDRVAAAARE DVQMKLEEC SQRANNGRFTL
RDLLMVP MQR VLKYHLLLQE LVKHTQEAME KENLRLALDA MRDLAQCVNE VKRDNETLRQ
ITNFQLS IEN LDQSLAHYGR PKIDGELKIT SVERRSKMDR YAFLLDKALL ICKRRGDSYD
LKDFVNLH SF QVRDDSSGDR DNKKWSHMFL LIEDQGAQGY ELFFKTRELK KKWMEQFEMA
ISNIYPENAT ANGHDFQMFS FEETTCKAC QMLLRGTFYQ GYRCHRCRAS AHKECLGRVP
PCGRHGQDFP GTM

```

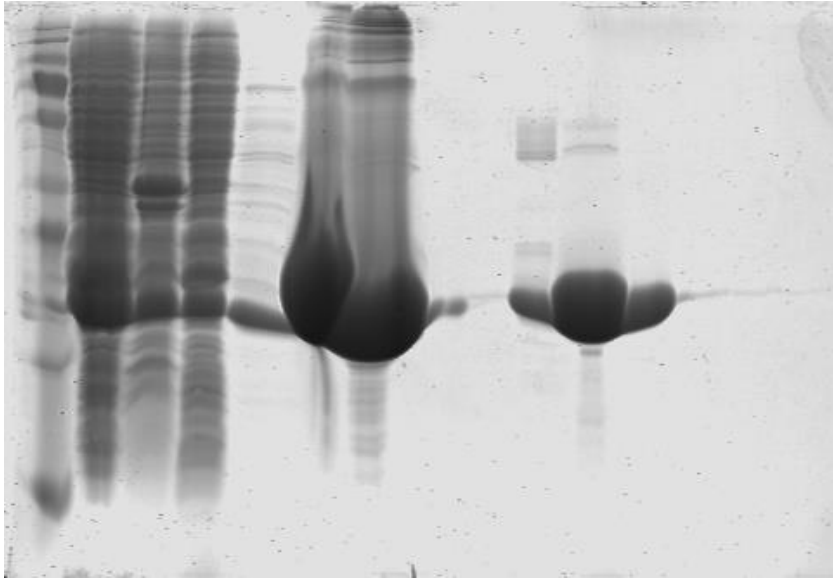
8.2 Original gels and blots

8.2.1 Protein expression and purification

Expression and purification of Rab5a

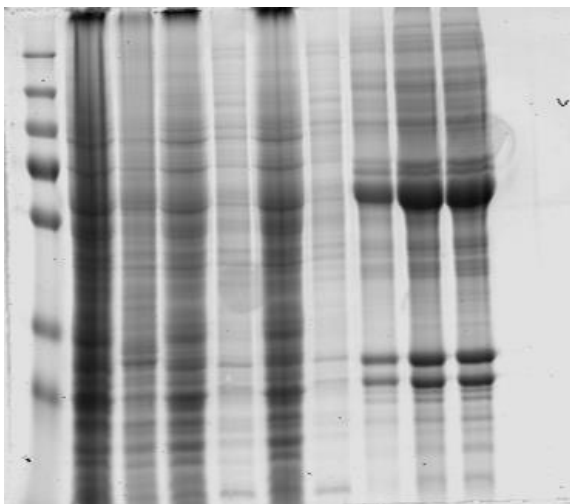


Supporting figure 11: Expression of Rab5a. Different volumes of the same samples have been loaded. Unlabelled original coomassie gel.

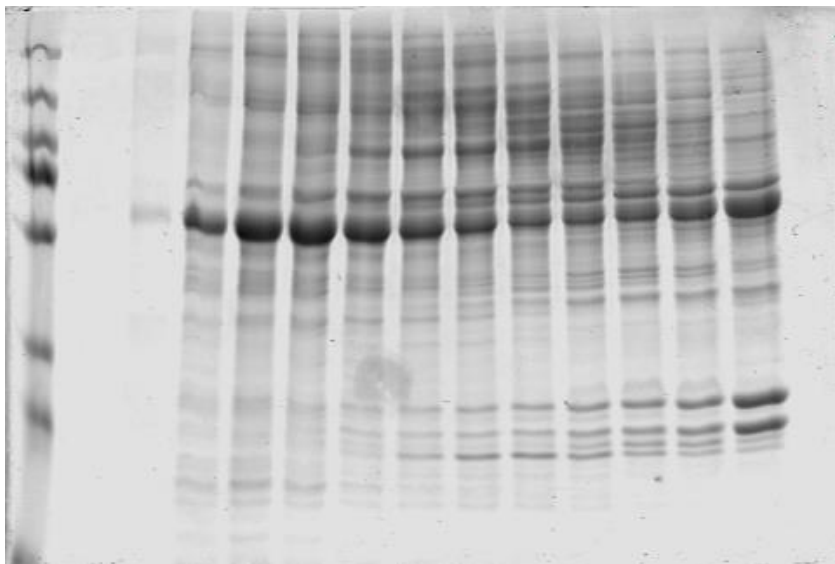


Supporting figure 12: Purification of Rab5a. Un-labelled original coomassie stained gel.

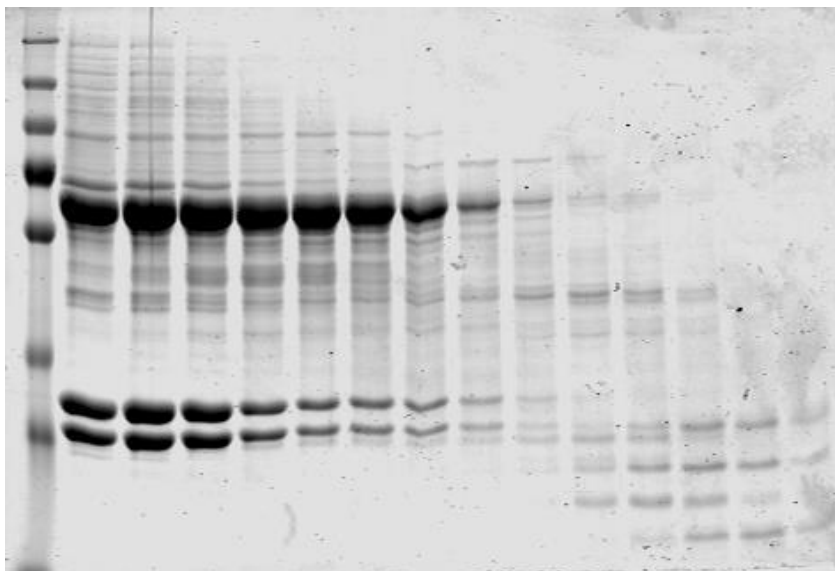
Purification of Rin1C



Supporting figure 13: Ni-NTA affinity chromatography of Rin1C. Un-labelled original coomassie stained gel.

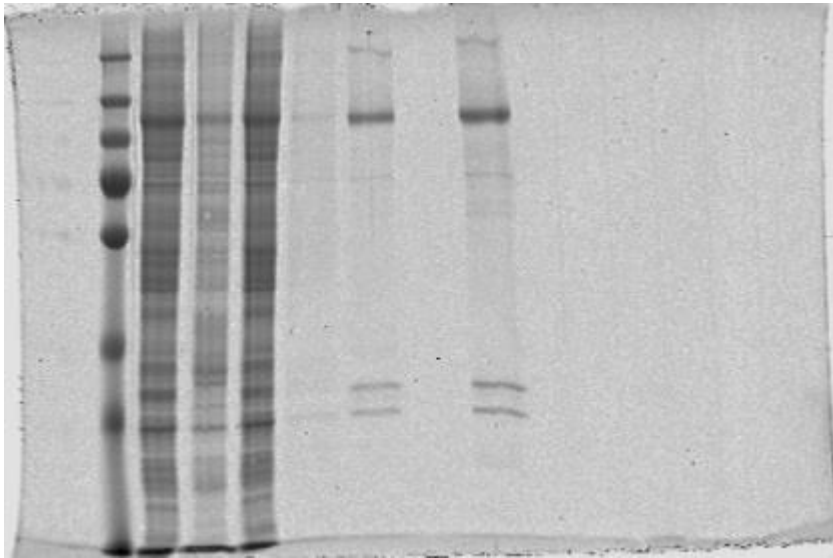


Supporting figure 14: First part of the Rin1C size exclusion chromatography. Un-labelled original coomassie stained gel.



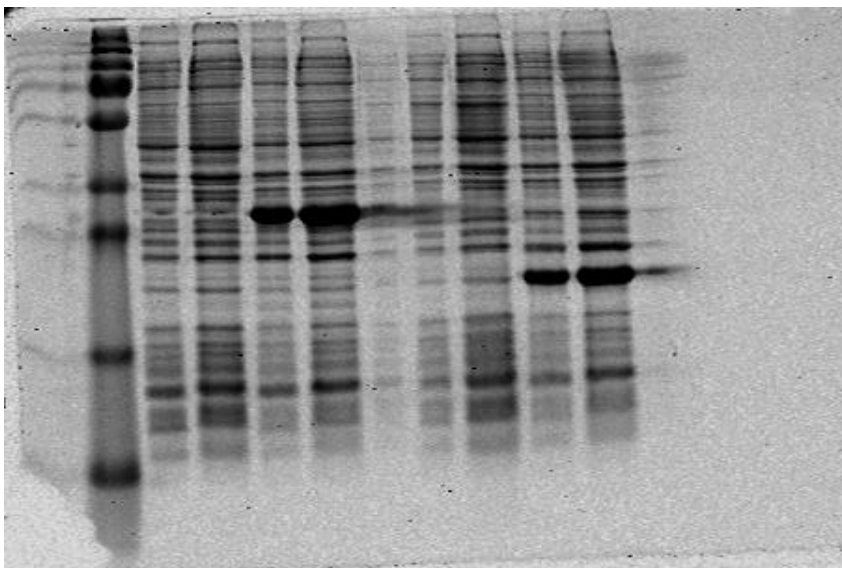
Supporting figure 15: Second part of the Rin1C size exclusion chromatography. Un-labelled original coomassie stained gel.

Purification of Rin1-TS

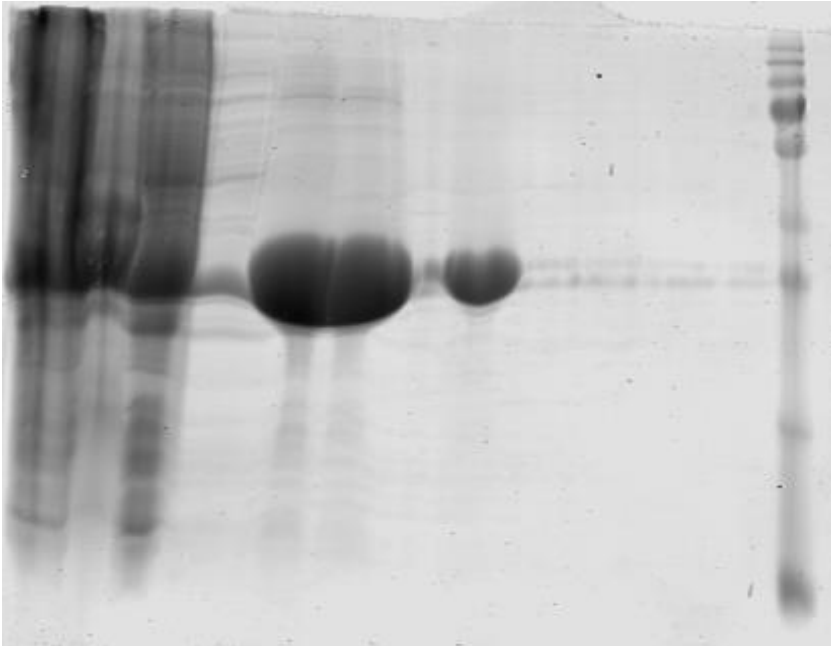


Supporting figure 16: Purification of Rin1-TS. Un-labelled original coomassie stained gel.

Expression and purification of Rabex-5_{GEF}

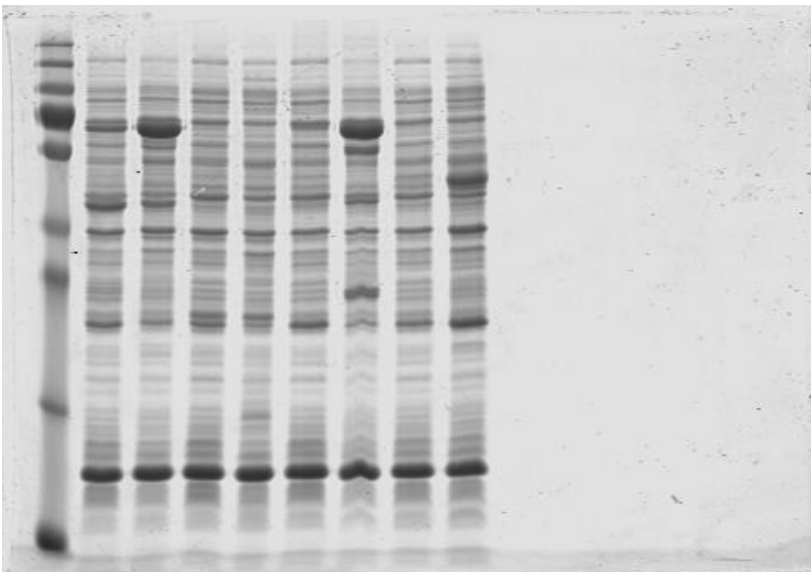


Supporting figure 17: Expression of Rabex-5_{GEF} and Rab5c. The right half of this gel contains samples corresponding to a simultaneously performed expression of Rab5c. Data covering Rab5c have not been used in this thesis. Un-labelled original coomassie stained gel.



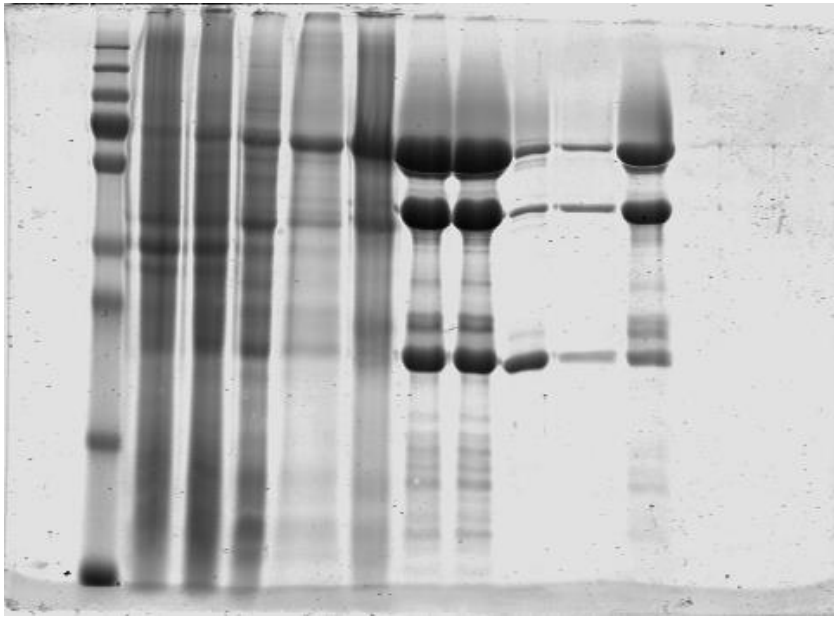
Supporting figure 18: Purification of Rabex-5_{GEF}. Un-labelled original coomassie stained gel.

Expression of Rab1, DrrA, Vav1 and Tiam1DHPH

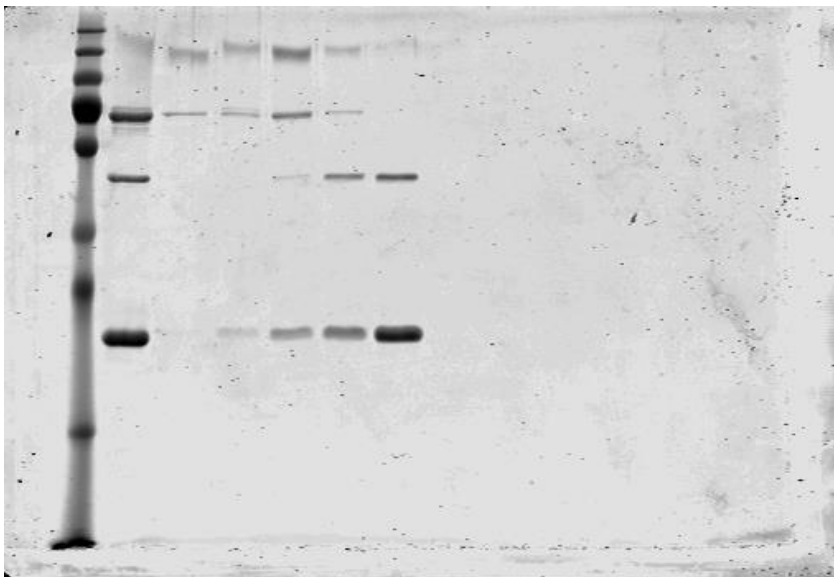


Supporting figure 19: Expression of Rab1, DrrA, Vav1 and Tiam1DHPH. This un-labelled original gel contains samples corresponding to four protein expressions that have been dealt separately with in this thesis. In the results part it is therefore cut and shown in four parts.

Purification of Rab1

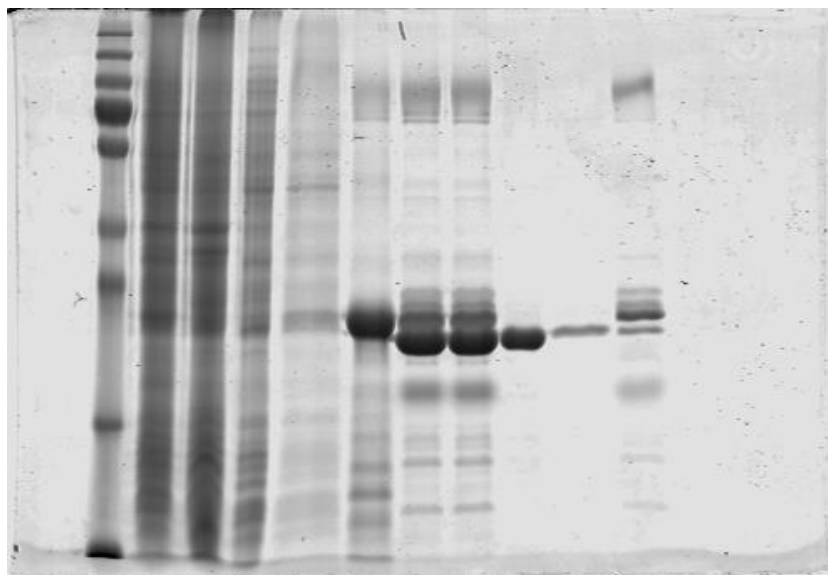


Supporting figure 20: First part of the Rab1 purification. Ni-NTA affinity chromatography and reverse Ni-NTA affinity chromatography. Un-labelled original coomassie stained gel.



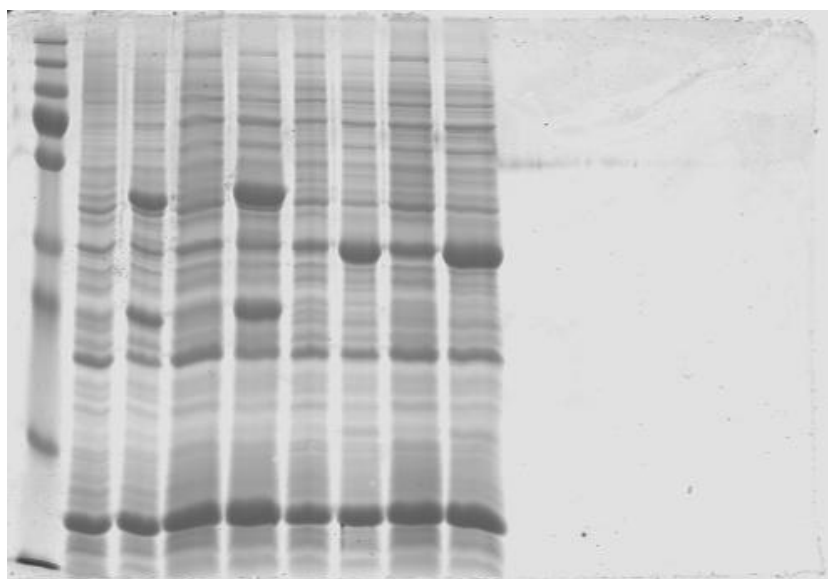
Supporting figure 21: Second part of the Rab1 purification. Size exclusion chromatography. Un-labelled original coomassie stained gel.

Purification of DrrA



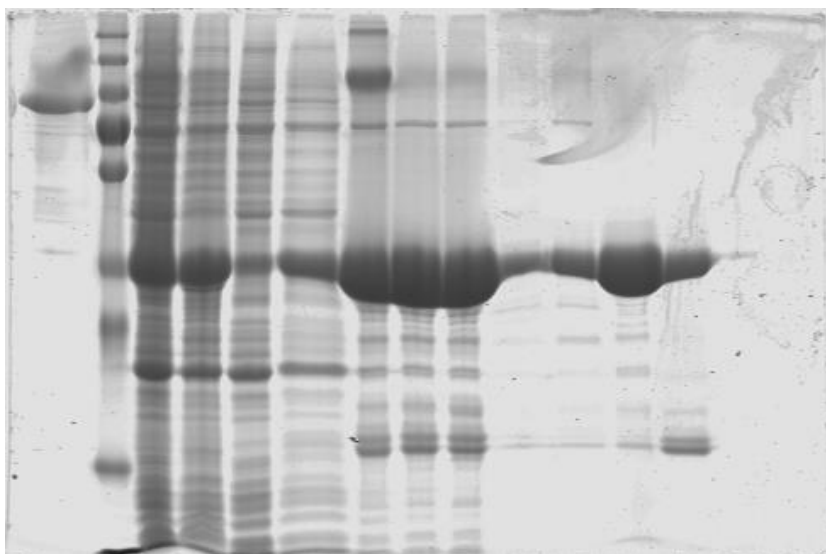
Supporting figure 22: Purification of DrrA. Un-labelled original coomassie stained gel.

Expression of Rac1 and Rac2



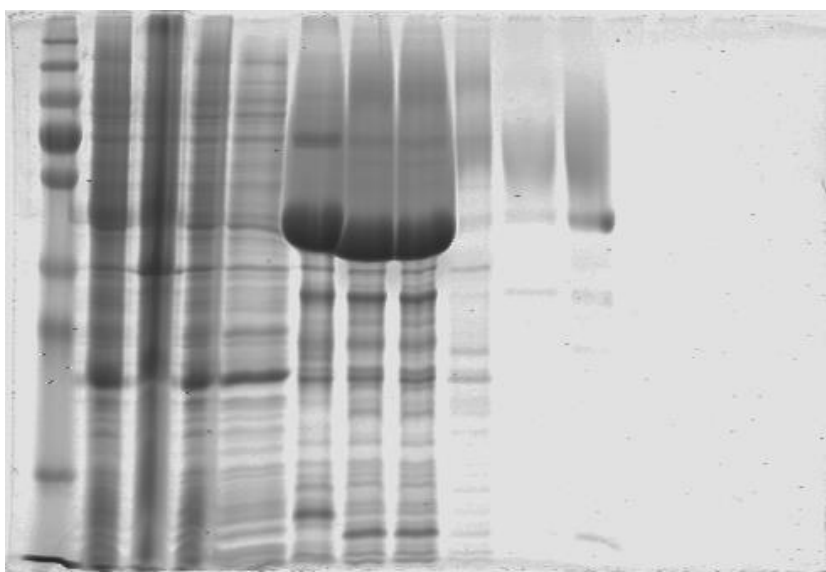
Supporting figure 23: Expression of Rac1 and Rac2. This un-labelled original gel contains samples corresponding to both protein expressions that have been dealt separately with in this thesis. In the results part it is therefore cut and shown in two parts. Two different volumes of the same samples have been loaded.

Purification of Rac2

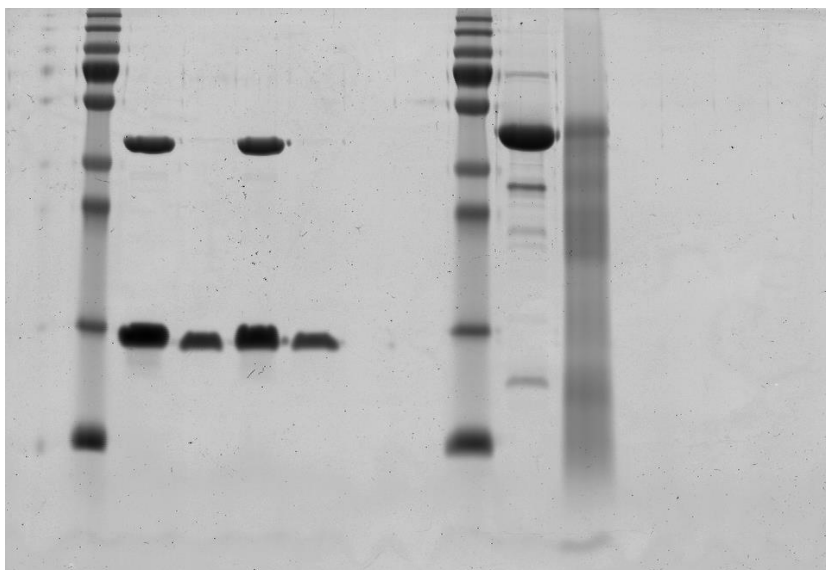


Supporting figure 24: Purification of Rac2. Un-labelled original coomassie stained gel.

Purification of Tiam1DHPH

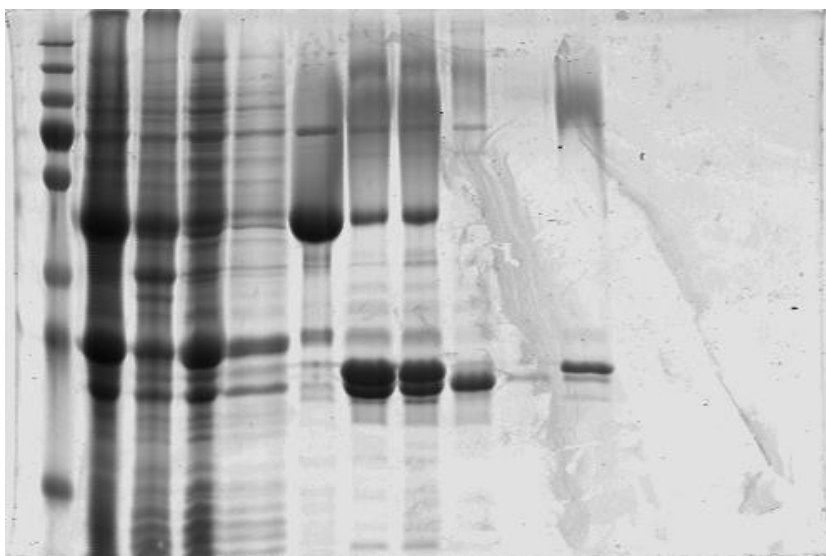


Supporting figure 25: Purification of Tiam1DHPH. Un-labelled original coomassie stained gel.



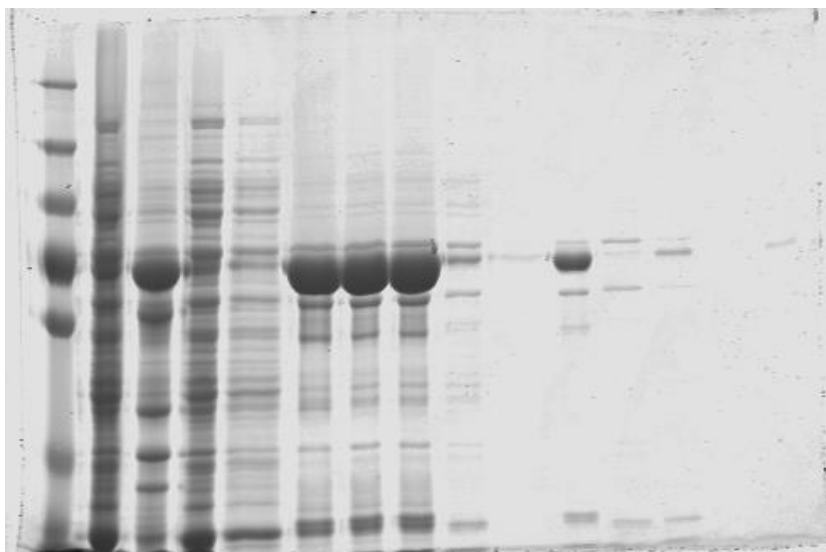
Supporting Figure 26: Final sample of Tiam1DHPH. The left side of this gel contains samples from an unrelated experiment performed by C. Sieg from the Famulok group. Un-labelled original coomassie stained gel.

Purification of Rac1



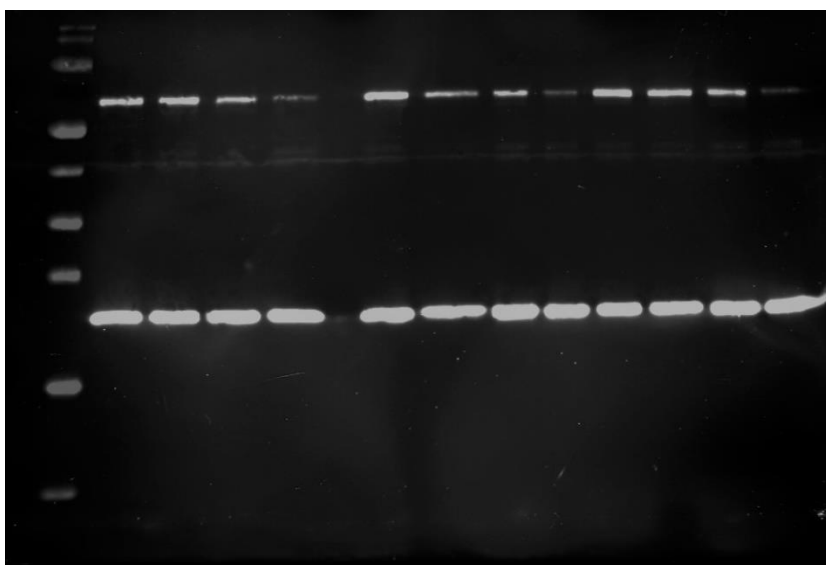
Supporting figure 27: Purification of Rac1. Un-labelled original coomassie stained gel.

Purification of Vav1

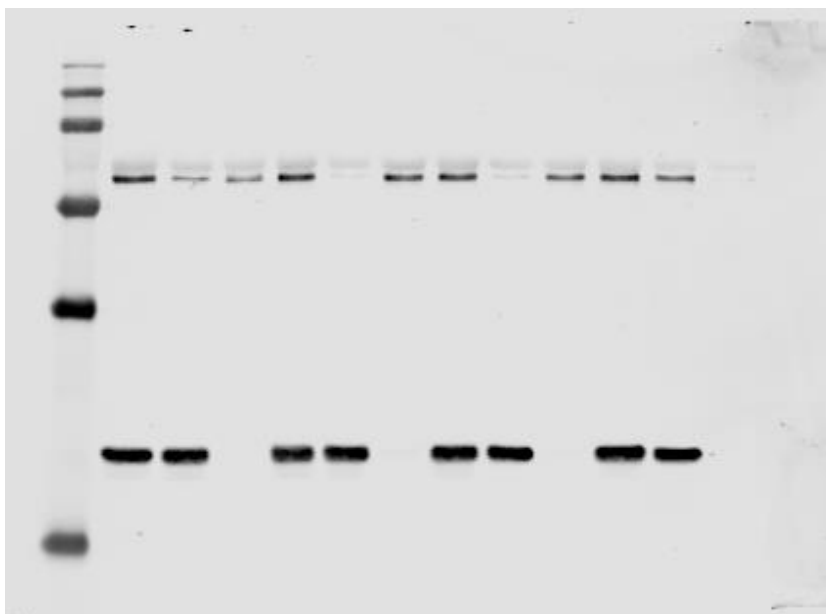


Supporting figure 28: Purification of Vav1. Un-labelled original coomassie stained gel.

8.2.2 Aggregation assay

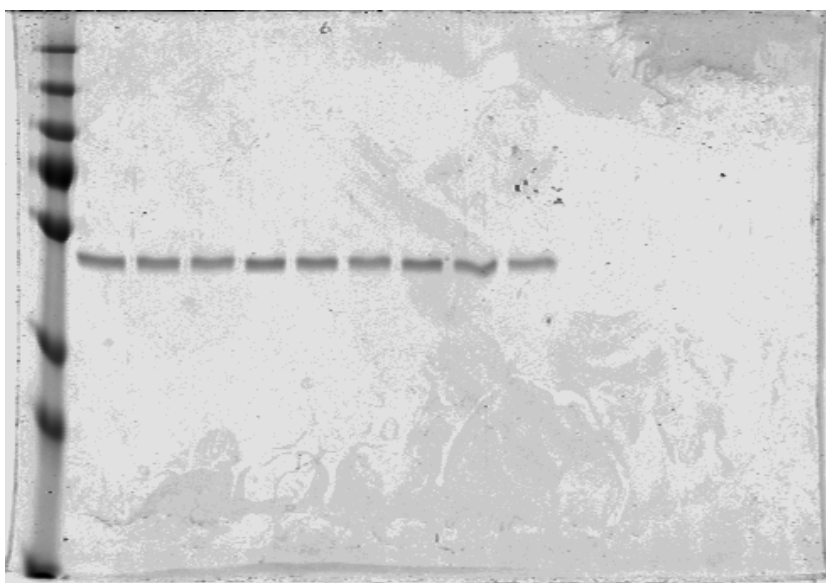


Supporting figure 29: Aggregation assay with the compounds CG3 05 A02 and CG6 25 G08. This Western blot was originally prepared to compare an aggregator (CG6 25 G08) with a non-aggregator (CG3 05 A02). All the samples have been loaded three times in the same order. Only the marker and the three lanes next to it have been shown in the results part. The lane next to those three contains the CG6 25 G08 sample. The colours have been inverted in the blot shown in the results part to match it with the other aggregation assay results. Un-labelled original anti-His₅ Western blot.

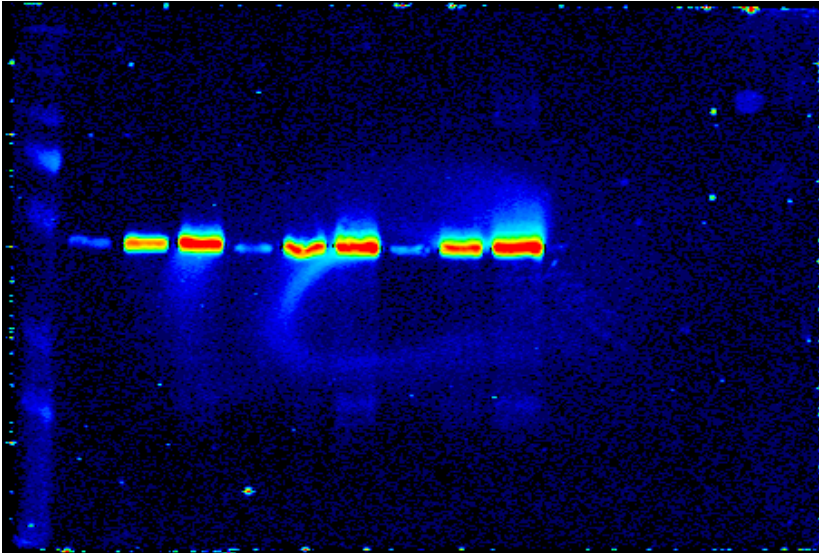


Supporting figure 30: Aggregation assay with the compounds CG55 08 H06, CG6 24 G06 and CG6 25 G08. Un-labelled original anti-His₅ Western blot.

8.2.3 The insulin receptor auto-phosphorylation assay

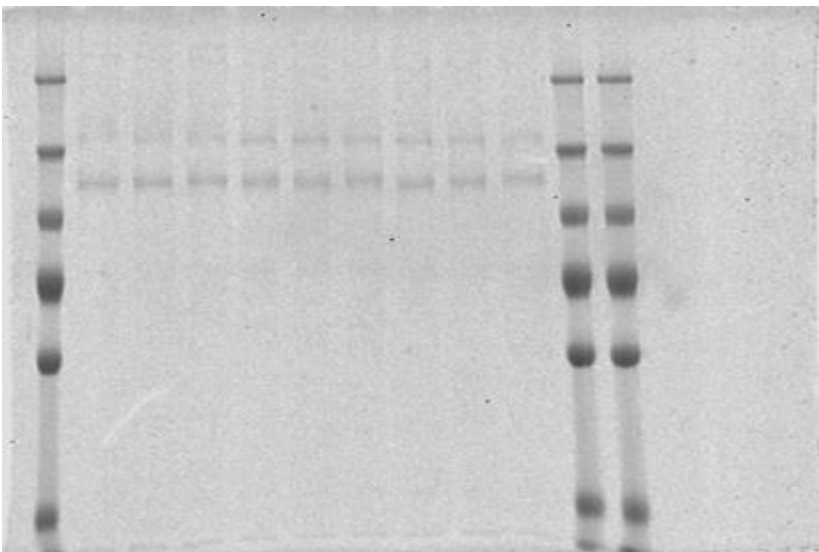


Supporting figure 31: Coomassie gel of the insulin receptor auto-phosphorylation assay. The un-labelled original coomassie stained gel shows that equal amounts of IR-ICD have been loaded.

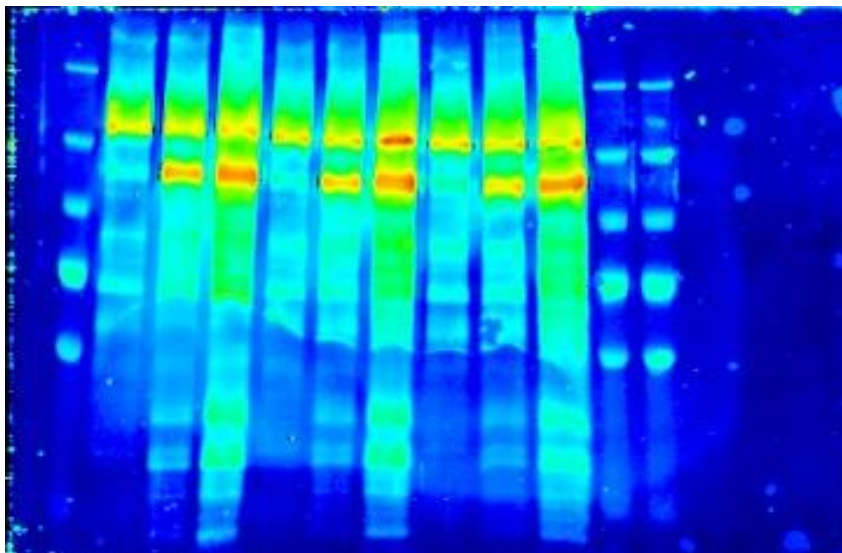


Supporting figure 32: Western blot of the insulin receptor auto-phosphorylation assay. Un-labelled original anti-phospho-tyrosine Western blot.

8.2.4 Influence of CG3 05 A02 on the ABL1-mediated Rin1 phosphorylation

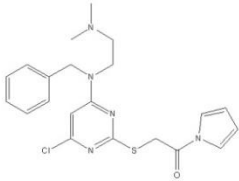
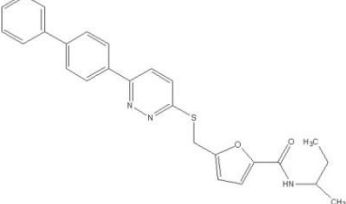
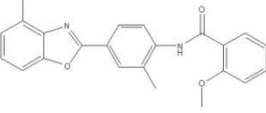
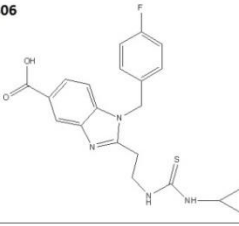
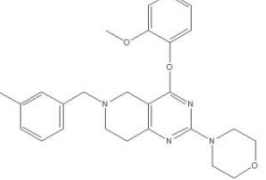
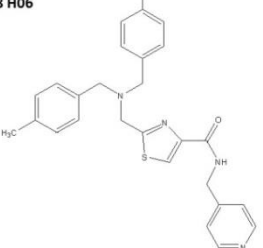
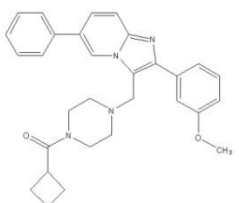
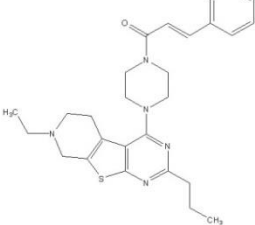
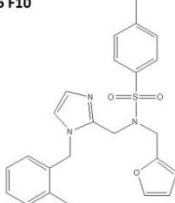
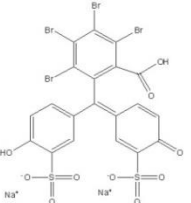
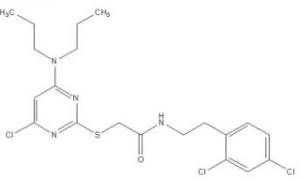
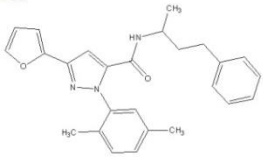
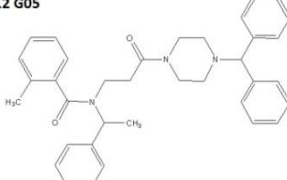
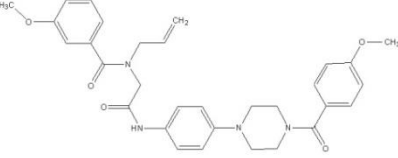


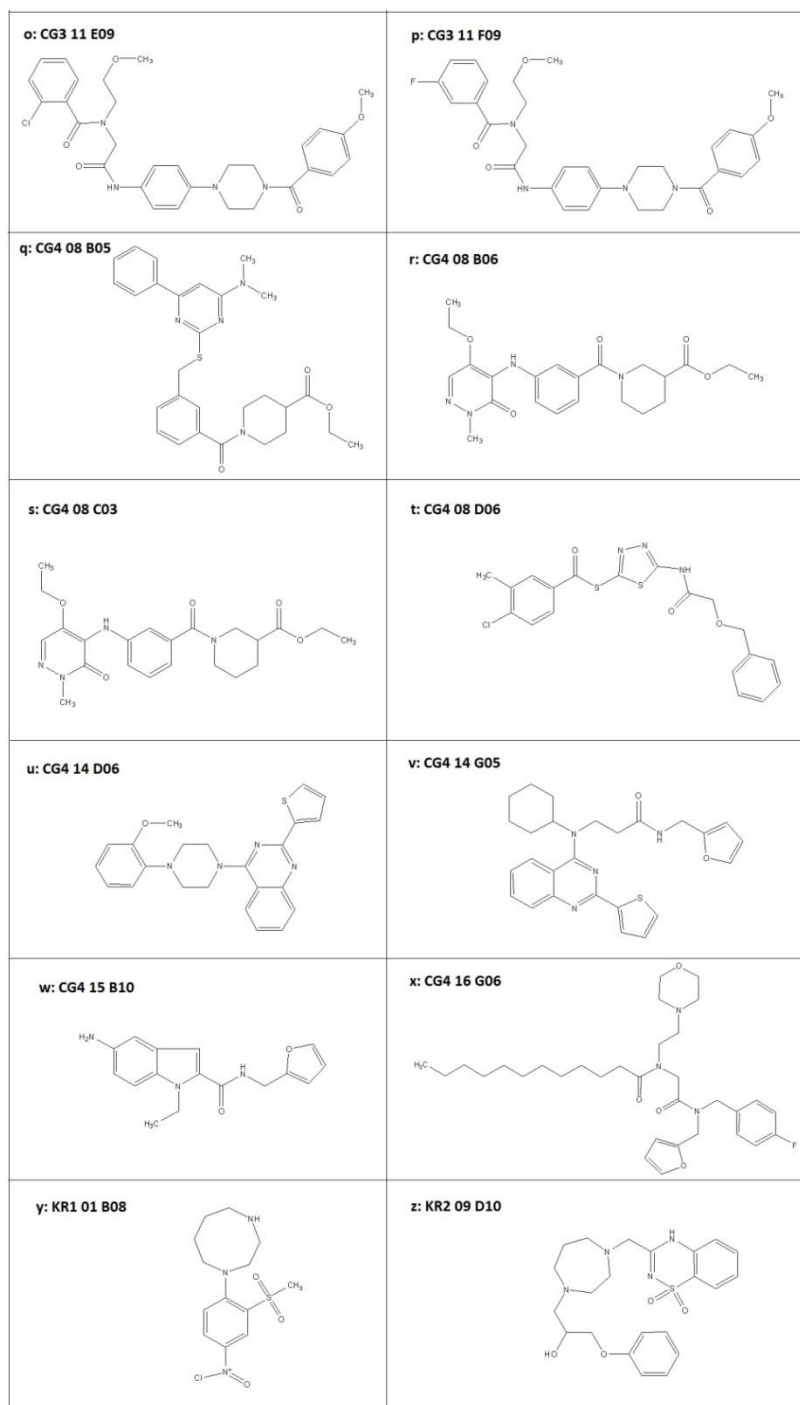
Supporting figure 33: Coomassie gel of the ABL1-mediated Rin1 phosphorylation assay. The un-labelled original coomassie stained gel shows that equal amounts of Rin1-TS and ABL1 have been loaded. The two marker lanes on the right side have been cut in the results part.



Supporting figure 34: Western blot of the ABL1-mediated Rin1 phosphorylation assay. Un-labelled original anti-phospho-tyrosine Western blot. The two marker lanes on the right side have been cut in the results part.

8.3 Structures of the 26 secondary hits

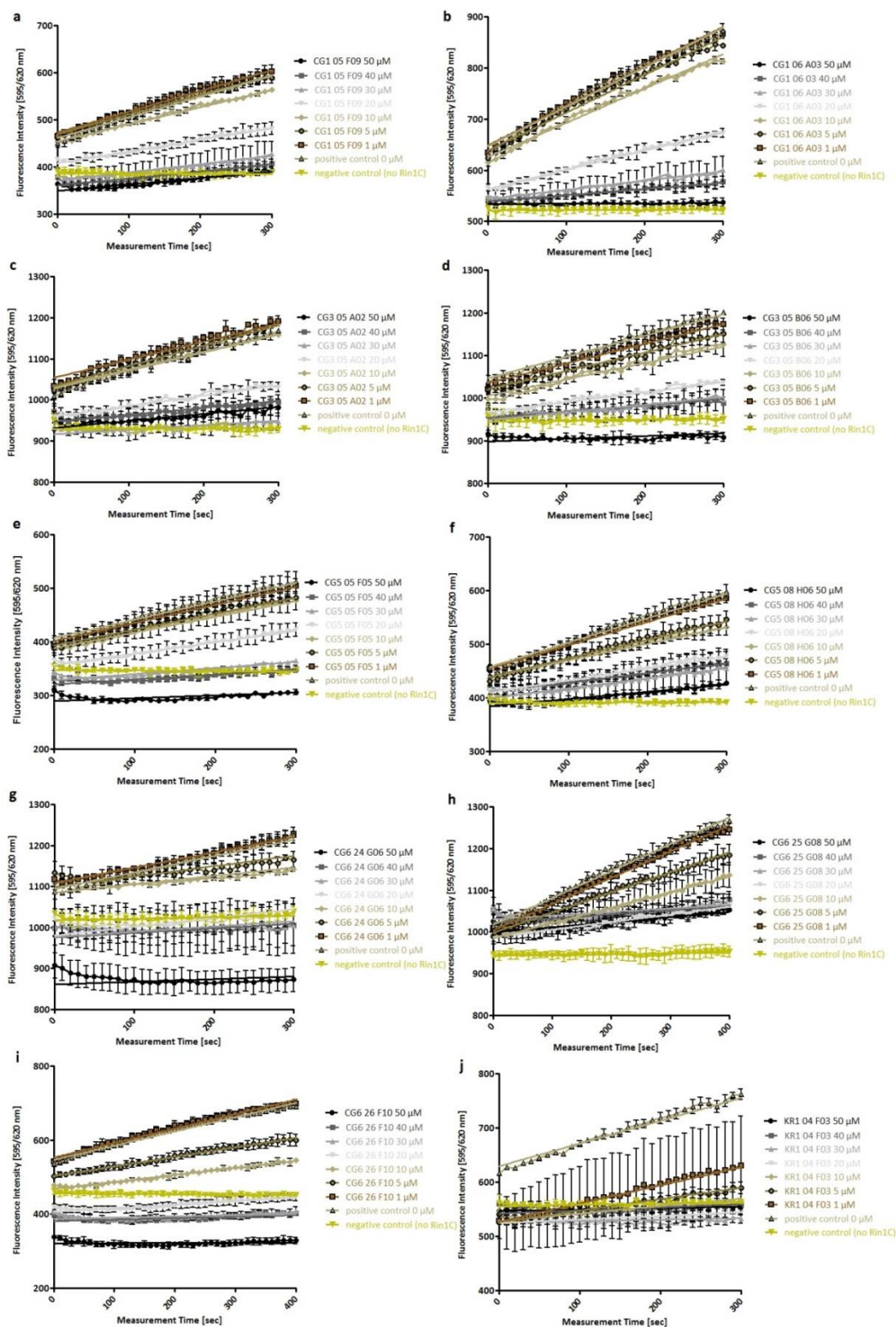
a: CG1 05 F09 	b: CG1 06 A03 
c: CG3 05 A02 	d: CG3 05 B06 
e: CG5 05 F05 	f: CG5 08 H06 
g: CG6 24 G06 	h: CG6 25 G08 
i: CG6 26 F10 	j: KR1 04 F03 
k: CG1 03 A01 	l: CG1 05 F01 
m: CG2 12 G05 	n: CG3 11 D10 



Supporting figure 35: Structures of the 26 secondary hits. a – j: Compounds that were active when tested from library stock solutions. These compounds are described in the results part. **k – z:** Compounds that were inactive when tested from library stock solutions and excluded from further analysis.

8.4 Raw data of the IC₅₀ measurements

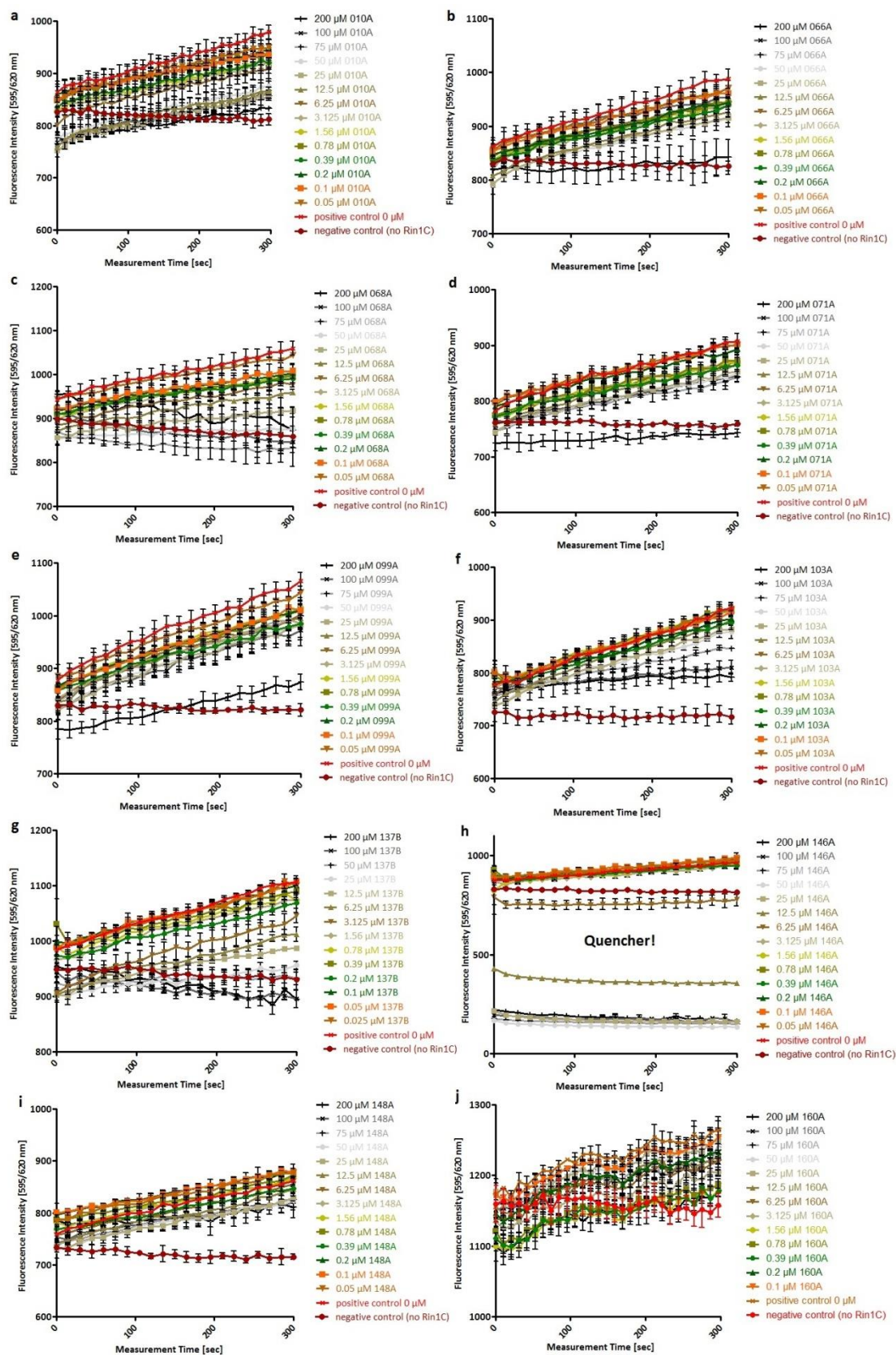
8.4.1 Secondary hits

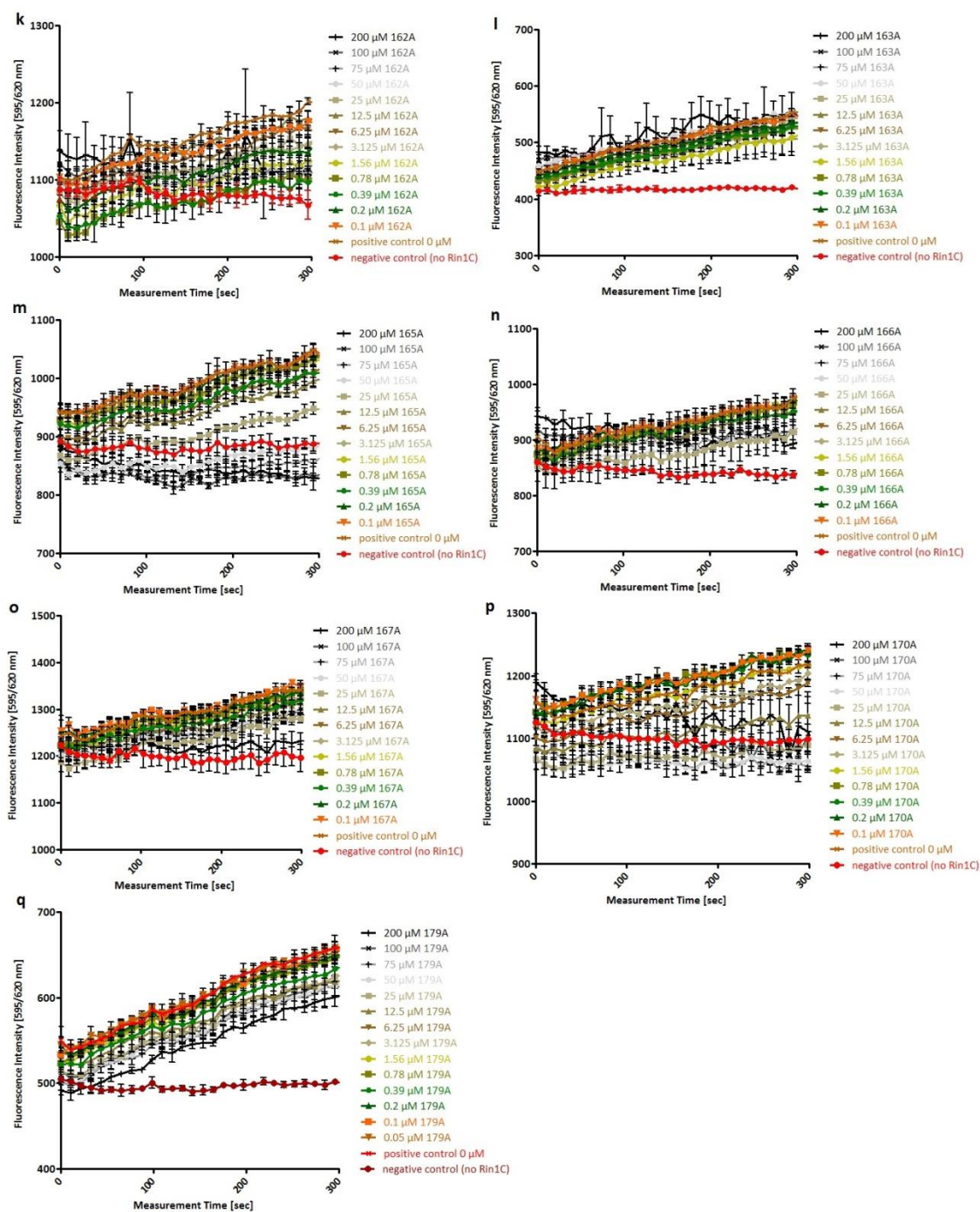


Supporting figure 36: Raw data of the IC₅₀ measurements. The linear phases of the reactions (first 300 seconds) were fitted and the corresponding slopes were calculated. Those slopes were used to generate the plots shown in the results part.

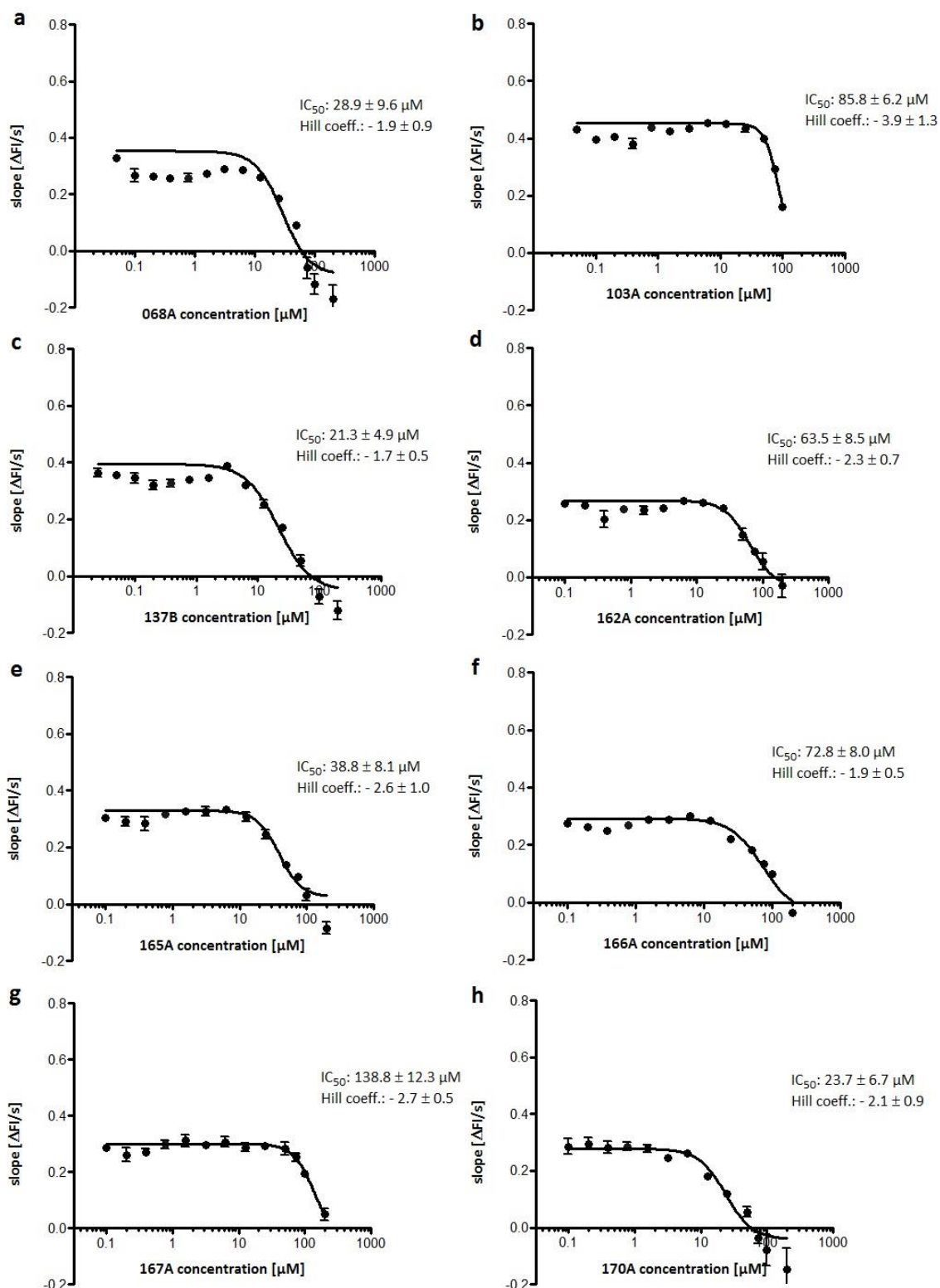
8.4.2 SAR compounds

8.4.2.1 Linear fits



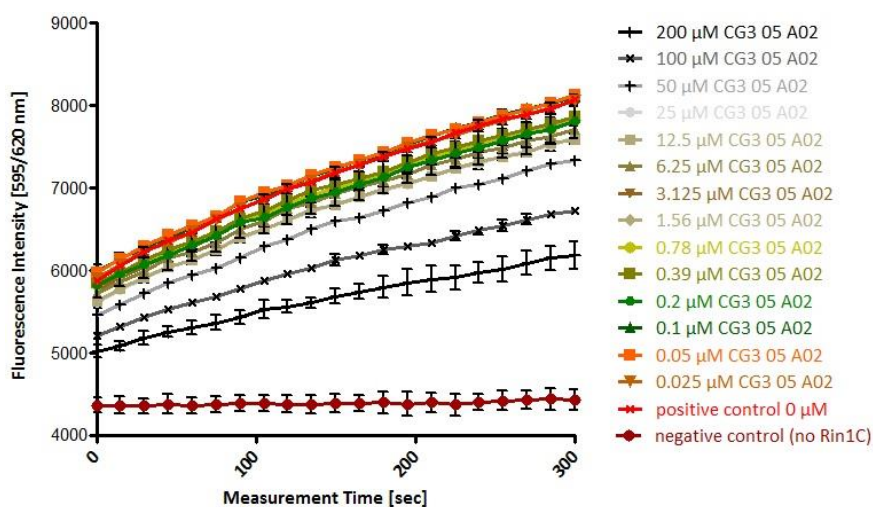


Supporting figure 37: Raw data of the SAR studies. No inhibition could be found for the compounds 010A (a), 066A (b), 071A (d), 099A (e), 146A (h), 148A (i), 160A (j), 163A (l) and 179A (q). For the compounds 068A (c), 103A (f), 137B (g), 162A (k), 165A (m), 166A (n), 167A (o) and 170A (p) the linear phases (the first 300 s) were fitted and the corresponding slopes were calculated. Those slopes were used to generate the plots shown in 8.5.2.2.

8.4.2.2 IC₅₀ calculations

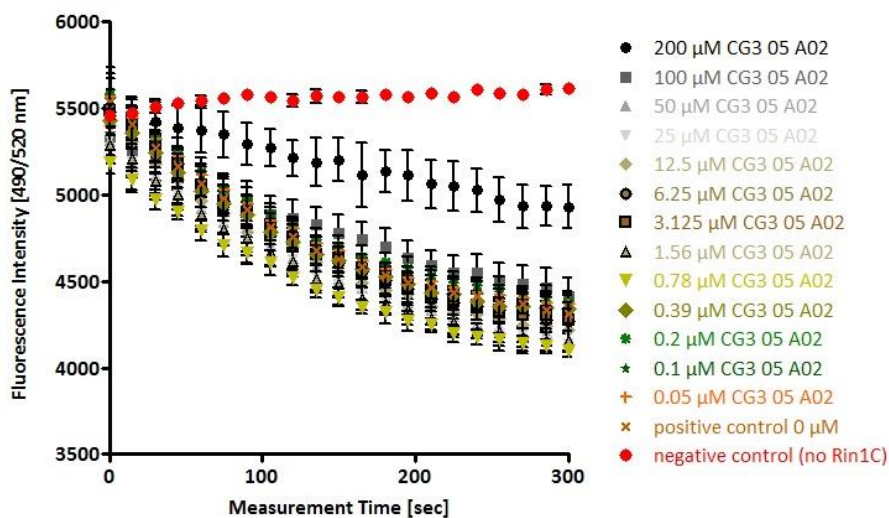
Supporting figure 38: IC₅₀ calculations for the active SAR compounds. The slopes calculated from the linear fits shown in 8.4.2.1 were plotted against the logarithmic compound concentrations to calculate the IC₅₀.

8.4.3 CG3 05 A02 in the Rin1C/Rab5a Bodipy-FL-GTP nucleotide exchange assay



Supporting figure 39: Raw data of the IC_{50} measurement for CG3 05 A02 in the Bodipy-FL-GTP nucleotide exchange assay. The linear phase was fitted to calculate the slopes used for the IC_{50} calculation shown in the results part.

8.4.4 CG3 05 A02 in the Rin1C/Rab5a Bodipy-FL-GDP release assay



Supporting figure 40: Raw data of the IC_{50} measurement for CG3 05 A02 in the Bodipy-FL-GDP release assay. The linear phase was fitted to calculate the slopes used for the IC_{50} calculation shown in the results part.

8.5 Solubility of the CG3 05 A02 derivatives

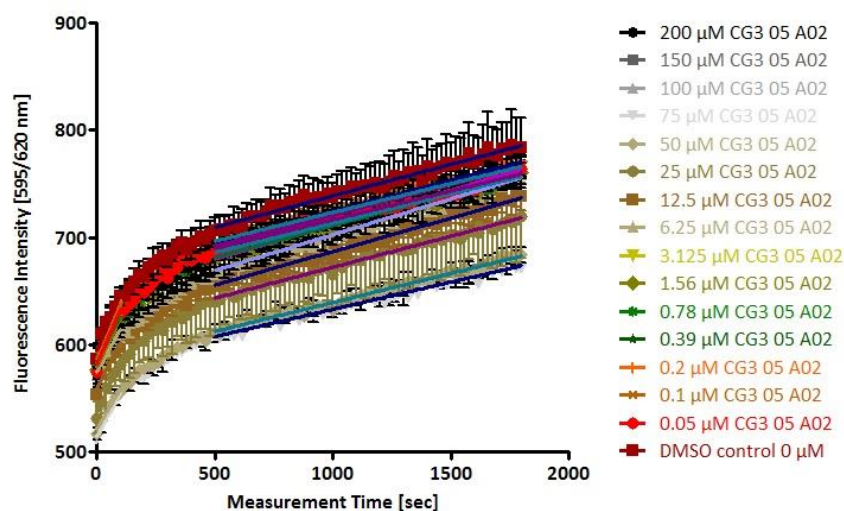
Table 25: Determination of the solubility of 068A.

Concentration [μM]	A_{350} before centrifugation	A_{350} after centrifugation
200	0.13	0.004
100	0.097	0.003
50	0.031	0.001
25	0.012	0.004
12.5	0.029	0.004
6.25	0.010	0.005
3.13	0.010	0.005
1.6	0.004	0.004

Table 26: Determination of the solubility of 137B.

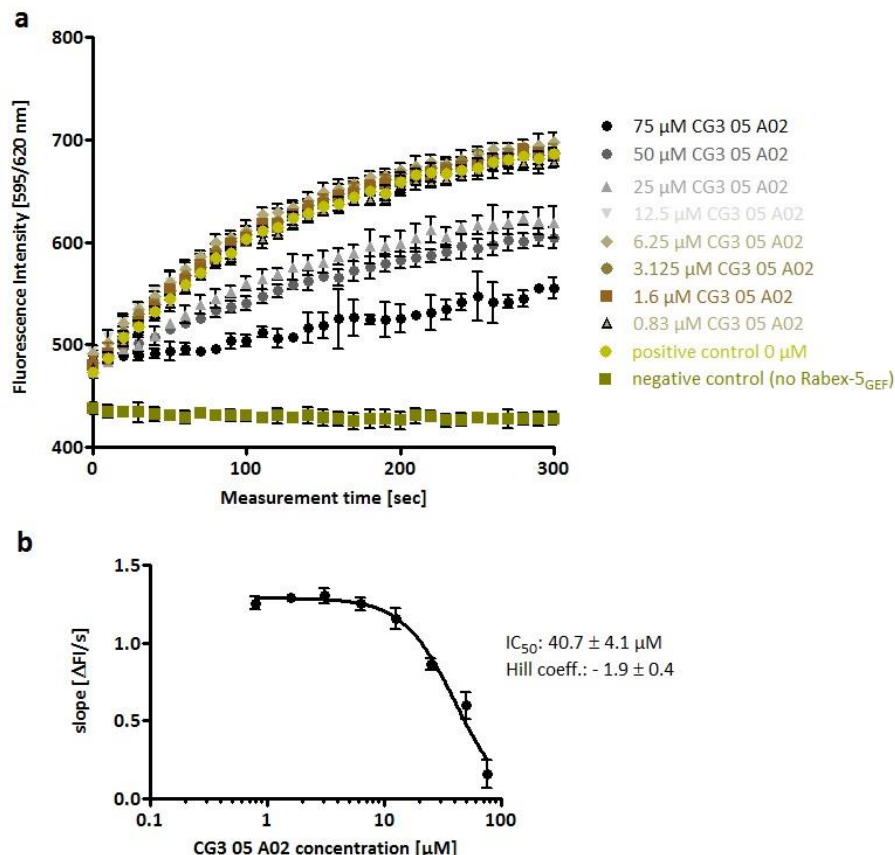
Concentration [μM]	A_{350} before centrifugation	A_{350} after centrifugation
200	0.276	0.002
100	0.171	0.003
50	0.101	0.002
25	0.042	0.001
12.5	0.025	0.002
6.25	0.016	0.003
3.13	0.007	0.003
1.6	0.007	0.001

8.6 Bodipy-TR-GTP binding to Rab5a



Supporting figure 41: Raw data showing the loading of Rab5a with Bodipy-TR-GTP. Rab5a was loaded with Bodipy-TR-GTP in presence of EDTA and different concentrations of CG3 05 A02 in absence of a GEF. A bi-phasic increase in the fluorescence signal can be seen. First the signal increases very fast for about 100 seconds. This linear phase has been used to calculate the slopes depicted in the results part. It is followed by a phase showing signs of saturation and then by another, slower, linear signal increase. This second linear phase has been fitted and is shown in shades of blue. It has not been used in the analysis shown in the results part, although the conclusions would have been the same, namely that there is no effect of CG3 05 A02 on the binding of Bodipy-TR-GTP to Rab5a. This bi-phasic signal increase could be explained with a phenomenon based on equilibration of the two isoforms of Bodipy-TR-GTP as has already been described by Guo et al.¹²⁹ for mant-GDP.

8.7 IC₅₀ of CG3 05 A02 in the Rabex-5_{GEF}/Rab5a Bodipy-TR-GTP nucleotide exchange assay



Supporting figure 42: IC₅₀ calculation of the compound CG3 05 A02 in the Rabex-5_{GEF}/Rab5a Bodipy-TR-GTP nucleotide exchange assay. Different concentrations of CG3 05 A02 were tested. The data obtained in the first 300 s (a) was fitted linearly to calculate the slopes depicted in b.

8.8 MST binding studies

In order to perform microscale thermophoresis (MST) experiments, the proteins Rin1C and Rab5a were labelled with Alexa-647 (NHS-ester) by addition of a 10-fold excess of Alexa-647 (NHS-ester) over the proteins, respectively, in labelling buffer. The samples were incubated on ice for 1 h. Free dye was then removed using NAP-5 columns equilibrated with elution buffer. Elution buffer was also used to elute the labelled proteins. The degree of labelling was afterwards calculated using the following equation:

$$DOL = \frac{A_{650} \cdot \epsilon_{Protein}}{A_{Protein} \cdot \epsilon_{Alexa-647}}$$

239000 is the extinction coefficient ϵ of Alexa-647, $\epsilon_{Protein}$ is the extinction coefficient of the protein-to-be-labelled, A_{650} is the absorption of the sample at 650 nm and $A_{Protein}$ is the absorption of the protein without the dye. $A_{Protein}$ can be calculated as follows:

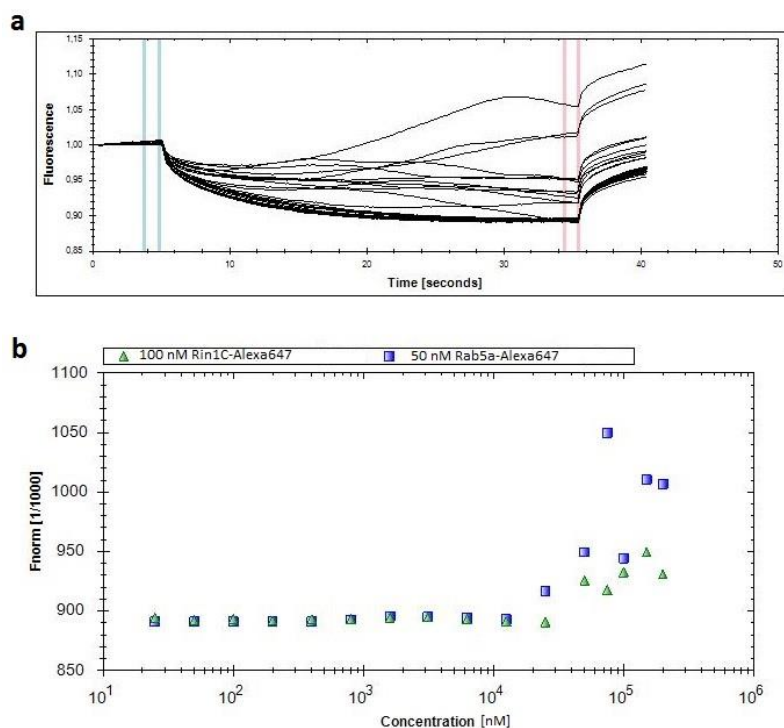
$$A_{Protein} = A_{280} - A_{650} \cdot CF$$

With A_{280} being the absorption of the sample at 280 nm and CF being 0.03, a correction factor for absorption readings, specific for Alexa-647.

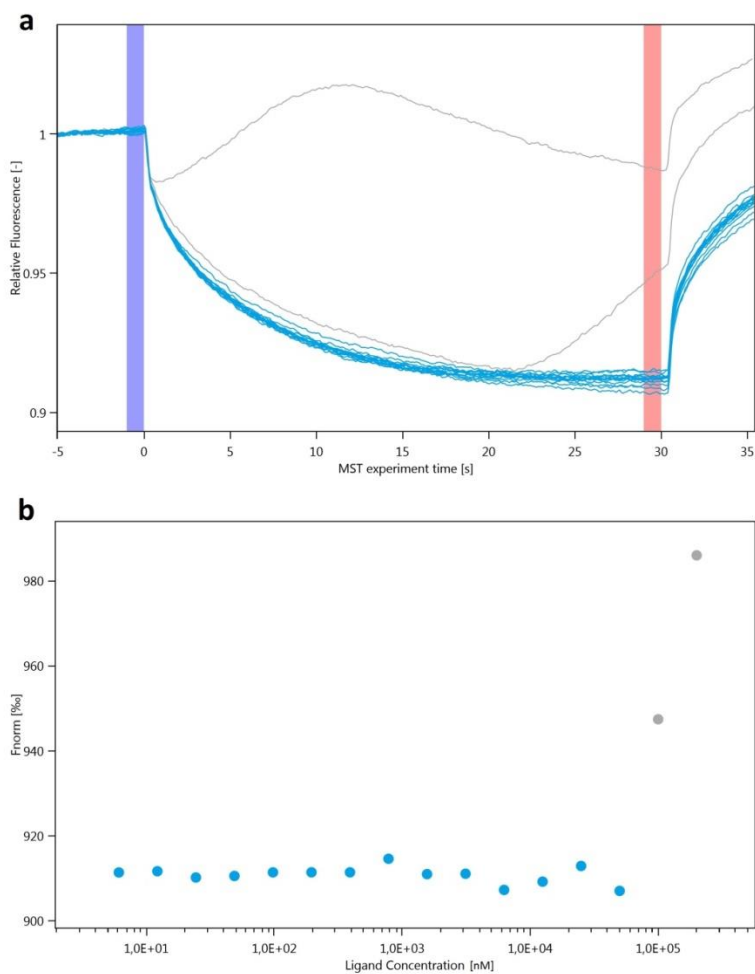
Table 27: Buffers for Alexa-647 (NHS-ester) labelling.

Buffer	Composition
Labelling Buffer	50 mM HEPES, pH 8 150 mM NaCl 1 mM MgCl ₂ 5 % Glycerol
Elution Buffer	50 mM HEPES, pH 7.5 150 mM NaCl 1 mM MgCl ₂ 5 % Glycerol

In the MST experiments CG3 05 A02 concentrations from 0 – 200 μ M were tested with a final DMSO concentration of 2 % in nucleotide exchange buffer (cp. section 7.2.3.1). 50 nM of labelled Rab5a and 100 nM of labelled Rin1C were used, respectively. When the GEF/GTPase complex was analysed, 1 μ M of un-labelled Rab5a and 200 nM of labelled Rin1C were used. The compound was pre-diluted in DMSO before the protein samples were mixed with the compound dilutions. The samples were aspirated in standard coated glass capillaries (NanoTemper) and then measured using 40 % LED power (red) and 20 % MST power. Thermophoresis and temperature jump were included in the evaluation shown in the supporting figures 43 and 44.



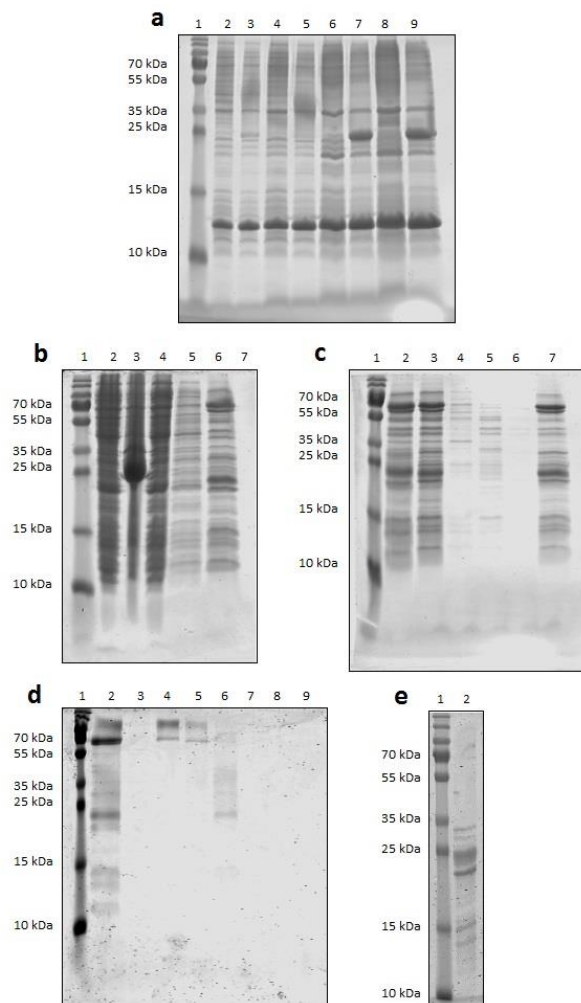
Supporting figure 43: MST binding studies for CG3 05 A02 on Rin1C and Rab5a. The compound was tested in concentrations between 0 and 200 μ M on each labelled protein. Compound concentrations > 50 μ M resulted in deformed thermophoresis curves (cp. **a**), probably due to compound aggregation, and were therefore excluded from the analysis. No concentration-dependent binding to any of the proteins could be detected in concentrations < 50 μ M (**b**).



Supporting figure 44: MST binding studies for CG3 05 A02 on the complex between Rin1C and Rab5a. The compound was tested in concentrations between 0 and 200 μM on 1 μM un-labelled Rab5a and 200 nM labelled Rin1C. Compound concentrations $> 50 \mu\text{M}$ resulted in deformed thermophoresis curves (cp. **a**), probably due to compound aggregation, and were therefore excluded from the analysis (grey dots, **b**). No concentration-dependent binding to the protein complex could be detected in concentrations $< 50 \mu\text{M}$ (**b**).

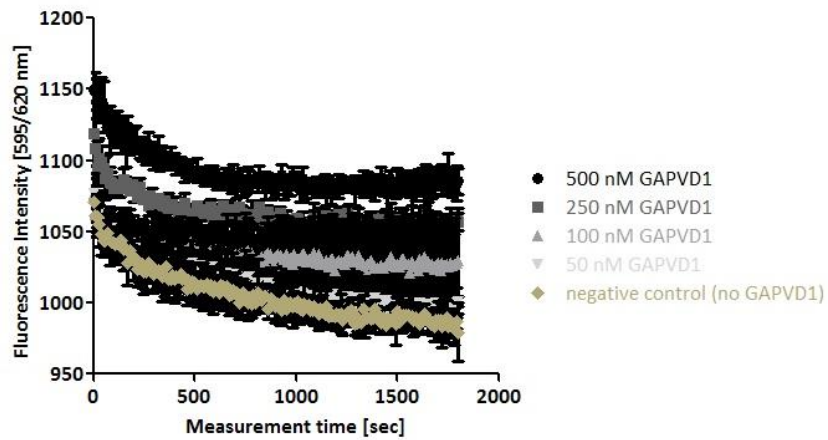
8.9 Expression, purification and nucleotide exchange activity of GAPVD1

GAPVD1 was expressed in *E. coli* and the protein expression was monitored on an SDS-PAGE gel as described in sections 7.2.1.1. It was then purified by Ni-NTA affinity chromatography, reverse Ni-NTA binding and size exclusion chromatography. The expression and the purification were analysed at every step as shown on the gels depicted in the supporting figure 45.



Supporting figure 45: Expression and purification of GAPVD1. A pre-stained molecular weight marker has been loaded in lane 1 on each gel. **a:** The protein expression was monitored on this 15 % SDS-PAGE gel. The lanes 2 and 3 show 3 μ L of an *E. coli* whole-cell lysate before (lane 2) and after (lane 3) induction of the expression with IPTG. In lanes 4 and 5 5 μ L of the lysates have been loaded. 7.5 μ L have been loaded in the lanes 6 and 7 and the lanes 8 and 9 contain 10 μ L of the lysates before and after IPTG induction. After induction a strong band can be seen approx. at the height of the 25 kDa marker band. The expected molecular weight of GAPVD1 is supposed to be \sim 31 kDa, it therefore runs a little low in the gel, what might be due to its hydrodynamic properties. **b:** 15 % SDS-PAGE gel showing step by step the GAPVD1 purification via Ni-NTA affinity chromatography. The cleared lysate is shown in lane 2. Lane 3 shows the insoluble cell debris from the pellet after the lysate was cleared. The unbound material after Ni-NTA binding (flow-through) is shown in lane 4. Lane 5 shows the washing fraction and lane 6 contains the eluate. Unfortunately a lot of the protein of interest appears to be insoluble and can be seen in the pellet sample. There is, however, some amount to be found in the eluate, although it is not very pure. **c:** 15 % SDS-PAGE gel analysing the reverse Ni-NTA binding and TEV digestion of GAPVD1. Lane 2 shows the eluate as it was already shown in lane 6 in **b**. The sample after TEV digestion is shown in lane 3. Lane 4 shows the unbound material after reverse Ni-NTA binding. The lanes 5 and 6 contain two washing fractions and the eluate is shown in lane 7. There is no molecular weight shift in any of the bands visible when comparing lanes 2 and 3, which argues against a successful TEV digestion. This is supported by the absence of the protein of interest in the flow-through fraction. It appears to be found in the eluate again and seems to be rather impure. **d:** Size exclusion chromatography of the eluate after reverse Ni-NTA binding analysed on a 15 % SDS-PAGE gel. Lane 2 shows the eluate after reverse Ni-NTA binding as already shown in lane 7 in **c**. The fractions were pooled by peaks. Lane 3 shows the fractions 1 – 4, the fractions 7 – 11 are shown in lane 4. In lane 5 the fractions 14 – 19 have been loaded and lane 6 shows the fractions 20 – 27. The lanes 7, 8 and 9 show the fractions 28 – 31, 36 – 39 and 41 – 47, respectively. The protein of interest could be seen in lane 6 corresponding to the fractions 20 – 27. These fractions were concentrated afterwards. **e:** The concentrated final sample of GAPVD1 is shown in lane 2. If it is the correct protein it is rather impure. It was used for activity testing next.

The concentrated final sample from the GAPVD1 purification was used in different concentrations on 1 μ M Rab5a. The results are shown in the supporting figure 46.



Supporting figure 46: Activity testing of GAPVD1. Different concentrations of GAPVD1 have been tested on 1 μ M Rab5a using Bodipy-TR-GTP. No increase in the fluorescence signal could be seen for any of the tested conditions. The GEF GAPVD1 appears to be inactive.

References

1. Sessa, G. & Weissmann, G. Phospholipid spherules (liposomes) as a model for biological membranes. *J. Lipid Res.* **9**, 310–318 (1968).
2. Syrovatkina, V., Alegre, K. O., Dey, R. & Huang, X.-Y. Regulation, Signaling, and Physiological Functions of G-Proteins. *J. Mol. Biol.* **428**, 3850–3868 (2016).
3. Yavropoulou, M. P. & Yovos, J. G. The molecular basis of bone mechanotransduction. *J. Musculoskelet. Neuronal Interact.* **16**, 221–236 (2016).
4. Zhang, X. Molecular sensors and modulators of thermoreception. *Channels Austin Tex* **9**, 73–81 (2015).
5. Suescún-Bolívar, L. P. & Thomé, P. E. Osmosensing and osmoregulation in unicellular eukaryotes. *World J. Microbiol. Biotechnol.* **31**, 435–443 (2015).
6. Becucci, L. & Guidelli, R. What Ion Flow along Ion Channels Can Tell us about Their Functional Activity. *Membranes* **6**, (2016).
7. Pan, Z. *et al.* Zinc transporters and dysregulated channels in cancers. *Front. Biosci. Landmark Ed.* **22**, 623–643 (2017).
8. Pakkala, S. & Ramalingam, S. S. Epidermal Growth Factor Receptor Mutated Advanced Non-Small Cell Lung Cancer: A Changing Treatment Paradigm. *Hematol. Oncol. Clin. North Am.* **31**, 83–99 (2017).
9. Gomez-Navarro, N. & Miller, E. Protein sorting at the ER-Golgi interface. *J. Cell Biol.* **215**, 769–778 (2016).
10. Di Fiore, P. P. & De Camilli, P. Endocytosis and Signaling: An Inseparable Partnership. *Cell* **106**, 1–4 (2001).
11. Miaczynska, M., Pelkmans, L. & Zerial, M. Not just a sink: endosomes in control of signal transduction. *Curr. Opin. Cell Biol.* **16**, 400–406 (2004).

12. Novick, P. Regulation of membrane traffic by Rab GEF and GAP cascades. *Small GTPases* **7**, 252–256 (2016).
13. Tzeng, H.-T. & Wang, Y.-C. Rab-mediated vesicle trafficking in cancer. *J. Biomed. Sci.* **23**, 70 (2016).
14. Bos, J. L. ras oncogenes in human cancer: a review. *Cancer Res.* **49**, 4682–4689 (1989).
15. Baines, A. T., Xu, D. & Der, C. J. Inhibition of Ras for cancer treatment: the search continues. *Future Med. Chem.* **3**, 1787–1808 (2011).
16. Bourne, H. R., Sanders, D. A. & McCormick, F. The GTPase superfamily: a conserved switch for diverse cell functions. *Nature* **348**, 125–132 (1990).
17. Weiss, O., Holden, J., Rulka, C. & Kahn, R. A. Nucleotide binding and cofactor activities of purified bovine brain and bacterially expressed ADP-ribosylation factor. *J. Biol. Chem.* **264**, 21066–21072 (1989).
18. Vetter, I. R. & Wittinghofer, A. The guanine nucleotide-binding switch in three dimensions. *Science* **294**, 1299–1304 (2001).
19. Grosshans, B. L., Ortiz, D. & Novick, P. Rabs and their effectors: achieving specificity in membrane traffic. *Proc. Natl. Acad. Sci. U. S. A.* **103**, 11821–11827 (2006).
20. Scolnick, E. M., Papageorge, A. G. & Shih, T. Y. Guanine nucleotide-binding activity as an assay for src protein of rat-derived murine sarcoma viruses. *Proc. Natl. Acad. Sci. U. S. A.* **76**, 5355–5359 (1979).
21. Zhao, W. *et al.* Direct Targeting of the Ras GTPase Superfamily Through Structure-Based Design. *Curr. Top. Med. Chem.* **17**, 16–29 (2017).
22. Wennerberg, K., Rossman, K. L. & Der, C. J. The Ras superfamily at a glance. *J. Cell Sci.* **118**, 843–846 (2005).
23. Zerial, M. & McBride, H. Rab proteins as membrane organizers. *Nat. Rev. Mol. Cell Biol.* **2**, 107–117 (2001).

24. Mizuno-Yamasaki, E., Rivera-Molina, F. & Novick, P. GTPase networks in membrane traffic. *Annu. Rev. Biochem.* **81**, 637–659 (2012).
25. Etienne-Manneville, S. & Hall, A. Rho GTPases in cell biology. *Nature* **420**, 629–635 (2002).
26. Yudin, D. & Fainzilber, M. Ran on tracks--cytoplasmic roles for a nuclear regulator. *J. Cell Sci.* **122**, 587–593 (2009).
27. Seabra, M. C. Membrane association and targeting of prenylated Ras-like GTPases. *Cell. Signal.* **10**, 167–172 (1998).
28. Seabra, M. C. & Wasmeier, C. Controlling the location and activation of Rab GTPases. *Curr. Opin. Cell Biol.* **16**, 451–457 (2004).
29. Ullrich, O., Horiuchi, H., Bucci, C. & Zerial, M. Membrane association of Rab5 mediated by GDP-dissociation inhibitor and accompanied by GDP/GTP exchange. *Nature* **368**, 157–160 (1994).
30. Soldati, T., Shapiro, A. D., Svejstrup, A. B. & Pfeffer, S. R. Membrane targeting of the small GTPase Rab9 is accompanied by nucleotide exchange. *Nature* **369**, 76–78 (1994).
31. Goody, R. S. & Hofmann-Goody, W. Exchange factors, effectors, GAPs and motor proteins: common thermodynamic and kinetic principles for different functions. *Eur. Biophys. J. EBJ* **31**, 268–274 (2002).
32. Itzen, A. & Goody, R. S. GTPases involved in vesicular trafficking: Structures and mechanisms. *Semin. Cell Dev. Biol.* **22**, 48–56 (2011).
33. Goody, P. R. Intrinsic protein fluorescence assays for GEF, GAP and post-translational modifications of small GTPases. *Anal. Biochem.* **515**, 22–25 (2016).
34. Stenmark, H. & Olkkonen, V. M. The Rab GTPase family. *Genome Biol.* **2**, REVIEWS3007 (2001).
35. Pereira-Leal, J. B. & Seabra, M. C. Evolution of the Rab family of small GTP-binding proteins. *J. Mol. Biol.* **313**, 889–901 (2001).

36. Pfeffer, S. R. Rab GTPases: specifying and deciphering organelle identity and function. *Trends Cell Biol.* **11**, 487–491 (2001).
37. Pereira-Leal, J. B. & Seabra, M. C. The mammalian Rab family of small GTPases: definition of family and subfamily sequence motifs suggests a mechanism for functional specificity in the Ras superfamily. *J. Mol. Biol.* **301**, 1077–1087 (2000).
38. Moore, I., Schell, J. & Palme, K. Subclass-specific sequence motifs identified in Rab GTPases. *Trends Biochem. Sci.* **20**, 10–12 (1995).
39. Chavrier, P. *et al.* Hypervariable C-terminal domain of rab proteins acts as a targeting signal. *Nature* **353**, 769–772 (1991).
40. Echard, A. *et al.* Alternative splicing of the human Rab6A gene generates two close but functionally different isoforms. *Mol. Biol. Cell* **11**, 3819–3833 (2000).
41. Anant, J. S. *et al.* Mechanism of Rab geranylgeranylation: formation of the catalytic ternary complex. *Biochemistry (Mosc.)* **37**, 12559–12568 (1998).
42. Wright, L. P. & Philips, M. R. Thematic review series: lipid posttranslational modifications. CAAX modification and membrane targeting of Ras. *J. Lipid Res.* **47**, 883–891 (2006).
43. Stenmark, H. Rab GTPases as coordinators of vesicle traffic. *Nat. Rev. Mol. Cell Biol.* **10**, 513–525 (2009).
44. Dirac-Svejstrup, A. B., Sumizawa, T. & Pfeffer, S. R. Identification of a GDI displacement factor that releases endosomal Rab GTPases from Rab-GDI. *EMBO J.* **16**, 465–472 (1997).
45. Sivars, U., Aivazian, D. & Pfeffer, S. R. Yip3 catalyses the dissociation of endosomal Rab-GDI complexes. *Nature* **425**, 856–859 (2003).
46. Cabrera, M. & Ungermann, C. Guanine nucleotide exchange factors (GEFs) have a critical but not exclusive role in organelle localization of Rab GTPases. *J. Biol. Chem.* **288**, 28704–28712 (2013).

47. Blümer, J. *et al.* RabGEFs are a major determinant for specific Rab membrane targeting. *J. Cell Biol.* **200**, 287–300 (2013).
48. Alberts, B. *et al.* *Molecular Biology of the Cell.* (Garland Science, 2002).
49. Park, H. H. Structural basis of membrane trafficking by Rab family small G protein. *Int. J. Mol. Sci.* **14**, 8912–8923 (2013).
50. Wang, J., Morita, Y., Mazelova, J. & Deretic, D. The Arf GAP ASAP1 provides a platform to regulate Arf4- and Rab11-Rab8-mediated ciliary receptor targeting. *EMBO J.* **31**, 4057–4071 (2012).
51. Dong, B., Kakihara, K., Otani, T., Wada, H. & Hayashi, S. Rab9 and retromer regulate retrograde trafficking of luminal protein required for epithelial tube length control. *Nat. Commun.* **4**, 1358 (2013).
52. Burd, C. & Cullen, P. J. Retromer: a master conductor of endosome sorting. *Cold Spring Harb. Perspect. Biol.* **6**, (2014).
53. Saxena, S., Bucci, C., Weis, J. & Kruttgen, A. The small GTPase Rab7 controls the endosomal trafficking and neuritogenic signaling of the nerve growth factor receptor TrkA. *J. Neurosci. Off. J. Soc. Neurosci.* **25**, 10930–10940 (2005).
54. Carroll, K. S. *et al.* Role of Rab9 GTPase in facilitating receptor recruitment by TIP47. *Science* **292**, 1373–1376 (2001).
55. Wandinger-Ness, A. & Zerial, M. Rab Proteins and the Compartmentalization of the Endosomal System. *Cold Spring Harb. Perspect. Biol.* **6**, (2014).
56. Hoepfner, S. *et al.* Modulation of receptor recycling and degradation by the endosomal kinesin KIF16B. *Cell* **121**, 437–450 (2005).
57. Bananis, E. *et al.* Microtubule-dependent movement of late endocytic vesicles in vitro: requirements for Dynein and Kinesin. *Mol. Biol. Cell* **15**, 3688–3697 (2004).

58. Barbero, P., Bittova, L. & Pfeffer, S. R. Visualization of Rab9-mediated vesicle transport from endosomes to the trans-Golgi in living cells. *J. Cell Biol.* **156**, 511–518 (2002).
59. Cantalupo, G., Alifano, P., Roberti, V., Bruni, C. B. & Bucci, C. Rab-interacting lysosomal protein (RILP): the Rab7 effector required for transport to lysosomes. *EMBO J.* **20**, 683–693 (2001).
60. Jordens, I. *et al.* The Rab7 effector protein RILP controls lysosomal transport by inducing the recruitment of dynein-dynactin motors. *Curr. Biol. CB* **11**, 1680–1685 (2001).
61. Johansson, M. *et al.* Activation of endosomal dynein motors by stepwise assembly of Rab7-RILP-p150Glued, ORP1L, and the receptor betaIII spectrin. *J. Cell Biol.* **176**, 459–471 (2007).
62. Delevoeye, C. & Goud, B. Rab GTPases and kinesin motors in endosomal trafficking. *Methods Cell Biol.* **130**, 235–246 (2015).
63. Lapierre, L. A. *et al.* Myosin vb is associated with plasma membrane recycling systems. *Mol. Biol. Cell* **12**, 1843–1857 (2001).
64. Lindsay, A. J. *et al.* Identification and characterization of multiple novel Rab-myosin Va interactions. *Mol. Biol. Cell* **24**, 3420–3434 (2013).
65. McNew, J. A. *et al.* Compartmental specificity of cellular membrane fusion encoded in SNARE proteins. *Nature* **407**, 153–159 (2000).
66. Weber, T. *et al.* SNAREpins: minimal machinery for membrane fusion. *Cell* **92**, 759–772 (1998).
67. Pfeffer, S. R. Rab GTPase regulation of membrane identity. *Curr. Opin. Cell Biol.* **25**, 414–419 (2013).
68. Gruenberg, J. & Maxfield, F. R. Membrane transport in the endocytic pathway. *Curr. Opin. Cell Biol.* **7**, 552–563 (1995).

69. Gu, F. & Gruenberg, J. Biogenesis of transport intermediates in the endocytic pathway. *FEBS Lett.* **452**, 61–66 (1999).
70. Haucke, V. Phosphoinositide regulation of clathrin-mediated endocytosis. *Biochem. Soc. Trans.* **33**, 1285–1289 (2005).
71. Doherty, G. J. & McMahon, H. T. Mechanisms of endocytosis. *Annu. Rev. Biochem.* **78**, 857–902 (2009).
72. Donaldson, J. G., Johnson, D. L. & Dutta, D. Rab and Arf G proteins in endosomal trafficking and cell surface homeostasis. *Small GTPases* **7**, 247–251 (2016).
73. Dutta, D. & Donaldson, J. G. Sorting of Clathrin-Independent Cargo Proteins Depends on Rab35 Delivered by Clathrin-Mediated Endocytosis. *Traffic Cph. Den.* **16**, 994–1009 (2015).
74. Su, H. *et al.* Small GTPase Rab14 down-regulates UT-A1 urea transport activity through enhanced clathrin-dependent endocytosis. *FASEB J. Off. Publ. Fed. Am. Soc. Exp. Biol.* **27**, 4100–4107 (2013).
75. Lampe, M., Vassilopoulos, S. & Merrifield, C. Clathrin coated pits, plaques and adhesion. *J. Struct. Biol.* **196**, 48–56 (2016).
76. Elkin, S. R., Lakoduk, A. M. & Schmid, S. L. Endocytic pathways and endosomal trafficking: a primer. *Wien. Med. Wochenschr.* **166**, 196–204 (2016).
77. Kadlecova, Z. *et al.* Regulation of clathrin-mediated endocytosis by hierarchical allosteric activation of AP2. *J. Cell Biol.* **216**, 167–179 (2017).
78. Avinoam, O., Schorb, M., Beese, C. J., Briggs, J. A. G. & Kaksonen, M. ENDOCYTOSIS. Endocytic sites mature by continuous bending and remodeling of the clathrin coat. *Science* **348**, 1369–1372 (2015).
79. Massol, R. H., Boll, W., Griffin, A. M. & Kirchhausen, T. A burst of auxilin recruitment determines the onset of clathrin-coated vesicle uncoating. *Proc. Natl. Acad. Sci. U. S. A.* **103**, 10265–10270 (2006).

80. Kirsten, M. L., Baron, R. A., Seabra, M. C. & Ces, O. Rab1a and Rab5a preferentially bind to binary lipid compositions with higher stored curvature elastic energy. *Mol. Membr. Biol.* **30**, 303–314 (2013).
81. Pfeffer, S. R. Rab GTPase localization and Rab cascades in Golgi transport. *Biochem. Soc. Trans.* **40**, 1373–1377 (2012).
82. Christine Irene Wosnitza. Chemical modulation of guanine nucleotide exchange factor activity - A small molecule inhibitor for the Rabex-5 mediated Rab5 activation. (Rheinische Friedrich-Wilhelms Universität Bonn, 2013).
83. Simpson, J. C. & Jones, A. T. Early endocytic Rabs: functional prediction to functional characterization. *Biochem. Soc. Symp.* 99–108 (2005).
84. Barbieri, M. A. *et al.* Epidermal growth factor and membrane trafficking. EGF receptor activation of endocytosis requires Rab5a. *J. Cell Biol.* **151**, 539–550 (2000).
85. Arnett, A. L. H. *et al.* Antisense oligonucleotide against GTPase Rab5b inhibits metabotropic agonist DHPG-induced neuroprotection. *Brain Res.* **1028**, 59–65 (2004).
86. Haobam, B. *et al.* Rab17-mediated recycling endosomes contribute to autophagosome formation in response to Group A Streptococcus invasion. *Cell. Microbiol.* **16**, 1806–1821 (2014).
87. Callaghan, J., Nixon, S., Bucci, C., Toh, B. H. & Stenmark, H. Direct interaction of EEA1 with Rab5b. *Eur. J. Biochem.* **265**, 361–366 (1999).
88. Mishra, A., Eathiraj, S., Corvera, S. & Lambright, D. G. Structural basis for Rab GTPase recognition and endosome tethering by the C2H2 zinc finger of Early Endosomal Autoantigen 1 (EEA1). *Proc. Natl. Acad. Sci. U. S. A.* **107**, 10866–10871 (2010).
89. Zhu, G. *et al.* Structural basis of Rab5-Rabaptin5 interaction in endocytosis. *Nat. Struct. Mol. Biol.* **11**, 975–983 (2004).
90. Eathiraj, S., Pan, X., Ritacco, C. & Lambright, D. G. Structural basis of family-wide Rab GTPase recognition by rabenosyn-5. *Nature* **436**, 415–419 (2005).

91. Horiuchi, H. *et al.* A Novel Rab5 GDP/GTP Exchange Factor Complexed to Rabaptin-5 Links Nucleotide Exchange to Effector Recruitment and Function. *Cell* **90**, 1149–1159 (1997).
92. Nishimura, N., Nakamura, H., Takai, Y. & Sano, K. Molecular cloning and characterization of two rab GDI species from rat brain: brain-specific and ubiquitous types. *J. Biol. Chem.* **269**, 14191–14198 (1994).
93. Wu, Y.-W. *et al.* Membrane targeting mechanism of Rab GTPases elucidated by semisynthetic protein probes. *Nat. Chem. Biol.* **6**, 534–540 (2010).
94. Amor, J. C., Harrison, D. H., Kahn, R. A. & Ringe, D. Structure of the human ADP-ribosylation factor 1 complexed with GDP. *Nature* **372**, 704–708 (1994).
95. Stenmark, H. *et al.* Inhibition of rab5 GTPase activity stimulates membrane fusion in endocytosis. *EMBO J.* **13**, 1287–1296 (1994).
96. Albert, S., Will, E. & Gallwitz, D. Identification of the catalytic domains and their functionally critical arginine residues of two yeast GTPase-activating proteins specific for Ypt/Rab transport GTPases. *EMBO J.* **18**, 5216–5225 (1999).
97. Liu, O. & Grant, B. D. Basolateral Endocytic Recycling Requires RAB-10 and AMPH-1 Mediated Recruitment of RAB-5 GAP TBC-2 to Endosomes. *PLoS Genet.* **11**, e1005514 (2015).
98. Bernards, A. GAPs galore! A survey of putative Ras superfamily GTPase activating proteins in man and Drosophila. *Biochim. Biophys. Acta* **1603**, 47–82 (2003).
99. Chotard, L. *et al.* TBC-2 Regulates RAB-5/RAB-7-mediated Endosomal Trafficking in *Caenorhabditis elegans*. *Mol. Biol. Cell* **21**, 2285–2296 (2010).
100. Carney, D. S., Davies, B. A. & Horazdovsky, B. F. Vps9 domain-containing proteins: activators of Rab5 GTPases from yeast to neurons. *Trends Cell Biol.* **16**, 27–35 (2006).
101. Simon, I., Zerial, M. & Goody, R. S. Kinetics of interaction of Rab5 and Rab7 with nucleotides and magnesium ions. *J. Biol. Chem.* **271**, 20470–20478 (1996).

102. Tall, G. G., Barbieri, M. A., Stahl, P. D. & Horazdovsky, B. F. Ras-activated endocytosis is mediated by the Rab5 guanine nucleotide exchange activity of RIN1. *Dev. Cell* **1**, 73–82 (2001).
103. Woller, B. *et al.* Rin-like, a novel regulator of endocytosis, acts as guanine nucleotide exchange factor for Rab5a and Rab22. *Biochim. Biophys. Acta BBA - Mol. Cell Res.* **1813**, 1198–1210 (2011).
104. Hadano, S. *et al.* ALS2CL, the novel protein highly homologous to the carboxy-terminal half of ALS2, binds to Rab5 and modulates endosome dynamics. *FEBS Lett.* **575**, 64–70 (2004).
105. Kunita, R. *et al.* The Rab5 activator ALS2/alsin acts as a novel Rac1 effector through Rac1-activated endocytosis. *J. Biol. Chem.* **282**, 16599–16611 (2007).
106. Zhu, H., Qian, H. & Li, G. Delayed onset of positive feedback activation of Rab5 by Rabex-5 and Rabaptin-5 in endocytosis. *PloS One* **5**, e9226 (2010).
107. Sandri, C. *et al.* The R-Ras/RIN2/Rab5 complex controls endothelial cell adhesion and morphogenesis via active integrin endocytosis and Rac signaling. *Cell Res.* **22**, 1479–1501 (2012).
108. Kajihito, H. *et al.* RIN3: a novel Rab5 GEF interacting with amphiphysin II involved in the early endocytic pathway. *J. Cell Sci.* **116**, 4159–4168 (2003).
109. Hunker, C. M. *et al.* Rab5-activating protein 6, a novel endosomal protein with a role in endocytosis. *Biochem. Biophys. Res. Commun.* **340**, 967–975 (2006).
110. Zhang, X., He, X., Fu, X.-Y. & Chang, Z. Varp is a Rab21 guanine nucleotide exchange factor and regulates endosome dynamics. *J. Cell Sci.* **119**, 1053–1062 (2006).
111. Fukuda, M. Multiple Roles of VARP in Endosomal Trafficking: Rabs, Retromer Components and R-SNARE VAMP7 Meet on VARP. *Traffic Cph. Den.* **17**, 709–719 (2016).

112. Davies, B. A., Carney, D. S. & Horazdovsky, B. F. Ubiquitin regulation of the Rab5 family GEF Vps9p. *Methods Enzymol.* **403**, 561–583 (2005).
113. Wang, Y. *et al.* The RAS effector RIN1 directly competes with RAF and is regulated by 14-3-3 proteins. *Mol. Cell. Biol.* **22**, 916–926 (2002).
114. Balaji, K. *et al.* RIN1 orchestrates the activation of RAB5 GTPases and ABL tyrosine kinases to determine the fate of EGFR. *J. Cell Sci.* **125**, 5887–5896 (2012).
115. Barbieri, M. A., Kong, C., Chen, P.-I., Horazdovsky, B. F. & Stahl, P. D. The SRC homology 2 domain of Rin1 mediates its binding to the epidermal growth factor receptor and regulates receptor endocytosis. *J. Biol. Chem.* **278**, 32027–32036 (2003).
116. Kong, C., Su, X., Chen, P.-I. & Stahl, P. D. Rin1 interacts with signal-transducing adaptor molecule (STAM) and mediates epidermal growth factor receptor trafficking and degradation. *J. Biol. Chem.* **282**, 15294–15301 (2007).
117. Han, L. *et al.* Protein binding and signaling properties of RIN1 suggest a unique effector function. *Proc. Natl. Acad. Sci. U. S. A.* **94**, 4954–4959 (1997).
118. Galvis, A. *et al.* Inhibition of early endosome fusion by Rab5-binding defective Ras interference 1 mutants. *Arch. Biochem. Biophys.* **482**, 83–95 (2009).
119. Hu, H., Bliss, J. M., Wang, Y. & Colicelli, J. RIN1 is an ABL tyrosine kinase activator and a regulator of epithelial-cell adhesion and migration. *Curr. Biol. CB* **15**, 815–823 (2005).
120. Ziegler, S. *et al.* A novel protein kinase D phosphorylation site in the tumor suppressor Rab interactor 1 is critical for coordination of cell migration. *Mol. Biol. Cell* **22**, 570–580 (2011).
121. Liu, X. *et al.* ABL SH3 mutant inhibits BCR-ABL activity and increases imatinib sensitivity by targeting RIN1 protein in CML cell. *Cancer Lett.* **369**, 222–228 (2015).
122. Afar, D. E. *et al.* Regulation of the oncogenic activity of BCR-ABL by a tightly bound substrate protein RIN1. *Immunity* **6**, 773–782 (1997).

123. Shuster, M. I. *et al.* A consistent pattern of RIN1 rearrangements in oral squamous cell carcinoma cell lines supports a breakage-fusion-bridge cycle model for 11q13 amplification. *Genes. Chromosomes Cancer* **28**, 153–163 (2000).
124. Senda, K., Goi, T., Hirono, Y., Katayama, K. & Yamaguchi, A. Analysis of RIN1 gene expression in colorectal cancer. *Oncol. Rep.* **17**, 1171–1175 (2007).
125. Tomshine, J. C. *et al.* Cell Proliferation and Epidermal Growth Factor Signaling in Non-small Cell Lung Adenocarcinoma Cell Lines Are Dependent on Rin1. *J. Biol. Chem.* **284**, 26331–26339 (2009).
126. Milstein, M. *et al.* RIN1 is a breast tumor suppressor gene. *Cancer Res.* **67**, 11510–11516 (2007).
127. Bos, J. L., Rehmann, H. & Wittinghofer, A. GEFs and GAPs: critical elements in the control of small G proteins. *Cell* **129**, 865–877 (2007).
128. Delprato, A. & Lambright, D. G. Structural basis for Rab GTPase activation by VPS9 domain exchange factors. *Nat. Struct. Mol. Biol.* **14**, 406–412 (2007).
129. Guo, Z., Ahmadian, M. R. & Goody, R. S. Guanine nucleotide exchange factors operate by a simple allosteric competitive mechanism. *Biochemistry (Mosc.)* **44**, 15423–15429 (2005).
130. Cherfils, J. & Chardin, P. GEFs: structural basis for their activation of small GTP-binding proteins. *Trends Biochem. Sci.* **24**, 306–311 (1999).
131. Delprato, A., Merithew, E. & Lambright, D. G. Structure, exchange determinants, and family-wide rab specificity of the tandem helical bundle and Vps9 domains of Rabex-5. *Cell* **118**, 607–617 (2004).
132. Yavas, S., Macháň, R. & Wohland, T. The Epidermal Growth Factor Receptor Forms Location-Dependent Complexes in Resting Cells. *Biophys. J.* **111**, 2241–2254 (2016).

133. Wang, Y.-N. *et al.* Membrane-bound Trafficking Regulates Nuclear Transport of Integral Epidermal Growth Factor Receptor (EGFR) and ErbB-2. *J. Biol. Chem.* **287**, 16869–16879 (2012).
134. Kaplan, M. *et al.* EGFR Dynamics Change during Activation in Native Membranes as Revealed by NMR. *Cell* **167**, 1241–1251.e11 (2016).
135. Ferguson, K. M. Structure-based view of epidermal growth factor receptor regulation. *Annu. Rev. Biophys.* **37**, 353–373 (2008).
136. Kozer, N. *et al.* Differential and synergistic effects of epidermal growth factor receptor antibodies on unliganded ErbB dimers and oligomers. *Biochemistry (Mosc.)* **50**, 3581–3590 (2011).
137. Colicelli, J. Human RAS superfamily proteins and related GTPases. *Sci. STKE Signal Transduct. Knowl. Environ.* **2004**, RE13 (2004).
138. Singh, B., Carpenter, G. & Coffey, R. J. EGF receptor ligands: recent advances. *F1000Research* **5**, (2016).
139. Bertelsen, V. *et al.* A chimeric pre-ubiquitinated EGF receptor is constitutively endocytosed in a clathrin-dependent, but kinase-independent manner. *Traffic Cph. Den.* **12**, 507–520 (2011).
140. Han, L. & Colicelli, J. A human protein selected for interference with Ras function interacts directly with Ras and competes with Raf1. *Mol. Cell. Biol.* **15**, 1318–1323 (1995).
141. Hu, H. *et al.* Integration of transforming growth factor beta and RAS signaling silences a RAB5 guanine nucleotide exchange factor and enhances growth factor-directed cell migration. *Mol. Cell. Biol.* **28**, 1573–1583 (2008).
142. Medts, T. *et al.* Acute ligand-independent Src activation mimics low EGF-induced EGFR surface signalling and redistribution into recycling endosomes. *Exp. Cell Res.* **316**, 3239–3253 (2010).

143. Roepstorff, K. *et al.* Differential effects of EGFR ligands on endocytic sorting of the receptor. *Traffic Cph. Den.* **10**, 1115–1127 (2009).
144. Colicelli, J. ABL tyrosine kinases: evolution of function, regulation, and specificity. *Sci. Signal.* **3**, re6 (2010).
145. Pluk, H., Dorey, K. & Superti-Furga, G. Autoinhibition of c-Abl. *Cell* **108**, 247–259 (2002).
146. Nagar, B. *et al.* Organization of the SH3-SH2 unit in active and inactive forms of the c-Abl tyrosine kinase. *Mol. Cell* **21**, 787–798 (2006).
147. Brasher, B. B. & Van Etten, R. A. c-Abl has high intrinsic tyrosine kinase activity that is stimulated by mutation of the Src homology 3 domain and by autophosphorylation at two distinct regulatory tyrosines. *J. Biol. Chem.* **275**, 35631–35637 (2000).
148. Tanis, K. Q., Veach, D., Duewel, H. S., Bornmann, W. G. & Koleske, A. J. Two distinct phosphorylation pathways have additive effects on Abl family kinase activation. *Mol. Cell. Biol.* **23**, 3884–3896 (2003).
149. Cao, X., Tanis, K. Q., Koleske, A. J. & Colicelli, J. Enhancement of ABL Kinase Catalytic Efficiency by a Direct Binding Regulator Is Independent of Other Regulatory Mechanisms. *J. Biol. Chem.* **283**, 31401–31407 (2008).
150. Fang, P., Zhao, Z., Tian, H. & Zhang, X. RIN1 exhibits oncogenic property to suppress apoptosis and its aberrant accumulation associates with poor prognosis in melanoma. *Tumor Biol.* **33**, 1511–1518 (2012).
151. Wang, Q. *et al.* Prognostic significance of RIN1 gene expression in human non-small cell lung cancer. *Acta Histochem.* **114**, 463–468 (2012).
152. Drews, J. Drug discovery: a historical perspective. *Science* **287**, 1960–1964 (2000).
153. Patel, D. V. & Gordon, E. M. Applications of small-molecule combinatorial chemistry to drug discovery. *Drug Discov. Today* **1**, 134–144 (1996).

154. Alaimo, P. J., Shogren-Knaak, M. A. & Shokat, K. M. Chemical genetic approaches for the elucidation of signaling pathways. *Curr. Opin. Chem. Biol.* **5**, 360–367 (2001).
155. Ohlmeyer, M. & Zhou, M.-M. INTEGRATION OF SMALL MOLECULE DISCOVERY IN ACADEMIC BIOMEDICAL RESEARCH. *Mt. Sinai J. Med. N. Y.* **77**, 350–357 (2010).
156. Weiss, W. A., Taylor, S. S. & Shokat, K. M. Recognizing and exploiting differences between RNAi and small-molecule inhibitors. *Nat. Chem. Biol.* **3**, 739–744 (2007).
157. Tijsterman, M., May, R. C., Simmer, F., Okihara, K. L. & Plasterk, R. H. A. Genes required for systemic RNA interference in *Caenorhabditis elegans*. *Curr. Biol. CB* **14**, 111–116 (2004).
158. Spring, D. R. Chemical genetics to chemical genomics: small molecules offer big insights. *Chem. Soc. Rev.* **34**, 472–482 (2005).
159. Verkman, A. S. Drug discovery in academia. *Am. J. Physiol. Cell Physiol.* **286**, C465–474 (2004).
160. Arkin, M. R., Tang, Y. & Wells, J. A. Small-molecule inhibitors of protein-protein interactions: progressing toward the reality. *Chem. Biol.* **21**, 1102–1114 (2014).
161. Hong, L. *et al.* A Pan-GTPase Inhibitor as a Molecular Probe. *PloS One* **10**, e0134317 (2015).
162. Shima, F. *et al.* Current status of the development of Ras inhibitors. *J. Biochem. (Tokyo)* **158**, 91–99 (2015).
163. Cox, A. D., Fesik, S. W., Kimmelman, A. C., Luo, J. & Der, C. J. Drugging the undruggable RAS: Mission possible? *Nat. Rev. Drug Discov.* **13**, 828–851 (2014).
164. Spiegel, J., Cromm, P. M., Zimmermann, G., Grossmann, T. N. & Waldmann, H. Small-molecule modulation of Ras signaling. *Nat. Chem. Biol.* **10**, 613–622 (2014).

165. Cromm, P. M., Spiegel, J., Grossmann, T. N. & Waldmann, H. Direct Modulation of Small GTPase Activity and Function. *Angew. Chem. Int. Ed Engl.* **54**, 13516–13537 (2015).
166. Vigil, D., Cherfils, J., Rossman, K. L. & Der, C. J. Ras superfamily GEFs and GAPs: validated and tractable targets for cancer therapy? *Nat. Rev. Cancer* **10**, 842–857 (2010).
167. Reuther, G. W. *et al.* RasGRP4 is a novel Ras activator isolated from acute myeloid leukemia. *J. Biol. Chem.* **277**, 30508–30514 (2002).
168. Ebinu, J. O. *et al.* RasGRP, a Ras guanyl nucleotide- releasing protein with calcium- and diacylglycerol-binding motifs. *Science* **280**, 1082–1086 (1998).
169. Tognon, C. E. *et al.* Regulation of RasGRP via a Phorbol Ester-Responsive C1 Domain. *Mol. Cell. Biol.* **18**, 6995–7008 (1998).
170. Fernandez-Zapico, M. E. *et al.* Ectopic expression of VAV1 reveals an unexpected role in pancreatic cancer tumorigenesis. *Cancer Cell* **7**, 39–49 (2005).
171. Qin, J. *et al.* Upregulation of PIP3-dependent Rac exchanger 1 (P-Rex1) promotes prostate cancer metastasis. *Oncogene* **28**, 1853–1863 (2009).
172. Muralidharan-Chari, V. *et al.* ADP-ribosylation factor 6 regulates tumorigenic and invasive properties in vivo. *Cancer Res.* **69**, 2201–2209 (2009).
173. Li, M. *et al.* EFA6A enhances glioma cell invasion through ADP ribosylation factor 6/extracellular signal-regulated kinase signaling. *Cancer Res.* **66**, 1583–1590 (2006).
174. Morishige, M. *et al.* GEP100 links epidermal growth factor receptor signalling to Arf6 activation to induce breast cancer invasion. *Nat. Cell Biol.* **10**, 85–92 (2008).
175. Boulay, P.-L., Cotton, M., Melançon, P. & Claing, A. ADP-ribosylation factor 1 controls the activation of the phosphatidylinositol 3-kinase pathway to regulate epidermal growth factor-dependent growth and migration of breast cancer cells. *J. Biol. Chem.* **283**, 36425–36434 (2008).

176. Wells, J. A. & McClendon, C. L. Reaching for high-hanging fruit in drug discovery at protein-protein interfaces. *Nature* **450**, 1001–1009 (2007).
177. Blumberg, P. M. *et al.* Wealth of opportunity - the C1 domain as a target for drug development. *Curr. Drug Targets* **9**, 641–652 (2008).
178. Margarit, S. M. *et al.* Structural evidence for feedback activation by Ras.GTP of the Ras-specific nucleotide exchange factor SOS. *Cell* **112**, 685–695 (2003).
179. Roberts, A. E. *et al.* Germline gain-of-function mutations in SOS1 cause Noonan syndrome. *Nat. Genet.* **39**, 70–74 (2007).
180. Lopez, I., Mak, E. C., Ding, J., Hamm, H. E. & Lomasney, J. W. A novel bifunctional phospholipase c that is regulated by Galpha 12 and stimulates the Ras/mitogen-activated protein kinase pathway. *J. Biol. Chem.* **276**, 2758–2765 (2001).
181. Nishikimi, A. *et al.* Blockade of inflammatory responses by a small-molecule inhibitor of the Rac activator DOCK2. *Chem. Biol.* **19**, 488–497 (2012).
182. Shang, X. *et al.* Small-molecule inhibitors targeting G-protein-coupled Rho guanine nucleotide exchange factors. *Proc. Natl. Acad. Sci. U. S. A.* **110**, 3155–3160 (2013).
183. Schmidt, S., Diriong, S., Méry, J., Fabbrizio, E. & Debant, A. Identification of the first Rho-GEF inhibitor, TRIPalpha, which targets the RhoA-specific GEF domain of Trio. *FEBS Lett.* **523**, 35–42 (2002).
184. Bouquier, N. *et al.* A cell active chemical GEF inhibitor selectively targets the Trio/RhoG/Rac1 signaling pathway. *Chem. Biol.* **16**, 657–666 (2009).
185. Viaud, J. *et al.* Structure-based discovery of an inhibitor of Arf activation by Sec7 domains through targeting of protein-protein complexes. *Proc. Natl. Acad. Sci. U. S. A.* **104**, 10370–10375 (2007).
186. Shima, F. *et al.* In silico discovery of small-molecule Ras inhibitors that display antitumor activity by blocking the Ras–effector interaction. *Proc. Natl. Acad. Sci. U. S. A.* **110**, 8182–8187 (2013).

187. Lim, S. M. *et al.* Therapeutic targeting of oncogenic K-Ras by a covalent catalytic site inhibitor. *Angew. Chem. Int. Ed Engl.* **53**, 199–204 (2014).
188. Ostrem, J. M., Peters, U., Sos, M. L., Wells, J. A. & Shokat, K. M. K-Ras(G12C) inhibitors allosterically control GTP affinity and effector interactions. *Nature* **503**, 548–551 (2013).
189. Taveras, A. G. *et al.* Ras oncoprotein inhibitors: the discovery of potent, ras nucleotide exchange inhibitors and the structural determination of a drug-protein complex. *Bioorg. Med. Chem.* **5**, 125–133 (1997).
190. Patgiri, A., Yadav, K. K., Arora, P. S. & Bar-Sagi, D. An Orthosteric Inhibitor of the Ras-Sos Interaction. *Nat. Chem. Biol.* **7**, 585–587 (2011).
191. Leshchiner, E. S. *et al.* Direct inhibition of oncogenic KRAS by hydrocarbon-stapled SOS1 helices. *Proc. Natl. Acad. Sci. U. S. A.* **112**, 1761–1766 (2015).
192. Hocker, H. J. *et al.* Andrographolide derivatives inhibit guanine nucleotide exchange and abrogate oncogenic Ras function. *Proc. Natl. Acad. Sci. U. S. A.* **110**, 10201–10206 (2013).
193. Maurer, T. *et al.* Small-molecule ligands bind to a distinct pocket in Ras and inhibit SOS-mediated nucleotide exchange activity. *Proc. Natl. Acad. Sci. U. S. A.* **109**, 5299–5304 (2012).
194. Spoerner, M., Graf, T., König, B. & Kalbitzer, H. R. A novel mechanism for the modulation of the Ras-effector interaction by small molecules. *Biochem. Biophys. Res. Commun.* **334**, 709–713 (2005).
195. Rosnizeck, I. C. *et al.* Stabilizing a weak binding state for effectors in the human ras protein by cyclen complexes. *Angew. Chem. Int. Ed Engl.* **49**, 3830–3833 (2010).
196. Lu, Y. *et al.* Solution phase parallel synthesis and evaluation of MAPK inhibitory activities of close structural analogues of a Ras pathway modulator. *Bioorg. Med. Chem. Lett.* **14**, 3957–3962 (2004).

197. Yan, C. *et al.* Discovery and characterization of small molecules that target the GTPase Ral. *Nature* **515**, 443–447 (2014).
198. Bidaud-Meynard, A. *et al.* A novel small-molecule screening strategy identifies mitoxantrone as a RhoGTPase inhibitor. *Biochem. J.* **450**, 55–62 (2013).
199. Hong, L. *et al.* Characterization of a Cdc42 protein inhibitor and its use as a molecular probe. *J. Biol. Chem.* **288**, 8531–8543 (2013).
200. Désiré, L. *et al.* RAC1 inhibition targets amyloid precursor protein processing by gamma-secretase and decreases Abeta production in vitro and in vivo. *J. Biol. Chem.* **280**, 37516–37525 (2005).
201. Shang, X. *et al.* Rational design of small molecule inhibitors targeting RhoA subfamily Rho GTPases. *Chem. Biol.* **19**, 699–710 (2012).
202. Friesland, A. *et al.* Small molecule targeting Cdc42–intersectin interaction disrupts Golgi organization and suppresses cell motility. *Proc. Natl. Acad. Sci. U. S. A.* **110**, 1261–1266 (2013).
203. Gao, Y., Dickerson, J. B., Guo, F., Zheng, J. & Zheng, Y. Rational design and characterization of a Rac GTPase-specific small molecule inhibitor. *Proc. Natl. Acad. Sci. U. S. A.* **101**, 7618–7623 (2004).
204. Montalvo-Ortiz, B. L. *et al.* Characterization of EHop-016, Novel Small Molecule Inhibitor of Rac GTPase. *J. Biol. Chem.* **287**, 13228–13238 (2012).
205. Cardama, G. A. *et al.* Preclinical Development of Novel Rac1-GEF Signaling Inhibitors using a Rational Design Approach in Highly Aggressive Breast Cancer Cell Lines. *Anticancer Agents Med. Chem.* **14**, 840–851 (2014).
206. Pelish, H. E. *et al.* Secramine inhibits Cdc42-dependent functions in cells and Cdc42 activation in vitro. *Nat. Chem. Biol.* **2**, 39–46 (2006).

207. Ohashi, Y. *et al.* AMF-26, a Novel Inhibitor of the Golgi System, Targeting ADP-ribosylation Factor 1 (Arf1) with Potential for Cancer Therapy. *J. Biol. Chem.* **287**, 3885–3897 (2012).
208. Spiegel, J. *et al.* Direct targeting of Rab-GTPase-effector interactions. *Angew. Chem. Int. Ed Engl.* **53**, 2498–2503 (2014).
209. Cromm, P. M. *et al.* Protease-Resistant and Cell-Permeable Double-Stapled Peptides Targeting the Rab8a GTPase. *ACS Chem. Biol.* **11**, 2375–2382 (2016).
210. Johnson, J. L. *et al.* Identification of Neutrophil Exocytosis Inhibitors (Nexinhibs), Small Molecule Inhibitors of Neutrophil Exocytosis and Inflammation DRUGGABILITY OF THE SMALL GTPase Rab27a. *J. Biol. Chem.* **291**, 25965–25982 (2016).
211. Agola, J. O. *et al.* A competitive nucleotide binding inhibitor: in vitro characterization of Rab7 GTPase inhibition. *ACS Chem. Biol.* **7**, 1095–1108 (2012).
212. Kato-Stankiewicz, J. *et al.* Inhibitors of Ras/Raf-1 interaction identified by two-hybrid screening revert Ras-dependent transformation phenotypes in human cancer cells. *Proc. Natl. Acad. Sci. U. S. A.* **99**, 14398–14403 (2002).
213. Shutes, A. *et al.* Specificity and mechanism of action of EHT 1864, a novel small molecule inhibitor of Rac family small GTPases. *J. Biol. Chem.* **282**, 35666–35678 (2007).
214. Evelyn, C. R. *et al.* Combined Rational Design and a High Throughput Screening Platform for Identifying Chemical Inhibitors of a Ras-activating Enzyme. *J. Biol. Chem.* **290**, 12879–12898 (2015).
215. Evelyn, C. R. *et al.* Rational design of small molecule inhibitors targeting the Ras GEF, SOS1. *Chem. Biol.* **21**, 1618–1628 (2014).
216. Niebel, B., Wosnitza, C. I. & Famulok, M. RNA-aptamers that modulate the RhoGEF activity of Tiam1. *Bioorg. Med. Chem.* **21**, 6239–6246 (2013).

217. Bouquier, N. *et al.* Aptamer-Derived Peptides as Potent Inhibitors of the Oncogenic RhoGEF Tgat. *Chem. Biol.* **16**, 391–400 (2009).
218. Blangy, A. *et al.* Identification of TRIO-GEFD1 chemical inhibitors using the yeast exchange assay. *Biol. Cell* **98**, 511–522 (2006).
219. Blangy, A. & Fort, P. Targeting the Dbl and dock-family RhoGEFs: a yeast-based assay to identify cell-active inhibitors of Rho-controlled pathways. *The Enzymes* **33 Pt A**, 169–191 (2013).
220. Renault, L., Guibert, B. & Cherfils, J. Structural snapshots of the mechanism and inhibition of a guanine nucleotide exchange factor. *Nature* **426**, 525–530 (2003).
221. Hafner, M. *et al.* Inhibition of cytohesins by SecinH3 leads to hepatic insulin resistance. *Nature* **444**, 941–944 (2006).
222. Stumpfe, D. *et al.* Targeting Multifunctional Proteins by Virtual Screening: Structurally Diverse Cytohesin Inhibitors with Differentiated Biological Functions. *ACS Chem. Biol.* **5**, 839–849 (2010).
223. Mayer, G. *et al.* Controlling small guanine–nucleotide–exchange factor function through cytoplasmic RNA intramers. *Proc. Natl. Acad. Sci. U. S. A.* **98**, 4961–4965 (2001).
224. Stenmark, H. *et al.* Distinct structural elements of rab5 define its functional specificity. *EMBO J.* **13**, 575–583 (1994).
225. Steele-Mortimer, O. *et al.* The N-terminal domain of a rab protein is involved in membrane-membrane recognition and/or fusion. *EMBO J.* **13**, 34–41 (1994).
226. Merithew, E., Stone, C., Eathiraj, S. & Lambright, D. G. Determinants of Rab5 Interaction with the N Terminus of Early Endosome Antigen 1. *J. Biol. Chem.* **278**, 8494–8500 (2003).
227. Keefe, A. D., Wilson, D. S., Seelig, B. & Szostak, J. W. One-step purification of recombinant proteins using a nanomolar-affinity streptavidin-binding peptide, the SBP-Tag. *Protein Expr. Purif.* **23**, 440–446 (2001).

228. Lippé, R., Miaczynska, M., Rybin, V., Runge, A. & Zerial, M. Functional synergy between Rab5 effector Rabaptin-5 and exchange factor Rabex-5 when physically associated in a complex. *Mol. Biol. Cell* **12**, 2219–2228 (2001).
229. Baumeister, M. A. *et al.* Loss of phosphatidylinositol 3-phosphate binding by the C-terminal Tiam-1 pleckstrin homology domain prevents in vivo Rac1 activation without affecting membrane targeting. *J. Biol. Chem.* **278**, 11457–11464 (2003).
230. Aghazadeh, B., Lowry, W. E., Huang, X. Y. & Rosen, M. K. Structural basis for relief of autoinhibition of the Dbl homology domain of proto-oncogene Vav by tyrosine phosphorylation. *Cell* **102**, 625–633 (2000).
231. invitrogen - ThermoFisher Scientific. Molecular Probes Handbook. in *Molecular Probes Handbook 11th Edition*, (2010).
232. Nelson, S. L. Academic HTS: diverse portraits. *Drug Discov. Today Technol.* **5**, e29–e33 (2008).
233. Inglese, J. *et al.* High-throughput screening assays for the identification of chemical probes. *Nat. Chem. Biol.* **3**, 466–479 (2007).
234. Zhang, null, Chung, null & Oldenburg, null. A Simple Statistical Parameter for Use in Evaluation and Validation of High Throughput Screening Assays. *J. Biomol. Screen.* **4**, 67–73 (1999).
235. Evelyn, C. R. *et al.* High-Throughput Screening for Small Molecule Inhibitors of LARG-Stimulated RhoA Nucleotide Binding via a Novel Fluorescence Polarization Assay. *J. Biomol. Screen.* **14**, 161–172 (2009).
236. Beck, B. *et al.* Assay Operations for SAR Support. in *Assay Guidance Manual* (eds. Sittampalam, G. S. *et al.*) (Eli Lilly & Company and the National Center for Advancing Translational Sciences, 2004).
237. Heck, H. d'A. Statistical theory of cooperative binding to proteins. Hill equation and the binding potential. *J. Am. Chem. Soc.* **93**, 23–29 (1971).

238. Lombardino, J. G. & Lowe, J. A. The role of the medicinal chemist in drug discovery — then and now. *Nat. Rev. Drug Discov.* **3**, 853–862 (2004).
239. Irwin, J. J. *et al.* An Aggregation Advisor for Ligand Discovery. *J. Med. Chem.* **58**, 7076–7087 (2015).
240. Abate, F. *et al.* Activating mutations and translocations in the guanine exchange factor VAV1 in peripheral T-cell lymphomas. *Proc. Natl. Acad. Sci.* **114**, 764–769 (2017).
241. Seidler, J., McGovern, S. L., Doman, T. N. & Shoichet, B. K. Identification and prediction of promiscuous aggregating inhibitors among known drugs. *J. Med. Chem.* **46**, 4477–4486 (2003).
242. Niebel, B. Modulierung der Guaninnukleotid Austauschfaktoren Tiam1 und Vav1 durch RNA-Aptamere. (2011).
243. Benjamin Felix Crispin Weiche. Biochemical and structural studies of the interaction between ARNO and the Epidermal Growth Factor Receptor. (2014).
244. Goody, R. S. How not to do kinetics: examples involving GTPases and guanine nucleotide exchange factors. *FEBS J.* **281**, 593–600 (2014).
245. Niebel, B. *et al.* ADLOC: an aptamer-displacement assay based on luminescent oxygen channeling. *Chem. Weinh. Bergstr. Ger.* **16**, 11100–11107 (2010).
246. Schwedt, Georg & Vogt, Carla. *Analytische Trennmethoden.* (Wiley-VCH, 2010).
247. Li, T. *et al.* High-throughput screening against thioredoxin glutathione reductase identifies novel inhibitors with potential therapeutic value for schistosomiasis. *Infect. Dis. Poverty* **4**, 40 (2015).
248. Arora, S. *et al.* Identification of small molecule inhibitors of ERCC1-XPF that inhibit DNA repair and potentiate cisplatin efficacy in cancer cells. *Oncotarget* **7**, 75104–75117 (2016).
249. Cottom, J. *et al.* Assay development and high-throughput screening of small molecular c-Abl kinase activators. *J. Biomol. Screen.* **16**, 53–64 (2011).

250. Xiao, T., Liu, R., Proud, C. G. & Wang, M.-W. A high-throughput screening assay for eukaryotic elongation factor 2 kinase inhibitors. *Acta Pharm. Sin. B* **6**, 557–563 (2016).
251. Ramos-Espiritu, L. *et al.* Discovery of LRE1 as a specific and allosteric inhibitor of soluble adenylyl cyclase. *Nat. Chem. Biol.* **12**, 838–844 (2016).
252. Voter, A. F., Manthei, K. A. & Keck, J. L. A High-Throughput Screening Strategy to Identify Protein-Protein Interaction Inhibitors That Block the Fanconi Anemia DNA Repair Pathway. *J. Biomol. Screen.* **21**, 626–633 (2016).
253. Terry-Lorenzo, R. T. *et al.* High-Throughput Screening Strategy Identifies Allosteric, Covalent Human D-Amino Acid Oxidase Inhibitor. *J. Biomol. Screen.* **20**, 1218–1231 (2015).
254. Posner, B. A., Xi, H. & Mills, J. E. J. Enhanced HTS hit selection via a local hit rate analysis. *J. Chem. Inf. Model.* **49**, 2202–2210 (2009).
255. Blevitt, J. M. *et al.* Structural Basis of Small-Molecule Aggregate Induced Inhibition of a Protein-Protein Interaction. *J. Med. Chem.* (2017).
256. Gupta, K. *et al.* Structural Basis for Inhibitor-Induced Aggregation of HIV Integrase. *PLoS Biol.* **14**, e1002584 (2016).
257. Rix, U. & Superti-Furga, G. Target profiling of small molecules by chemical proteomics. *Nat. Chem. Biol.* **5**, 616–624 (2009).
258. Han, L. *et al.* Protein binding and signaling properties of RIN1 suggest a unique effector function. *Proc. Natl. Acad. Sci. U. S. A.* **94**, 4954–4959 (1997).
259. Morand, K. L. & Cheng, X. Organic Compound Stability in Large, Diverse Pharmaceutical Screening Collections. in *Analysis and Purification Methods in Combinatorial Chemistry* (ed. Yan, B.) 321–350 (John Wiley & Sons, Inc., 2003).
doi:10.1002/0471531979.ch13
260. Kozikowski, B. A. *et al.* The effect of freeze/thaw cycles on the stability of compounds in DMSO. *J. Biomol. Screen.* **8**, 210–215 (2003).

261. Waybright, T. J., Britt, J. R. & McCloud, T. G. Overcoming problems of compound storage in DMSO: solvent and process alternatives. *J. Biomol. Screen.* **14**, 708–715 (2009).
262. Bowes, S. *et al.* Quality assessment and analysis of Biogen Idec compound library. *J. Biomol. Screen.* **11**, 828–835 (2006).
263. Popa-Burke, I. G. *et al.* Streamlined system for purifying and quantifying a diverse library of compounds and the effect of compound concentration measurements on the accurate interpretation of biological assay results. *Anal. Chem.* **76**, 7278–7287 (2004).
264. Gallagher, S. R. One-dimensional SDS gel electrophoresis of proteins. *Curr. Protoc. Protein Sci.* **Chapter 10**, Unit 10.1.1-44 (2012).
265. Laemmli, U. K. Cleavage of structural proteins during the assembly of the head of bacteriophage T4. *Nature* **227**, 680–685 (1970).
266. Gallagher, S. & Sasse, J. Protein analysis by SDS-PAGE and detection by Coomassie blue or silver staining. *Curr. Protoc. Pharmacol.* **Appendix 3**, 3B (2001).
267. Kyhse-Andersen, J. Electroblothing of multiple gels: a simple apparatus without buffer tank for rapid transfer of proteins from polyacrylamide to nitrocellulose. *J. Biochem. Biophys. Methods* **10**, 203–209 (1984).
268. Towbin, H., Staehelin, T. & Gordon, J. Electrophoretic transfer of proteins from polyacrylamide gels to nitrocellulose sheets: procedure and some applications. 1979. *Biotechnol. Read. Mass* **24**, 145–149 (1992).
269. Hochuli, E., Bannwarth, W., Döbeli, H., Gentz, R. & Stüber, D. Genetic Approach to Facilitate Purification of Recombinant Proteins with a Novel Metal Chelate Adsorbent. *Nat. Biotechnol.* **6**, 1321–1325 (1988).
270. Smith, D. B. & Johnson, K. S. Single-step purification of polypeptides expressed in *Escherichia coli* as fusions with glutathione S-transferase. *Gene* **67**, 31–40 (1988).

271. Majorek, K. A., Kuhn, M. L., Chruszcz, M., Anderson, W. F. & Minor, W. Double trouble-Buffer selection and His-tag presence may be responsible for nonreproducibility of biomedical experiments. *Protein Sci. Publ. Protein Soc.* **23**, 1359–1368 (2014).
272. Sabaty, M. *et al.* Detrimental effect of the 6 His C-terminal tag on YedY enzymatic activity and influence of the TAT signal sequence on YedY synthesis. *BMC Biochem.* **14**, 28 (2013).
273. Panek, A., Pietrow, O., Filipkowski, P. & Synowiecki, J. Effects of the polyhistidine tag on kinetics and other properties of trehalose synthase from *Deinococcus geothermalis*. *Acta Biochim. Pol.* **60**, 163–166 (2013).
274. Pace, C. N., Vajdos, F., Fee, L., Grimsley, G. & Gray, T. How to measure and predict the molar absorption coefficient of a protein. *Protein Sci. Publ. Protein Soc.* **4**, 2411–2423 (1995).
275. Bradford, M. M. A rapid and sensitive method for the quantitation of microgram quantities of protein utilizing the principle of protein-dye binding. *Anal. Biochem.* **72**, 248–254 (1976).
276. Feng, B. Y. *et al.* A high-throughput screen for aggregation-based inhibition in a large compound library. *J. Med. Chem.* **50**, 2385–2390 (2007).
277. Alsenz, J. & Kansy, M. High throughput solubility measurement in drug discovery and development. *Adv. Drug Deliv. Rev.* **59**, 546–567 (2007).

Acknowledgements

There are several people who contributed to this thesis in one way or another.

First of all I'd like to express my thankfulness to Anton Schmitz, Michael Famulok and Günter Mayer. They gave me the opportunity to perform the research on this great project and always supported me. Thank you for many interesting scientific discussions, the encouragement to work independently, your expert guidance and the excellent infrastructure in the lab.

Moreover I sincerely thank Matthias Geyer for his interest in my work and for kindly accepting to be the third referee in my examination.

I am also very grateful to Anton Bovier for accepting to be the fourth referee of this thesis.

There are many colleagues and collaborators who supported my research and expanded this thesis. I especially want to thank Anton Schmitz for cloning of most of the plasmids I used for protein expression. Special thanks also to Yvonne Aschenbach-Paul who took care of the *Sf9* insect-cell culture and expressed some of my constructs. Jeffrey Hannam synthesized my compounds and the derivatives used during the SAR studies and he was always there for me with his opinion from "a chemist's point of view". I want to thank Klaus Rotscheidt for operating the screening roboter and taking care of the compound library. Special thanks to Christine Wosnitza for her fantastic support at the beginning of my work in the lab. She helped me to get started and shared her experiences in working with Rab5 GEFs as well as committed plasmids I used for protein expression. I am very grateful to Mark Kerzhner for his expertise on LCMS measurements and enduring my many questions. I moreover thank Christian Sieg and Benjamin Weiche for kindly providing the proteins IR-ICD, ARNO-Sec7 and Arf1. Special thanks to Dongsheng Yin, who also works on a Rin1-related project, for constant exchange of insights on Rin1.

It is a pleasure to thank all of my great colleagues from the Famulok, Geyer and Mayer groups, who generated a nice working atmosphere and became friends over the years. Special thanks at this point to „the caesar guys“: Martina Bettio, Christian Sieg, Nora Karnowski, Dongsheng (Max) Yin, Anton Schmitz, Volkmar Fieberg and Yvonne Aschenbach for lighting up every-day life in the lab and funny free-time activities. I had a great time working and laughing with you.

I am very grateful to Anton Schmitz and Christoph Schür for proofreading and commenting on longer or shorter parts of this thesis.

I sincerely thank my dear friends Christoph Schür, Ilka Knigge and Linda Schaub for encouraging me when possible and distracting me when necessary. Special thanks at this point also to Aljoscha Weigand, who always believed in me, lovingly supported me and endured my moodiness during the ups and downs of this project.

My heartfelt gratitude I wish to express to my whole family, especially to my mother Ingrid Hamann, who was always there for me, constantly supported me and never stopped (and never will stop) believing in me. Thank you for your faith in me and being the best I could wish for.